Nonlinear elastic properties and vibrational anharmonicity of very high purity quartz

Wang, Qingxian

Award date:
1993

Awarding institution:
University of Bath

NONLINEAR ELASTIC PROPERTIES AND VIBRATIONAL ANHARMONICITY OF VERY HIGH PURITY QUARTZ

submitted by

QINGXIAN WANG

for the degree of PhD

of the University of Bath

1993

ProQuest LLC
789 East Eisenhower Parkway
P.O. Box 1346
Ann Arbor, MI 48106-1346

ACKNOWLEDGEMENTS

I am extremely grateful to Professor G.A. Saunders for his supervision, support, help and encouragement during the whole period of my time at Bath University. I have gained an enormous amount of knowledge and working experience during my studies here which will benefit me greatly in the future.

I would like to thank the Hirst Research Centre of the General Electric Company for its financial support during this project and also for providing me with the samples of very high purity quartz needed for the measurements. I owe a particular debt of gratitude to Dr. B.J. James for his advice on my work and for his kindness in giving me some extremely valuable research literature.

Many thanks go to Mr. E.F. Lambson for his capable assistance in the operation of the ultrasonic equipment and pressure system.

I am indebted to Dr. P.J. Ford for his kindness in reading the manuscript, particularly with reference to the written English and for his useful comments on my thesis.

I would like to thank Mr R.C.J. Draper, Mrs W.A. Lambson, and all my colleagues in the ultrasonics group for their help during this work.

Finally, I am most grateful to Mrs E. Birks, Mr B. Ring, Mrs D.J. Pennock and Mrs A.K. Soboslay for their administrative help and support during my work.

ABSTRACT

The nonlinear elastic properties and the lattice vibrational anharmonicity of very high purity monocrystalline α-quartz have been investigated as a function of temperature from 243K to 393K, the range of an industrial applications.

The temperature dependences of the all fourteen independent third order elastic constants C_{IJK} and the hydrostatic pressure derivatives $(\partial C_{IJ}/\partial P)_{T,P=0}$ of the six independent second order elastic constants at zero electric field have been determined by using the ultrasonic pulse echo overlap and the ultrasonic pulse superposition techniques in combination with a hydrostatic pressure system and a uniaxial compression apparatus. The results show strong temperature dependences of C_{IJK} and $(\partial C_{IJ}/\partial P)_{T,P=0}$. When the temperature is increased, C_{111}, C_{113}, C_{114}, C_{133}, C_{134}, C_{144} and C_{155} decrease while C_{112}, C_{123}, C_{124}, C_{133}, C_{222} and C_{344} increase. C_{444} shows a maximum at around 303K. These strong temperature dependences of the TOEC indicate unsuspected complications in the interatomic interactions in monocrystalline α-quartz. The derivation of the general equations for the calculation of the third order elastic constants from ultrasonic data for piezoelectric crystals has been given in detail. The hydrostatic pressure derivatives $(\partial C_{IJ}/\partial P)_{T,P=0}$ increase approximately linearly with temperature, when the contributions from piezoelectric effects are deducted. However the temperature dependences of the $(\partial C_{11}/\partial P)_{T,P=0}$, $(\partial C_{13}/\partial P)_{T,P=0}$ and $(\partial C_{66}/\partial P)_{T,P=0}$ are considerably affected by the contributions from the piezoelectric effects. In general the piezoelectric effects provide considerable contributions to C_{IJK}, $(\partial C_{IJ}/\partial P)_{T,P=0}$ and the vibrational anharmonicity of monocrystalline α-quartz. The analysis of these results reveals that the temperature

dependences of volume compression and the pressure induced changes of the lattice parameters of very high purity α-quartz become considerable at high pressures. For the requirements of quartz device design the temperature coefficients of the second and third order elastic constants have been extracted from the results.

To quantify the lattice vibrational anharmonicity of the very high purity crystalline quartz, the long wavelength acoustic mode Grüneisen parameters which characterise the contributions of the relevant phonon modes to thermal expansion have been determined from the measured ultrasonic data using the equations developed for piezoelectric crystals. A complicated dependence of the parameters on the acoustic wave propagation direction has been found. The results show the responses of the zone centre acoustic phonon modes to the variation of temperature. The temperature dependences of the mode Grüneisen parameters indicate that the contribution of the long wavelength acoustic mode phonons to the thermal expansion changes with temperature and plays a dominant role at low temperature. There is acoustic mode softening which contributes for the negative thermal expansion tensor α_{33} . The hydrostatic pressure derivatives $(\partial C_{66}/\partial P)_{T,P=0}$ and $(\partial C_{14}/\partial P)_{T,P=0}$ which have negative values at low temperature may be related to the "soft" phonon mode which induces the $\alpha-\beta$ phase transition.

CONTENTS

Chapter 1 Introduction

α-Quartz crystal is one of the most important and useful materials. Applications for quartz crystals have grown from their early use in frequency standards and radio communications to the present wide spectrum of uses encompassing many electrical products. Quartz crystal units are extensively employed in the fields of telecommunications and radio communications for precise frequency control and in quartz clocks for timing control. They are also used as timing control elements in computers, as surface wave correlators, discriminators and filters in instrumentation and communication, and as sensors of temperature and pressure.

The elastic properties of α-quartz are interesting because of their important applications to device designs. In the linear limit, the fundamental resonant frequency of each quartz device is determined by its physical dimensions, the SOEC and density. The elastic behaviour of quartz have been studied for nearly a century. The early work on the determination of the SOEC has been reviewed by Cady (1946, 1964), Koga et al. (1958) and Bechmann (1958). The earliest publication of the most complete data for the elastic coefficients can be traced to Voigt (1910). In 1922, Perrier and de Mandrot (1922) published the first complete set of high temperature data which showed that the elastic coefficients of quartz undergo very pronounced changes in the neighbourhood of the $\alpha-\beta$ phase transition at 846K. To obtain more accurate data for quartz design and investigation, many workers have measured the elastic constants and the temperature coefficients of quartz at, or around, room temperature, e.g. Bechmann (1958), Koga et al. (1958), Bechmann et al. (1962), McSkimin (1962), Ludanov et al. (1976), Shevel'ko

and Yakovlev (1977) and James (1987). A review and commentary on determinations of currently used data sets of the SOEC has been given by James (1987). Up to now, most of the available data are for the second-order elastic compliances and stiffnesses, and their temperature coefficients, around room temperature (298K). In a review article on the properties of quartz, Brice (1985) gives the mean and the standard deviation of the values of C_{IJ} measured by Bechmann (1958), Koga et al. (1958), McSkimin et al. (1965), Ludanov et al. (1976), and Shevel'ko and Yakovlev (1977). Brice suggested that the mean values could be regarded as unbiased estimates of the C_{IJ} values. No data of very high purity quartz (VHPQ) were available until 1987 when James (1987) reported the measurements of the velocities of the five ultrasonic wave propagation modes in the VHPQ from 213K to 393K.

With the development of electronic devices utilizing quartz crystal, there is a need for the higher order elastic coefficients and their temperature dependences. A determination of high order coefficients would enable a correct interpretation of non-linear effects in resonators. The nonlinear behaviour of quartz crystal is responsible for most of the frequency instabilities of resonators and oscillators (Gagnepain 1981). The available data for higher order elastic constants are far less extensive than that required. Thurston et al. (1966) determined all of the fourteen independent third order elastic constants (TOEC) of α-quartz at 298K by using an ultrasonic pulse superposition system with the sample under a hydrostatic pressure and a uniaxial stress, respectively. Fowles (1967), Graham (1972) and Gerlich and Breazeale (1990) reported some of TOEC and the fourth order elastic constants C_{111}, C_{333}, C_{1111} and C_{3333} of quartz at room temperature. Recently Hruska (1990a) has determined the five combinations of the TOEC and the third order piezoelectric coefficients by measuring the dc-field induced change in the resonant frequency of the extension mode of the quartz rod. However the results cannot give all the information needed of the individual independent TOEC. It is imperative

in quartz device design to have a knowledge of the temperature dependences of the third order elastic constants in the commonly used temperature range.

Hence the main objective of this work is to determine the all fourteen independent TOEC of VHPQ as a function of temperature from 243K to 393K by using ultrasonic methods with samples under a hydrostatic and an uniaxial stress respectively.

A description of the fundamental relationships in theory of nonlinear elasticity is given in Chapter 2 in which the hydrostatic and uniaxial pressure effects on velocities of ultrasonic waves are related to the TOEC for a piezoelectric crystal with an arbitrary symmetry. In the long wavelength limit, crystals can be treated as continuum media for elastic wave propagation. To investigate the nonlinear elastic properties, finite strain tensors are introduced into the equation of wave motion and the constitutive relations. For piezoelectric media elastic strains are coupled with elastic field and, hence, the Maxwell field equations are involved. The application of the quasi-electrostatic approximation simplifies the derivation of the nonlinear form of the piezoelectric constitutive relations. Solving the linearized equations of wave motion and the linearized Maxwell field equations gives the eigenequations of the wave motion. The equations relating the TOEC with the ultrasonically measured data can be eventually obtained by finding the pressure derivatives of the eigen values for the eigenequations. As a direct result of the measurements, the pressure derivatives of the SOEC can also be determined. As combinations of the TOEC these pressure derivatives are directly related to the nonlinear properties of crystals and can be used to analyse the properties such as the volume compression of a crystal under high pressures. A method to calculate the hydrostatic pressure derivatives of the SOEC is also discussed in Chapter 2.

Thermal properties such as thermal expansion and phonon-phonon interactions arise from lattice vibrational anharmonicity which is due to the nonlinearity of interatomic forces with respect to atomic displacements. Knowledge of the TOEC, and also of the

pressure derivatives of the SOEC, is fundamental for understanding these properties. The generalized mode Grüneisen parameters measure the contributions of phonons of different modes to thermal expansion of a crystal. Chapter 3 describes the methods for determination of the acoustic mode Grüneisen parameters in long wavelength limit by using the TOEC and the hydrostatic pressure derivatives of the SOEC respectively. Applications of the parameters to the thermal expansion is also discussed in the chapter.

A description of the ultrasonic measurement techniques and equipments is given in Chapter 4. An ultrasonic pulse echo overlap system has been used to determine the hydrostatic pressure dependence of the velocity of ultrasonic waves propagated in VHPQ while an ultrasonic pulse superposition technique has been used to determine the uniaxial compression effects on the wave velocities. The other facilities used in the measurements are presented and the errors which may occur in the measurements are discussed.

After a brief description of the structure of α-quartz, Chapter 5 surveys its physical properties and the coefficients related to this work, such as the tensor components of the elasticity, piezoelectricity and electrostrictivity. The conventions used are described. The specific expressions for the functions in the general equations obtained in Chapter 2 for determination of the TOEC are given for the individual ultrasonic wave modes in quartz crystal.

The data measured in this work for determination of the TOEC are presented in Chapter 6. The hydrostatic pressure derivatives of the SOEC of VHPQ are given as a function of temperature. Some nonlinear elastic properties of α-quartz such as volume compression and the changes of the lattice parameters at high pressure are calculated at selected temperatures by using the measured values of the hydrostatic pressure derivatives of the SOEC. The pressure derivatives which have negative values are related to the structural stability of α-quartz. The results of the central task of the work, i.e. the measurement of the temperature dependences of the TOEC from 243K and 393K, are

given eventually in section 6.6. The TOEC as functions of temperature are given both in values and figures. To enable the use of our data in quartz device design, the temperature coefficients of the fourteen independent TOEC are also tabulated. As an application to the lattice vibrational anharmonicity, the temperature dependences of the acoustic mode Grüneisen parameters in the long wavelength limit calculated by using the pressure derivatives of the SOEC are given in Chapter 7 as a function of wave propagation direction. The mean long wavelength acoustic Grüneisen parameter in high temperature limit is also given as a function of temperature in this chapter. The TOEC have been used in the calculation of the elastic thermal expansion tensor components. The calculated components at low temperature are compared with the thermal expansion tensor components determined experimentally at 5K.

In Chapter 8 a summary is given of the present findings of the properties of the nonlinear elasticity and lattice vibrational anharmonicity of α-quartz.

Chapter 2 Determination of the Third Order Elastic Constants of Piezoelectric Crystals

2.1 Introduction

The theory of elasticity, in its broad aspects, deals with the study of the behaviour of media that possess the property of recovering their size and shape when the forces producing deformations are removed. A body is deformed, or strained, whenever the distance between its particles changes. The force exerted on the surface of an element in the medium by the material surrounding it is proportional to the area of the surface of the element. The force per unit area is called the stress. The deformation of the medium, resulting in a particle displacement from its original position to a new position, is defined as the strain. An elastic property is characterized mathematically by a particular functional relationship connecting stress with strain. Fig. 2.1 (Auld 1973) gives a schematic representation of the relation between the stress and the strain. For small deformations, the strain in a deformed body is linearly proportional to the applied stress. This is Hooke's law. In this region the body is subjected to a linear elastic deformation and gives rise to linear elastic properties which are characterized by the second order elastic constants (SOEC). As an increasing deformation is applied, the relation between stress and strain becomes increasingly nonlinear, although the body can still return to its original state when the stress is removed. The deformation in this region is elastically nonlinear. Hooke's law is not valid in this region. Nonlinear elastic properties are described by the third and higher order elastic constants. If the strain is increased above a certain limit, known as the elastic limit, the deformation is no longer elastic. Beyond

this elastic limit, the medium deforms permanently; i.e. it undergos a plastic deformation. Increasing strain ultimately leads to fracture of the solid. In the present work only the deformation in the elastic region is of interest.

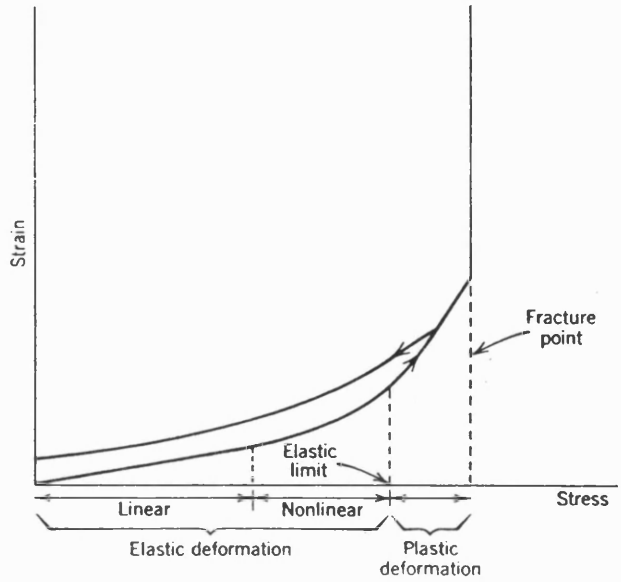

Fig. 2.1 Typical stress-strain relation for a solid material (Auld 1973).

In some cases, the relations represented by Fig. 2.1 do not describe fully the response of a solid to stress. Certain materials are piezoelectric becoming electrically polarized when they are squeezed, or becoming strained when placed in an electric field. Piezoelectricity, as an interdependence of elastic and electric properties in piezoelectric crystalline materials, is intimately related to the study of elastic waves. α-Quartz is a typical piezoelectric material.

The third order elastic constants (TOEC) are essential to understand the nonlinear elastic properties of materials. From the dynamic equations of elastic wave motion, Thurston and Brugger (1964) have derived equations to calculate the TOEC from velocity measurements on small amplitude sound waves in statically stressed crystals of arbitrary

symmetry. These equations do not include piezoelectric effects. For piezoelectric materials, the equations for solving the TOEC must involve the second and third order piezoelectric coefficients (SOPC and TOPC). Based on the Langrangian theory of elastic dielectrics, Nelson (1978, 1979) discussed in detail nonlinear phenomena related with the interactions between acoustic and electric fields in dielectrics and presented the general dynamic equations and constitutive relations for the phenomena, which include TOEC. By using the nonlinear form constitutive relations including the third order terms, McMahon (1968) and Ljamov (1971) analysed the nonlinear wave equations for piezoelectrics. Nakagawa et al. (1973) applied Thurston and Brugger's method (1964) to piezoelectrics and derived the general equations to calculate TOEC from velocity measurements of the ultrasonic wave propagated in piezoelectrics with arbitrary symmetry under a static uniaxial stress. Cho and Yamanouchi (1987) extended the work of Nakagawa et al. (1973) to include the piezoelectrics under a static electric field and derived the whole sets of equations to determine the various third order coefficients from ultrasonic velocity measurements and capacitance measurements of arbitrary piezoelectric crystals under a static uniaxial stress or in a static electric field.

In the present work, measurements of the ultrasonic wave velocity have been made under hydrostatic pressure and uniaxial compression respectively. Beside the equations for the TOEC, determined by measurements under uniaxial compression, the equations determining the combination of the TOEC coupled with other third order coefficients for the modes measured under hydrostatic pressure are also needed. Following the methods used by Thurston and Brugger (1964) and Cho and Yamanouchi (1987), the general equations have been derived in this work to calculate the TOEC coupled with other third order coefficients from ultrasonic velocity measurements of piezoelectric crystals with arbitrary symmetry under hydrostatic pressure and uniaxial compression. The derivation gives the same results as Cho and Yamanouchi (1987) for the

measurements under uniaxial compression. The details of the derivation are given in this chapter as a description of the fundamental theory of electromechanics. The fundamental concepts of deformation, thermodynamic functions, the piezoelectric constitutive relations and Maxwell's electromagnetic equations in the material representation are introduced in sections 2.2 and 2.3. Section 2.4 discusses the nonlinear form of the piezoelectric constitutive relations. Section 2.5 describes the details of the derivation of the equations for determining the TOEC of the piezoelectric crystals from the velocity measurements of acoustic waves propagated in crystals under hydrostatic pressure and uniaxial compression.

The pressure derivatives of the SOEC of piezoelectric crystals also include a contribution from piezoelectric effects. Thurston's method (1965a) for the calculation of the pressure derivatives of the SOEC of crystals with arbitrary symmetry has been developed for piezoelectric crystals in section 2.6.

2.2 Deformation and stress

There are two basic ways of describing deformation and motion in continuum mechanics. These are the material, or Lagrangian, and spatial, or Eulerian, descriptions. In the material description, the coordinates of a material point, or particle, in its undeformed position, are used as independent variables while in the spatial description the coordinates of the particle in the deformed position are taken as the independent variables. The two descriptions are the same when the deformation is infinitesimal (Nelson 1979). However, for finite deformations, they give different descriptions of strains (Miklowitz 1980). For consistency with most of the literatures the material or Lagrangian description is used in the work reported here.

Following the conventions of Thurston and Brugger (1964) the configurations used to define a deformed state of a solid are:

(i) $(a_1,\ a_2,\ a_3)$ is the reference configuration corresponding to zero stress, or the natural state. Hence, $\vec{a}(a_1,\ a_2,\ a_3)$ indicates a point in an undeformed state referred to a rectangular Cartesian coordinate system.

(ii) $(X_1,\ X_2,\ X_3)$ is the reference configuration corresponding to some "initial" stress and $\vec{X}(X_1,\ X_2,\ X_3)$ indicates a point in an initially stressed state.

(ii) $(x_1,\ x_2,\ x_3)$ is the reference configuration corresponding to a current (stressed) state of the solid and $\vec{x}(x_1,\ x_2,\ x_3)$ indicates a point in a currently deformed state.

Consider an unstrained body initially occupying a space R . After straining, the body then occupies the region R'. A general position $P(\vec{a})$ has been strained into position $P'(\vec{x})$ and there exists a relation of the form

$$x_i = x_i(\vec{a}) \quad . \tag{2.1}$$

It is assumed that: (1) the deformation is continuous and reversible, therefore $x_i(\vec{a})$ must be continuous functions (i.e. no dislocations can occur) and have a unique continuous inverse

$$a_i = a_i(\vec{x}) \quad , \tag{2.2}$$

(2) the functions $x_i(\vec{a})$ and $a_i(\vec{x})$ have continuous derivatives; then their functional determinant (or Jacobian) J of deformation of $(x_1,\ x_2,\ x_3)$ with respect to $(a_1,\ a_2,\ a_3)$ is given by (Thurston 1964 and Nelson 1979):

$$J = \begin{Vmatrix} \dfrac{\partial x_1}{\partial a_1} & \dfrac{\partial x_1}{\partial a_2} & \dfrac{\partial x_1}{\partial a_3} \\ \dfrac{\partial x_2}{\partial a_1} & \dfrac{\partial x_2}{\partial a_2} & \dfrac{\partial x_2}{\partial a_3} \\ \dfrac{\partial x_3}{\partial a_1} & \dfrac{\partial x_3}{\partial a_2} & \dfrac{\partial x_3}{\partial a_3} \end{Vmatrix} \tag{2.3}$$

and this cannot be infinite or zero. These two assumptions are the requirements for continuity of the deformation.

A body element that is initially a rectangular parallelepiped of volume $dV_0 = da_1 da_2 da_3$

at any time t has a volume dV such that the volume dV and dV_0 satisfy the Jacobian J (Thurston 1964 and Nelson 1979); in an abbreviated form:

$$\lim_{dV_0 \to 0}\left(\frac{dV}{dV_0}\right)=\left\| \frac{\partial x_r}{\partial a_s} \right\| \quad , \tag{2.4}$$

or

$$J \equiv \left\| \frac{\partial x_r}{\partial a_s} \right\| = \frac{\rho_0}{\rho} \tag{2.5}$$

where ρ_0 and ρ are the mass densities in the natural and in an arbitrary state respectively.

The displacement vector $\vec{u}(u_1,\ u_2,\ u_3)$ of a particle is defined by

$$\vec{u} = \vec{x} - \vec{X} \quad . \tag{2.6}$$

If a curve PQ, with a differential arc length ds in the region R, deforms into $P'Q'$ with a differential arc length ds' in the region R', there exist the relations:

$$(ds)^2 = da_i da_i \quad , \quad (ds')^2 = dx_i dx_i \tag{2.7}$$

where

$$dx_i = \frac{\partial x_i}{\partial a_j} da_j \quad . \tag{2.8}$$

Here the Einstein convention is used, i.e. a summation is inferred if the same subscript repeats on one side of the equal symbol. Let

$$\eta_{jk} = \frac{1}{2}\left(\frac{\partial x_i}{\partial a_j}\frac{\partial x_i}{\partial a_k} - \delta_{jk}\right) \tag{2.9}$$

where

$$\delta_{ij} = \begin{cases} 1, & i = j; \\ 0, & i \neq j, \end{cases}$$

is the Kronecker delta. Then

$$(ds')^2 - (ds)^2 = 2\eta_{jk} da_j da_k \quad . \tag{2.10}$$

From Eq. (2.1), (2.6) and (2.8) it is clear that

$$\frac{\partial x_i}{\partial a_j} = \frac{\partial u_i}{\partial a_j} + \delta_{ij} \quad . \tag{2.11}$$

From this relation, η_{jk} can be written as

$$\eta_{jk} = \frac{1}{2}\left(\frac{\partial u_j}{\partial a_k} + \frac{\partial u_k}{\partial a_j} + \frac{\partial u_i}{\partial a_j}\frac{\partial u_i}{\partial a_k} \right) \quad . \tag{2.12}$$

The nine quantities η_{jk} constitute a second rank tensor and are called the material or Lagrangian strain tensor components. They represent a finite deformation. The values of the components depend on the position P where the deformation is observed. Only six components of the material strains are distinct, since η_{jk} are symmetric tensors, i.e.,

$$\eta_{jk} = \eta_{kj} \quad . \tag{2.13}$$

In the spatial frame, the stress at any point P on a body is described by a tensor whose Cartesian component σ_{ij} equals the i-component of the force per unit area acting across a surface with a normal in the j-direction, as shown in Fig. 2.2. The i-component of force per unit area across a surface of unit normal $\vec{n}$ is

$$\sigma_i = \sigma_{ij} n_j \quad . \tag{2.14}$$

Hence, the force per unit area exerted across the surface at P is

$$\vec{\sigma} = \sigma_1 \vec{i} + \sigma_2 \vec{j} + \sigma_3 \vec{k} \quad . \tag{2.15}$$

The stress tensor σ_{ij} is a symmetric tensor expressed by the equation (Fedorov 1968):

$$\sigma_{ij} = \sigma_{ji} \quad . \tag{2.16}$$

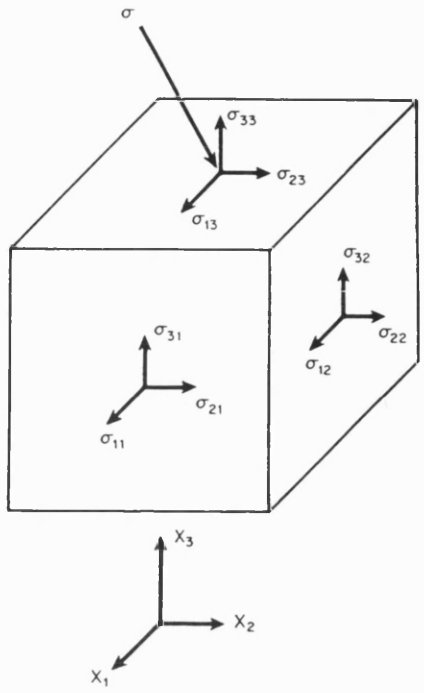

Fig. 2.2 Stress components on the faces of a rectangular parallelepiped.

In the material frame a tensor t_{ij}, called the thermodynamic tension (Brugger 1964), is used. It is related to the stress tensor σ_{ij} by the expression (Thurston and Brugger 1964)

$$\sigma_{ij} = \frac{1}{J} \frac{\partial x_i}{\partial a_p} \frac{\partial x_j}{\partial a_q} t_{pq} \quad . \tag{2.17}$$

Similarly with σ_{ij} , t_{ij} is also a symmetric tensor

$$t_{ij} = t_{ji} \quad . \tag{2.18}$$

2.3 Electromagnetic equations in the material description and the quasi-electrostatic approximation

Electromagnetic equations in the material description can be transformed from the equations in the spatial representation. For the spatial description italic letters are adopted and Maxwell's field equations can be written in the form:

$$\nabla \times \vec{E} = -\frac{\partial \vec{B}}{\partial t} \quad , \tag{2.19}$$

$$\nabla \times \vec{H} = \frac{\partial \vec{D}}{\partial t} + \vec{j} \quad , \tag{2.20}$$

$$\nabla \cdot \vec{B} = 0 \quad , \tag{2.21}$$

$$\nabla \cdot \vec{D} = \rho_e \quad , \tag{2.22}$$

with

$$\vec{D} = \varepsilon_0 \vec{E} + \vec{P} \quad , \tag{2.23}$$

$$\vec{H} = \frac{\vec{B}}{\mu_0} - \vec{M} \quad . \tag{2.24}$$

In Eqs. (2.19)-(2.24) $\vec{E}$, $\vec{D}$, $\vec{B}$ and $\vec{H}$ are the electrical field, electrical displacement, magnetic flux density and magnetic intensity respectively. $\vec{P}$ and $\vec{M}$ are the electric and magnetic moment per unit volume. ρ_e and $\vec{j}$ are the densities of free electric charge and electric current. The divergence and curl operations in spatial coordinates are:

$$(\nabla \times) \equiv \left(\frac{\partial}{\partial x_1}\vec{i} + \frac{\partial}{\partial x_2}\vec{j} + \frac{\partial}{\partial x_3}\vec{k} \right) \times \quad , \tag{2.25}$$

and

$$(\nabla \cdot) \equiv \left(\frac{\partial}{\partial x_1}\vec{i} + \frac{\partial}{\partial x_2}\vec{j} + \frac{\partial}{\partial x_3}\vec{k} \right) \cdot \quad . \tag{2.26}$$

In the material presentation, ordinary roman letters are used for electric and magnetic field quantities, which are defined as follows (Thurston 1974):

$$\vec{\mathrm{E}}: \quad \mathrm{E}_j = E_i \frac{\partial x_i}{\partial a_j} \quad ; \quad E_i = \mathrm{E}_j \frac{\partial a_j}{\partial x_i} \quad , \tag{2.27}$$

$$\vec{\mathrm{D}}: \quad \mathrm{D}_j = JD_i \frac{\partial a_j}{\partial x_i} \quad ; \quad D_i = \frac{1}{J}\mathrm{D}_j \frac{\partial x_i}{\partial a_j} \quad , \tag{2.28}$$

$$\vec{\mathrm{P}}: \quad \mathrm{P}_j = JP_i \frac{\partial a_j}{\partial x_i} \quad ; \quad P_i = \frac{1}{J}\mathrm{P}_j \frac{\partial x_i}{\partial a_j} \quad , \tag{2.29}$$

$$\vec{\mathrm{H}}: \quad \mathrm{H}_j = JH_i \frac{\partial x_i}{\partial a_j} \quad ; \quad H_i = \mathrm{H}_j \frac{\partial a_j}{\partial x_i} \quad , \tag{2.30}$$

$$\vec{\mathrm{E}}: \quad \mathrm{M}_j = M_i \frac{\partial x_i}{\partial a_j} \quad ; \quad M_i = \mathrm{M}_j \frac{\partial a_j}{\partial x_i} \quad , \tag{2.31}$$

$$\vec{\mathrm{B}}: \quad \mathrm{B}_j = JB_i \frac{\partial a_j}{\partial x_i} \quad ; \quad B_i = \frac{1}{J}\mathrm{B}_j \frac{\partial x_i}{\partial a_j} \quad , \tag{2.32}$$

Here J is the Jacobian of the deformation defined in Eq. (2.5). By using the transformation equations (2.27)-(2.32), in the case of the particle motion associated with a mechanical wave, the material representations of Maxwell's field equations can be obtained as (Thurston 1974, Nelson 1979)

$$\nabla_a \times \vec{\mathrm{E}} = -\frac{\partial \vec{\mathrm{B}}}{\partial t} \quad , \tag{2.33}$$

$$\nabla_a \times \vec{\mathrm{H}} = \frac{\partial \vec{\mathrm{D}}}{\partial t} + \vec{\mathrm{j}} \quad , \tag{2.34}$$

$$\nabla_a \cdot \vec{\mathrm{B}} = 0 \quad , \tag{2.35}$$

$$\nabla_a \cdot \vec{\mathrm{D}} = J\rho_e \quad , \tag{2.36}$$

with

$$\mathrm{D}_j = \varepsilon_0 J \frac{\partial a_i}{\partial x_j}\frac{\partial a_k}{\partial x_j}\mathrm{E}_k + \mathrm{P}_j \quad . \tag{2.37}$$

The divergence and curl operations in material coordinates are

$$(\nabla_a \times) = \left(\frac{\partial}{\partial a_1}\vec{i} + \frac{\partial}{\partial a_2}\vec{j} + \frac{\partial}{\partial a_3}\vec{k} \right) \times \quad , \tag{2.38}$$

$$(\nabla_a \cdot) = \left(\frac{\partial}{\partial a_1}\vec{i} + \frac{\partial}{\partial a_2}\vec{j} + \frac{\partial}{\partial a_3}\vec{k} \right) \cdot \quad . \tag{2.39}$$

In a piezoelectric solid electric and acoustic fields are coupled together. Because of this coupling propagation of acoustic waves in a piezoelectric solid is accompanied by propagation of electromagnetic waves. When an acoustic plane wave propagates in a piezoelectric crystal, it drives the electric field wave through the direct piezoelectric effect. This piezoelectrically generated electric field then affects the propagation of the acoustic wave that generates it through the converse piezoelectric effect. Applied electric and magnetic fields will affect the propagation of the acoustic wave. Therefore, measurements of the elastic properties depend on the electromagnetic conditions imposed on the specimen.

In general, the acoustic, electric and magnetic fields interact with one another. When considering the nonlinear properties, the magnetostrictive effect can be important even in a nonmagnetic dielectric, if an applied magnetic field is sufficiently strong (Nelson, 1979). The involvement of electric and magnetic fields makes the analysis of the elastic properties of piezoelectric crystals complicated. However, the analysis can be simplified by using the quasi-electrostatic approximation. The velocity of sound is very small compared with that of an electromagnetic wave. As a result, a polarization wave induced by the sound wave cannot be propagated in the form of an electromagnetic wave. The piezoelectrically generated electric field of a plane acoustic wave is associated with a mechanical vibration as an electrostatic field. Nelson (1979) has shown that, if the free space wavelength λ of an electromagnetic wave, with an angular frequency ω, is large compared with a typical dimension L of the piezoelectric crystal studied, i.e.

$$\frac{\omega L}{c} = \frac{2\pi L}{\lambda} \ll 1 \quad , \tag{2.40}$$

then all time derivative terms in, or caused by, Maxwell's field equations can be dropped and hence:

$$\nabla \times \vec{E} = 0 \tag{2.41}$$

$$\nabla \times \vec{H} = \vec{j} \quad . \tag{2.42}$$

In dielectrics

$$\rho_e = 0 \quad , \qquad \vec{j} = 0 \tag{2.43}$$

and

$$\vec{M} = 0 \quad . \tag{2.44}$$

Hence,

$$\nabla \times \vec{B} = 0 \quad . \tag{2.45}$$

Therefore in these circumstances the magnetic field $\vec{B}$ is not coupled to either the acoustic or electric fields. $\vec{B}$ represents only an applied magnetic field. However, in piezoelectric studies a magnetic field is generally not applied, the magnetostriction is not involved and as a consequence

$$\vec{B} = 0 \quad . \tag{2.46}$$

Under these conditions, the electric field in a piezoelectric solid can be considered to be an electrostatic field, i.e.

$$\vec{E} = -\nabla\phi \quad , \tag{2.47}$$

where ϕ is the electric scale potential. This is called the quasi-electrostatic approximation so that the piezoelectrically generated electric field is a quasi-electrostatic field.

In the piezoelectric problems with which we are concerned, the quasi-electrostatic approximation always holds. By taking a quasi-electrostatic approximation, Maxwell's

field equations for piezoelectric dielectrics are reduced (in the material representation) to the form:

$$\nabla_a \times \vec{\mathrm{E}} = 0 \quad , \tag{2.48}$$

$$\vec{\mathrm{E}} = -\nabla_a \phi \quad , \tag{2.49}$$

$$\frac{\partial \vec{\mathrm{D}}}{\partial t} = 0 \quad , \tag{2.50}$$

$$\nabla_a \cdot \vec{\mathrm{D}} = 0 \quad , \tag{2.51}$$

with

$$\mathrm{D}_j = \varepsilon_0 J \frac{\partial a_i}{\partial x_j} \frac{\partial a_k}{\partial x_j} \mathrm{E}_k + \mathrm{P}_j \quad . \tag{2.52}$$

If a electromagnetic field does exist, an additional stress tensor, called the Maxwell stress, is imposed on piezoelectric crystals. The Maxwell stress tensor m_{ij} is defined (Toupin 1963, Nelson 1979) as

$$m_{ij} \equiv \varepsilon_0 E_i E_j + \frac{1}{\mu_0} B_i B_j - \frac{1}{2}\left(\varepsilon_0 E_k E_k + \frac{1}{\mu_0} B_k B_k \right) \delta_{ij} = m_{ji} \quad . \tag{2.53}$$

In the quasi-electrostatic approximation, the tensor is reduced to

$$m_{ij} \equiv \varepsilon_0 E_i E_j - \frac{1}{2} \varepsilon_0 E_k E_k \delta_{ij} = m_{ji} \quad . \tag{2.54}$$

By using the transformation equation (2.27) the Maxwell stress tensor can be expressed in terms of the electric field in material frame and denoted by roman letter m_{ij}:

$$\mathrm{m}_{ij} = \varepsilon_0 \mathrm{E}_i \mathrm{E}_j \frac{\partial a_i}{\partial x_m} \frac{\partial a_j}{\partial x_n} - \frac{1}{2} \varepsilon_0 \mathrm{E}_k \mathrm{E}_k \delta_{ij} \frac{\partial a_k}{\partial x_l} \frac{\partial a_k}{\partial x_l} \quad . \tag{2.55}$$

2.4 The nonlinear form of the constitutive relations

In order to concentrate on the elastic and electric properties of piezoelectric crystals, thermal effects are not considered. The piezoelectric constitutive relations can be derived by defining the appropriate thermodynamic functions for piezoelectric solids. Consider the thermodynamic function per unit mass $\Phi(S, \eta_{ij}, \mathrm{E}_k)$, where S is the entropy per unit mass. The thermodynamic tension and electric displacement components in the material frame are defined as

$$\frac{1}{\rho_0} t_{ij} = \left(\frac{\partial \Phi}{\partial \eta_{ij}} \right)_{S,\mathrm{E}} , \qquad -\frac{1}{\rho_0} D_k = \left(\frac{\partial \Phi}{\partial \mathrm{E}_k} \right)_{S,\eta} . \tag{2.56}$$

The constitutive relations in the material frame can be written as follows:

$$t_{ij} = C_{ijlm}^{S,\mathrm{E}} \eta_{lm} - e_{kij} \mathrm{E}_k , \tag{2.57}$$

$$\mathrm{D}_k = \varepsilon_{ki}^{\eta} \mathrm{E}_i + e_{kij} \eta_{ij} . \tag{2.58}$$

Similarly, another pair of the constitutive relations can be obtained:

$$\eta_{ij} = s_{ijlm}^{S,\mathrm{E}} t_{lm} + d_{kij} \mathrm{E}_k , \tag{2.59}$$

$$\mathrm{D}_k = \varepsilon_{ki}^{t} \mathrm{E}_i + d_{kij} t_{ij} , \tag{2.60}$$

where $C_{ijlm}^{S,\mathrm{E}}$ are the second order isentropic thermodynamic elastic stiffness (SOEC) at zero electric field, e_{ijk} the second order piezoelectric coefficients (SOPC), ε_{ki}^{η} the dielectric constants at zero strain, ε_{ki}^{t} the dielectric constants at zero stress, d_{kij} the second order converse piezoelectric coefficients (or the piezoelectric strain coefficients), $s_{ijlm}^{S,\mathrm{E}}$ the isentropic elastic compliances at zero electric field.

In practical cases, the response of solids to external actions are nonlinear and it is necessary to look for relations in a nonlinear form. When discussing nonlinear properties of piezoelectric crystals, in addition to the nonlinear elastic, piezoelectric and dielectric properties, the electrostriction is also involved. The electrostrictive effect is a universal

property of dielectrics and independent of the direction of the electric field. The electrostrictive strain is proportional to the square of the electric field intensity and occurs simultaneously with the piezoelectric effect. Unlike piezoelectric effects, the electrostriction has no particular requirement on the internal structure of materials. The piezoelectric strain is usually larger by several orders of magnitude than the electrostrictive strain (Bottom 1982). Therefore, the introduction of the electrostrictive coefficients arises only from the consideration of the nonlinear deformation. Electrostriction comes from two contributions: one is from the dependence of the dielectric coefficients on strain and the other is from the Maxwell stress (Nelson 1979). The stress caused by the electrostrictive effects can be written as:

$$\tau_{ij} = -\frac{1}{2} l_{khij} \mathrm{E}_k \mathrm{E}_h \quad , \tag{2.61}$$

where l_{khij} is the electrostrictive tensor and is defined as (Nelson 1978)

$$l_{khij} \equiv l^r_{khij} - \varepsilon_0(\delta_{ik}\delta_{jh} + \delta_{ih}\delta_{jk} - \delta_{kh}\delta_{ij}) \quad , \tag{2.62}$$

with l^r_{khij} being the relative electrostrictive coefficient (Nelson 1978) which is the inherent part of substances.

By using Brugger's definition (1964) for the higher order elastic coefficients to piezoelectric materials, the elastic, electric and piezoelectric coefficients to third order can be defined as follows:

the isentropic thermodynamic elastic stiffness at zero electric field

$$C^{S,\mathrm{E}}_{ijlmpq} = \rho_0 \left(\frac{\partial^3 \Phi}{\partial \eta_{ij} \partial \eta_{lm} \partial \eta_{pq}} \right)_{S,\mathrm{E}} = \left(\frac{\partial^2 t_{ij}}{\partial \eta_{lm} \partial \eta_{pq}} \right)_{S,\mathrm{E}} \quad , \tag{2.63}$$

the piezoelectric coefficients

$$e_{kijlm} = -\rho_0 \left(\frac{\partial^3 \Phi}{\partial \mathrm{E}_k \partial \eta_{ij} \partial \eta_{lm}} \right)_S = \left(\frac{\partial^2 \mathrm{D}_k}{\partial \eta_{ij} \partial \eta_{lm}} \right)_S \quad , \tag{2.64}$$

the dielectric coefficients at zero strain

$$\varepsilon^{\eta}_{khn} = -\rho_0\left(\frac{\partial^3\Phi}{\partial E_k \partial E_h \partial E_n}\right)_{S,\eta} = \left(\frac{\partial^2 D_k}{\partial E_h \partial E_n}\right)_{S,\eta} \quad , \tag{2.65}$$

and the electrostrictive coefficients

$$l_{khij} = -\rho_0\left(\frac{\partial^3\Phi}{\partial E_k \partial E_h \partial \eta_{ij}}\right)_{S} = \left(\frac{\partial^2 D_k}{\partial E_h \partial \eta_{ij}}\right)_{S} \quad . \tag{2.66}$$

By using the above definitions, the potential function Φ for the electromechanical interaction of a piezoelectric system can then be written to third order as (Nakagawa et al. 1973, Gagnepain and Besson 1975, Maugin 1985, Kittinger et al. 1986)

$$\begin{aligned}\rho_0\Phi(S,\ \eta,\ E) - \rho_0\Phi(S,\ 0,\ 0) = &\frac{1}{2}C^{S,E}_{ijlm}\eta_{ij}\eta_{lm} + \frac{1}{6}C^{S,E}_{ijlmpq}\eta_{ij}\eta_{lm}\eta_{pq} - e_{kij}\eta_{ij}E_k \\ &-\frac{1}{2}e_{k,ijlm}E_k\eta_{ij}\eta_{lm} - \frac{1}{2}l_{khij}\eta_{ij}E_kE_h \\ &-\frac{1}{2}\varepsilon^{\eta}_{kh}E_kE_h - \frac{1}{6}\varepsilon^{\eta}_{khg}E_kE_hE_g \quad .\end{aligned} \tag{2.67}$$

The third order coefficients satisfy the following symmetry relations:

$$C_{ijlmpq} = C_{jimlqp} = C_{lmijpq} = C_{ijpqlm} \quad , \quad etc. \quad , \tag{2.68}$$

$$e_{kijlm} = e_{kjilm} = e_{kijml} = e_{klmij} \quad , \quad etc. \quad , \tag{2.69}$$

$$\varepsilon^{\eta}_{khn} = \varepsilon^{\eta}_{hkn} = \varepsilon^{\eta}_{knh} = \varepsilon^{\eta}_{nkh} = \varepsilon^{\eta}_{hnk} = \varepsilon^{\eta}_{nhk} \quad , \tag{2.70}$$

$$l_{khij} = l_{hkij} = l_{khji} \quad . \tag{2.71}$$

By using the definition (2.56), the nonlinear form of the piezoelectric constitutive relations to third order can then be written as:

$$t_{ij} = C^{S,E}_{ijlm}\eta_{lm} - e_{kij}E_k + \frac{1}{2}C^{S,E}_{ijlmpq}\eta_{lm}\eta_{pq} - \frac{1}{2}l_{khij}E_kE_h - e_{kijlm}\eta_{lm}E_k \quad , \tag{2.72}$$

$$D_k = \varepsilon^{\eta}_{kh}E_h + e_{kij}\eta_{ij} + \frac{1}{2}\varepsilon^{\eta}_{khg}E_hE_g + l_{khij}E_h\eta_{ij} + \frac{1}{2}e_{kijlm}\eta_{ij}\eta_{lm} \quad . \tag{2.73}$$

Another pair of piezoelectric constitutive relations can be written as

$$\eta_{ij} = s^{T,E}_{ijkm} t_{km} + d^{T}_{lij} E_l + \frac{1}{2} s^{T,E}_{ijkmpq} t_{km} t_{pq} + \frac{1}{2} \lambda_{lhij} E_l E_h + d^{T}_{lijkm} t_{km} E_l \quad , \tag{2.74}$$

$$D_k = \varepsilon^{t}_{kh} E_h + d^{T}_{kij} t_{ij} + \frac{1}{2} \varepsilon^{t}_{khg} E_h E_g + \lambda_{khij} E_h t_{ij} + \frac{1}{2} d^{T}_{kijlm} t_{ij} t_{lm} \quad , \tag{2.75}$$

where

$$d^{T}_{lijkm} = \left(\frac{\partial^2 D_l}{\partial t_{ij} t_{km}} \right)_T \tag{2.76}$$

are the converse piezoelectric coefficients (or the piezoelectric strain coefficients) and

$$\lambda_{lhij} = \left(\frac{\partial D^2_l}{\partial E_h \partial t_{ij}} \right)_T \tag{2.77}$$

are the converse electrostrictive coefficients.

Using Voigt's notation, the tensor form of the coefficients can be transformed into the matrix form. The transformation is shown below:

Tensor	11	22	33	23,32	13,31	12,21
Matrix	1	2	3	4	5	6

For instance, the transformations of the second order coefficients are as follows:

$$C_{\alpha\beta} \sim C_{ijlm} \quad ; \quad s_{\alpha\beta} \sim 2^{p} s_{ijkl} \quad , \quad p = \begin{cases} 0, & \alpha \text{ and } \beta \le 3 \quad , \\ 1, & \alpha \text{ or } \beta > 3 \quad , \\ 2, & \alpha \text{ and } \beta > 3 \quad ; \end{cases} \tag{2.78}$$

and

$$e_{i\alpha} \sim e_{ijk} \quad ; \quad d_{i\alpha} \sim \begin{cases} d_{ijk}, & \alpha \le 3 \quad , \\ 2d_{ijk}, & \alpha > 3 \quad ; \end{cases} \tag{2.79}$$

where $i, \ j = 1, \ 2, \ 3$, and $\alpha, \ \beta = 1, \ldots 6$. The transformations of the third order coefficients to Voigt's notation are as follows:

$$C_{IJK} \sim C_{ijlmpq} \quad ; \quad e_{kIJ} \sim e_{kijlm} \quad . \tag{2.80}$$

The symmetry relations (2.68) and (2.69) become

$$C_{IJK} = C_{JIK} = C_{IKJ} = C_{KIJ} \quad , \tag{2.81}$$

$$e_{kIJ} = e_{kJI} \quad . \tag{2.82}$$

Although electrostriction is a nonlinear phenomenon, the coefficients in Voigt's notation are conventionally written in the form with two subscripts (Nakagawa et al. 1973, Cho and Yamanouchi 1987, Adam et al. 1988, Hruska and Brendel 1990), i.e.

$$l_{khij} \sim l_{IJ} \quad . \tag{2.83}$$

But

$$l_{IJ} \neq l_{JI} \quad . \tag{2.84}$$

2.5 Determination of the third order elastic constants from ultrasonic measurements

2.5.1 Linearization of the equations of wave motion

The determination of the nonlinear coefficients involves measurements of interactions between strain fields and electric fields in piezoelectric solids. The interaction is represented by the electric field term in the equation of wave motion and the strain term in Maxwell's electric field equations.

In the spatial frame, the equations of motion are

$$\rho \ddot{x}_j = \frac{\partial \sigma_{kj}}{\partial x_k} \quad . \tag{2.85}$$

By substituting Eq. (2.17) into the above equation, denoting

$$P_{jp} = \left(\frac{\partial x_j}{\partial a_q} \right) t_{pq} \quad , \tag{2.86}$$

which is called the Piola-Kirchhoff stress tensor (Truesdell and Toupin 1960), and then using the identity (Thurston and Brugger 1964)

$$\frac{\partial}{\partial x_k}\left(\frac{1}{J}\frac{\partial x_k}{\partial a_p}\right)\equiv 0 \quad , \tag{2.87}$$

the equations of motion (2.85) become:

$$\rho\ddot{x}_j = \frac{1}{J}\frac{\partial P_{jp}}{\partial a_p} \quad , \tag{2.88}$$

or

$$\rho_0\ddot{x}_j = \frac{\partial P_{jp}}{\partial a_p} \quad . \tag{2.89}$$

To obtain the linearized equations of wave motion, P_{jp} can be expanded to the first order about the initial state of coordinates X_i and the electric potential ϕ, denoting the initial values by a tilde " ~ " above the symbols,

$$P_{jp} - \tilde{P}_{jp} = \left(\frac{\partial P_{jp}}{\partial(\partial x_k/\partial a_m)}\right)_{X,S}\left(\frac{\partial x_k}{\partial a_m} - \frac{\partial X_k}{\partial a_m}\right) + \left(\frac{\partial P_{jp}}{\partial(\partial\phi/\partial a_m)}\right)_{\tilde{\phi},S}\left(\frac{\partial\phi}{\partial a_m} - \frac{\partial\tilde{\phi}}{\partial a_m}\right)$$

$$= \tilde{A}^{S,E}_{jkpm}\frac{\partial u_k}{\partial a_m} + \tilde{A}^{S,\eta}_{jpm}\frac{\partial\phi'}{\partial a_m} \quad , \tag{2.90}$$

where

$$\tilde{A}^{S,E}_{jkpm} = \left(\frac{\partial P_{jp}}{\partial(\partial x_k/\partial a_m)}\right)_{X,S} \quad , \tag{2.91}$$

$$\tilde{A}^{S,\eta}_{jpm} = \left(\frac{\partial P_{jp}}{\partial(\partial\phi/\partial a_m)}\right)_{\tilde{\phi},S} \quad , \tag{2.92}$$

and

$$\phi' = \phi - \tilde{\phi} \quad . \tag{2.93}$$

Similarly, the components of the electric displacement D_p can be expanded to the first order about the initial state of coordinates X_i and the electric potential ϕ as follows:

$$\mathrm{D}_p - \tilde{\mathrm{D}}_p = \left(\frac{\partial \mathrm{D}_p}{\partial(\partial x_k/\partial a_m)}\right)_{X,S}\left(\frac{\partial x_k}{\partial a_m} - \frac{\partial X_k}{\partial a_m}\right) + \left(\frac{\partial \mathrm{D}_p}{\partial(\partial\phi/\partial a_m)}\right)_{\tilde{\phi},S}\left(\frac{\partial\phi}{\partial a_m} - \frac{\partial\tilde{\phi}}{\partial a_m}\right)$$

$$= \tilde{B}^{S,E}_{pkm}\frac{\partial u_k}{\partial a_m} + \tilde{B}^{S,\eta}_{pm}\frac{\partial\phi'}{\partial a_m} \quad , \tag{2.94}$$

where

$$\tilde{B}^{S,\mathrm{E}}_{pkm} = \left(\frac{\partial \mathrm{D}_p}{\partial(\partial x_k/\partial a_m)}\right)_{X,S} \quad , \tag{2.95}$$

$$\tilde{B}^{S,\eta}_{pm} = \left(\frac{\partial \mathrm{D}_p}{\partial(\partial\phi/\partial a_m)}\right)_{\tilde{\phi},S} \quad . \tag{2.96}$$

At an arbitrary stressed state, there exists the relation (Thurston and Brugger 1964)

$$\frac{\partial\eta_{ij}}{\partial(\partial x_k/\partial a_m)} = \frac{1}{2}\left(\frac{\partial x_k}{\partial a_j}\delta_{mi} + \frac{\partial x_k}{\partial a_i}\delta_{mj}\right) \quad . \tag{2.97}$$

With the help of Eq. (2.72), (2.73) and (2.97), the coefficients (2.91), (2.92), (2.95) and (2.96) can be expressed as:

$$A^{S,\mathrm{E}}_{jkpm} = \delta_{jk}t_{pm} + \frac{\partial x_j}{\partial a_q}\frac{\partial x_k}{\partial a_i}\left(\frac{\partial t_{pq}}{\partial\eta_{mi}}\right)_{S,\mathrm{E}} = \delta_{jk}t_{pm} + \frac{\partial x_j}{\partial a_q}\frac{\partial x_k}{\partial a_i}C'_{pqmi} \quad , \tag{2.98}$$

where

$$C'_{pqmi} = \left(\frac{\partial t_{pq}}{\partial\eta_{mi}}\right)_{S,\mathrm{E}} = C^{S,\mathrm{E}}_{pqmi} + C_{pqmirs}\eta_{rs} - e_{lpqmi}\mathrm{E}_l \tag{2.99}$$

$$A^{S,\eta}_{jpm} = \frac{\partial x_j}{\partial a_q}\frac{\partial t_{pq}}{\partial(\partial\phi/\partial a_m)} = \frac{\partial x_j}{\partial a_q}e'_{mpq} \quad , \tag{2.100}$$

where

$$e'_{mpq} = \frac{\partial t_{pq}}{\partial(\partial\phi/\partial a_m)} = -\frac{\partial t_{pq}}{\partial \mathrm{E}_m} = e_{mpq} + l_{mrpq}\mathrm{E}_r + e_{mpqrs}\eta_{rs} \quad ; \tag{2.101}$$

$$B^{S,\mathrm{E}}_{pkm} = \frac{\partial \mathrm{D}_p}{\partial\eta_{mi}}\left(\frac{\partial\eta_{mi}}{\partial(\partial x_k/\partial a_m)}\right) = \frac{\partial x_k}{\partial a_i}\frac{\partial \mathrm{D}_p}{\partial\eta_{mi}} = \frac{\partial x_k}{\partial a_i}e'_{pmi} \quad , \tag{2.102}$$

where

$$e'_{pmi} = \frac{\partial D_p}{\partial \eta_{mi}} = e_{pmi} + l_{prmi} E_r + e_{pmirs} \eta_{rs} \quad ; \tag{2.103}$$

and

$$B^{S,\eta}_{pm} = \frac{\partial D_p}{\partial(\partial\phi/\partial a_m)} = -\frac{\partial D_p}{\partial E_m} = -\varepsilon'_{pm} \quad , \tag{2.104}$$

where

$$\varepsilon'_{pm} = \frac{\partial D_p}{\partial E_m} = \varepsilon^{\eta}_{pm} + \varepsilon^{\eta}_{pmr} E_r + l_{pmrs} \eta_{rs} \quad . \tag{2.105}$$

Comparing Eq. (2.100) with Eq. (2.102) it follows that

$$A^{S,\eta}_{jpm} = B^{S,E}_{jpm} \quad . \tag{2.106}$$

From the above discussion, and maintaining the first order of the particle displacement and the increment of the electric potential, the linearized equations for the elastic wave motion in the piezoelectric medium for u_j and ϕ' are obtained in the form:

$$\rho_0 \ddot{u}_j = \tilde{A}^{S,E}_{jkpm} \frac{\partial^2 u_k}{\partial a_p \partial a_m} + \tilde{A}^{S,\eta}_{jpm} \frac{\partial^2 \phi'}{\partial a_p \partial a_m} \quad . \tag{2.107}$$

Substituting Eq.(2.94) into Eq.(2.51), we obtain

$$\tilde{B}^{S,E}_{pkm} \frac{\partial^2 u_k}{\partial a_p \partial a_m} + \tilde{B}^{S,\eta}_{pm} \frac{\partial^2 \phi'}{\partial a_p \partial a_m} = 0 \quad . \tag{2.108}$$

2.5.2 Eigenequations and eigenvalues of wave motion

Assume that the displacement $\vec{u}$ and the increment ϕ' of the electrical potential ϕ are in the form of plane sinusoidal waves:

$$u_j = A_j \exp\left[j\omega \left(t - N_i \frac{a_i}{W} \right) \right] \quad , \tag{2.109}$$

$$\phi' = \phi'_0 \exp\left[j\omega\left(t - N_i \frac{a_i}{W} \right)\right] \quad , \tag{2.110}$$

where N_i is the ith component of the direction vector of the wave propagation described in the material frame and W is the natural velocity defined by Thurston and Brugger (1964)

$$W = 2l_0 f \quad . \tag{2.111}$$

Here l_0 is the transit length of the wave and f is the measured frequency of the round-trips of the wave in the sample. Substituting Eq.(2.109) and (2.110) into Eq.(2.107) and (2.108) gives

$$\rho_0 W^2 u_j = (\bar{A}^{S,E}_{jkpm} u_k + \bar{A}^{S,\eta}_{jpm}\phi')N_p N_m \quad , \tag{2.112}$$

and

$$\bar{B}^{S,E}_{pkm} u_k N_p N_m + \bar{B}^{S,\eta}_{pm}\phi' N_p N_m = 0 \quad . \tag{2.113}$$

By deleting the electrical potential ϕ' from the above two equations and considering the relation Eq. (2.106), it is found that

$$\rho_0 W^2 u_j = \bar{C}_{jkpm} N_p N_m u_k \quad , \tag{2.114}$$

where

$$\bar{C}_{jkpm} = \bar{A}^{S,E}_{jkpm} + \frac{\bar{B}^{S,E}_{njk} N_n \bar{B}^{S,E}_{lpm} N_l}{(-\bar{B}^{S,\eta}_{nl} N_n N_l)} \quad . \tag{2.115}$$

The direction vector of the particle displacement $\vec{u}$ can be transformed to the natural, undeformed direction of the material line with the direction vector of the particle displacement $\vec{U}$ in the material frame by using Thurston and Brugger's method (Thurston and Brugger 1964). Then Eq. (2.114) can be written as:

$$\rho_0 W^2 U_j = w_{jk} U_k \quad , \tag{2.116}$$

$\rho_0 W^2$ and $\overrightarrow{U}$ are the eigenfunction and the eigenvector of the equation (2.116) respectively. w_{jk} is:

$$w_{jk} = N_r N_s \tilde{A}^{S,E}_{jrks} + \frac{\tilde{B}^{S,E}_{njr} N_n N_r \tilde{B}^{S,E}_{lks} N_l N_s}{(-\tilde{B}^{S,\eta}_{nl} N_n N_l)} \quad , \tag{2.117}$$

and from Eq. (2.98)-Eq. (2.105) it can be shown that

$$w_{jk} = N_r N_s \left[\delta_{jk} f_{rs} + \tilde{C}_{jk} \left(\tilde{C}'_{jrks} + \frac{\tilde{e}'_{njr} N_n \tilde{e}'_{lks} N_l}{\tilde{\varepsilon}'_{nl} N_n N_l} \right) \right] \quad , \tag{2.118}$$

where

$$\tilde{C}_{jk} = \frac{\partial X_i}{\partial a_j} \frac{\partial X_i}{\partial a_k} = (\delta_{jk} + 2\tilde{\eta}_{jk}) \quad . \tag{2.119}$$

When the initial state is a natural state, i.e. $P \to 0, \quad \vec{E} \to 0,$

$$w_{jk}(0) = N_r N_s C^{st}_{jrks} \quad , \tag{2.120}$$

where

$$C^{st}_{jrks} = C^{S,E}_{jrks} + \frac{e_{njr} N_n e_{lks} N_l}{\varepsilon_{nl} N_n N_l} \quad , \tag{2.122}$$

are called the "stiffened" elastic coefficients (Dieulesaint and Royer 1980).

Let $\overrightarrow{U}^0$ be the eigenvector and w the eigenvalue of Eq.(2.116) at the initial state of the equation, i.e.,

$$w = (\rho_0 W^2)_{P=0} = (\rho v^2)_{P=0} \quad . \tag{2.122}$$

From Eq.(2.116) it follows that

$$w_{jk}(0) U^0_j = w U^0_k \quad . \tag{2.123}$$

2.5.3 The pressure derivatives of $\rho_0 W^2$

In this section the variation of the natural velocity of sound waves under an applied static stress with zero electric field is discussed in the material configuration. The results obtained can then be used to determine the TOEC coupled with other nonlinear coefficients by using the data from ultrasonic measurements.

By defining

$$(\rho_0 W^2)' = \left(\frac{\partial(\rho_0 W^2)}{\partial P} \right)_T \quad , \tag{2.124}$$

the pressure derivative of Eq. (2.116) at constant temperature can be written as

$$(\rho_0 W^2)' U_j + \rho_0 W^2 U_j' = w_{jk}' U_k + w_{jk} U_k' \quad . \tag{2.125}$$

Since

$$\vec{U} \cdot \vec{U} = 1 \quad , \qquad \text{and} \qquad \vec{U} \cdot \vec{U}' = 0 \quad , \tag{2.126}$$

Eq. (2.125) reduces to

$$(\rho_0 W^2)' = U_j w_{jk}' U_k + U_j w_{jk} U_k' \quad . \tag{2.127}$$

When P approaches zero,

$$(\rho_0 W^2)'_{P=0} = (U_j w_{jk}' U_k)_{P=0} \quad . \tag{2.128}$$

This pressure derivative can be transformed to the partial differential with respect to the Lagrangian strain in the form

$$\left(\frac{\partial}{\partial P} \right)_T = \left(\frac{\partial t_{km}}{\partial P} \right)_T \left(\frac{\partial \eta_{ij}}{\partial t_{km}} \right)_T \left(\frac{\partial}{\partial \eta_{ij}} \right)_T \quad . \tag{2.129}$$

By differentiating Eq.(2.74) we obtain

$$\left(\frac{\partial \eta_{ij}}{\partial t_{km}} \right)_T = s^{T,E}_{ijkm} + s^{T,\mathrm{E}}_{ijkmpq} t_{pq} + d^T_{lijkm} \mathrm{E}_l = s'_{ijkm} \quad . \tag{2.130}$$

and therefore the transformation Eq.(2.130) becomes

$$\left(\frac{\partial}{\partial P} \right)_T = t_{km}' s'_{ijkm} \left(\frac{\partial}{\partial \eta_{ij}} \right)_T \quad , \tag{2.131}$$

where

$$t_{km}{}' = \left(\frac{\partial t_{km}}{\partial P}\right)_T \quad . \tag{2.132}$$

When P and $\vec{E} = 0$ at the initial state, the pressure derivative $w_{jk}{}'$ of Eq. (2.118) is

$$w_{jk}{}'(0) = N_r N_s \{\delta_{jk} t_{rs}{}'(0) + t_{ab}{}'(0) s^{T,E}_{jkab} [2\left(C^{S,E}_{jrks} + \frac{e_{njr} N_n e_{lks} N_l}{\varepsilon_{nl} N_n N_l}\right)$$

$$+ C_{jrksip} + \frac{e_{njrip} N_n e_{lks} N_l}{\varepsilon^{\eta}_{nl} N_n N_l} + \frac{e_{njr} N_n e_{lksip} N_l}{\varepsilon^{\eta}_{nl} N_n N_l}$$

$$- \frac{e_{njr} N_n e_{lks} N_l}{(\varepsilon^{\eta}_{nl} N_n N_l)^2} l_{nlip} N_n N_l]\} \quad , \tag{2.133}$$

with

$$\left(\frac{\partial \tilde{C}_{qk}}{\partial \eta_{ip}}\right)_{T,P=0} = 2 \quad , \qquad (\tilde{C}_{qk})_{P=0} = 1 \tag{2.134}$$

and

$$C_{jrksip} = \left(\frac{\partial C^{S,E}_{jrks}}{\partial \eta_{ip}}\right)_T \quad . \tag{2.135}$$

Let F_{U^0} be the eigenfunction of eigenvector $\vec{U}^0$ as P approaching to zero and $\vec{E} = 0$, then

$$F^0_{qk} U^0_k = F_{U^0} U^0_q \quad , \tag{2.136}$$

with the definition

$$F^0_{qk} = \left(\frac{\partial \eta_{qk}}{\partial P}\right)_{P=0} = s^{T,E}_{qkab} t_{ab}{}'(0) \quad . \tag{2.137}$$

Substituting Eq.(2.133) into Eq.(2.128) and considering the above relations and definitions gives

$$(\rho_0 W^2)'_{P=0} = 2w F_{U^0} + N_r N_s (t_{ab}{}'(0) + t_{ab}{}'(0) s^{T,E}_{jkab} C_{jrksip}$$

$$+ t_{ab}{}'(0) s^{T,E}_{jkab} C^{e}_{jrksip}) U_j U_k \tag{2.138}$$

where C^{e}_{jrksip} is the quantity containing the piezoelectric coefficients

$$C^{e}_{jrksip} = \frac{e_{njrip}N_n e_{lks}N_l}{\varepsilon^{\eta}_{nl}N_nN_l} + \frac{e_{njr}N_n e_{lksip}N_l}{\varepsilon^{\eta}_{nl}N_nN_l} - \frac{e_{njr}N_n e_{lks}N_l}{(\varepsilon^{\eta}_{nl}N_nN_l)^2} l_{nlip}N_nN_l \quad . \tag{2.129}$$

From Eq.(2.17) the thermal stress can be expressed as

$$t_{rs} = J\frac{\partial a_r}{\partial X_k}\frac{\partial a_s}{\partial X_j}\sigma_{kj} \quad . \tag{2.140}$$

For hydrostatic pressures

$$\sigma_{kj} = -P\delta_{kj} \quad , \tag{2.141}$$

and hence,

$$t_{rs}'(0) = -\delta_{rs} \quad , \tag{2.142}$$

and

$$N_rN_st_{rs}'(0) = -1 \quad . \tag{2.143}$$

For uniaxial compression in the direction of a unit vector $\vec{M}$

$$\sigma_{kj} = -\sigma M_kM_j = -P\left(\frac{A_0}{A}\right)M_kM_j \quad , \tag{2.144}$$

where σ is the actual magnitude of the compressing stress on the area A and P is the compressing force per unit of original area A_0. Hence,

$$t_{rs}'(0) = -M_rM_s \quad , \tag{2.145}$$

and

$$N_rN_st_{rs}'(0) = -(\vec{N}\cdot\vec{M})^2 \quad . \tag{2.146}$$

2.5.4 Determination of the TOEC

To summarize, the pressure derivatives of ρ_0W^2 referred to the natural state when P approaches zero and $E = 0$, obtained from velocity measurements of ultrasonic waves

under hydrostatic pressure and uniaxial compression, are written as follows:

A. For hydrostatic pressure experiments:

$$(\rho_0 W^2)'_{P=0} = -1 - 2wF_H - G_H - H_H \tag{2.147}$$

with

$$w = C^{st}_{jrks} N_j N_k U_r U_s \quad , \tag{2.148}$$

$$F_H = s^{T,E}_{aars} U_r U_s \quad , \tag{2.149}$$

$$G_H = s^{T,E}_{aauv} C_{uvjrks} N_j N_k U_r U_s \quad , \tag{2.150}$$

$$H_H = s^{T,E}_{aauv} C^{e}_{uvjrks} N_j N_k U_r U_s \quad . \tag{2.151}$$

Here

$$C^{st}_{jrks} = C^{S,E}_{jrks} + \frac{e_{njr} N_n e_{lks} N_l}{\varepsilon_{nl} N_n N_l} \tag{2.152}$$

and

$$C^{e}_{uvjrks} = \frac{e_{nuvjr} N_n e_{lks} N_l}{\varepsilon^{\eta}_{nl} N_n N_l} + \frac{e_{njr} N_n e_{luvks} N_l}{\varepsilon^{\eta}_{nl} N_n N_l} - \frac{e_{njr} N_n e_{lks} N_l}{(\varepsilon^{\eta}_{nl} N_n N_l)^2} l_{nluv} N_n N_l \quad . \tag{2.153}$$

B. For uniaxial compression

$$(\rho_0 W^2)'_{P=0} = -(\vec{N} \cdot \vec{M})^2 - 2wF_U - G_U - H_U \tag{2.154}$$

with

$$w = C^{st}_{jrks} N_j N_k U_r U_s \quad , \tag{2.155}$$

$$F_U = s^{T,E}_{abrs} M_a M_b U_r U_s \quad , \tag{2.156}$$

$$G_U = s^{T,E}_{abuv} C_{uvjrks} M_a M_b N_j N_k U_r U_s \quad , \tag{2.157}$$

$$H_U = s^{T,E}_{abuv} C^{e}_{uvjrks} M_a M_b N_j N_k U_r U_s \quad . \tag{2.158}$$

Here

$$C_{jrks}^{st} = C_{jrks}^{S,E} + \frac{e_{njr}N_n e_{lks}N_l}{\varepsilon_{nl}N_n N_l} \tag{2.159}$$

and

$$C_{uvjrks}^{e} = \frac{e_{nuvjr}N_n e_{lks}N_l}{\varepsilon_{nl}^{\eta}N_n N_l} + \frac{e_{njr}N_n e_{luvks}N_l}{\varepsilon_{nl}^{\eta}N_n N_l} - \frac{e_{njr}N_n e_{lks}N_l}{(\varepsilon_{nl}^{\eta}N_n N_l)^2} l_{nluv}N_n N_l \quad . \tag{2.160}$$

2.6 The hydrostatic pressure derivatives of $C_{IJ}^{S,E}$

One advantage of using the natural velocity is that $(\rho_0 W^2)'_{P=0}$ is directly related to the initial slope and intercept of the measured frequency versus pressure curve of ultrasonic measurements:

$$(\rho_0 W^2)'_{P=0} = 2\rho_0 v_0^2 \frac{f'}{f_0} \quad , \tag{2.161}$$

where f' is the pressure derivative of the measured frequency. To relate the pressure derivatives of ρv^2 to the measured frequency data and the elastic coefficients, Thurston (1965a) derived an equation given by:

$$[(\rho v^2)' - (\rho_0 W^2)']_{P=0} = \rho_0 v_0^2 (s_{kkii}^T - 2N_k N_m s_{kmii}^T)_{P=0} \quad . \tag{2.162}$$

By combining Eq. (2.162) with Eq. (2.161) and noting that

$$s_{kkii}^T = \chi^T, \tag{2.163}$$

the following is obtained that

$$(\rho v^2)'_{P=0} = \rho_0 v_0^2 \left(\frac{2f'}{f_0} + \chi^T - 2N_k N_m s_{kmii}^T \right)_{P=0} \quad . \tag{2.164}$$

where χ^T is the isothermal volume compressibility.

In calculations of the pressure derivatives of the elastic constants, it is necessary to distinguish between the effective and thermodynamic elastic constants. Thurston (1965b) has given definitions for the effective elastic constants and their differences

from the thermodynamic ones. Under zero pressure, there are not significant differences between the absolute values of the two types of constants, but their pressure derivatives could be considerably different (Tu Hailin 1983). The general relations between effective and thermodynamic elastic constants are (Thurston 1965a):

$$C_{ijkm}^{ef} = \tilde{P}(\delta_{ij}\delta_{km} - \delta_{im}\delta_{jk} - \delta_{ik}\delta_{jm}) + \frac{\tilde{\rho}}{\rho_0}\frac{\partial X_i}{\partial a_p}\frac{\partial X_j}{\partial a_q}\frac{\partial X_k}{\partial a_r}\frac{\partial X_m}{\partial a_s}C_{ijkm}^{S,E} \quad . \tag{2.165}$$

Here $\tilde{P}$ and $\tilde{\rho}$ are the pressure and density at an initial state. From Eq.(2.165), it can be seen that at zero pressure the C_{ijkm}^{ef} are equal to the thermodynamic SOEC tensors $C_{ijkm}^{S,E}$.

The hydrostatic pressure derivatives of the thermodynamic "stiffened" elastic constants at zero pressure can be defined as

$$B_{jrks}^{st} \equiv \left(\frac{\partial C_{jrks}^{st}}{\partial P}\right)_T = \left(\frac{\partial C_{jrks}^{S,E}}{\partial P}\right)_T + \left[\partial\left(\frac{e_{njr}N_n e_{lks}N_l}{\varepsilon_{nl}N_n N_l}\right)/\partial P\right]_T$$

$$= B_{jrks} + \left[\partial\left(\frac{e_{njr}N_n e_{lks}N_l}{\varepsilon_{nl}N_n N_l}\right)/\partial P\right]_T \quad , \tag{2.166}$$

where

$$B_{jrks} = \left(\frac{\partial C_{jrks}^{S,E}}{\partial P}\right)_T \quad . \tag{2.167}$$

The pressure derivatives B_{jrks}^{st} can be related to the data from ultrasonic measurements by

$$2\rho_0 v_0^2 \frac{f'}{f_0} = (\rho_0 W^2)'_{P=0} = -1 - (2wF_H - U_j^0 U_k^0 N_r N_s B_{jrks}^{st}) \tag{2.168}$$

where w and F_H are defined by Eq. (2.148) and (2.149). Let

$$B_H = U_j^0 U_k^0 N_r N_s B_{jrks}^{st} \quad , \tag{2.169}$$

then Eq. (2.168) can be written as

$$2\rho_0 v_0^2 \frac{f'}{f_0} = (\rho_0 W^2)'_{P=0} = -1 - (2wF_H - B_H) \quad . \tag{2.170}$$

The pressure derivatives of the effective elastic constants, as P approaches zero, can be related to the B_{ijkm} by (Thurston 1965a):

$$\left(\frac{\partial C^{ef}_{ijkm}}{\partial P}\right)_{P=0} = \delta_{ij}\delta_{km} - \delta_{im}\delta_{jk} - \delta_{ik}\delta_{jm} + B_{ijkm} + \chi^T C^{S,\mathrm{E}}_{ijkm}$$

$$-C^{S,\mathrm{E}}_{pjkm}S^{T,\mathrm{E}}_{tip} - C^{S,\mathrm{E}}_{iqkm}S^{T,\mathrm{E}}_{tjq} - C^{S,\mathrm{E}}_{ijrm}S^{T,\mathrm{E}}_{tkr} - C^{S,\mathrm{E}}_{iiks}S^{T,\mathrm{E}}_{ttms} \quad . \qquad (2.171)$$

Thurston (1965b) has computed the differences between B_{jrks} and $(\partial C^{ef}_{jrks}/\partial P)_T$ for several different symmetries of crystals but not for those which are monoclinic and triclinic. Hence, a general method for finding the zero pressure values of the pressure derivatives of the effective elastic constants is to calculate the B^{st}_{ijkm} from the measured f'/f_0 and to determine B_{jrks} . The derivatives $(\partial C^{ef}_{ijkm}/\partial P)_{T,P=0}$ of the effective elastic constants with respect to pressure in the zero pressure limit are then evaluated employing Eq. (2.171)

.

Chapter 3 Acoustic Mode Vibrational Anharmonicity and Grüneisen Parameters

3.1 Lattice vibrational anharmonicity

The lattice vibrations in solids are responsible for many properties of crystals, such as thermal expansion, specific heat of crystals, elasticity, thermal conductivity etc. In the quantum mechanical treatment of lattice dynamics the lattice vibrations are treated as quasi-particles called phonons which have quantum numbers n_s and quasi-momenta $\hbar\vec{q}$, where s specifies the vibrational mode and $\vec{q}$ its wavevector.

The study of lattice vibrations is based on a fundamental principle proposed by Born and Oppenheimer (1927) called the adiabatic approximation, by which the lattice potential can be defined. The lattice vibrational potential Φ of a crystal can be written as a function of the displacements of all atoms: $\Phi = \Phi\left(\cdots\vec{u}\begin{pmatrix} l \\ k \end{pmatrix}\cdots\right)$, where $\vec{u}\begin{pmatrix} l \\ k \end{pmatrix}$ is the displacement of the kth atom in the l th unit cell. The potential can be written, in the form of a power series, as:

$$\Phi = \Phi_0 + \sum_{lk\alpha}\Phi_\alpha\begin{pmatrix} l \\ k \end{pmatrix}u_\alpha\begin{pmatrix} l \\ k \end{pmatrix} + \frac{1}{2}\sum_{lk\alpha l'k'\beta}\Phi_{\alpha\beta}\begin{pmatrix} l\,l' \\ k\,k' \end{pmatrix}u_\alpha\begin{pmatrix} l \\ k \end{pmatrix}u_\beta\begin{pmatrix} l' \\ k' \end{pmatrix}$$
$$+\frac{1}{3!}\sum_{lk\alpha l'k'\beta l''k''\gamma}\Phi_{\alpha\beta\gamma}\begin{pmatrix} l\,l'\,l'' \\ k\,k'\,k'' \end{pmatrix}u_\alpha\begin{pmatrix} l \\ k \end{pmatrix}u_\beta\begin{pmatrix} l' \\ k' \end{pmatrix}u_\gamma\begin{pmatrix} l'' \\ k'' \end{pmatrix}+\cdots \quad , \tag{3.1}$$

where α, β and γ indicate the direction cosines of the displacement. Eq. (3.1) can be written as

$$\Phi = \Phi_0 + \Phi_1 + \Phi_2 + \Phi_3 + \cdots \quad . \tag{3.2}$$

In the harmonic approximation, the series in Eq. (3.1) is terminated at the quadratic term. As a consequence of this approximation, lattice vibrations are the collection of independent harmonic oscillators with 3N normal modes, where N is the number of atoms in a solid. In this harmonic approximation phonons act independently of each other. This approximation gives a very simple picture of lattice vibrations, but it also provides a considerable discrepancies from actual observations. Brüesch (1982) has listed some of the most important consequences of this approximation. The one related directly to the elastic properties of crystals is that the elastic constants are independent of both temperature and pressure. In real crystals, none of the consequences of the harmonic approximation is satisfied and temperature and pressure dependences of elastic constants have been observed. In other words, real crystals show anharmonicity in their lattice vibrations.

One of the approaches (Brüesch 1982) to study anharmonic effects in crystals is to separate the thermodynamic properties into quasiharmonic and explicitly anharmonic contributions. In the quasiharmonic approximation, the effect of the higher order terms $(\Phi_3 + \Phi_4 + \cdots)$ neglected by the harmonic approximation are, to a first approximation, taken into account by evaluating the second derivatives $\Phi_{\alpha\beta}$ in Eq.(3.1) at the mean positions which the atoms actually occupy at temperature T. The force constants, and thereby the phonon frequencies, are dependent only on temperature through the lattice dimensions, i.e. they are volume dependent. These volume-dependent phonon frequencies are then used within the framework of harmonic theory to obtain the quasi-harmonic frequency spectrum and the quasiharmonic values of the Helmholtz free energy F, the entropy S, the heat capacity at constant volume C_V and an equation of state. In this quasi-harmonic approximation, the phonons are still assumed to be independent although their frequencies are allowed to depend on volume. However, it does give a useful first approximation for the anharmonic effects on the spectra of lattice vibrations

and enables the deviations from quasiharmonic behaviour observed in crystals to be treated as perturbations of the basic harmonic problem. In cases where the anharmonicity is small enough to be treated as a perturbation, the Helmholtz free energy may be written as

$$F(V,T) = F^{qh} + F^{a} \quad , \tag{3.3}$$

where F^{qh} represents the quasiharmonic contribution and F^{a} represents the explicitly anharmonic contribution. The F^{a} is directly related to the high-order terms $\Phi_3 + \Phi_4 + \cdots$ in Eq.(3.2) and can be derived, in principle, if the interatomic potential is known (Leibfried and Ludwig, 1961).

3.2 Grüneisen parameters

According to statistical mechanics, the Helmholtz free energy of a crystal with phonon frequency ν_i can be written as (Born and Huang 1954)

$$F = U_0 + \sum_i \left\{ \frac{1}{2} h\nu_i + k_B T ln[1 - \exp(-h\nu_i / k_B T)] \right\} \quad , \tag{3.4}$$

where U_0 is the static lattice energy, k_B is the Boltzmann constant and the terms of $h\nu_i/2$ correspond to the zero-point energy due to the quantum mechanical uncertainty principle. From the thermodynamic relation

$$P = -\left(\frac{\partial F}{\partial V} \right)_T \tag{3.5}$$

and Eq.(3.4) an equation of state can be obtained:

$$P = -\frac{dU_0}{dV} + \frac{1}{V} \sum_i \gamma_i \left[\frac{1}{2} h\nu_i + \frac{h\nu_i}{\exp(h\nu_i / k_B T) - 1} \right] \quad , \tag{3.6}$$

where the dimensionless quantities γ_i are defined as

$$\gamma_i = -\frac{V}{\nu_i} \frac{d\nu_i}{dV} = -\frac{d(\ln \nu_i)}{d(\ln V)} \tag{3.7}$$

and are called the mode Grüneisen parameters of the crystals. The negative sign indicates that in normal circumstances the phonon frequencies decrease as the lattice expands. Hence, for the normal behaviour of phonons γ_i have positive values.

In the quasiharmonic approximation, the thermal Grüneisen parameter γ^h of a solid is expressed as the weighed average of the mode Grüneisen parameters γ_i (Slater 1939):

$$\gamma^h = \frac{\sum_i \gamma_i c_i}{\sum_i c_i} \quad , \tag{3.8}$$

where

$$c_i = k_B \left(\frac{h\nu_i}{k_B T} \right)^2 \frac{\exp(h\nu_i / k_B T)}{[\exp(h\nu_i / k_B T) - 1]^2} \tag{3.9}$$

is the Einstein specific heat (Slater 1939) associated with the mode i. c_i is a temperature dependent weighting factor for each γ_i and reflects the contribution of the ith mode to the heat capacity C_V. A thermodynamic expression for the thermal Grüneisen parameter can be obtained (Slater 1939, Reissland 1973) as:

$$\gamma^h = \frac{\alpha V B^T}{C_V} = \frac{\alpha V B^S}{C_P} \quad , \tag{3.10}$$

where α is the volume thermal expansion coefficient, B^T and B^S are the isothermal and isentropic bulk moduli, and C_V and C_P are the heat capacity at constant volume and under constant pressure respectively. Eq. (3.10) relates the Grüneisen parameter to measurable quantities, while Eq. (3.8) shows how it depends on the contributions from each phonon mode.

The relations of the mode Grüneisen parameters with thermal expansion can be obtained by introducing the thermal expansion tensors. The thermal expansion tensor α_{jk} at constant thermodynamic tension is defined by (Thurston 1964)

$$\alpha_{ij} = \left(\frac{\partial \eta_{ij}}{\partial T} \right)_t \quad . \tag{3.11}$$

In the quasiharmonic approximation, by using the free energy expression (3.4), Brugger and Fritz (1967) expressed the tensor components α_{im} as

$$\alpha_{im} = \sum_{jk} \sum_{p\vec{q}} s^T_{imjk} \gamma_{jk}(p,\vec{q}) c(p,\vec{q}) \quad , \tag{3.12}$$

where

$$\gamma_{jk}(p,\vec{q}) = -\left\{ \frac{1}{\omega(p,\vec{q})} \left[\frac{\partial \omega(p,\vec{q})}{\partial \eta_{jk}} \right]_T \right\}_{\eta=0} \tag{3.13}$$

are the generalized Grüneisen parameters (Brugger 1965a) and ω is the angular frequency of the phonons. Here, p (=1, 2, 3) is the index indicating the mode branch for different polarizations. The principal thermal expansion coefficient tensors α_{ii} are

$$\alpha_{ii} = \sum_{jk} \sum_{p\vec{q}} s^T_{iijk} \gamma_{jk}(p,\vec{q}) c(p,\vec{q}) \qquad (i = 1, 2, 3) \quad . \tag{3.14}$$

The volume thermal expansion coefficient α is related to the generalized Grüneisen parameters by

$$\alpha = \sum_i \alpha_{ii} = \sum_i \sum_{jk} \sum_{p\vec{q}} s^T_{iijk} \gamma_{jk}(p,\vec{q}) c(p,\vec{q}) \quad . \tag{3.15}$$

Eqs. (3.12) and (3.15) show how the Grüneisen gamma characterizes the quasiharmonic thermal expansion.

Since in the quasiharmonic approximation phonon frequencies change with temperature only through the lattice dimension, they are strain-dependent as shown in Eq. (3.13), which allows us to calculate the generalized Grüneisen parameter from the ultrasonically measured elastic constants. By using the standing wave condition of the Debye model, Brugger (1965) introduced the natural wave velocity W into the strain-dependent definition of the generalized Grüneisen parameter and derived the equations to calculate the generalised Grüneisen parameter $\gamma_{jk}(p,\vec{N})$ of nonpiezoelectric

materials from the second and third order elastic constants, where $\vec{N}$ is the unit vector along wave propagation direction. In the Debye model, where dispersion is neglected, the mode wave velocities depend only on their propagation directions. Eq. (3.13) can then be written as (Brugger 1965)

$$\gamma_{jk}(p,\vec{N}) = -\left\{ \frac{1}{2W(p,\vec{N})} \left[\frac{\partial \rho_0 W^2(p,\vec{N})}{\partial \eta_{jk}} \right]_T \right\}_{\eta=0} . \tag{3.18}$$

By using Brugger's method (1965) and following the procedures in section 2.5 the equations for the calculation of $\gamma_{jk}(p,\vec{N})$ for piezoelectric crystals can be obtained as follows:

$$\gamma_{jk}(p,\vec{N}) = -\frac{1}{2w(p,\vec{N})} \{ 2w(p,\vec{N}) U_j U_k + [C^T_{jkmn} + (C_{jkmuv} + C^e_{jkmuv}) U_u U_v] N_m N_n \} , \tag{3.17}$$

with

$$w(p,\vec{N}) = C^{st}_{muv} N_m N_n U_u U_v \tag{3.18}$$

and

$$C^e_{jkmuv} = \frac{e_{sjknv} N_s e_{lmu} N_l}{\varepsilon^\eta_{sl} N_s N_l} + \frac{e_{sjk} N_s e_{lmunv} N_l}{\varepsilon^\eta_{sl} N_s N_l} - l_{slnv} \frac{e_{sjk} N_s e_{lmu} N_l}{(\varepsilon^\eta_{sl} N_s N_l)^2} . \tag{3.19}$$

For the case where a volume change is produced by hydrostatic pressure P, Brugger (1965) introduced the generalized Grüneisen parameter defined by the volume derivative

$${}_H\gamma(p,\vec{q}) = \left\{ \frac{V}{\omega(p,\vec{q})} \left[\frac{\partial \omega(p,\vec{q})}{\partial V} \right]_T \right\}_{P=0} . \tag{3.20}$$

For piezoelectric crystals ${}_H\gamma(p,\vec{q})$ can be expressed as

$${}_H\gamma(p,\vec{N}) = -\frac{B^T}{2w(p,\vec{N})} \{ 1 + s^T_{aajk} [2w(p,\vec{N}) U_j U_k + (C_{jkmuv} + C^e_{jkmuv}) U_u U_v N_m N_n] \} , \tag{3.21}$$

or

$$ {}_H\gamma(p,\vec{N}) = -\frac{B^T}{2w(p,\vec{N})}[1 + 2s^T_{aajk} w(p,\vec{N}) U_j U_k - B^{st}_{jrks} U_j U_k N_r N_s] \quad . \qquad (3.22) $$

From the relations between B^{st}_{jrks} and B_{jrks} and also between B_{jrks} and the pressure derivatives of the effective elastic stiffnesses, the equation for calculating ${}_H\gamma(p,\vec{N})$ from the hydrostatic pressure derivatives of the effective elastic stiffnesses can be obtained. For piezoelectric crystals in Laue group RI, the equation can be written as:

$$
\begin{aligned}
{}_H\gamma(p,\vec{N}) = -\frac{B^T}{2w}\{1 + 2w[s_1(U_1^2 + U_2^2) + s_3 U_3^2] \\
-\left[\left(\frac{\partial C^{ef}_{11}}{\partial P}\right)_T + \left(\frac{\partial e_1}{\partial P}\right)_T + 1 + (2s_1 - s_3) C^{S,E}_{11}\right](N_1U_1 + N_2U_2)^2 \\
-\left[\left(\frac{\partial C^{ef}_{66}}{\partial P}\right)_T + \left(\frac{\partial e_1}{\partial P}\right)_T + 1 + (2s_1 - s_3) C^{S,E}_{66}\right](N_1U_2 - N_2U_1)^2 \\
-\left[\left(\frac{\partial C^{ef}_{33}}{\partial P}\right)_T + 1 + (3s_3 - 2s_1) C^{S,E}_{33}\right] N_3^2 U_3^2 \\
-\left[\left(\frac{\partial C^{ef}_{44}}{\partial P}\right)_T + 1 + s_3 C^{S,E}_{44}\right][(N_2U_3 + N_3U_2)^2 + (N_1U_3 + N_3U_1)^2] \\
-2\left[\left(\frac{\partial C^{ef}_{13}}{\partial P}\right)_T - 1 + s_3 C^{S,E}_{13}\right][(N_1U_1 + N_2U_2) N_3U_3 \\
-2\left[\left(\frac{\partial C^{ef}_{14}}{\partial P}\right)_T + s_1 C^{S,E}_{14}\right][(N_1^2 - N_2^2) U_2U_3 + (U_1^2 - U_2^2) N_2N_3 \\
+2N_1U_1(N_2U_3 + N_3U_2)] \quad , \qquad (3.23)
\end{aligned}
$$

where

$$w = C_{11}^{S,E}(N_1U_1 + N_2U_2)^2 + C_{66}^{S,E}(N_1U_2 - N_2U_1)^2$$
$$+C_{33}^{S,E}N_3^2U_3^2 + C_{44}^{S,E}[(N_2U_3 + N_3U_2)^2 + (N_1U_3 + N_3U_1)^2]$$
$$+2C_{13}^{S,E}(N_1N_3U_1U_3 + N_2N_3U_2U_3)$$
$$+2C_{14}^{S,E}[(N_1^2 - N_2^2)U_2U_3 + N_2N_3(U_1^2 - U_2^2) + 2N_1U_1(N_2U_3 + N_3U_2)]$$
$$+\frac{\{e_{11}[(N_1^2 - N_2^2)U_1 - 2N_1N_2U_2] + e_{14}(N_1N_3U_2 - N_2N_3U_1)\}^2}{[\varepsilon_{11}^{\eta}(N_1^2 + N_2^2) + \varepsilon_{33}^{\eta}N_3^2]}, \tag{3.24}$$

$$e_1 = \frac{e_{11}^2}{\varepsilon_{11}^{\eta}}, \tag{3.25}$$

and

$$s_1 = s_{11}^T + s_{12}^T + s_{13}^T, \tag{3.26}$$

$$s_3 = 2s_{13}^T + s_{33}^T. \tag{3.27}$$

Similarly, for the volume change produced by a uniaxial compressive stress along the direction of $\vec{M}$ the equations for piezoelectric crystals are:

$${}_M\gamma(p,\vec{N}) = -\frac{B^T}{2w(p,\vec{N})}\{(\vec{N}\cdot\vec{M})^2 + M_aM_bs_{abjk}^T[2w(p,\vec{N})U_jU_k$$
$$+(C_{jkmuv} + C_{jkmuv}^e)U_uU_vN_mN_n]\}. \tag{3.28}$$

The acoustic mode Grüneisen parameters, measured using ultrasonic techniques, reflect the contributions of the modes of long wavelength acoustic phonons to lattice vibrational anharmonicity. To examine the overall contributions from the long wavelength acoustic phonons, the mean acoustic (or elastic) Grüneisen parameter γ^l can be obtained by summing all the long wavelength acoustic modes (Brugger and Fritz 1967)

$$\gamma^l = \frac{\sum_{p=1}^{3}\int_{\Omega}\gamma(p,\vec{N})c(p,\vec{N})d\Omega}{\sum_{p=1}^{3}\int_{\Omega}c(p,\vec{N})d\Omega}, \tag{3.29}$$

where the subscript Ω means integration over the whole solid angle. The method to calculate the function $c(p,\vec{N})$ depends on the lattice dynamic model used (i.e. Debye model or Born-von Karman model) (Brugger and Fritz 1967). The mode Grüneisen gamma $\gamma(p,\vec{N})$ satisfy the relation (Brugger and Fritz 1967)

$$\gamma(p,\vec{N}) = B^T \sum_i \sum_{jk} s^T_{iijk} \gamma_{jk}(p,\vec{N}) \quad . \tag{3.30}$$

From Eq. (3.15) it can be seen that the volume thermal expansion coefficient α includes the contribution from all phonon modes. Axial crystals have two principal thermal expansion coefficients $\alpha_{11} = \alpha_{22}$ and α_{33}. Hence

$$\alpha = 2\alpha_{11} + \alpha_{33} \quad . \tag{3.31}$$

The principal thermal expansion coefficients are related to the main thermal Grüneisen parameters by (Barron et al. 1980)

$$\alpha_{11} = \frac{C_P}{V}[(s^S_{11} + s^S_{12})\gamma^{th}_{11} + s^S_{13}\gamma^{th}_{33}] \quad , \tag{3.32}$$

$$\alpha_{33} = \frac{C_P}{V}(2s^S_{13}\gamma^{th}_{11} + s^S_{33}\gamma^{th}_{33}) \quad . \tag{3.33}$$

In the above equations γ^{th}_{11} and γ^{th}_{33} include the contributions from both acoustic and optic modes. The contributions of long wavelength acoustic phonons to the principal thermal expansion coefficients are represented by the long wavelength mean acoustic principal Grüneisen parameters γ^{el}_{11} and γ^{el}_{33}. Here γ^{el}_{11} and γ^{el}_{33} are the weighted average of the Grüneisen parameter tensors of the modes perpendicular or parallel to the unique axis of the crystal (Brugger and Fritz 1967):

$$\gamma^{el}_{11} = \frac{\sum_{p=1}^{3} \int_\Omega \Gamma_{11}(p,\vec{N}) c(p,\vec{N}) d\Omega}{\sum_{p=1}^{3} \int_\Omega c(p,\vec{N}) d\Omega} \tag{3.34}$$

and

$$\gamma_{33}^{el} = \frac{\sum_{p=1}^{3} \int_{\Omega} \Gamma_{33}(p,\vec{N}) c(p,\vec{N}) d\Omega}{\sum_{p=1}^{3} \int_{\Omega} c(p,\vec{N}) d\Omega} \quad . \tag{3.35}$$

The expressions for the two parameters, Γ_{11} and Γ_{33}, given by Brugger and Fritz (1967) for nonpiezoelectric solids can be expanded for piezoelectric crystals. The expression for Γ_{11} is

$$2\Gamma_{11} = -\frac{B^T}{2w}(N_1^2 + N_2^2 + 2w_{11} + r_{11} + r_{11}^e) \tag{3.36}$$

with w defined by Eq. (3.26)

$$w_{11} = w[(s_{11}^T + s_{12}^T)(U_1^2 + U_2^2) + 2s_{13}^T U_3^2] \quad , \tag{3.37}$$

$$r_{11} = \sum_{i=1}^{6} M_{11}^i R_i \quad , \tag{3.38}$$

$$r_{11}^e = 2p_{11}\left(\frac{e}{\varepsilon}\right) - o_{11}\left(\frac{e}{\varepsilon}\right)^2 \quad , \tag{3.39}$$

with

$$M_{11}^i = (s_{11}^T + s_{12}^T)C'_i + 2s_{13}^T C''_i \quad , \tag{3.40}$$

$$R_1 = (N_1U_1 + N_2U_2)^2 \quad ,$$

$$R_2 = (N_1U_2 - N_2U_1)^2 \quad ,$$

$$R_3 = N_3^2U_3^2 \quad ,$$

$$R_4 = (N_2U_3 + N_3U_2)^2 + (N_3U_1 + N_1U_3)^3 \quad , \tag{3.41}$$

$$R_5 = 2(N_1U_1 + N_2U_2)N_3U_3 \quad ,$$

$$R_6 = 2[(N_1^2 - N_2^2)U_2U_3 + N_2N_3(U_1^2 - U_2^2) + 2N_1U_1(N_2U_3 + N_3U_2)] \quad ;$$

$$p_{11} = [(s_{11}^T + s_{12}^T)(e_{111} - e_{122}) + 4s_{13}^T e_{113}]\left[\frac{1}{2}(N_1^2 - N_2^2)U_1 - N_1 N_2 U_2\right]$$

$$+ [(s_{11}^T + s_{12}^T)(e_{114} + e_{124}) + 2s_{13}^T e_{134}](N_1 U_2 - N_2 U_1)N_3 \quad , \tag{3.42}$$

$$o_{11} = [(s_{11}^T + s_{12}^T)(l_{11} + l_{12}) + 2s_{13}^T l_{13}](N_1^2 + N_2^2) + 2[(s_{11}^T + s_{12}^T)l_{31} + s_{13}^T l_{33}]N_3^2 \quad , \tag{3.43}$$

$$e = [e_{11}(N_1^2 - N_2^2) - e_{14} N_2 N_3]U_1 + (e_{14} N_3 - 2\varepsilon_{11} N_2)N_1 U_2 \quad , \tag{3.44}$$

$$\varepsilon = \varepsilon_{11}^{\eta}(N_1^2 + N_2^2) + \varepsilon_{33}^{\eta} N_3^2 \quad , \tag{3.45}$$

and

$$C'_1 = C_{111} + C_{112} \quad , \qquad C''_1 = C_{113} \quad ;$$

$$C'_2 = \frac{1}{2}(-C_{112} + C_{222}) \quad , \qquad C''_2 = \frac{1}{2}(C_{113} - C_{123}) \quad ;$$

$$C'_3 = 2C_{133} \quad , \qquad C''_3 = C_{113} \quad ; \tag{3.46}$$

$$C'_4 = C_{144} + C_{155} \quad , \qquad C''_4 = C_{344} \quad ;$$

$$C'_5 = C_{113} + C_{123} \quad , \qquad C''_5 = C_{133} \quad ;$$

$$C'_6 = C_{114} + C_{124} \quad , \qquad C''_6 = C_{134} \quad .$$

The expression for Γ_{33} is

$$\Gamma_{33} = -\frac{B^T}{2w}(N_3^2 + 2w_{33} + r_{33} + r_{33}^e) \tag{3.47}$$

with

$$w_{33} = w[s_{13}^T(U_1^2 + U_2^2) + s_{33}^T U_3^2] \quad , \tag{3.48}$$

$$r_{33} = \sum_{i=1}^{6} M_{33}^i R_i \quad , \tag{3.49}$$

$$r_{33}^e = 2p_{33}\left(\frac{e}{\varepsilon}\right) - o_{33}\left(\frac{e}{\varepsilon}\right)^2 \quad , \tag{3.50}$$

with

$$M_{33}^i = s_{13}^T C'_i + s_{33}^T C''_i \quad , \tag{3.51}$$

$$p_{33} = [s_{13}^T(e_{111} - e_{122}) + 2s_{33}^T e_{113}]\left[\frac{1}{2}(N_1^2 - N_2^2)U_1 - N_1 N_2 U_2\right]$$

$$+ [s_{13}^T(e_{114} + e_{124}) + s_{33}^T e_{134}](N_1 U_2 - N_2 U_1)N_3 \quad , \tag{3.52}$$

$$o_{33} = [s_{13}^T(l_{11} + l_{12}) + s_{33}^T l_{13}](N_1^2 + N_2^2) + (2s_{13}^T l_{31} + s_{33}^T l_{33})N_3^2 \quad . \tag{3.53}$$

In the Debye model, at low temperatures where the T^3 law holds, the weighting function $c(p,\vec{N})$ is proportional to $v^{-3}(p,\vec{N})$ (Barron et al. 1980), where $v(p,\vec{N})$ is the sound wave velocity of the p th mode propagated along the direction $\vec{N}$. The long wavelength acoustic mean Grüneisen parameter in low temperature limit can be calculated from

$$\gamma_L^{el} = \frac{\sum_{p=1}^{3} \int_\Omega \gamma(p,\vec{N}) v^{-3}(p,\vec{N}) d\Omega}{\sum_{p=1}^{3} \int_\Omega v^{-3}(p,\vec{N}) d\Omega} \quad . \tag{3.54}$$

At high temperature ($T \gg \Theta_D$) all of the modes have the same weight and hence the long wavelength acoustic mean Grüneisen parameter in high temperature limit can be obtained by

$$\gamma_H^{el} = \frac{\sum_{p=1}^{3} \int_\Omega \gamma(p,\vec{N}) d\Omega}{\sum_{p=1}^{3} \int_\Omega d\Omega} \quad . \tag{3.55}$$

In general, the phonons of both acoustic and optical modes need to be examined in order to study the contribution from each mode to the lattice vibrational anharmonicity of a solid. However, the long wavelength acoustic mode Grüneisen parameters provide some valuable information on the properties of lattice vibrations. Since at low temperatures ($T \ll \Theta_D$, where Θ_D is the Debye temperature) the lattice vibrational anharmonicity is mainly dominated by the acoustic phonon modes, the mean long wavelength acoustic Grüneisen parameter at low temperatures characterizes the low temperature

thermal expansion. The anharmonicity of lattice vibrations is enhanced as the temperature increases above the Debye temperature. At those temperatures the higher frequency phonons become increasingly important.

3.3 Temperature dependence of the Grüneisen parameters and the soft phonon modes

Variation of the Grüneisen parameter γ^{th} with temperature comes from two sources implied by Eq. (3.8): 1) the temperature dependence of the mode Grüneisen parameter γ_i , 2) the temperature dependence of the weighting factor or mode specific heat c_i . Eq. (3.8) has two limiting forms at low and high temperatures respectively. In the Debye model at low temperature ($T \rightarrow 0$K), c_i is proportional to T^3, whereas at high temperature c_i approaches k_B . Therefore, γ^{th} approaches different values at high and low temperatures. At low temperatures, the long wavelength acoustic phonons dominate. Due to the $v^{-3/2}$ in the Debye model (Eq. (3.54)), the Grüneisen parameter will be closer to the values for the transverse acoustic phonon branches. For piezoelectric crystals, the long wavelength acoustic mode Grüneisen tensors $\gamma_{jk}(p,\vec{N})$ in different wave propagation directions are determined by the SOEC, the TOEC and the second and third order piezoelectric coefficients (Eq. (3. 17)-(3.27)). The $\gamma_{jk}(p,\vec{N})$ varies with temperature as a consequence of the temperature dependence of those coefficients. Hence, the variation of the weighted average γ^{el} with temperature is an overall effect of the temperature dependence of all mode Grüneisen parameters and mode specific heats.

The Grüneisen parameter γ^{th} can have negative values. From Eq. (3.10) a negative γ^{th} means that the thermal expansion coefficient α would be expected to be negative. A negative thermal expansion has been observed in some materials especially at low temperatures (Barron 1980). This phenomenon implies that for some modes the γ_i have

negative values. For these modes, according to Eq. (3.7), the phonon frequencies or the interatomic force constants decrease when the volume of the solid is reduced. These modes are "softer" than others and then the weighted average of the γ_i on all modes gives a negative γ^h. The existence of soft modes is also possible even if the thermal expansion is positive, which causes a small value of the γ^h. For piezoelectric crystals under hydrostatic pressure, the negative acoustic mode Grüneisen parameters are caused by the negative values of the hydrostatic pressure derivatives B^{st}_{jrks} of the stiffened thermodynamic second order elastic constants in Eq. (3.22). When

$$B^{st}_{jrks}U_jU_kN_rN_s < (1 + 2s^T_{aajk}w(p,\vec{N})U_jU_k)$$

the ${}_H\gamma(p,\vec{N})$ will be negative.

The soft modes could also exist in materials undergoing a phase transition accompanied by crystal distortions or displacements of ions (Aubry and Pick 1971, Fleury 1973, Rao and Rao 1978). The mean value of the displacements corresponds to an order parameter. The order parameter measures the magnitude of the change in atomic configuration from the old structure. The phonon mode associated with the order parameter will describe the thermal fluctuations in the order parameter. As the temperature approaches the transition point T_C, the mode softens, i.e. the phonon frequency decreases. In a second-order phase transition, the frequency decreases to zero at the transition temperature T_C. In an elastic phase transition the order parameter is the corresponding strain (Aubry and Pick 1971) and the corresponding mode is an acoustic phonon. In the case when the order parameter is the amplitude of a relative atomic displacement the corresponding soft mode is an optical phonon (Aubry and Pick 1971). As a driving force for the structural phase transition the mode softening occurs even at temperatures which are far below or above T_C (Brassington and Saunders 1982). The Grüneisen parameter γ_i for the corresponding mode will therefore have a negative value owing to the strain-related mode softening.

Chapter 4 Experimental Techniques and Equipment

4.1 Introduction

In experimental techniques which have been developed to measure the elastic properties of solid, the dynamic methods, particularly those using ultrasonics, are most widely used nowadays. The dynamic measurements are based upon the principle that the natural frequency of vibration of an elastic solid depends on the geometry, density and elastic constants of the specimen. Methods used include either the measurement of the resonant frequency of a device containing the sample to be tested or the measurement of the round-trip frequency (or time delay) of an ultrasonic wave pulse generated in a specimen. The measured frequencies are usually so high that the elastic constants are essentially adiabatic. Another kind of dynamic method is to measure the optical effect of ultrasonic waves in materials, from which the ultrasonic wavelength can be determined (Breazeale et al. 1981).

Ultrasonic pulse techniques have been used widely to measure directly ultrasonic wave velocities in various solids from the kHz to GHz range. The velocity of ultrasonic waves propagated in specimens can be used for two purposes. The first is to determine the absolute values of the elastic constants of a solid and the second is to determine the change of the elastic properties with variations in the environment of solids, such as temperature or pressure.

A pulse system measures the transit time of ultrasonic waves propagated in a sample. The system mainly consists of two sections: a pulse generation section and a pulse receiving section. A pulsed rf signal of a given frequency is generated by a pulse source

and converted by means of a transducer into a pulsed ultrasonic wave of the same frequency. The ultrasonic pulse travels through the sample and is reflected at the sample boundaries until it has decayed completely. Each time the ultrasonic pulse is picked up by the transducer an electrical signal is generated and sent to a receiver. The receiver amplifies the signal and feeds it to an oscilloscope so as to display it. If the pulse length is small compared to a round-trip transit time in the sample, a pulse echo train develops and is shown on the screen of the oscilloscope. The velocity of ultrasonic wave propagation is determined by measuring the transit time between the reflected pulses and the corresponding pulse propagation distance in the sample. In the present work, both the pulse echo overlap and the pulse superposition methods have been used in the MHz range. The former technique was used for measurements of the hydrostatic pressure effects on the ultrasonic wave velocities and the latter was used for measuring the uniaxial stress effects on the wave velocities.

4.2 The pulse echo overlap system

The pulse echo overlap method was developed by Papadakis (1964) based on the method reported by May (1958). A pulse echo overlap system measures the transit time between any pair of echoes in a pulse-echo pattern shown in Fig. 4.1. This corresponds to the round-trip phase delay of ultrasonic wave in the sample. The repetition rate of the pulses is low enough so that all echoes from a given rf pulse decay away before the next pulse is applied. The selected echoes in one pulse-echo pattern are overlapped with each another. By driving the X-axis of an oscilloscope at a frequency equal to the reciprocal of the round-trip travel time of the echoes in the sample, or at an integer multiple of that frequency, the echo-overlap can be obtained on the scope. The measured overlapping frequency can then be used to calculate the sound wave velocity.

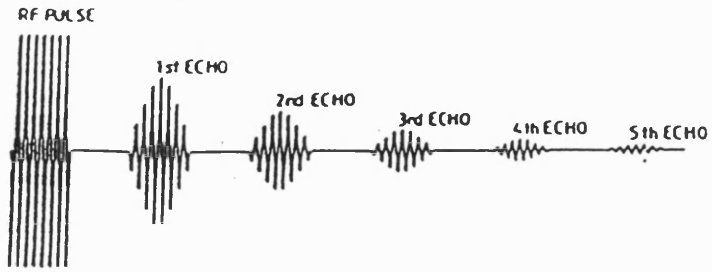

Fig. 4.1 The pulse-echo pattern displayed on the screen.

The system construction (Lichnowski 1975) is based on Papadakis' developments (1964, 1966, 1967) of this method. It gives a sensitivity of the measured wave velocity change to 10^{-4} (Yogurtcu 1980).

The system is shown in the block diagram Fig. 4.2. The equipment used in the system is:

(1) MATEC high resolution frequency source (0.5Hz-50MHz, Model 110);

(2) MATEC pulse modulator and receiver (Model 6600);

(3) MATEC rf plug-in (10-90MHz, Model 760V);

(4) HITACHI oscilloscope V-1050F (100MHz);

(5) HEWLETT-PACKARD Model 5382A 225MHz frequency counter;

(6) Decade divider and strobe generator.

The high resolution frequency source generates a synchroniser square wave in the kHz range as seen in Fig. 4.3(1), which is used to trigger the rf pulse generator contained in the MATEC pulse modulator and receiver (Model 6600). The rf pulse generator, in which the carrier frequency is set to the resonant frequency of the quartz transducer, produces a short duration high voltage rf pulse with three microseconds time width and a maximum amplitude of 630 volts peak-to-peak. To enable a complete set of echoes to be observed, the rf pulse generator has to be triggered at a low frequency which ensures that all the echoes from one rf pulse have died away before the next rf pulse is applied.

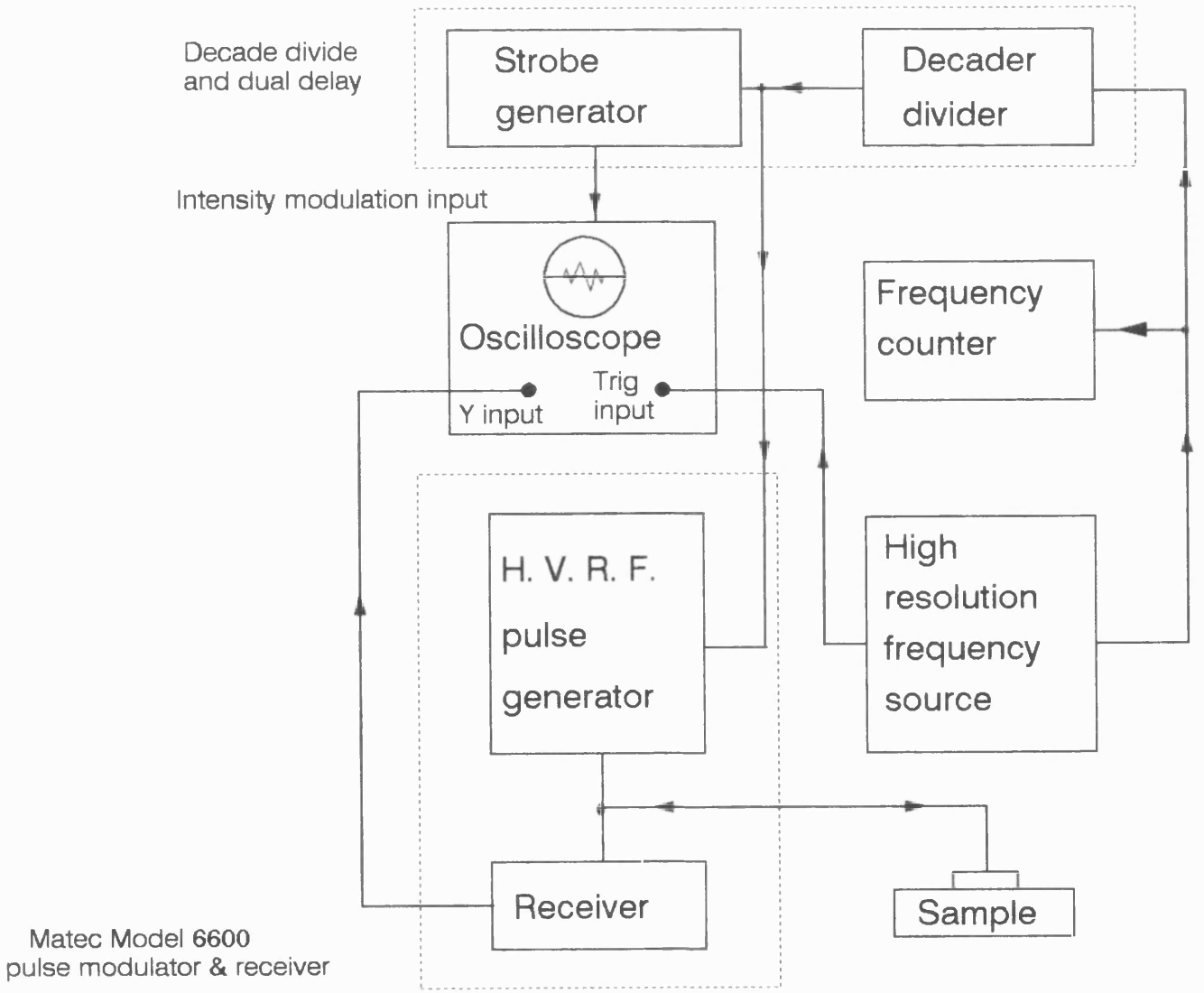

Fig. 4.2 Block diagram of the pulse echo overlap apparatus.

This low triggering frequency is achieved by dividing the output signal of the high resolution source by a factor of 10, using the decade divider. The rf pulse generator is then triggered by the divided signal at the low frequency required (Fig. 4.3(2)). When the rf pulse (Fig. 4.3(3)) is applied to a transducer mounted on a sample, the electrical signal is converted into a mechanical vibration which passes through the sample and is reflected back and forth at the faces of the sample. As a result, a train of ultrasonic echoes is produced. They are picked up by the transducer and converted into electrical signals which are fed to the amplifier in the receiver.

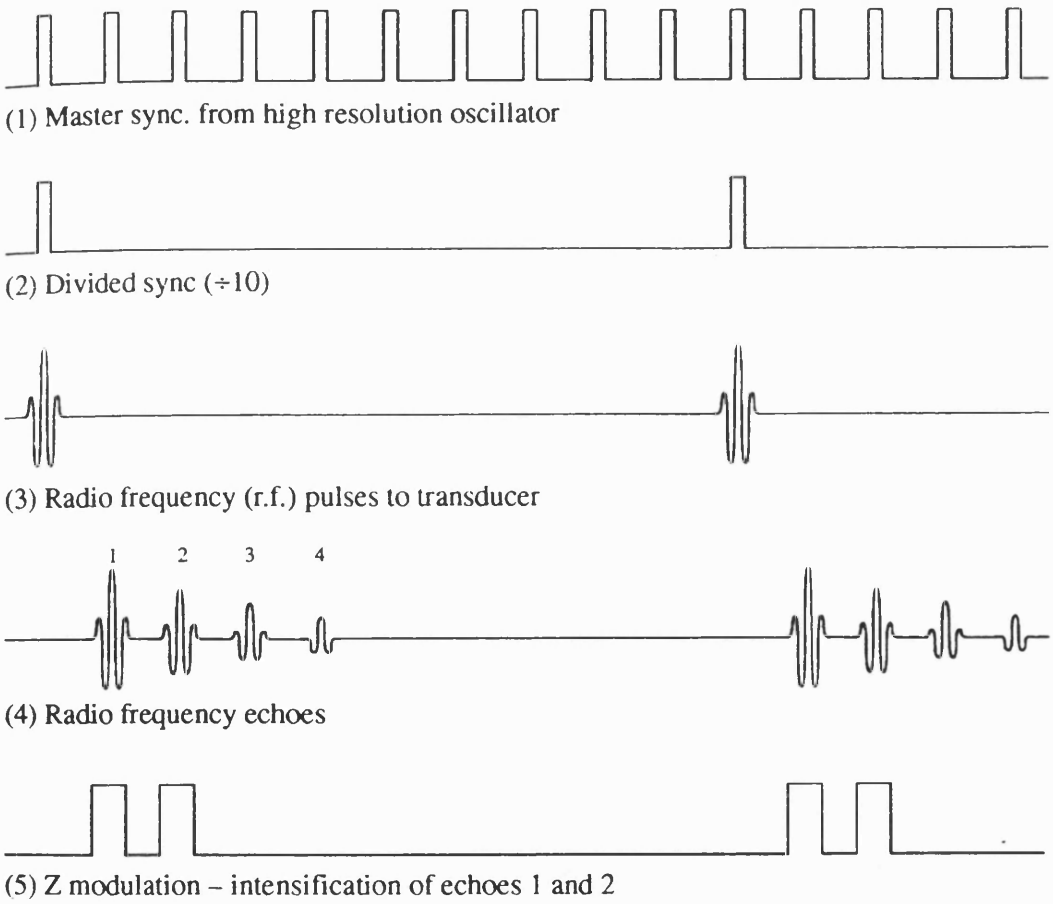

(1) Master sync. from high resolution oscillator

(2) Divided sync (÷10)

(3) Radio frequency (r.f.) pulses to transducer

(4) Radio frequency echoes

(5) Z modulation – intensification of echoes 1 and 2

Fig. 4.3 Signals in the pulse echo overlap system.

The output from the amplifier is observed on the oscilloscope and displayed as seen in Fig 4.3(4) or Fig. 4.1. The strobe generator is triggered by the output signal from the decade divider to produce a pair of square wave pulses. The pair of pulses (Fig. 4.3(5)) are fed to the Z-mode of the oscilloscope to intensify two selected echoes. Reducing the brightness of the oscilloscope obscures other echoes. When the frequency of the output signal from the high resolution source is adjusted to equal approximately to the reciprocal of the time delay between the selected echoes, the frequency sweep rate of the oscilloscope is synchronous with this time delay and the two intensified echoes can be seen overlapped on the screen. A fine adjustment of the high resolution source brings the rf cycles within the two echo envelopes to overlap cycle-by-cycle as in Fig. 4.4; the reading of the frequency counter indicates the overlap frequency of the echoes. The criterion proposed by McSkimin and Andreatch (1962) can be used to decide which cycle is the correct one for matching in each echo.

Fig. 4.4 Two overlapped echoes.

4.3 The pulse superposition system

Hydrostatic pressure measurements cannot give all the information needed for the calculation of the whole set of TOEC. To complete the work, the effect of uniaxial stress on the ultrasonic wave velocities has to be measured. Since a uniaxial stress will generate a shear component leading to dislocation movement in a sample, only a relatively small

uniaxial stress can be applied to reduce the effects on the measurements of transit time. In this work the uniaxial stress is in the range from several bar to 300 bar. Such small stresses will cause changes in ultrasonic wave velocities of the order of only 10^{-5} to 10^{-3}. To reduce the measurement error to within 1%, the sensitivity of the equipment has to be at least 10^{-7}. Hence, the pulse superposition system, which is more sensitive than the pulse echo overlap method, has been used. The pulse superposition method was devised by McSkimin (McSkimin 1961, McSkimin and Andreatch 1962) and developed by McSkimin (1965), Holder (1970) and Yogurtcu (1980). This method measures the time delay between superimposed "in-phase" pulses. In a pulse superposition system, a series of rf pulses from a generator is introduced into the sample. The repetition rate of the pulses is adjusted to be either equal to the reciprocal of the acoustic round-trip transit time in the sample or to the submultiples of that rate. In contrast to the pulse echo overlap method, the successive rf pulses generate acoustic waves in the sample before the former generated waves decay. The echoes of these waves are superposed simultaneously at the transducer bonded onto the sample.

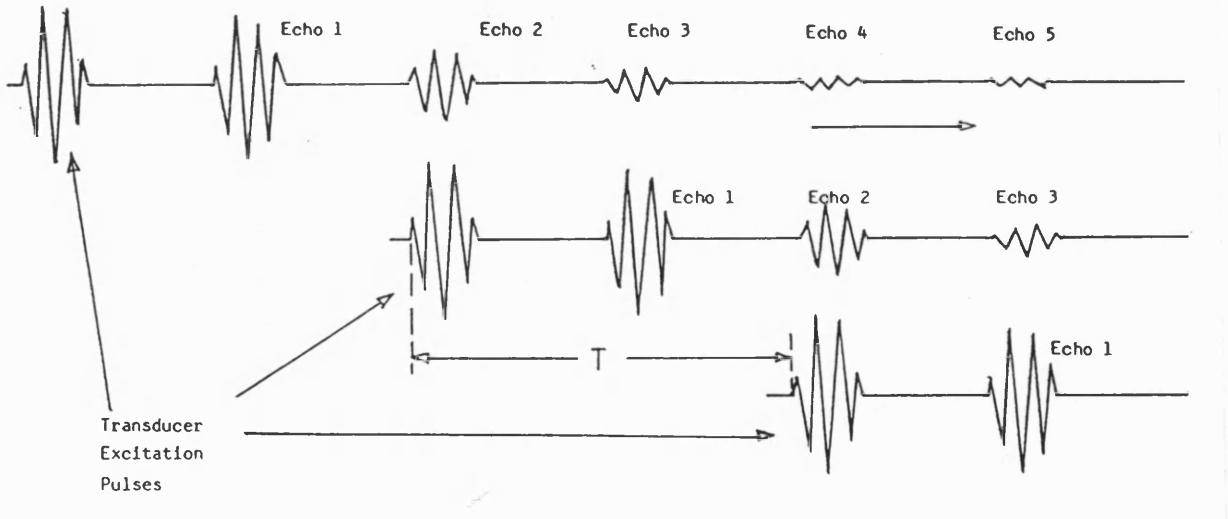

Fig. 4.5 The excited pulses and the echo patterns.

Fig. 4.5 shows the pulses excited by the transducer and the echo patterns to be superposed. The sound velocity can be determined from the measured time delay between the pulses and the wave transit distance.

The system used was built and modified by Yogurtcu (1980) based on a sensitive interference method developed by McSkimin (1961). The apparatus is capable of measuring changes in ultrasonic wave velocities to 1 part in 10^8.

A block diagram of the apparatus is shown in Fig. 4.6. The instruments comprising the system are:

1) GENERAL RADIO 1061 frequency synthesizer (0.4-160MHz range).

2) RACAL-DANA 9917 UHF frequency meter.

3) RACAL-DANA instrument interface 9932.

4) ORTEC Brookdeal 9503 precision lock-in amplifier (P.S.D.).

5) Reference generator.

6) Variable attenuator.

7) Programmable frequency divider.

8) ARULAB pulse oscillator model PG-650C (gated amplifier).

9) ARULAB wide band amplifier WA-600-E.

10) ARULAB preamplifier PA-620-B.

11) GOULD Advance OS 3300B oscilloscope.

12) FARNELL PG5112 pulse generator.

13) T/R (Transmit/Receive) Switch Unit.

14) Low Pass Active Filter.

The GENERAL RADIO 1061 frequency synthesizer is a C.W. generator. Its stability is 1 part in 10^{10} which is two orders of magnitude greater than the overall system stability. Hence the instrumental errors in the measurements of the ultrasonic wave transit time can be ignored. When the operation is started, the rf synthesizer frequency is set to the resonant frequency of the transducer and is determined by the frequency meter which

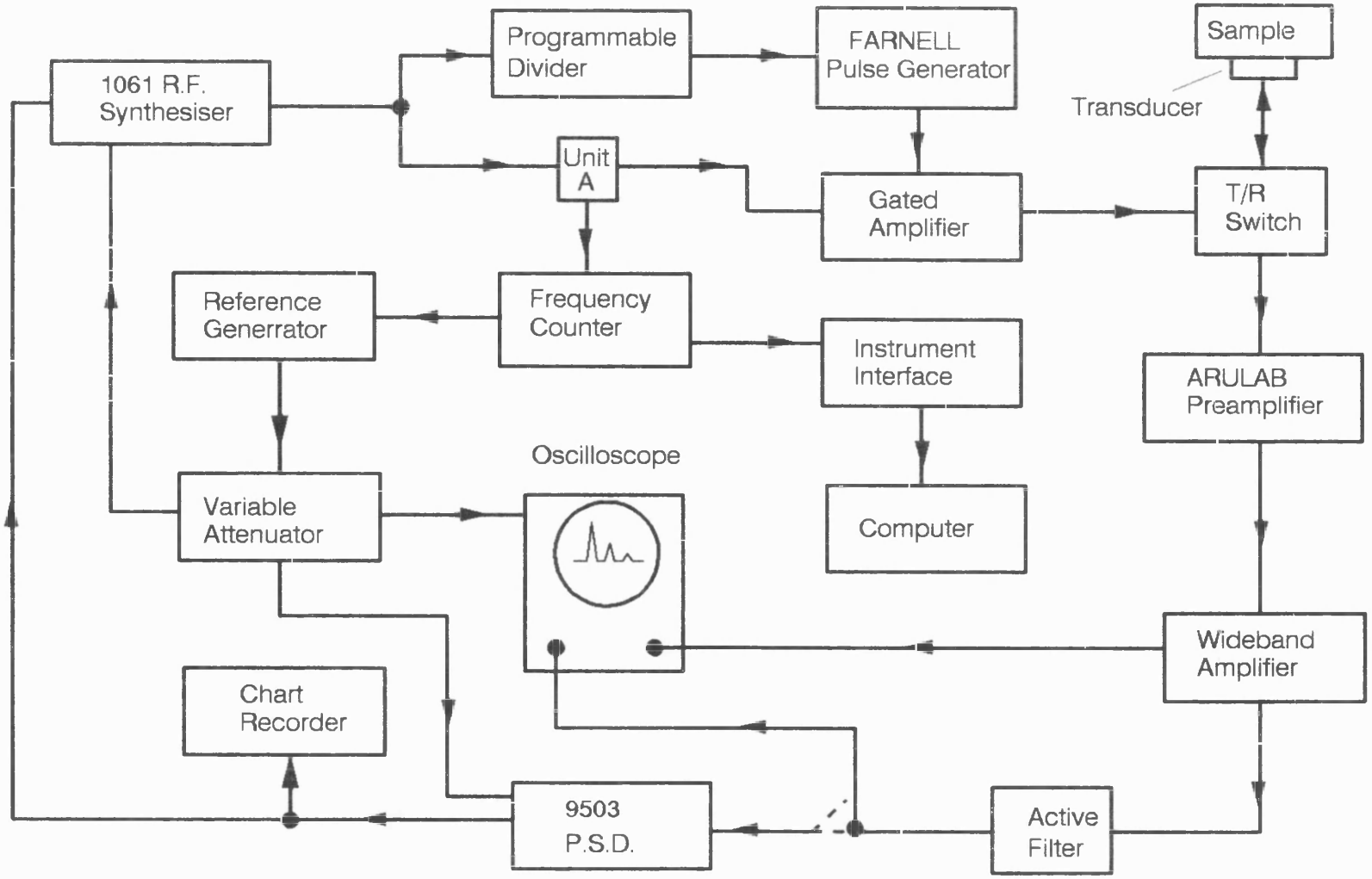

Fig. 4.6 Block diagram of the pulse superposition system.

has a nine digit display with an accuracy of ±1 count and covers a frequency range of 10Hz to 60MHz with a resolution of 0.1Hz. Its input level is restricted to 5V by the unit A (Fig. 4.6) in order to prevent the overload of the input signal.

Rf pulses are generated by gating the output of the C.W. generator, using the gated amplifier which can generate rf pulses in the frequency range of 2MHz to 100MHz. The input of a 3V peak-to-peak signal is provided by the unit A and then amplified for a short, controllable duration of 1μs. Its output impedance is 90 Ohms. The amplifier is triggered synchronously with the input signal so as to generate coherent rf pulses. The triggering signal is a pulse generated by a programmable frequency divider. The input frequency of the divider can be divided by any integer from 1 to 9999. The division ratio is determined by setting thumbwheel switches on the divider front panel. If the switch setting is X, the division ratio D will be D=10000-X. The frequency of the output sine wave of the frequency synthesizer is divided by D. The divided output pulse has a duration of 1/2 of the period of the input wave and is synchronous with the input frequency. The FARNELL PG5112 pulse generator is used to amplify the divided output pulse so as to match the input level of the gated amplifier. The output of the gated amplifier is applied to a 10MHz quartz transducer bonded onto a sample.

The echoes picked up by the transducer are detected and amplified by the ARULAB wideband amplifier WA-600-E. It has a band width of 5MHz to 60MHz and a 90dB gain. The gain is highly stable and free from drift. In order to prevent damage of the wideband amplifier, caused by excessive voltages from the gated amplifier, the signals of the ultrasonic echoes are picked up and transmitted by a T/R switch unit to the wideband amplifier. The unit limits the input signal to the wideband amplifier at 0.6V. To provide sufficient gain along with a low noise to the wideband amplifier, the preamplifier (PA-620-B) which works at frequencies between 5MHz and 60MHz is inserted between the wideband amplifier and the T/R switch unit. The preamplifier also narrows the pass band and improves the signal-to-noise ratio. The video output of the wideband

amplifier is applied to the CH2 (channel 2, Y-axis) of the oscilloscope so that the echo trains can be monitored. An echo train in maximum amplitude can be achieved by adjusting the synthesizer frequency and the preamplifier. If the programmable divider is set to a high division ratio, e.g. 2000 or 4000 and the high voltage of the gated amplifier is increased, a complete set of echo trains can be observed as shown in Fig. 4.7. To obtain the pulse superposition, the repetition rate of the rf pulse must be high enough to superpose successive echo trains. Reducing the division ratio will make the appropriately chosen echoes in successive echo trains coincide with one another so that an maximum peak will be seen as shown in Fig. 4.8a. When the synthesizer frequency is changed, the locus of this peak forms a resonance curve as seen in Fig. 4.8b.

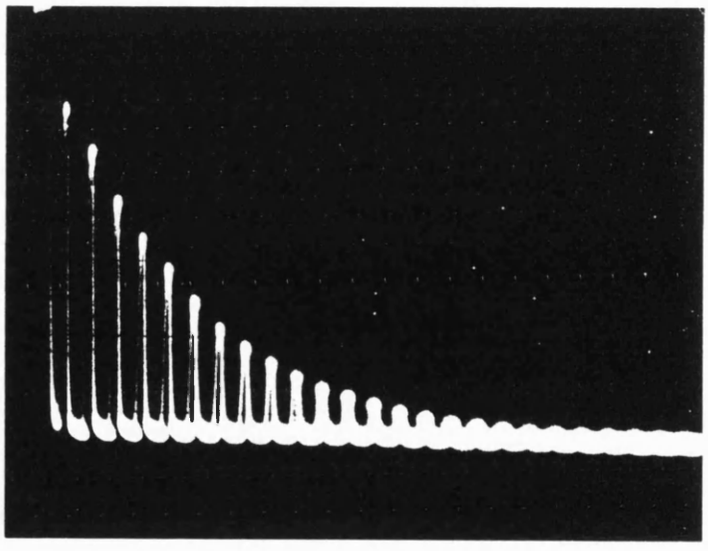

Fig. 4.7 The echo train on the screen.

The video output from the wideband amplifier is also fed to a low pass active filter to retrieve the amplitude modulation present on the pulses. The filter attenuates any harmonics of the modulation frequency which may be present in the signal and attenuates any high frequency noise associated with the signal. The output of the filter is applied to the CH1 (channel 1, Y-axis) of the oscilloscope so that the demodulation signal can be observed.

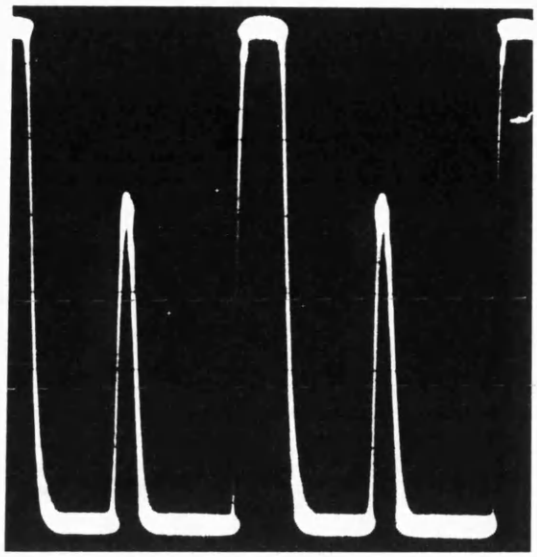

Fig. 4.8 (a) Maximum peaks on the screen.

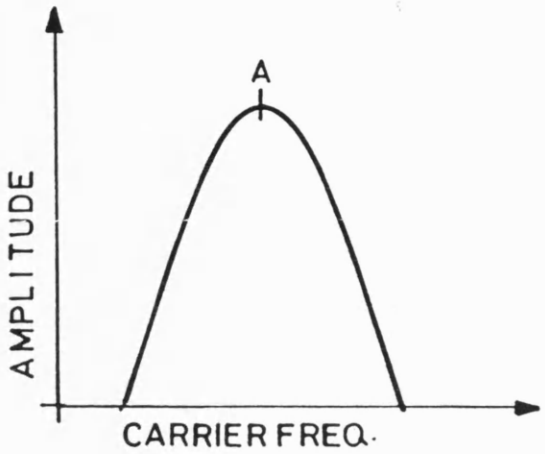

Fig. 4.8 (b) The resonance curve formed by the locus of a maximum peak.

A reference frequency generator produces a highly stable reference signal to the P.S.D. and supplies a modulation voltage for the rf synthesizer. The generator also provides an input signal to the oscilloscope for X-axis triggering. The amplitude of the modulation signal is controlled by a variable attenuator. When the synthesizer frequency is modulated sinusoidally at a low rate (222Hz), the amplitude of the summed echoes will vary proportionally to the slope of the resonance curve. If the x100kHz button of the synthesizer is pressed down, a series of resonance peaks as shown in Fig. 4.9a can be seen on the screen by switching off the timebase of the oscilloscope, increasing the modulation amplitude and adjusting the division ratio. The maximum peak can be selected by reducing the modulation amplitude. The input signal of the P.S.D. (phase sensitive detector) is provided by the low pass filter. The P.S.D. multiplies the demodulation signal (the input signal) with the modulation signal (the reference signal) and outputs a signal proportional to the resonance curve. As the rf frequency is swept across the resonance curve, the output of the P.S.D. will change from positive to negative or vice versa. At the peak of the resonance curve, where the successive echoes are in phase and the demodulation signal has twice the frequency of the modulation signal, the

P.S.D. will give zero output. On the both sides of the peak the successive echoes are out of phase and then the P.S.D. will give an output to the rf synthesizer according to the polarity of the signal. The output frequency of the synthesizer will be adjusted automatically until the echoes are brought back to the in-phase position and the interference condition is maintained at the peak. To monitor the output from the active filter the mode of the oscilloscope is switched to CH1 and the timebase is switched on. A waveform containing a 444Hz modulation frequency harmonic content can be seen on the oscilloscope screen-the successive echoes are in phase, i.e. the peak of the resonance curve is reached. Then the timebase is switched off and a Lissajou's figure of eight will be seen as shown in Fig. 4.9b. When the output of the filter to the oscilloscope CH1 is also fed to the input channel of the P.S.D. the superposition frequency will be measured automatically. The data are collected by a programmed computer through an IEEE interface connected to the frequency counter, from which the ultrasonic wave velocity can be determined.

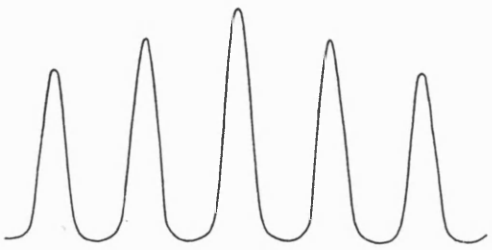

Fig. 4.9 (a) The resonance peaks.

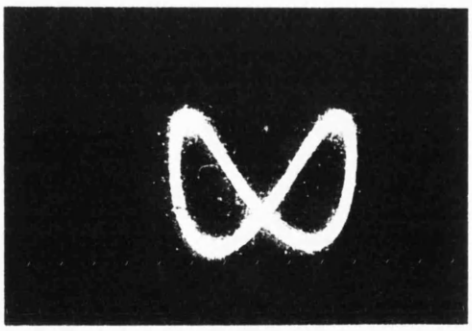

Fig. 4.9 (b) The Lissajous figure of layed-down eight.

4.4 The transducers and bonding agents

A transducer converts a mechanical vibration into an electrical signal or vice versa by means of the piezoelectric effect. It is used as both the transmitter and receiver of mechanical vibrations. Although many solids which do not have a centre of symmetry can show the piezoelectric effect, practical piezoelectric transducers are fabricated from only a small number of materials that possess a favourable combination of mechanical, electrical and piezoelectric properties. Some transducer materials are crystalline such as quartz, tourmaline, ammonium dihydrogen phosphate (ADP), Rochelle Salt, cadmium sulphide, diamine tartrate (EDT), dipotassium tartrate (DKT), and lithium sulphate (LH) (Mason 1958, Ikeda 1990). Alternatively man-made ferroelectric ceramics are used such as barium titanates, lead zirconate-titanates (PZT) and lead metaniobates (O'Donnell et al. 1981). Crystals such as quartz are inherently piezoelectric, while ferroelectric ceramics are initially isotropic and need to be polarized above the Curie temperature by the application of strong electric fields to introduce the anisotropy responsible for their strong piezoelectric properties.

In ultrasonic measurements quartz transducers have been used widely. Among the commonly used quartz transducers for ultrasonic measurements are X-, Y- and AT-cut transducers. As shown in Fig. 4.10a, the transducer cut with its length along the Y-crystallographic axis and its thickness normal to the X-axis is called an X-cut transducer. The Y-cut transducer is cut with its length along the X-axis and its thickness normal to the Y-axis. The AT-cut transducer is cut with its length along the X-axis and with a rotation about X-axis for 35°15′ apart from Z-axis (IEEE 1978).

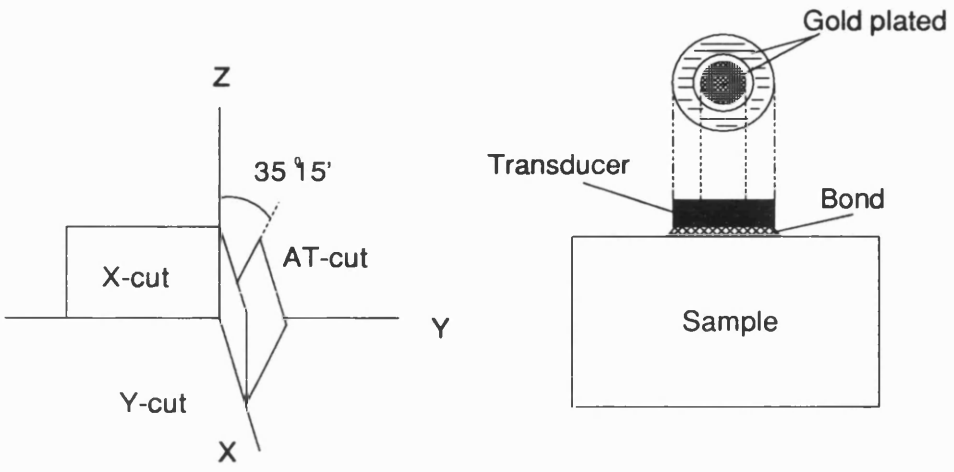

a. The transducer cuts. b. The bonded Transducer.

Fig. 4.10 The transducer cuts and the bonded transducer.

Transducers can produce longitudinal or shear modes at frequencies governed by their thickness. The relationship between the thickness of a transducer and the wavelength of a driven mode is given by

$$l = \lambda/2 \tag{4.1}$$

where λ is the wavelength of the generated sound wave at the fundamental resonance frequency f_0 and l is the thickness of the transducer plate. For this application, the quartz plate is usually given a square or circular cross section. Transducers can be driven at odd harmonics of a fundamental frequency, which obey the condition

$$f_n = (2n-1)f_0 \qquad (n = 1,2,3,\ldots) \tag{4.2}$$

A relationship between the frequencies of the generated modes of a transducer and its thickness may obtained by combining Eq. (4.1) and (4.2):

$$f_n = \left(n - \frac{1}{2}\right)\frac{v_0}{l} \quad , \qquad (n = 1,2,3,\ldots) \tag{4.3}$$

where v_0 is the velocity with the fundamental frequency f_0.

In the measurements made here the circular plates of the X- and Y-cut quartz transducers with a diameter of 6mm were employed for generating 10 MHz longitudinal and shear

waves. One side of a transducer is coated coaxially with gold to form two electrodes with an insulating region between them. This is used as a high voltage connection. The other side is fully coated to obtain the earth connection. Fig. 4.10b shows a transducer with two electrodes bonded on to a sample.

A circular transducer attached to a sample generates a wave which is essentially plane and has a width equal to the diameter of the transducer up to the distance given by

$$d = \frac{a^2}{\lambda} \tag{4.4}$$

where d is the axial distance which the plane wave travels and a is the radius of the transducer. This region is called the Fresnel region (Mason 1958). For an infinite medium, the sound energy spreads out at an angle β given by the equation

$$\sin\beta = 1.22\frac{\lambda}{2a} = 0.61\frac{\lambda}{a} \quad , \tag{4.5}$$

as shown in Fig. 4.11. Hence, in order to maintain a plane wave within a sample, the size of transducers should be chosen to match the dimension of the sample in order to prevent the sound energy from diverging.

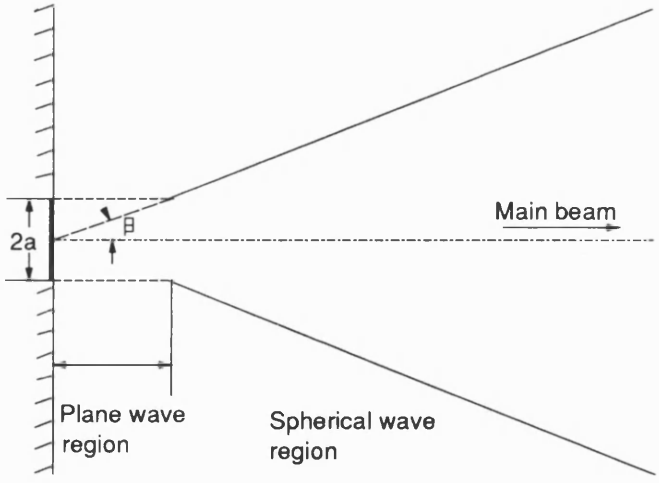

Fig. 4.11 The Fresnel region of the sound wave emitted from a transducer.

An ultrasonic wave will lose its energy due to reflection when it impinges on a transducer-sample boundary. An intermediary bond must be used to couple the wave energy into the sample. The reflection coefficient r is expressed by the equation

$$r = \frac{Z_t - Z_b}{Z_t + Z_b} \quad , \tag{4.6}$$

where Z_t and Z_b are the characteristic acoustic impedances of the transducer and the bonding material respectively and are defined by the expression

$$Z = \rho v \tag{4.7}$$

where ρ is the density of the material and v the velocity of the sound wave propagated in the material. There are two points have to be considered in choosing a bonding material. One is its acoustic characteristic impedance Z_b which should result in a low reflection coefficient. The second is that the bonding material should be easy to use and the bonded transducer removable after used. Normally, viscous liquids are used. The bonding materials used in this work are Dow Resin 276-V9 (Dow-Corning Corp., U.S.A.) and Du Pont Thick Film Conductor Composition (Du Pont Ltd., U.K.). The former gives a good acoustic energy coupling in the temperature range of measurements, 243K to 393K, for longitudinal waves measured by both the pulse echo overlap system and the pulse superposition method, but gives a poor coupling for shear waves above 313K in a pressure transmitting fluid (silicone fluid) and above 333K in air when it is not viscous enough. The Du Pont bonding agent was used to overcome this problem in the measurements using the pulse echo overlap method up to 393K. The procedure for using the Du Pont agent is: 1) attach a transducer with Du Pont on the work face of a sample; 2) bake the sample bonded with the transducer at an room temperature at 353 to 373K for 8 to 12 hours; 3) leave the sample to cool down naturally to room temperature. The bond between the transducer and the sample must be very thin and uniform to ensure that the echoes displayed on the oscilloscope screen are clear and decay exponentially. The pulse superposition system requires high quality echoes which the Du Pont agent cannot give.

Therefore indium has been used as a bonding material for shear modes under uniaxial stress above 363K. The procedure used to make an indium bonding is as follows: (1) lay a thin indium sheet with a thickness of about 0.5mm between the sample and the transducer; (2) place the sample-transducer set in a sample holder with an electrode squeezing the transducer lightly to hold the set tightly; (3) heat the sample, transducer and the indium sheet from the bottom of the sample holder by using a heat gun gradually up to 433K; (4) leave the set to cool down naturally to room temperature.

4.5 The hydrostatic pressure apparatus

In this work two different hydrostatic rigs have been used to determine the effects of hydrostatic pressure on the elastic properties. One is for use above room temperature and the other below.

As shown in Fig 4.12, the hydrostatic rig consists of a cylinder and two pistons made from EN26 nickel alloy carbon steel. A hydraulic pressure pump provides hydrostatic pressure from 1 bar to 1.6 kbar for the rig used above room temperature. Another pump, matched with the rig used for measurements below room temperature, provides pressure from 1 bar to 1.2 kbar. The sample holder is fixed onto the top piston which has several pins to connect the manganin wire coil which acts as a pressure gauge. This coil has a linear resistance-pressure relationship with a pressure coefficient of 2.4×10^{-6} bar^{-1} and a temperature coefficient of $+1.0 \times 10^{-7}$ K^{-1} (Yogurtcu 1980). On the top piston, a NiCr/NiAl thermocouple is mounted to allow temperature measurement. An electrode on the sample holder is connected to the pulse generator of the pulse echo overlap system. The pressure is transmitted by "Dow Corning" 200/1000cs silicone fluid which works in a temperature range of 243K to 453K, the limits being set to prevent the fluid freezing or igniting. Rubber "O" rings and the PTFE delta rings have been used as seals between the pistons and the inner cylinder wall. The "O" rings used for room temperature and above are made from black VIT (viton). The maximum operating temperature of these "O" rings

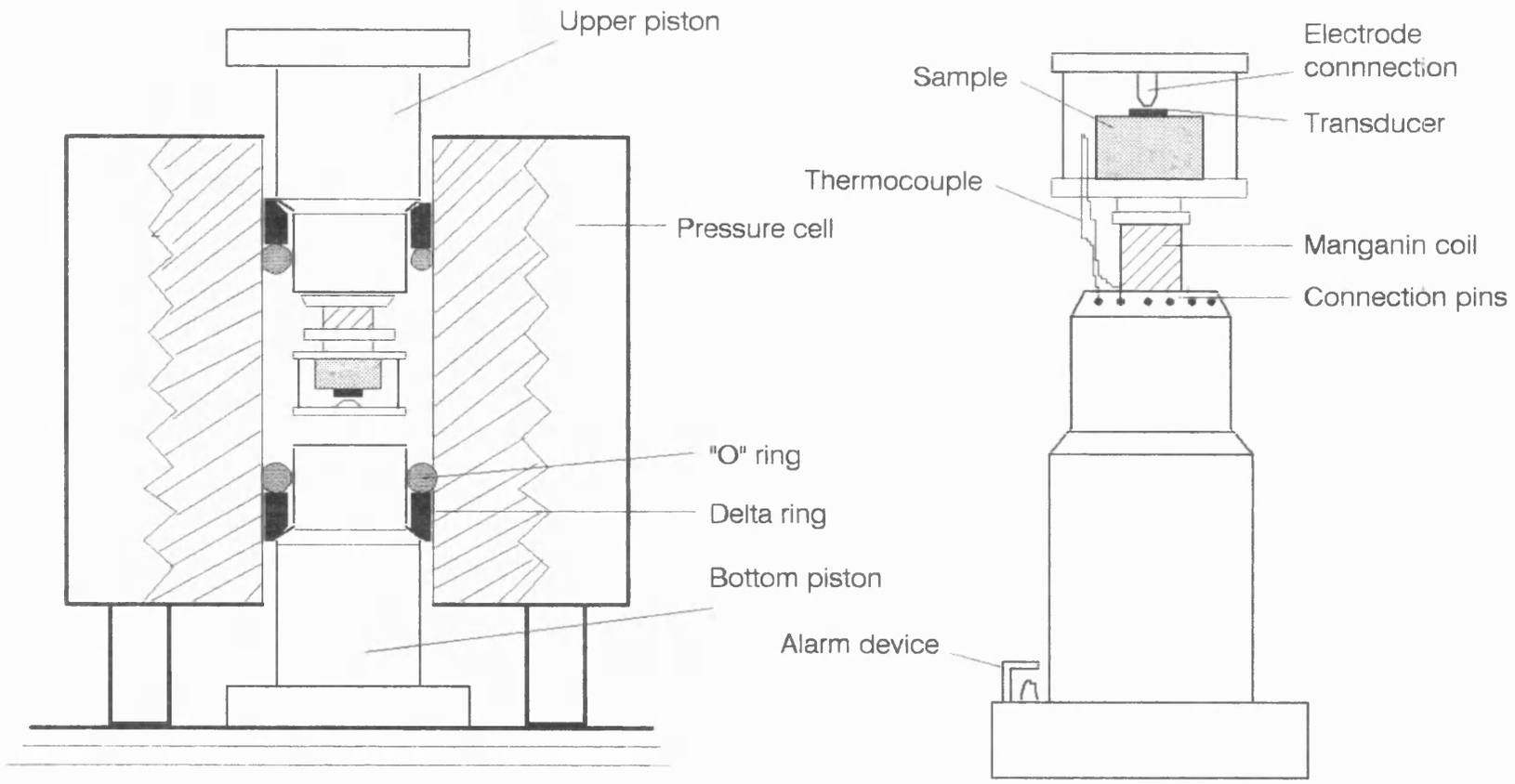

Fig. 4.12 Diagram of the hydrostatic pressure cell and sample holder.

in air is 473K but they become hard below room temperature, which results in oil leakage. Therefore brown silicone rubber "O" rings of the same diameter (Bearing Services Ltd., U.K.) are used below room temperature and these remain flexible down to 213K. Pressure is created and transmitted to the sample when the top piston is pressed downwards. A simple safety alarm device is connected to the top piston to prevent crushing of the sample if there is any leak in the seals. A "Thurlby" 1905a Intelligent multimeter (Thurlby Electronic Ltd.), with a sensitivity of $1m\Omega$, is used to measure the electric resistance of the manganin coil under pressure. The pressure data are converted from the resistance by the relation (Yogurtcu, 1980)

$$P = \frac{1}{2.4 \times 10^{-3}} \left(\frac{R}{R_0} - 1 \right) \quad \text{(kbar)} \quad , \tag{4.8}$$

where R and R_0 are the resistances of the manganin coil under arbitrary pressure P and initial pressure P_0 respectively.

Temperatures below room temperature can be obtained by pumping cold antifreeze fluid around a cooling jacket surrounding the pressure cylinder. An electrically heated jacket is used to reach temperatures above room temperature, which is controlled by a "Eurotherm" temperature controller (type 810, Eurotherm Ltd.). A "Digitron" digital thermometer (Digitron Instrumentation Ltd.) gives the temperature readings to an accuracy of 0.1K.

4.6 The uniaxial apparatus

Uniaxial pressure is applied in a manual controlled system. A diagram of the apparatus is shown in Fig. 4.13a. A screw shaft is used to apply stress. The stress is transmitted by a proving ring and a thrust rod to a sample. A thrust bearing is attached to the screw to ensure that no twisting forces are applied to the proving ring. The proving ring has been calibrated and used in its elastic deformation range, which can be used up to a maximum force of 10 kilo Newtons, to measure the stress applied. When the ring is

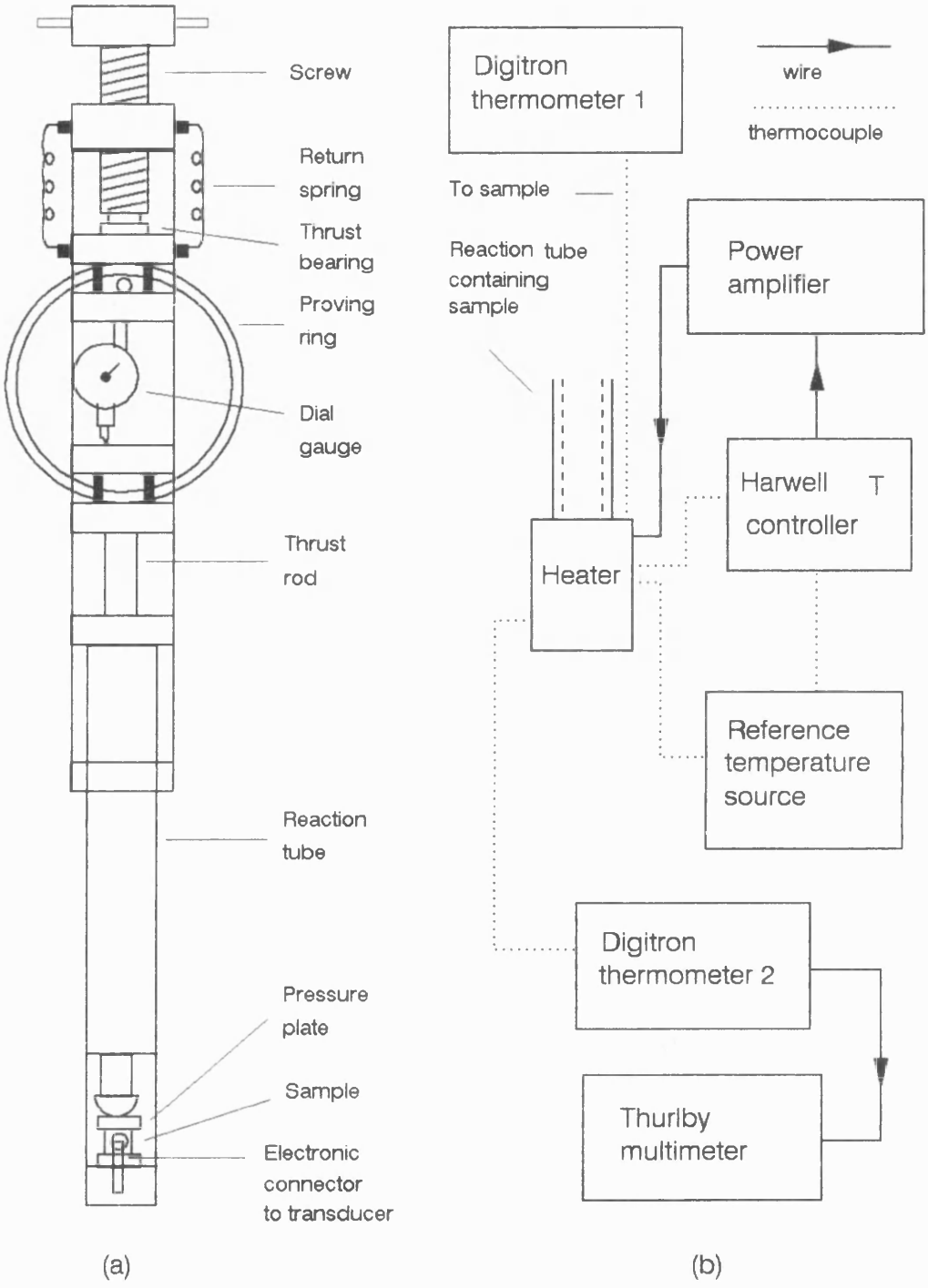

Fig. 4.13 (a) Diagram of the iniaxial stress apparatus, (b) block diagram of the temperature control system.

squeezed diametrically, a dial gauge reads the change of the diameter and the force is determined from calibration data. If the reading of the dial gauge is R and the stressed sample area is A, then the stress P applied on the sample is

$$P = \frac{(6.35R - 1.25 \times 10^{-4}R^2) \times 10^{-5}}{A} \quad \text{(bar)} \qquad (4.9)$$

where the unit of the stressed area is m^2. The thrust rod is centralised in the reaction tube by two sets of three-point nylon blocks fixed in the tube, which allow the tube to move vertically and in an almost frictionless manner. Two springs are used to release the stress when the screw is released. The end of the reaction tube is sealed with a steel plug to support the sample. The sample is placed between two stainless steel pressure plates, which have optically flat faces, to ensure an even pressure distribution on the sample. In order to align the thrust rod with the sample, a steel ball bearing has been attached to the end of the thrust rod. The electrical connection to the transducers bonded on the sample is made by using two spring probes which are fixed onto a perspex plate screwed onto the thrust rod. The complete apparatus is mounted in a frame.

To measure the temperature dependence of the uniaxial stress effects on ultrasonic velocities, a temperature control system has been used. The block diagram of the system is shown in Fig. 4.13b. The heater is a 60 Ohm nichrome wire coil wound on a copper former which is hung on the reaction tube, surrounding the sample. The temperature controller uses a NiCr/NiAl thermocouple. The measurement junction of the thermo-couple is attached to the heater, and, depending on the temperature range, the reference junction is either kept in iced water (for measurements above 273K) or dry ice (CO_2) which has a sublimation temperature of 194.7K (for measurements below 273K). The temperature of the heater is controlled by a Harwell temperature controller. The backoff voltage range of this temperature controller is from zero to 5000 μV with a resolution of 2 μV. The required temperature of the heater can be preset by tuning the 'SET CONTROL POINT' which determines the operating temperature by backing off the

thermocouple voltage by a calibrated amount. The amount of output power given to the heater is determined by the error voltage. The gain of the error amplifier is set by the 'RANGE SWITCH' control. The voltages indicated on the panel represent the thermocouple inputs necessary to give full scale deflection of the meter. The 'ZERO CONTROL' is used to zero the error amplifier with its input short circuited. The power output of the Harwell temperature controller is 15W maximum. A power amplifier is used to increase the power output to the heater by 60 watts. The temperature of the heater is monitored by a 'Digitron' thermometer and a 'Thurlby 1905a' multimeter which gives a temperature reading to 3 digits. Another 'Digitron' thermometer is used to monitor the temperature of the sample. To control the temperature efficiently, liquid nitrogen contained in a dewar surrounding the heater has been used as a cold source.

4.7 Errors of measurement and corrections

Some possible sources of error exist in the ultrasonic wave velocity measurements which include measurements of the sound wave transit time and density measurement, temperature and pressure measurement, and sample preparation. In addition, changes in the environmental conditions (e.g., temperature, pressure etc.) of the specimen during the experiments can have a considerable influence on the measured data.

Errors from echo mismatch and phase shift

In these pulse methods the time measured between echoes corresponds to the phase delay of the elastic wave in a sample with a given length. This phase delay can be affected by the bonding medium between a transducer and the sample. The travelling time measured between the pairs of echoes is (McSkimin 1961)

$$t = p\delta - \frac{p\gamma}{360f} + \frac{n}{f} \quad , \tag{4.10}$$

where δ is the true round-trip travel time, p is the number of round-trips between the echoes used in the measurement, γ is the phase angle upon reflection from the specimen-transducer interface, f is the rf frequency and n is the number of cycles of mismatch in the overlap measurement. For a proper cycle-to-cycle match between overlapped echoes, n is equal to zero (Papadakis 1967). In the pulse echo overlap method the echoes chosen to overlap were two successive echoes, i.e., $p = 1$ in our measurements, while in our pulse superposition method p was chosen to be equal to 2. Hence, Eq.(4.10) is in the form

$$t = \delta - \frac{\gamma}{360f} \tag{4.11a}$$

for the pulse echo overlap method, or

$$t = 2\delta - \frac{\gamma}{180f} \tag{4.11b}$$

for the pulse superposition method. The phase shift γ, in terms of a transmission line analysis of the sample-bond-transducer system (Williams and Lamb 1958,McSkimin 1961), is

$$\gamma = -2\tan^{-1}\left(\frac{Z_d}{jZ_s}\right) \quad , \tag{4.12}$$

where Z_s is the characteristic acoustic impedance of the sample and Z_d is the terminating impedance of the acoustic transmission line. Z_d is given by (McSkimin 1961)

$$Z_d = jZ_b \frac{(Z_b/Z_t)\tan B_b l_b + \tan B_t l_t}{(Z_b/Z_t) - \tan B_t l_t \cdot \tan B_b l_b} \quad , \tag{4.13}$$

where l_b and l_t, Z_b and Z_t, and B_b and B_t are the thickness, the characteristic impedance and the phase shift constants of the bond and transducer respectively. In this equation

$$B_b = \frac{2\pi f}{v_b} \quad , \tag{4.14}$$

and

$$B_t = \frac{2\pi f}{v_t} \quad , \tag{4.15}$$

where v_b and v_t are the sound velocities in the bond and the transducer respectively. The true round-trip time is given by

$$\delta = t + \frac{\gamma}{360f} \tag{4.16a}$$

for the pulse echo overlap method, or

$$\delta = \frac{1}{2}\left(t + \frac{\gamma}{180f}\right) \tag{4.16b}$$

for the pulse superposition method. McSkimin and Andreatch (1962) have given the experimental results of the time increment versus different bond thickness and sample impedances due to the phase shift for Dow Resin 276-V9 bonding material and X- and Y-cut quartz transducers on a quartz specimen in the X, Y and Z directions. The characteristic impedances of Dow Resin 276-V9 at 298K for longitudinal and shear waves are 2.25×10^5 kgs^{-1}m^{-2} and 0.9×10^5 kgs^{-1}m^{-2} respectively (McSkimin and Andreatch 1962). By using these results an estimation gives an average increment of about 0.02% in wave velocity.

Errors from multiple reflection in the transducer

When a pulse from a sample is incident onto an air-backed transducer through a sample-transducer boundary, the wave is partly reflected back to the sample and partly transmitted into the transducer. The transmitted wave is reflected back and forth within the transducer and part of it is transmitted back into the sample each time it strikes the boundary until it has decayed totally. Such multiple internal reflections within a transducer may lead to a considerable distortion of the pulse envelope and to a time lag of the centre of the reflected pulse relative to a signal reflected from the surface of the

transducer (Altman and Beyer 1976). Kittinger (1977) has given a method for correction of the time lag. First, it is necessary to calculate the reflection coefficient from

$$r_{st} = \frac{Z_t - Z_s}{Z_t + Z_s} \quad , \tag{4.17}$$

where Z_t and Z_s are the characteristic impedances of the transducer and the sample. Next, the echo delay time τ (in units of $1/f_0$ where f_0 is the resonance frequency of the transducer) is found from the curve given by Kittinger (1977) and then τ is transformed into the real time unit. Finally, the real transit time t_r is calculated by using $t_r = t - \tau$. The errors caused by this multiple reflection in the calculation of the wave velocity are 1~2.5%. This correction has been done in a computer programme (Brassington 1982).

Errors from diffraction

An acoustic wave emitted by a transducer into a sample is not in fact confined to a region defined by the area of the transducer and the normal to its emitting surface, since the acoustic beam spreads out into a diffraction field due to the finite size of the transducer. The wave beam from such a finite size source diverges in the sample and the wave front is neither plane nor spherical. The diffraction field is characterized by the dimensions of the transducer and the properties of the propagation medium. It introduces errors in the velocity measurement. In particular, the smaller the size of the transducer, the larger the error. A method to calculate the diffraction field and the correction for velocity measurements has been given by Papadakis (1966). Assume that the diffraction field is radiated into an anisotropic solid and is received by a circular, longitudinal transducer with electrodes covering the surfaces. The transducer is treated as a circular piston source on the plane surface of an infinite half-space and a circular receiver sensitive to both pressure and phase. The distance of a signal travelling from the generator to the receiver is

$$Z = 2nl \quad , \tag{4.18}$$

where n is the echo number and l is the thickness of the sample. The process of the analysis of the diffraction field is: (1) to find the pressure and phase profiles at several distances from the input, and (2) to find the response of the receiver to these profiles. Papadakis' results indicate that the phase change increases monotonically to a limit of $\pi/2$ from the normalized distance S=0 to infinity, where S is defined as $S = Z\lambda/a^2$ with λ being the wavelength of the ultrasonic wave, a the transducer radius and Z the echo travelling distance as in Eq. (4.18). By analysing the angular spectrum of the plane waves, James (1987) used a similar approach to that of Kharusi and Farnell (1970) to analyse a diffraction field generated by a square transducer of the same area with a circular transducer. The result agrees very closely with those of Papadakis (James 1987). The correction procedures for velocity measurements are: (1) to find the normalized distances S corresponding to two overlapped echoes respectively, using the equations given above; (2) to find the phase advance $\phi(S)$ corresponding to each S from the result of the diffraction field analysis given by Papadakis (1966) or James (1987); (3) to calculate the increment in time interval

$$\Delta t = \frac{\phi(S_n) - \phi(S_m)}{2\pi f} \quad , \tag{4.19}$$

where ϕ is in radians, n and m $(n > m)$ are the integers representing the echo numbers and f is the resonance frequency of the transducer; (4) to add the increment Δt to the measured value t of the travel time to get the true travel time

$$t_r = t + \Delta t \quad . \tag{4.20}$$

From Eq. (4.19), and the definition of S, it can be seen that the increment Δt decreases as the resonance frequency f increases. An estimation, by using Papadakis' analysis, shows that in a three-fold axis (Z axis) direction in quartz, the error caused by the diffraction field in wave velocity measurements for longitudinal waves is about twice that for shear wave, but both are less than 1%.

Errors from pressure dependence of transducer resonant frequency

In a pressure dependence measurement, such as with the hydrostatic method, an effect of pressure on a transducer is to change its resonant frequency. It is necessary to make a correction for the transducer phase shift due to this effect. The correction for the pressure derivative of the appropriate combination of elastic constants ρv_{ij}^2 is given by the expression (Davies and O'Connell 1977)

$$\left[\frac{\partial(\rho v_{ij}^2)}{\partial P}\right]_{corr} = \frac{v_{ij}^2}{l}\left[\frac{Z_t}{f_r}\left(\frac{\partial \ln f_r}{\partial P}\right)_{P=0}\right] \quad , \tag{4.21}$$

where l is the thickness of the sample, f_r is the resonance frequency of the transducer and v_{ij} is the wave velocity of the relevant mode. The $(\partial \ln f_r/\partial P)_{P=0}$ for quartz transducers are given by McSkimin et al. (1965) as follows:

$$\left(\frac{\partial \ln f_r}{\partial p}\right)_l = 1.51 \quad (10^{-11} Pa^{-1}),$$

$$\left(\frac{\partial \ln f_r}{\partial p}\right)_s = -3.68 \quad (10^{-11} Pa^{-1}).$$

The actual pressure derivatives of ρv_{ij}^2, after the correction, is then

$$\left[\frac{\partial(\rho v_{ij}^2)}{\partial P}\right] = \left[\frac{\partial(\rho v_{ij}^2)}{\partial P}\right]_m + \left[\frac{\partial(\rho v_{ij}^2)}{\partial P}\right]_{corr} \quad , \tag{4.22}$$

where $[\partial(\rho v_{ij}^2)/\partial P]_m$ is the measured data. In the present work the corrections for the pressure derivatives of ρv_{ij}^2 of the modes have been made in the programme calculating the pressure derivatives of the second order elastic constants. The resonant frequency of each mode in the measurements under hydrostatic pressure at 298K is listed in Table 4.1. The definition of the modes are given in Table 5.10. It has been found that the values of the corrections for shear modes are greater than those for longitudinal modes and that the correction is rather significant for some modes.

Table 4.1 The resonant frequency of wave modes under hydrostatic pressure

Mode	1H	2H	5H	6H	7H	9H	10H	13H
$f_r(MHz)$	12.86	10	11.24	10.26	10	10	11.02	10.46

Errors from non-parallelism and misorientation

A quartz piezoelectric transducer is a phase sensitive device. The phase variations over the area of the transducer lead to interference and therefore affect the integrated response of the transducer over its area, i.e., the measured quantity (voltage). The non-parallelism of the wave reflecting surfaces of a sample will reflect a wave through a small angle, even if it is originally plane. After multiple reflections, the different surface area elements of the transducer detect different phases of the wave, which thereby lead to an interference.

In anisotropic crystals, the value of wave velocity depends on the wave propagation direction. In the ultrasonic measurement, the wave propagation directions measured are those of pure modes (Brugger 1965b), i.e. propagations of one longitudinal and two shear mode waves are allowed. Misorientation of crystallographic axes will lead to departures from the pure mode direction and cause a mismeasurement of the ultrasonic wave mode velocities.

The samples used were prepared by the Hirst Research Centre of the GEC company at Wembley, Middlesex. In order to avoid the above effects, the samples were polished and checked carefully by the Hirst Research Centre, to make sure that the physical parallelism of each face is the same as the optical parallelism. On the right-handed XYZ block, the worst face misorientation is of the order of 25 seconds of arc and the worst parallelism is approximately 1 fringe (633 nm). All faces are flat to better than a quarter of a wavelength. On the left-handed rotated block at 45° from +Y to +Z, the

misorientation of the rotated Y'-axis is - 2′48″ and the face misorientation of the work faces is -33″ of arc. The parallelism of the working faces is approximately 0 fringe (James 1989 and 1990). The well prepared samples reduce the errors from non-parallelism and orientation to the extent that they can be ignored.

If the bond between the faces of the sample and transducer is not uniform, such interference can also occur. The effect of a poor bonding can be recognized by the quality of the echo train. Hence, in the measurements, great efforts were made to achieve good echo patterns.

Errors from other measurements

Errors possibly exist in other parameters, such as pressure, temperature, sample dimensions and density etc, due to the precision of the equipment. This kind of error causes some uncertainty of the measured data and has been estimated in the deviations of the data. When the ambient temperature changes the dimensions and density of a sample will also change due to thermal expansion. A correction for thermal expansion has been made in a calculation programme. The thermal expansion coefficients used are those for the synthetic standard grade quartz (James 1987) because those for VHPQ are unavailable.

Chapter 5 Crystalline Structure and Physical Properties of α-Quartz

5.1 Introduction

Silica, with its chemical formula of SiO_2, occurs in many forms. Sosman (1965) has divided condensed forms of SiO_2 into 22 different phases, five of them are amorphous while 17 are crystalline. The formation of each phase depends on ambient temperature, pressure etc. Among the crystalline phases, only four are stable under atmospheric pressure over the temperature ranges indicated in Table 5.1 (Sosman 1965, Megaw 1973).

Table 5.1 Four stable crystalline phases of silica

Phases	T-range (K)	Symmetry	Point group
α-quartz	0 to 846	Trigonal	32
β-quartz	846 to 1140	Hexagonal	622
High-tridymite	1140 to 1743	Hexagonal	6/mmm
High-cristoballite	1743 to 1996	Face-centred cubic	m3m

In all of these phases, the structure is 4:2 coordinated, i.e. each silicon atom is coordinated by four oxygens and each oxygen atom is coordinated by two silicon atoms. The difference in electronegativity between silicon and oxygen is 1.7. This value corresponds to a bond which is about 40 per cent ionic (Evans 1966). Therefore, the bonding in the materials is about 60 per cent covalent and 40 per cent ionic (Evans 1966, Brice 1985). Although the materials are all built from SiO_4 tetrahedron sharing each of their corners

with one other tetrahedron in a continuous three dimensional network, they have different crystal structures (see Table 5.1) due to the different arrangements of the tetrahedra. Among the isomorphous α-quartz is the most common and most widely used in industry and daily life and, is therefore the most interesting in scientific research. The next section gives a brief review of the crystalline structure of α-quartz. Whether α-quartz is natural or cultured, it has internal defects such as substitutions, interstitial or dislocations, which can affect the physical properties of the crystal. Possible impurities in α-quartz are described in section 5.3.

The numbers of independent tensor components for elasticity, piezoelectricity and electrostrictivity of a crystal are confined by its symmetry. The corresponding independent tensor components for α-quartz are given in matrix notation in section 5.4. The signs of the coefficients describing elastic, piezoelectric and electrostrictive properties of α-quartz are determined by the reference frame which is used. Different conventions for piezoelectric crystals have been used in the literature for a long time. To avoid a possible confusion, the conventions used in this work and how they affect the signs of the second order coefficients are described in section 5.4. The functions needed for determination of the third order elastic constants (TOEC), which are given in section 2.5, are dependent on the directions of wave propagation, particle displacement and stress. They are tabulated for certain acoustic wave modes propagated in α-quartz in section 5.4.

Section 5.5 reviews briefly some selected data given by other scientists for the thermodynamic and piezoelectric properties of α-quartz, which are relevant to this work.

5.2 Crystalline structure

α-Quartz is also called quartz, low quartz (Sosman 1965 and Megaw 1973), or trigonal quartz (Dieulestaint and Royer 1980). It has two enantiomorphous forms. Therefore, both right-handed and left-handed crystals can occur which are mirror images of each other. Fig. 5.1 shows a photograph of a bar of cultured quartz produced commercially (Bottom 1982) and a morphology exhibited by a perfectly grown right-handed quartz crystal. Crystals with faces s and x are rarely seen although when present, they enable us to distinguish between left- and right-handed quartz (Bottom 1982). In right-handed quartz, the s and x faces occur at the lower-right corner of a major rhombohedral face (the largest cap face) in Fig. 5.1(b). In left-handed quartz, they are at the lower-left corner of the major rhombohedral face. Fig. 5.2 (Evans 1966) shows a plan of the trigonal (or rhombohedral) structure projected perpendicular to the principal axis of left-handed α-quartz. For comparison, a projected plan of the hexagonal structure of β-quartz is also given in the figure. Only silicon atoms are shown in the figures; the oxygen atoms are tetrahedrally disposed about those of silicon in such a way that all corners of the SiO_4 tetrahedron are shared. It can be seen from the figure, that the arrangement of the Si ions of the trigonal (rhombohedral) structure appears as a distortion of the hexagonal structure. When compared with the hexagonal structure of β-quartz, the oxygen atoms in α-quartz are rotated and lifted from their positions in the hexagonal structure (Smith 1982). This distorted-like arrangement of the silicon and oxygen atoms makes α-quartz lose the six-fold axis and mirror planes existing in the hexagonal structure of β-quartz. The positions of the silicon and oxygen atoms in right-handed α-quartz are shown in Fig. 5.3 (Dieulestaint and Royer 1980) with the principle c axis perpendicular to the paper. Marks inside the circles stand for the vertical altitude of atoms with the c value being taken as unity. Hence, silicon atoms are at height $0, \frac{1}{3}, \frac{2}{3}$ and oxygen atoms are at

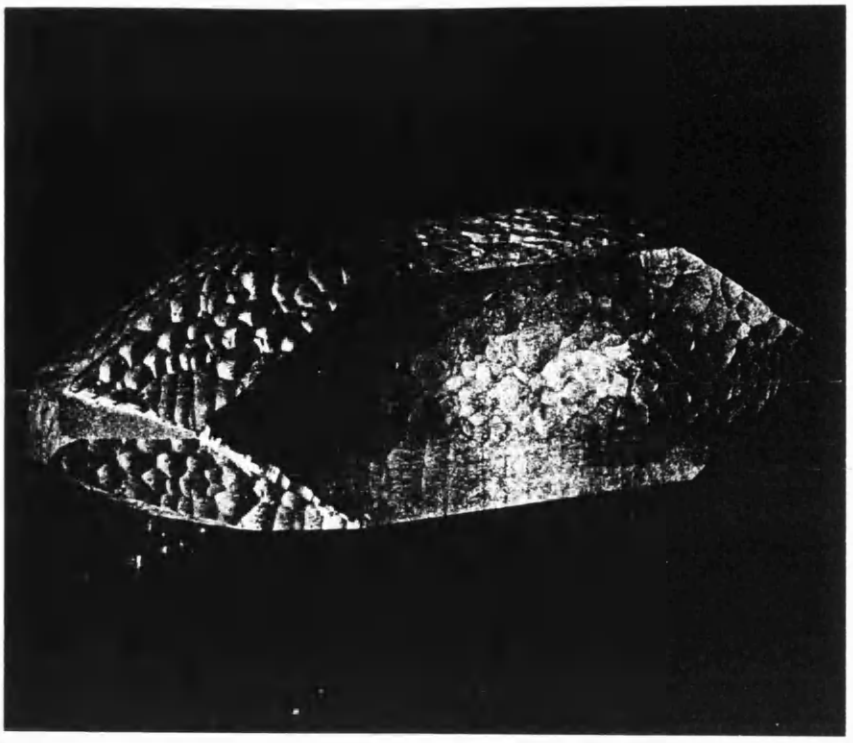

Fig. 5.1 (a) A photograph of a bar of cultured α-quartz crystal (by Sawyer Research Products, Inc.).

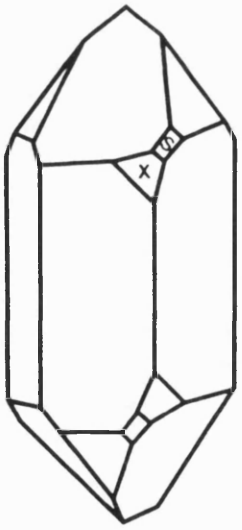

Fig. 5.1 (b) The growth morphology of a right-handed α-quartz crystal (Dieulesaint and Royer, 1980).

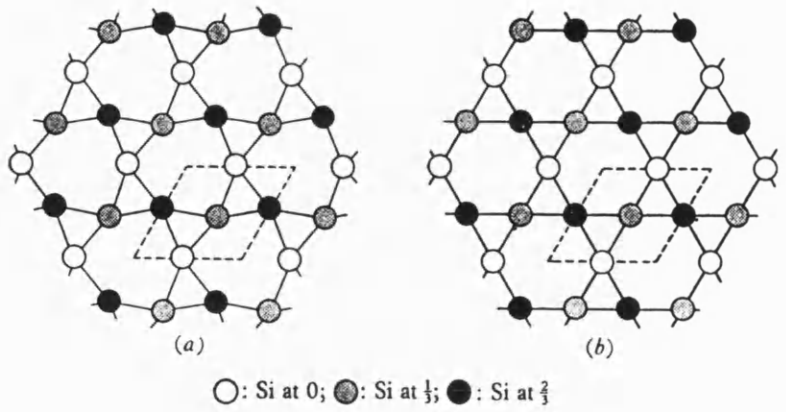

Fig. 5.2 (a) Plan of the trigonal structure of α-quartz, projected perpendicular to the principal axis. (b) Plan of the hexagonal structure of β-quartz projected on a plane perpendicular to the Z-axis. Only silicon atoms are shown (by Evans, 1966).

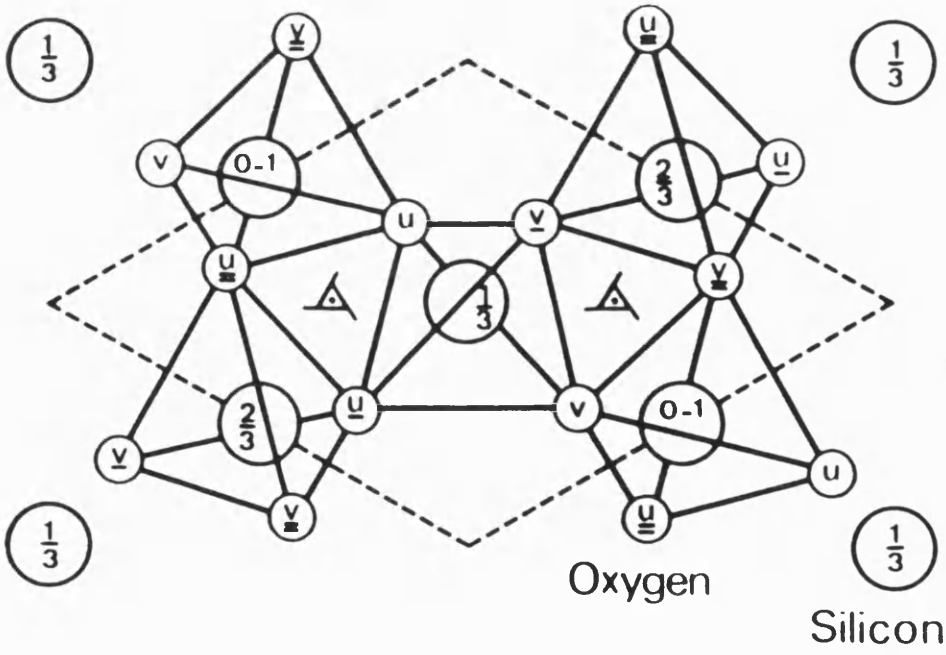

Fig. 5.3 α-quartz structure has a screw axis (3_1) perpendicular to the paper plane. Marks in the circles stand for the vertical altitude of atoms (see the text), the length of the c edge being taken as unity (Dieulesaint and Royer, 1980).

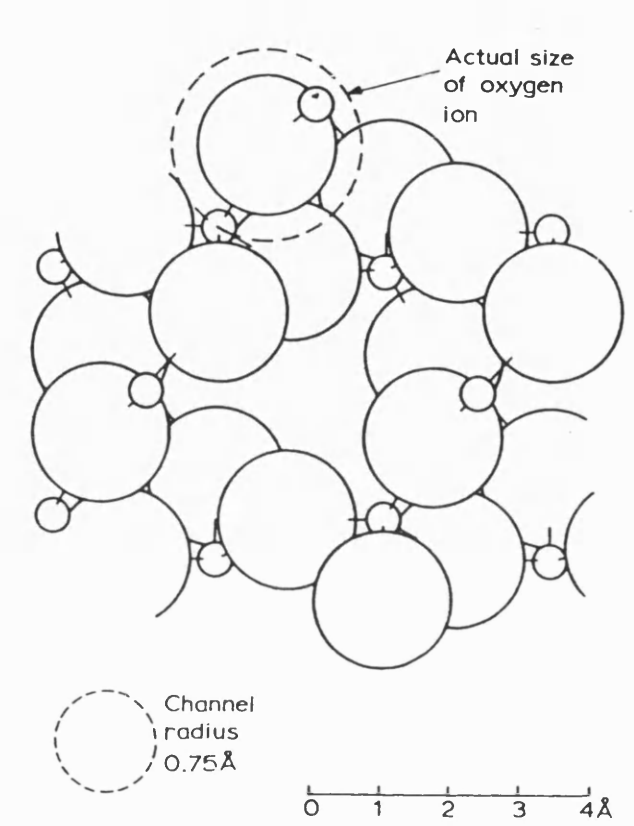

Fig. 5.4 A vertical projection of the α-quartz structure. The c axis is normal to the plane of the diagram. The small circles are Si atoms and the large ones O atoms (Brice, 1985).

densities in VHPQ are typically 10^2-10^3 times lower. A review of VHPQ and a comparison of its properties with those of the standard synthetic quartz have been given by James (1987).

5.4 Symmetry and the elastic, piezoelectric and electrostrictive coefficients of α-quartz

The structure of α-quartz belongs to the class 32 symmetry (Schoenflies symbol D_3, Laue group RI), which is characterized by a *c* axis of threefold symmetry, with three *a* axes of twofold symmetry perpendicular to the *c* axis and mutually orientated to angles of 120°. It does not have a centre of inversion and any mirror plane symmetry. The right-handed enantiomorph has the space group $P3_221$, while the left-handed one is in the space group $P3_121$. The definition of the X, Y and Z axes is shown in Fig. 5.5 (IEEE 1978). The Z axis is parallel to the *c* axis. The X axis coincides in direction with any one of the *a* axes. The Y axis is perpendicular to Z and X, and is so oriented as to form a right-handed system. According to the convention of the IEEE Standard on Piezoelectricity of 1978, the positive sense of the X axis is the sense such that the piezoelectric strain constant d_{11} is positive for a right-handed crystal. The signs of all the piezoelectric coefficients for right- and left-handed quartz in this convention are as follows:

right-handed quartz	left-handed quartz
$e_{11}>0$, $e_{14}>0$,	all have the opposite signs to that
$d_{11}>0$, $d_{14}<0$,	of right-handed quartz.

All of the elastic constants are positive for left- and right-handed quartz. Under the convention, right-handed axial systems are used for all crystals, whether right- or left-handed as shown in Fig. 5.5, and in this case, the left-handed form should be regarded

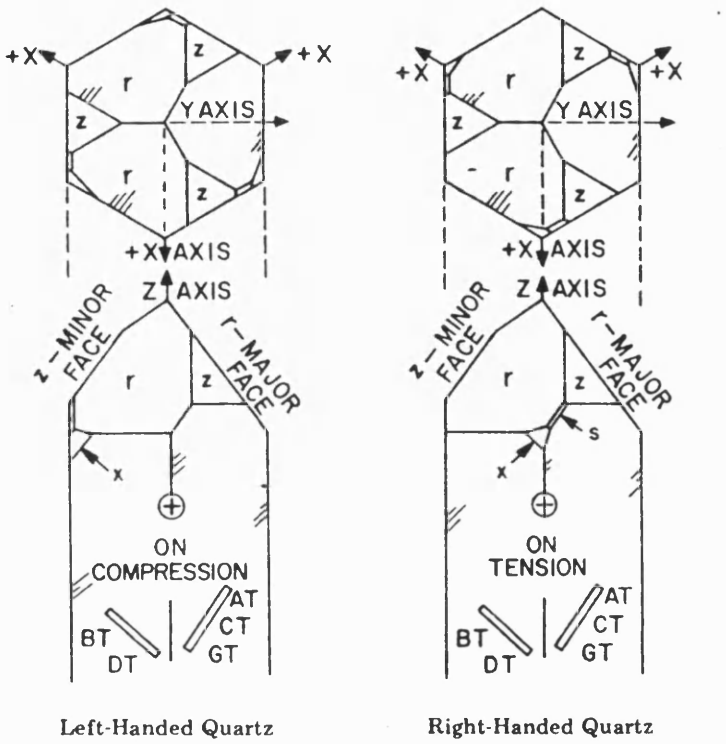

Left-Handed Quartz Right-Handed Quartz

Fig. 5.5 The definitions of the axes of left- and right-handed quartz and some principal cuts (IEEE Standard on Piezoelectricity, 176-1978).

as the crystallographic inversion of the right-handed form, rather than its mirror image (IEEE 1978).

The requirement that the elastic and piezoelectric tensor components be invariant under a symmetry operation leads to a reduction in the number of the independent coefficients. The non-zero second order coefficients C_{IJ}, $e_{i\alpha}$ and ε_{ij} for α-quartz crystal are listed in Table 5.2; only six C_{IJ} , two $e_{i\alpha}$ and two ε_{ij} are independent.

Table 5.2 Second order elastic stiffness , piezo-electric and dielectric coefficients of α-quartz

C_{11}	C_{12}	C_{13}	C_{14}	0	0	e_{11}	0	0
C_{12}	C_{11}	C_{13}	$-C_{14}$	0	0	$-e_{11}$	0	0
C_{13}	C_{13}	C_{33}	0	0	0	0	0	0
C_{14}	$-C_{14}$	0	C_{44}	0	0	e_{14}	0	0
0	0	0	0	C_{44}	C_{14}	0	$-e_{14}$	0
0	0	0	0	C_{14}	C_{66}	0	$-e_{11}$	0
e_{11}	$-e_{11}$	0	e_{14}	0	0	ε_{11}	0	0
0	0	0	0	$-e_{14}$	$-e_{11}$	0	ε_{11}	0
0	0	0	0	0	0	0	0	ε_{33}

In this table $C_{66} = \frac{1}{2}(C_{11} - C_{12})$.

According to Eq. (2.148) and (2.152) the SOEC and SOPC can be determined by measuring the natural ultrasonic wave velocities W . The formulae for W for 13 wave modes propagated in α-quartz are given in Table 5.3, following the notations given by McSkimin et al. (1965), with the sign "| " meaning "perpendicular to".

Table 5.3 Mode configuration and corresponding formulae for natural velocity W for α-quartz

Mode	Prop. Dir.	Pol. dir.	Type[a]	$w = (\rho_0 W^2)_{P=0}$
1	X	X	L	$C_{11}^{S,E} + e_{11}^2/\varepsilon_{11}^{\eta}$
2	X	$\perp$ X	S	$\left(C_{66}^{S,E} + C_{44}^{S,E} - \sqrt{(C_{66}^{S,E} - C_{44}^{S,E})^2 + 4(C_{14}^{S,E})^2}\right)/2$
3	X	$\perp$ X	S	$\left(C_{66}^{S,E} + C_{44}^{S,E} + \sqrt{(C_{66}^{S,E} - C_{44}^{S,E})^2 + 4(C_{14}^{S,E})^2}\right)/2$
4	Y	Y	QL	$\left(C_{11}^{S,E} + C_{44}^{S,E} + \sqrt{(C_{11}^{S,E} - C_{44}^{S,E})^2 + 4(C_{14}^{S,E})^2}\right)/2$
5	Y	$\perp$ X	QS	$\left(C_{11}^{S,E} + C_{44}^{S,E} - \sqrt{(C_{11}^{S,E} - C_{44}^{S,E})^2 + 4(C_{14}^{S,E})^2}\right)/2$
6	Y	X	S	$C_{66}^{S,E} + e_{11}^2/\varepsilon_{11}^{\eta}$
7	Z	Z	L	$C_{33}^{S,E}$
8	Z	X	S	$C_{44}^{S,E}$
9	Z	Y	S	$C_{44}^{S,E}$
10	Y+45° [b]	$\perp$ X	QL	$[(C_{11}^{S,E} + C_{33}^{S,E})/2 + C_{44}^{S,E} - C_{14}^{S,E} + \sqrt{(C_{11}^{S,E} - C_{33}^{S,E} - 2C_{14}^{S,E})^2/4 + (C_{13}^{S,E} + C_{44}^{S,E} - C_{14}^{S,E})^2}]/2$
11	Y+45° [b]	$\perp$ X	QS	$[(C_{11}^{S,E} + C_{33}^{S,E})/2 + C_{44}^{S,E} - C_{14}^{S,E} - \sqrt{(C_{11}^{S,E} - C_{33}^{S,E} - 2C_{14}^{S,E})^2/4 + (C_{13}^{S,E} + C_{44}^{S,E} - C_{14}^{S,E})^2}]/2$
12	Y+45° [b]	X	S	$(C_{66}^{S,E} + C_{44}^{S,E})/2 + C_{14}^{S,E} + (e_{11} + e_{14})^2/(2\varepsilon_{11}^{\eta} + 2\varepsilon_{33}^{\eta})$
13	Y-45° [c]	X	S	$(C_{66}^{S,E} + C_{44}^{S,E})/2 - C_{14}^{S,E} + (e_{11} - e_{14})^2/(2\varepsilon_{11}^{\eta} + 2\varepsilon_{33}^{\eta})$

a L=longitudinal, S=shear, QL=quasi-longitudinal, QS=quasi-shear.

b turning +45° around X.

c turning -45° around X.

α-quartz has 14 independent and 17 related third order elastic constants (TOEC), making up 31 non-zero coefficients. The fourteen independent TOEC are listed in Table 5.4.

Table 5.4 14 independent TOEC C_{IJK} of α-quartz

C_{111}	C_{113}	C_{123}	C_{133}	C_{144}	C_{222}	C_{344}
C_{112}	C_{114}	C_{124}	C_{134}	C_{155}	C_{333}	C_{444}

The non-zero TOEC of α-quartz satisfy the relations in Table 5.5 (Thurston 1974).

Table 5.5 The relations between the TOEC C_{IJK}

$C_{122}=C_{111}+C_{112}-C_{222}$	$C_{233}=C_{113}$	$C_{355}=C_{344}$
$C_{156}=(C_{114}+3C_{124})/2$	$C_{234}=-C_{134}$	$C_{356}=C_{134}$
$C_{166}=(-2C_{111}-C_{112}$	$C_{244}=C_{155}$	$C_{366}=(C_{113}-C_{123})/2$
$+3C_{222})/4$	$C_{255}=C_{144}$	$C_{455}=-C_{444}$
$C_{223}=C_{113}$	$C_{256}=(C_{114}-C_{124})/2$	$C_{456}=(-C_{144}+C_{155})/2$
$C_{224}=-(C_{114}+2C_{124})$	$C_{266}=(2C_{111}-C_{112}-C_{222})/4$	$C_{466}=C_{124}$

There are 23 non-zero third order piezoelectric coefficients (TOPC) for α-quartz crystal, 8 being independent. To be consistent with the normal convention used in recent years (Kittinger et al. 1986, Hruska 1987, Adam et al. 1988, Hruska 1989), the independent piezo-electric coefficients are chosen as listed in Table 5.6.

Table 5.6 8 independent TOPC e_{IJK} of α-quartz

e_{111}	e_{113}	e_{114}	e_{122}	e_{124}	e_{134}	e_{144}	e_{315}

The relations between the non-zero TOPC are given in Table 5.7 (Gagnepain and Besson 1975).

Table 5.7 The relations between the TOPC e_{IJK}

$e_{112}=-(e_{111}+e_{122})/2$	$e_{215}=-e_{124}$	$e_{236}=-e_{113}$
$e_{123}=-e_{113}$	$e_{216}=(e_{111}+3e_{122})/4$	$e_{245}=e_{144}$
$e_{155}=-e_{144}$	$e_{225}=-e_{114}$	$e_{246}=(e_{114}-e_{124})/2$
$e_{156}=(e_{124}-e_{114})/2$	$e_{226}=-(e_{122}+3e_{111})/4$	$e_{325}=-e_{315}$
$e_{166}=-(e_{111}+e_{122})/2$	$e_{235}=-e_{134}$	$e_{346}=-e_{315}$

α-quartz crystals have 8 independent electrostrictive coefficients. The total number of non-zero electrostrictive coefficients is 18. Table 5.8 lists the independent coefficients.

Table 5.8 The independent tensor components of electrostrictive coefficients l_{IJ} of α-quartz

l_{11}	l_{12}	l_{13}	l_{14}	l_{31}	l_{33}	l_{41}	l_{44}

The relations between the nonzero electrostrictive coefficients are as in Table 5.9 (Gagnepain and Besson 1975).

Table 5.9 The relations between the electrostrictive coefficients l_{IJ}

$l_{21}=l_{12}$	$l_{32}=l_{31}$	$l_{56}=l_{41}$
$l_{22}=l_{11}$	$l_{42}=-l_{41}$	$l_{65}=2l_{14}$
$l_{23}=l_{13}$	$l_{55}=l_{44}$	$l_{66}=(l_{11}-l_{12})$
$l_{24}=-l_{14}$		

The TOEC for α-quartz can be determined by using Eqs. (2.149)-(2.162) when the TOPC and the electrostrictive coefficients are known. The functions F_H , G_H , H_H , F_U , G_U and H_U in the equations are listed in Tables 5.10-5.15 for the ultrasonic wave modes in α-quartz under hydrostatic pressure or uniaxial compression. The definitions of the modes follows those of Thurston et al. (1966). The expressions for the G_U and H_U for many modes under uniaxial compression are lengthy; therefore, only those for measured modes are given here. In the tables $\vec{N}$ and $\vec{U}$ are the unit vectors along direction of wave propagation and particle displacement respectively. $\vec{M}$ is the unit vector along the direction of applied uniaxial stress.

Table 5.10 The function F_H for α-quartz

Mode	N_1	N_2	N_3	U_1	U_2	U_3	F_H
1H	1	0	0	1	0	0	s_1
2H	1	0	0	0	β_1	β_2	$\beta_1^2 s_1 + \beta_2^2 s_3$
3H	1	0	0	0	β_2	$-\beta_1$	$\beta_2^2 s_1 + \beta_1^2 s_3$
4H	0	1	0	0	$-\gamma_2$	γ_1	$\gamma_2^2 s_1 + \gamma_1^2 s_3$
5H	0	1	0	0	γ_1	γ_2	$\gamma_1^2 s_1 + \gamma_2^2 s_3$
6H	0	1	0	1	0	0	s_1
7H	0	0	1	0	0	1	s_3
8H	0	0	1	0	1	0	s_1
9H	0	0	1	0	0	1	s_1
10H	0	$1/\sqrt{2}$	$1/\sqrt{2}$	0	θ_1	θ_2	$\theta_1^2 s_1 + \theta_2^2 s_3$
11H	0	$1/\sqrt{2}$	$1/\sqrt{2}$	0	θ_2	$-\theta_1$	$\theta_2^2 s_1 + \theta_1^2 s_3$
12H	0	$1/\sqrt{2}$	$1/\sqrt{2}$	1	0	0	s_1
13H	0	$-1/\sqrt{2}$	$1/\sqrt{2}$	1	0	0	s_1

In Table 5.10 the expressions of F_H for mode 1H to 11H are from Thurston et al. (1966) and

$$s_1 = s_{11}^T + s_{12}^T + s_{13}^T \quad , \qquad s_3 = 2s_{13}^T + s_{33}^T \quad , \tag{5.1}$$

$$\beta_1 = \cos\left[ctg^{-1}\left(\frac{C_{14}^{S,E}}{w_2 - C_{66}^{S,E}} \right)\right] \quad , \qquad \beta_2 = \sin\left[ctg^{-1}\left(\frac{C_{14}^{S,E}}{w_2 - C_{66}^{S,E}} \right)\right] \quad , \tag{5.2}$$

$$\gamma_1 = \cos\left[ctg^{-1}\left(\frac{-C_{14}^{S,E}}{w_5 - C_{11}^{S,E}} \right)\right] \quad , \qquad \gamma_2 = \sin\left[ctg^{-1}\left(\frac{-C_{14}^{S,E}}{w_5 - C_{11}^{S,E}} \right)\right] \quad , \tag{5.3}$$

$$\theta_1 = \cos\left[ctg^{-1}\left(\frac{\frac{1}{2}(C_{13}^{S,E} - C_{14}^{S,E} + C_{44}^{S,E})}{w_{10} - \frac{1}{2}(C_{11}^{S,E} + C_{44}^{S,E} - C_{14}^{S,E})} \right)\right] \quad , \tag{5.4}$$

$$\theta_2 = \sin\left[ctg^{-1}\left(\frac{\frac{1}{2}(C_{13}^{S,E} - C_{14}^{S,E} + C_{44}^{S,E})}{w_{10} - \frac{1}{2}(C_{11}^{S,E} + C_{44}^{S,E} - C_{14}^{S,E})} \right)\right] \quad . \tag{5.5}$$

Table 5.11 The function G_H for α-quartz

Mode	G_H
1H	$s_1(C_{111} + C_{112}) + s_3 C_{113}$
2H	$\frac{1}{2}\beta_1^2[s_1(C_{222} - C_{112}) + s_3(C_{113} - C_{123})] + 2\beta_1\beta_2[s_1(C_{114} + C_{124}) + s_3 C_{134}]$ $+ \beta_2^2[s_1(C_{144} + C_{155}) + s_3 C_{344}]$
3H	$\frac{1}{2}\beta_2^2[s_1(C_{222} - C_{112}) + s_3(C_{113} - C_{123})] - 2\beta_1\beta_2[s_1(C_{114} + C_{124}) + s_3 C_{134}]$ $+\beta_1^2[s_1(C_{144} + C_{155}) + s_3 C_{344}]$
4H	$\gamma_2^2[s_1(C_{111} + C_{112}) + s_3 C_{113}] + 2\gamma_1\gamma_2[s_1(C_{114} + C_{124}) + s_3 C_{134}]$ $+\gamma_1^2[s_1(C_{144} + C_{155}) + s_3 C_{344}]$
5H	$\gamma_1^2[s_1(C_{111} + C_{112}) + s_3 C_{113}] - 2\gamma_1\gamma_2[s_1(C_{114} + C_{124}) + s_3 C_{134}]$ $+\gamma_2^2[s_1(C_{144} + C_{155}) + s_3 C_{344}]$

Table 5.11 (Continued)

Mode	G_H
6H	$\frac{1}{2}[s_1(C_{222}-C_{112})+s_3(C_{113}-C_{123})]$
7H	$2s_1C_{133}+s_3C_{333}$
8H=9H	$s_1(C_{144}+C_{155})+s_3C_{344}$
10H	$\frac{1}{2}\theta_1^2[s_1(C_{111}+C_{112})+s_3C_{113}]+\theta_1\theta_2[s_1(C_{113}+C_{123})+s_3C_{133}]$ $-(\theta_1^2+\theta_1\theta_2)[s_1(C_{114}+C_{124})+s_3C_{134}]+\frac{1}{2}\theta_2^2(2s_1C_{133}+s_3C_{333})$ $+\frac{1}{2}(1+2\theta_1\theta_2)[s_1(C_{144}+C_{155})+s_3C_{344}]$
11H	$\frac{1}{2}\theta_2^2[s_1(C_{111}+C_{112})+s_3C_{113}]-\theta_1\theta_2[s_1(C_{113}+C_{123})+s_3C_{133}]$ $-(\theta_2^2-\theta_1\theta_2)[s_1(C_{114}+C_{124})+s_3C_{134}]+\frac{1}{2}\theta_1^2(2s_1C_{133}+s_3C_{333})$ $+\frac{1}{2}(1-2\theta_1\theta_2)[s_1(C_{144}+C_{155})+s_3C_{344}]$
12H	$\frac{1}{2}[s_1\left(-\frac{1}{2}C_{112}+2C_{114}+2C_{124}+C_{144}+C_{155}+\frac{1}{2}C_{222}\right)$ $+s_3\left(\frac{1}{2}C_{113}-\frac{1}{2}C_{123}+2C_{134}+C_{344}\right)]$
13H	$\frac{1}{2}[s_1\left(-\frac{1}{2}C_{112}-2C_{114}-2C_{124}+C_{144}+C_{155}+\frac{1}{2}C_{222}\right)$ $+s_3\left(\frac{1}{2}C_{113}-\frac{1}{2}C_{123}+2C_{134}+C_{344}\right)]$

Table 5.12 The function H_H for α-quartz

Mode	H_H
1H	$[s_1(e_{111}-e_{122})+2s_3e_{113}]\left(\frac{e_{11}}{\varepsilon_{11}^{\eta}}\right)-[s_1(l_{11}+l_{12})+s_3l_{13}]\left(\frac{e_{11}}{\varepsilon_{11}^{\eta}}\right)^2$
6H	$[s_1(e_{111}-e_{122})+2s_3e_{113}]\left(\frac{e_{11}}{\varepsilon_{11}^{\eta}}\right)-[s_1(l_{11}+l_{12})+s_3l_{13}]\left(\frac{e_{11}}{\varepsilon_{11}^{\eta}}\right)^2$
12H	$[s_1(e_{111}-e_{122}+2e_{114}+2e_{124})+s_3(e_{113}+e_{134}]\left(\frac{e_{11}+e_{14}}{\varepsilon_{11}^{\eta}+\varepsilon_{33}^{\eta}}\right)$
	$-\frac{1}{2}[s_1(l_{11}+l_{12}+2l_{31})+s_3(l_{13}+l_{33})]\left(\frac{e_{11}+e_{14}}{\varepsilon_{11}^{\eta}+\varepsilon_{33}^{\eta}}\right)^2$
13H	$[s_1(e_{111}-e_{122}-2e_{114}-2e_{124})+s_3(e_{113}-e_{134}]\left(\frac{e_{11}-e_{14}}{\varepsilon_{11}^{\eta}+\varepsilon_{33}^{\eta}}\right)$
	$-\frac{1}{2}[s_1(l_{11}+l_{12}+2l_{31})+s_3(l_{13}+l_{33})]\left(\frac{e_{11}-e_{14}}{\varepsilon_{11}^{\eta}+\varepsilon_{33}^{\eta}}\right)^2$

$H_H = 0$ for other modes.

Table 5.13 The function F_U for α-quartz (Thurston et al. (1966))

Mode	$\vec{N}$	$\vec{U}$	$\vec{M}$	F_U
1A	1 0 0	1 0 0	0 1 0	s_{12}^T
1B			0 0 1	s_{13}^T
2A	1 0 0	0 β_1 β_2	0 1 1	$\beta_1^2 s_{11}^T + \beta_2^2 s_{13}^T + \beta_1\beta_2 s_{14}^T$
2B			0 0 0	$\beta_1^2 s_{13}^T + \beta_2^2 s_{33}^T$
3A	1 0 0	0 $-\beta_1$ β_2	0 1 0	$\beta_2^2 s_{11}^T + \beta_1^2 s_{13}^T - \beta_1\beta_2 s_{14}^T$
3B			0 0 1	$\beta_2^2 s_{13}^T + \beta_1^2 s_{33}^T$

Table 5.13 The function F_U for α-quartz

Mode	$\vec{N}$	$\vec{U}$	$\vec{M}$	F_U
4A	0 1 0	$0\ \gamma_1\ -\gamma_2$	1 0 0	$\gamma_2^2 s_{12}^T + \gamma_1^2 s_{13}^T - \gamma_1\gamma_2 s_{14}^T$
4B			0 0 1	$\gamma_2^2 s_{13}^T + \gamma_1^2 s_{33}^T$
5A	0 1 0	$0\ \gamma_2\ \gamma_1$	1 0 0	$\gamma_1^2 s_{12}^T + \gamma_2^2 s_{13}^T + \gamma_1\gamma_2 s_{14}^T$
5B			0 0 1	$\gamma_1^2 s_{13}^T + \gamma_2^2 s_{33}^T$
6A	0 1 0	1 0 0	1 0 0	s_{11}^T
6B			0 0 1	s_{13}^T
7A	0 0 1	0 0 1	1 0 0	s_{13}^T
7B			0 1 0	s_{13}^T
8A	0 0 1	0 1 0	1 0 0	s_{11}^T
8B			0 1 0	s_{12}^T
9A	0 0 1	0 0 1	1 0 0	s_{12}^T
9B			0 1 0	s_{11}^T
10A	$0\ \frac{1}{\sqrt{2}}\ \frac{1}{\sqrt{2}}$	$0\ \theta_2\ \theta_1$	1 0 0	$\theta_1^2 s_{12}^T + \theta_2^2 s_{13}^T + \theta_1\theta_2 s_{14}^T$
10B			$0\ \frac{1}{\sqrt{2}}\ -\frac{1}{\sqrt{2}}$	$[s_{13}^T + \theta_1^2(s_{11}^T + s_{12}^T) + \theta_2^2 s_{33}^T + \theta_1\theta_2(s_{44}^T + s_{14}^T)]/2$
11A	$0\ \frac{1}{\sqrt{2}}\ \frac{1}{\sqrt{2}}$	$0\ -\theta_1\ \theta_2$	1 0 0	$\theta_2^2 s_{12}^T + \theta_1^2 s_{13}^T - \theta_1\theta_2 s_{14}^T$
11B			$0\ \frac{1}{\sqrt{2}}\ -\frac{1}{\sqrt{2}}$	$[s_{13}^T + \theta_2^2(s_{11}^T + s_{12}^T) + \theta_1^2 s_{33}^T - \theta_1\theta_2(s_{44}^T + s_{14}^T)]/2$
12A	$0\ \frac{1}{\sqrt{2}}\ \frac{1}{\sqrt{2}}$	1 0 0	1 0 0	s_{11}^T
12B			$0\ -\frac{1}{\sqrt{2}}\ \frac{1}{\sqrt{2}}$	$(s_{12}^T + s_{13}^T - s_{14}^T)/2$
13A	$0\ \frac{1}{\sqrt{2}}\ -\frac{1}{\sqrt{2}}$	1 0 0	1 0 0	s_{11}^T
13B			$0\ \frac{1}{\sqrt{2}}\ \frac{1}{\sqrt{2}}$	$(s_{12}^T + s_{13}^T + s_{14}^T)/2$

Table 5.14 The function G_U for measured modes of α-quartz (Thurston et al. (1966))

Mode	G_U
1A	$s_{12}^T C_{111} + s_{11}^T C_{112} + s_{13}^T C_{113} - s_{14}^T C_{114}$
1B	$s_{13}^T (C_{111} + C_{112}) + s_{33}^T C_{113}$
4B	$\gamma_2^2 [s_{13}^T (C_{111} + C_{112}) + s_{33}^T C_{113}] - 2\gamma_1\gamma_2 [s_{13}^T (C_{114} + C_{124}) + s_{33}^T C_{134}]$ $+\gamma_1^2 [s_{13}^T (C_{144} + C_{155}) + s_{33}^T C_{344}]$
6A	$-\frac{1}{4}[s_{66}^T C_{111} + (s_{11}^T + s_{12}^T) C_{112}] + \frac{1}{2} s_{13}^T (C_{113} - C_{123}) + s_{14}^T C_{124} + \frac{1}{4}(3s_{11}^T - s_{12}^T) C_{222}$
6B	$\frac{1}{2}[s_{13}^T (C_{112} + C_{222}) + s_{33}^T (C_{113} - C_{123})]$
7A	$(s_{11}^T + s_{12}^T) C_{133} + s_{13}^T C_{333}$
8A	$s_{12}^T C_{144} + s_{11}^T C_{155} + s_{13}^T C_{344} - s_{14}^T C_{444}$
8B	$s_{11}^T C_{144} + s_{12}^T C_{155} + s_{13}^T C_{344} + s_{14}^T C_{444}$

Table 5.14 (Continue)

Mode	G_U
10B	$\frac{1}{4}\theta_1^2(s_{12}^T+s_{13}^T-s_{14}^T)(C_{111}+C_{112})+[\frac{1}{4}\theta_1^2(s_{13}^T+s_{33}^T)$ $+\frac{1}{2}\theta_1\theta_2(s_{11}^T+s_{13}^T+s_{14}^T)]C_{113}+[-\frac{1}{2}\theta_1\theta_2(s_{11}^T+s_{13}^T+s_{14}^T)$ $-\frac{1}{4}\theta_1^2(2s_{11}^T+2s_{13}^T+s_{14}^T-s_{44}^T)]C_{114}+\frac{1}{2}\theta_1\theta_2(s_{12}^T+s_{13}^T-s_{14}^T)C_{123}$ $+\left[(\theta_1^2+\theta_1\theta_2)\left(-s_{11}^T+\frac{1}{2}s_{12}^T-\frac{1}{2}s_{13}^T\right)+\frac{1}{2}\theta_1^2(s_{44}^T-2s_{14}^T)-\frac{3}{2}\theta_1\theta_2 s_{14}^T\right]C_{124}$ $+\left[\frac{1}{4}\theta^2(s_{11}^T+s_{12}^T+2s_{13}^T)+\frac{1}{2}\theta_1\theta_2(s_{13}^T+s_{33}^T)\right]C_{133}+[-\frac{1}{4}(\theta_2^2+\theta_1\theta_2)s_{66}^T$ $-\left(\frac{1}{2}\theta_1\theta_2-\theta^2\right)s_{14}^T+\frac{1}{2}\theta_1\theta_2 s_{44}^T-\frac{1}{2}(\theta_1^2+\theta_1\theta_2)(s_{13}^T+s_{33}^T)]C_{134}$ $+\frac{1}{4}(1+2\theta_1\theta_2)(s_{12}^T+s_{13}^T-s_{14}^T)C_{144}+[\frac{1}{4}(1+2\theta_1\theta_2)(s_{11}^T+s_{13}^T)$ $+\frac{1}{4}(\theta_2^2-\theta_1^2)s_{14}^T-\frac{1}{2}(\theta_1\theta_2+\theta_1^2)s_{14}^T]C_{155}+\left(\frac{1}{8}s_{66}^T+\frac{1}{2}s_{14}^T\right)\theta_1^2C_{222}$ $+\frac{1}{4}\theta_2^2(s_{13}^T+s_{33}^T)C_{333}+[\frac{1}{4}(1+2\theta_1\theta_2)(s_{13}^T+^T_{33})$ $-\frac{1}{2}(\theta_2^2+\theta_1\theta_2)(s_{14}^T+s_{44}^T)]C_{344}-\frac{1}{4}(1+2\theta_1\theta_2)(s_{14}^T+s_{44}^T)C_{444}$

Table 5.15 The function H_U for measured modes of α-quartz

Mode	H_U
1A	$[(2s_{12}^T - s_{11}^T)e_{111} - s_{12}^T e_{122} - 2s_{14}^T e_{144}]\frac{e_{11}}{\varepsilon_{11}^\eta} - (s_{12}^T l_{11} + s_{11}^T l_{12} + s_{13}^T l_{13} - s_{14}^T l_{14})\left(\frac{e_{11}}{\varepsilon_{11}^\eta}\right)^2$
1B	$s_{13}^T(e_{111} - e_{122})\frac{e_{11}}{\varepsilon_{11}^\eta} - [s_{13}^T(l_{11} + l_{12}) + s_{33}^T l_{13}]\left(\frac{e_{11}}{\varepsilon_{11}^\eta}\right)^2$
6A	$\left[\frac{1}{4}(s_{11}^T - 3s_{12}^T)e_{111} + \frac{1}{4}(3s_{11}^T - s_{12}^T)e_{122} - s_{13}^T e_{113} + \frac{1}{2}s_{14}^T(e_{114} - e_{124})\right]\left(\frac{e_{11}}{\varepsilon_{11}^\eta}\right)$ $- (s_{12}^T l_{11} + s_{11}^T l_{12} + s_{13}^T l_{13} - s_{14}^T l_{14})\left(\frac{e_{11}}{\varepsilon_{11}^\eta}\right)^2$
6B	$\frac{1}{2}(-s_{13}^T e_{111} + s_{13}^T e_{122} - 2s_{33}^T e_{113})\left(\frac{e_{11}}{\varepsilon_{11}^\eta}\right) - [s_{13}^T(l_{11} + l_{12}) + s_{33}^T l_{13})]\left(\frac{e_{11}}{\varepsilon_{11}^\eta}\right)^2$

5.5 Physical properties of α-quartz

The lattice constants and the axial ratio depend on the purity of the crystal. Brice (1980, 1985) has given a review of lattice parameter data for quartz. Natural quartz, which contains more impurities than very well made synthetic quartz, has a lattice constant a which varies from 4.9129 to 4.9138 Å and an axial ratio c/a which changes from 1.10012 to 1.10004. In contrast, the a values of premium synthetic quartz samples vary over the range 4.9132-4.9136 Å and the c/a value vary from 1.10008 to 1.10016. Brice (1985) gives reliable measured density values lie in the range 2648-2650 kgm^{-3} at 298K. James (1987) gives a density of 2648.38±0.2kgm^{-3} for synthetic quartz at 298K. He measured the density of VHPQ at 298K and found no significant difference between standard synthetic quartz and very high purity quartz (James 1987).

The thermal expansion of α-quartz is markedly anisotropic. The linear thermal expansivity along the threefold (Z) axis is much smaller than that along the direction

in X-Y plane (McSkimin et al. 1965, Brice 1985, White 1963). In acousto-electric device design, the linear thermal expansion coefficients are usually expressed as a third or fourth order polynomial of the form:

$$l_i = l_{i0}(1 + \alpha_{i1}t + \alpha_{i2}t^2 + \alpha_{i3}t^3 + \ldots) \quad , \tag{5.6}$$

where i (=1, 2, 3) indicates the i axis along which the measured dimension lies, l is a dimension at some temperature t (°C or K) and l_{i0} is the dimension at a reference temperature t_0. McSkimin et al. (1965) give data for $-196<t<30^0$C in a form of the fourth order polynomial with $t_0=0^0$C. The values of α_{in} (in units of $°C^{-n}$) are:

X axis	Y axis
$\alpha_{11}=13.20\text{x}10^{-6}$,	$\alpha_{31}=7.03\text{x}10^{-6}$,
$\alpha_{12}=22.85\text{x}10^{-9}$,	$\alpha_{32}=10.25\text{x}10^{-9}$,
$\alpha_{13}=86.36\text{x}10^{-12}$,	$\alpha_{33}=6.58\text{x}10^{-12}$,
$\alpha_{14}=276.2\text{x}10^{-15}$,	$\alpha_{34}=48.5\text{x}10^{-15}$.

James (1987) gives data in form of a third order polynomial over the range 213K to 393K, which was fitted to the thermal expansion coefficients data given by Brice (James 1987). The polynomial is in the form

$$l_i = l_{i0}(1 + \alpha_{i1}\Delta T + \alpha_{i2}\Delta T^2 + \alpha_{i3}\Delta T^3) \quad , \tag{5.7}$$

where l_{i0} is the dimension at 298K and $\Delta T=T$-298K. the values (in units of K^{-n}) are

X axis	Y axis
$\alpha_{11}=1.377\text{x}10^{-5}$,	$\alpha_{31}=7.483\text{x}10^{-6}$,
$\alpha_{12}=1.303\text{x}10^{-8}$,	$\alpha_{32}=9.405\text{x}10^{-9}$,
$\alpha_{13}=-6.329\text{x}10^{-12}$,	$\alpha_{33}=-5.440\text{x}10^{-12}$.

The coefficients provide a good "average" of the data used by other workers (James 1987) and are used in the data calculation and correction in this work.

Samsonov (1973) gives a molar specific heat (in unit of $Jmol^{-1}K^{-1}$) of

$$C_P = 47.0118 + 3.4358 \times 10^{-2}T - 1.131 \times 10^{6}T^{-2} \quad , \tag{5.8}$$

where T is the absolute temperature and the molar weight is 60.085g. The temperature dependence of C_P agrees well with the curve given by Brice (1985) which is based on the data of Weast (1964) and Touloukian (1967). The values of the Debye temperature from various sources are different. Gray (1972) quotes a value of 470K and a value of 552K is from Zeller and Pohl (1971). Brice (1985) suggests that a value of 700±50K is more appropriate for the temperature range in which devices are fabricated and used.

The SOEC have been measured by many workers as mentioned in Chapter 1. Frequently used data are those from Mason (1951), Bechmann et al. (1962) and McSkimin et al. (1965). There are no significant differences in the SOEC at room temperature for synthetic quartz crystals given by different workers. But there is a considerable divergence in the data of temperatures coefficients of the SOEC from different sources (e.g. see Brice 1985 and James 1987). Recently James (1987) measured the SOEC of standard synthetic quartz crystal and five independent SOEC (except for C_{13}) of VHPQ from 213K to 393K. He noted significant differences between the values of the SOEC for standard synthetic quartz and VHPQ. James' data are the only available ones for VHPQ prior to this work. James (1987) presented them (in units of Nm^{-2}) in the form of a polynomial to third order

$$C_{IJ}(T) = C_{IJ}(298K)(1 + a_1 dT + a_2 dT^2 + a_3 dT^3) \tag{5.9}$$

where $dT = T - 298K$. The coefficients in Eq. (5.9) are as follows:

	C_{11}	C_{12}	C_{14}
$C_{IJ}(298K)$	8.6822×10^{10}	7.1822×10^{9}	1.9008×10^{10}
a_1	-4.366×10^{-5}	-2.477×10^{-3}	9.021×10^{-5}
a_2	-1.086×10^{-7}	-3.07×10^{-6}	2.469×10^{-8}
a_3	-9.081×10^{-11}	-1.125×10^{-8}	-1.923×10^{-9}
	C_{33}	C_{44}	C_{66}
$C_{IJ}(298K)$	10.572×10^{10}	5.82862×10^{10}	3.9820×10^{10}
a_1	-1.909×10^{-4}	-1.702×10^{-4}	1.758×10^{-4}
a_2	-1.686×10^{-7}	-2.566×10^{-7}	1.585×10^{-7}
a_3	-3.606×10^{-11}	-2.004×10^{-10}	9.156×10^{-10}

The second order dielectric coefficients ε_{ij}^{T} determined experimentally are usually for constant stress. The coefficients for constant strain ε_{ij}^{η} can be determined from ε_{ij}^{T} by

$$\varepsilon_{ij}^{T} - \varepsilon_{ij}^{\eta} = d_{ik} e_{jk}. \tag{5.10}$$

Bottom (1972) has measured ε_{11}^{T} as $39.93\times10^{-12}\pm0.09\times10^{-12}$ Fm^{-1} and ε_{33}^{T} as $40.73\times10^{-12}\pm0.09\times10^{-12}$ Fm^{-1} at 293K for synthetic quartz. James (1987) measured the temperature dependences of ε_{ij}^{T} from 213K to 393K for standard synthetic quartz. A polynomial to the third order has been given by James (1987) for ε_{ij}^{T} and ε_{ij}^{η} (in units of Fm^{-1})

$$\varepsilon_{ij} = \varepsilon(298K)[1 + a_1 dT + a_2 dT^2 + a_3 dT^3] \tag{5.11}$$

where $dT = T - 298K$. The coefficients a_k for ε_{ij}^{T} and ε_{ij}^{η} are given as below:

	ε_{11}^{T}	ε_{33}^{T}	ε_{11}^{η}
$\varepsilon_{ij}(298K)$	$3.99205\text{x}10^{-11}$	$4.10395\text{x}10^{-11}$	$3.916\text{x}10^{-11}$
a_1	$7.06\text{x}10^{-6}$	$1.88\text{x}10^{-5}$	$1.47\text{x}10^{-5}$
a_2	$1.632\text{x}10^{-8}$	$3.29\text{x}10^{-8}$	$1.45\text{x}10^{-8}$
a_3	$-22.06\text{x}10^{-11}$	$-1.92\text{x}10^{-10}$	$-2.10\text{x}10^{-11}$

$\varepsilon_{33}^{\eta} = \varepsilon_{33}^{T}$. Since ε_{ij} for VHPQ are not available the temperature dependences of ε_{ij} given by James (1987) are used in this work.

There are no significant differences in the second order piezoelectric coefficients (SOPC) e_{ij} given by different workers (Koga et al. 1958, Shevel'ko and Yakovlev 1977, Ludanov et al. 1976, Bechmann 1958 and Graham 1972). The e_{ij} given by some workers and a "mean" value of e_{ij} calculated from these results are given in Table 5.16.

Table 5.16 Second order piezo-electric coefficients (Cm^{-2})

Source	e_{11}	e_{14}	IEEE Standard
(a)	-0.175	0.0407	1949
(b)	-0.171	0.04	1949
(c)	-0.174		1949
(d)	-0.171	0.0406	1949
(e)	-0.1711±0.00094		1949
(f)	0.173	0.040	1978
Mean value	0.1725	0.040	1978

(a) Koga et al. 1958.

(b) Shevel'ko and Yakovlev 1977.

(c) Ludanov et al. 1976.

(d) Bechmann 1958.

(e) Graham 1972.

(f) Bottom 1982.

The third order piezoelectric coefficients (TOPC) e_{IJK} at room temperature have been measured by several scientists (Hruska and Kazda 1968, Kusters 1970, Reider et al. 1982, Brendel 1984, Kittinger et al. 1986 and Hruska 1990b). But the values for the coefficients show a lack of agreement. The data are listed in Table 5.17. From measurements of the resonant frequency shift in quartz rods and plates caused by a dc electric field, Hruska (1989) and Hruska and Brendel (1989) have obtained some combinations M_{IJK} of the eight independent TOPC in a reference frame according to the IRE 1949 standard for piezoelectricity (Standards on Piezoelectric Crystals 1949). For the present work to get the best values of the coefficients, seven linearly independent combinations have been chosen and been transformed to the IEEE 1978 Standard for Piezoelectric Crystals (IEEE 1978):

$$
\begin{aligned}
M_{111} &= -e_{111} - 4.675e_{134} + 3.051e_{144} + 2.993e_{315} \\
M_{113} &= -e_{113} + 4.892e_{134} - 1.524e_{144} + 0.205e_{315} \\
M_{114} &= e_{114} + 9.211e_{134} - 5.639e_{144} - 0.309e_{315} \\
M_{122} &= -e_{122} - o.279e_{134} - 0.027e_{144} - 0.241e_{315} \\
M_{124} &= e_{124} + 1.195e_{134} - 0.438e_{144} + 0.309e_{315} \\
M_{144} &= e_{144} + 0.50e_{122} \\
M_{315} &= e_{315} + 0.61e_{122} + 0.52e_{134}
\end{aligned}
\qquad (5.12)
$$

The mean value of e_{134} calculated from the data of Reider et al. (1982), Kittinger et al. (1986) and Hruska (1990b) has been used as a known variable. Substitution of the mean e_{134} and other TOPC, listed in Table 5.17, into Eqs. (5.9) gives six sets of combinations as shown in Table 5.18. The combinations for the data of Reider et al. (1982), Kittinger et al. (1986) and Hruska (1990a) are in a very good agreement and hence, have been chosen to calculate the mean TOPC. Thus the mean TOPC to be used in the present work are given in Table 5.19.

The electrostrictive coefficients l_{IJ} of α-quartz are not so well known as the coefficients discussed above. However a whole set of electrostrictive coefficients l_{IJ}/ε_0 for α-quartz crystal has been given by Kittinger et al. (1986). Hruska (1990b) has determined some of the coefficients. A set of mean electrostrictive coefficients l_{IJ}/ε_0 determined by using the data given by Kittinger et al. (1986) and Hruska (1990b) are listed in Table 5.20 and are used here.

Table 5.17 The TOPC given by different authors (Cm^{-2})

e_{IJK}	Hruska and Kazda (1968)	Kusters (1970)	Reider et al. (1982)
e_{111}	2.30	-2.97	-2.61±0.09
e_{113}	8.71	-49.05	-0.49±0.17
e_{114}	3.91	28.81	-0.39±0.19
e_{122}	-2.38	-114.76	1.47±0.14
e_{124}	0.63	85.49	-1.13±0.08
e_{134}	-4.71	-2.12	-1.35±0.08
e_{144}	3.76	57.77	0.15±0.07
e_{315}	-0.46	70.72	0.64±0.08
e_{IJK}	Brendel (1984)	Kittinger et al. (1986)	Hruska (1990b)
e_{111}	-2.73±0.13	-2.18±0.02	-2.16±0.05
e_{113}	-12.00±1.2	0.50±0.03	0.43±0.07
e_{114}	33.40±6.1	-0.28±0.04	-0.16±0.04
e_{122}	3.05±1.9	1.10±0.03	1.12±0.03
e_{124}	34.57±7.2	-0.78±0.02	-0.74±0.02
e_{134}	50.46±8.2	-1.63±0.02	-1.65±0.03
e_{144}	-0.604±1.1	-0.05±0.02	-0.01±0.03
e_{315}	24.90±2.9	0.90±0.01	0.78±0.03

* The data of Reider et al. (1982), Kittinger et al. (1986) and Hruska (1990b) are referred to the coordinate system of the IEEE 1978 conventions, while those for others are originally referred to the coordinate system of the IRE 1949 conventions but are transferred to the IEEE 1978 conventions. The data of Hruska (1968) and Reider et al. (1982) are originally the electroelastic coefficients which have the same absolute values but opposite signs as the piezoelectric coefficients.

Table 5.18 The combinations M_{IJK} of the TOPC (Cm^{-2})

M_{IJK}	Hruska and Kazda (1968)	Kusters (1970)	Reider et al. (1984)
M_{111}	29.81	400.80	11.29
M_{113}	-37.56	-34.86	-6.21
M_{114}	-60.53	-338.33	-13.89
M_{122}	3.70	96.75	-1.25
M_{124}	-6.79	79.51	-2.61
M_{144}	2.57	0.39	0.88
M_{315}	-4.36	-0.39	0.83
M_{ijk}	Brendel (1984)	Kittinger et al. (1986)	Hruska (1990a)
M_{111}	-311.31	12.34	12.18
M_{113}	228.82	-8.21	-8.33
M_{114}	502.48	-15.29	-15.54
M_{122}	-5.04	-0.86	-0.85
M_{124}	86.91	-2.43	-2.47
M_{144}	-0.92	0.50	0.55
M_{315}	-0.52	0.72	0.60

Table 5.19 The mean TOPC (Cm^{-2})

e_{IJK}	e_{111}	e_{113}	e_{114}	e_{122}
Results	-2.32±0.03	0.15±0.06	-0.27±0.07	1.23±0.05
e_{IJK}	e_{124}	e_{134}	e_{144}	e_{315}
Results	-0.88±0.03	-1.54±0.03	0.03±0.03	0.77±0.03

Table 5.20 The mean electrostrictive coefficients l_{IJ}/ε_0

l_{IJ}/ε_0	l_{11}/ε_0	l_{12}/ε_0	l_{13}/ε_0	l_{14}/ε_0
Results	-3.9±0.5	0.11±0.6	10.2±1.6	-2.2±0.5
l_{IJ}/ε_0	l_{31}/ε_0	l_{33}/ε_0	l_{41}/ε_0	l_{44}/ε_0
Results	0.8±1.6	-5.8±3.7	-4.4±0.8	1.3±1.0

Chapter 6 Nonlinear Elastic Properties and Third Order Elastic Constants of Very High Purity Quartz (VHPQ)

6.1 Introduction

To determine the TOEC of α-quartz, two types of measurements are needed: 1) measurements of the effects of the hydrostatic pressure on the velocity of ultrasonic waves propagated in the crystal, 2) measurements of the effects of uniaxial stress on the velocity of ultrasonic waves. The former gives the hydrostatic pressure derivatives B_{jrks} (defined by Eq. (2.167)) which give the combinations of the TOEC and the latter gives G_U (defined in Eq. (2.157)) which also are the combinations of the TOEC (Table 5.14). From the first type of the measurements the hydrostatic pressure derivatives of the SOEC and the bulk modulus can be determined; these are also important in discussion of the nonlinear properties of VHPQ. The aim of the work in this chapter is to present the measured TOEC and the hydrostatic pressure derivatives of the SOEC of VHPQ as a function of temperature from 243K to 393K. Since the only other sources for the hydrostatic pressure derivatives of the SOEC and for the TOEC for α-quartz are McSkimin et al. (1965) and Thurston et al. (1966), their data are chosen for comparison of most of the measured data and the evaluated results in this work. Section 6.2 gives the data for the hydrostatic pressure derivatives of the natural velocities of measured wave modes and presents the six independent hydrostatic pressure derivatives of the SOEC and the hydrostatic pressure derivative of the bulk modulus determined as a direct output of the measured data. The data and the hydrostatic pressure derivatives at room temperature (298K) are then compared with those given by McSkimin et al. (1965). Section 6.3, 6.4 and 6.5 presents further derivatives of the data for hydrostatic pressure

effects on the velocity of ultrasonic waves propagated in VHPQ. In sections 6.3 and 6.4, by using the hydrostatic pressure derivatives of the bulk modulus $(\partial B/\partial P)_{T,P=0}$ and of the SOEC at zero pressure, volume compression and pressure-induced changes in the lattice parameters a and c of VHPQ have been extrapolated to high pressure, with the help of Murnaghan's equation of state (Murnaghan 1946) and Thurston's method (Thurston 1966) respectively. Next, the results are compared with those given by other authors. Section 6.5 suggests that the pressure derivatives of some SOEC can shed some light on the phase transformation from α-quartz to β-quartz, which occurs at 846K.

The central aim of the work has been to determine the temperature dependences of the TOEC of VHPQ from 243K to 393K, they are presented in section 6.6. In this section first given are the pressure derivatives of the natural velocities of the wave modes propagated under uniaxial compression. The fourteen independent TOEC are determined by using these data and the data of the wave modes propagated under hydrostatic pressure. The TOEC are found to change dramatically with increasing temperature. The contributions from the electromechanical effects to the TOEC for VHPQ at room temperature (293K) are also estimated. The TOEC determined in this work for VHPQ are compared with those given by Thurston et al. (1966) for α-quartz single crystals.

6.2 Hydrostatic pressure derivatives of the SOEC as a function of temperature

An important part of the project has been to measure the temperature dependences of the hydrostatic pressure derivatives of the natural velocity $(1/W_0)(\partial W/\partial P)_{T,P=0}$ of the relevant modes from 243K to 393K. The measured modes are mode 1H, 2H, 5H, 6H, 7H, 9H, 10H, and 13H (the definitions of the modes are in Table 5.10). The modes 10H and 13H have been measured on a left-handed specimen while the rest of the modes have been measured on a right-handed one. The ultrasonic wave velocities and their

pressure derivatives under zero pressure have been obtained by a least squares fit to the measured data and used to evaluate the SOEC and the pressure derivatives of the effective and thermodynamic SOEC, $(\partial C_{IJ}/\partial P)_{T,P=0}$ and B_{IJ} , by using Eqs. (2.148), (2.149), (2.152), (2.169), (2.170) and (2.171). The function B_H (Eq. (2.169)) for each of the thirteen ultrasound modes of α-quartz under hydrostatic pressure is tabulated in Table 6.1. The differences between the pressure derivatives of effective and thermodynamic SOEC (Thurston 1965b) are given in Table 6.2.

The hydrostatic pressure derivatives of the natural velocities $(1/W_0)(\partial W/\partial P)_{T,P=0}$ are listed in Table 6.3; they have been found to change markedly with temperature (Fig 6.1 (a)-(c)). With increasing temperature, $(1/W_0)(\partial W/\partial P)_{T,P=0}$ of modes 1H, 7H, 9H and 10H increase linearly while this function decreases for modes 2H and 13H. There is a minimum at 383K in the case of mode 13H (Fig. 6.1 (a)). For mode 5H $(1/W_0)(\partial W/\partial P)_{T,P=0}$ experiences a maximum at 298K (Fig. 6.1b) and for mode 6H a hump as the temperature approaches 310K (Fig. 6.1c). In Table 6.4, the hydrostatic pressure derivatives $(1/W_0)(\partial W/\partial P)_{T,P=0}$ measured at 298K are compared with those given by McSkimin et al. (1965) for α-quartz single crystals. The results for mode 6H, 7H and mode 9H are in good agreement. However for the other modes the values of $(1/W_0)(\partial W/\partial P)_{T,P=0}$ are markedly different from those given by McSkimin et al. (1965). The largest discrepancy is for mode 10H. In the present work this mode was examined on a left-handed VHPQ sample. The ultrasonic wave velocity of the mode is about 1000 m/s less than that given by McSkimin (1962) and $(1/W_0)(\partial W/\partial P)_{T,P=0}$ is nearly twice that given by McSkimin et al. (1965). These results would be expected to be the same. However a whole series of experiment showed that the present results are reproducible.

Table 6.1 The function B_H (Eq. (2.169)) of ultrasonic wave modes for α-quartz

mode	B_H
1H	$B_{11}+\left[\frac{\partial}{\partial P}\left(\frac{e_{11}^2}{\varepsilon_{11}^\eta}\right)\right]_T$
2H	$\beta_1^2 B_{66}+2\beta_1\beta_2 B_{14}+\beta_2^2 B_{44}$
3H	$\beta_2^2 B_{66}-2\beta_1\beta_2 B_{14}+\beta_1^2 B_{44}$
4H	$\gamma_2^2 B_{11}+2\gamma_1\gamma_2 B_{14}+\gamma_1^2 B_{44}$
5H	$\gamma_1^2 B_{11}-2\gamma_1\gamma_2 B_{14}+\gamma_2^2 B_{44}$
6H	$B_{66}+\left[\frac{\partial}{\partial P}\left(\frac{e_{11}^2}{\varepsilon_{11}^\eta}\right)\right]_T$
7H	B_{33}
8H=9H	B_{44}
10H	$[\theta_1^2 B_{11}+(1+2\theta_1\theta_2)B_{44}+2\theta_1\theta_2 B_{13}$ $-2(\theta_1^2+\theta_1\theta_2)B_{14}+\theta_2^2 B_{33}]/2$
11H	$[\theta_2^2 B_{11}+(1-2\theta_1\theta_2)B_{44}-2\theta_1\theta_2 B_{13}$ $-2(\theta_2^2-\theta_1\theta_2)B_{14}+\theta_1^2 B_{33}]/2$
12H	$(B_{44}+B_{66})/2+B_{14}+\left\{\frac{\partial}{\partial P}\left[\frac{(e_{11}+e_{14})^2}{2\left(\varepsilon_{11}^\eta+\varepsilon_{33}^\eta\right)}\right]\right\}_T$
13H	$(B_{44}+B_{66})/2-B_{14}+\left\{\frac{\partial}{\partial P}\left[\frac{(e_{11}-e_{14})^2}{2\left(\varepsilon_{11}^\eta+\varepsilon_{33}^\eta\right)}\right]\right\}_T$

Table 6.2 The differences between the effective and thermodynamic SOEC for α-quartz (Thurston 1965b)

$$(\partial C_{11}^{ef}/\partial P)_{P=0} - B_{11} = -1 + (s_3 - 2s_1)C_{11}^{S,E}$$

$$(\partial C_{12}^{ef}/\partial P)_{P=0} - B_{12} = 1 + (s_3 - 2s_1)C_{12}^{S,E}$$

$$(\partial C_{13}^{ef}/\partial P)_{P=0} - B_{13} = 1 - s_3 C_{13}^{S,E}$$

$$(\partial C_{14}^{ef}/\partial P)_{P=0} - B_{14} = -s_1 C_{14}^{S,E}$$

$$(\partial C_{33}^{ef}/\partial P)_{P=0} - B_{33} = -1 + (2s_1 - 3s_3)C_{33}^{S,E}$$

$$(\partial C_{44}^{ef}/\partial P)_{P=0} - B_{44} = -1 - s_3 C_{44}^{S,E}$$

$$(\partial C_{66}^{ef}/\partial P)_{P=0} - B_{66} = -1 + (s_3 - 2s_1)C_{66}^{S,E}$$

Table 6.3 $(1/W_0)(\partial W/\partial P)_{T,P=0}$ of the modes under hydrostatic pressure (10^{-11} Pa^{-1})

T (K)	Mode 1H	Mode 2H	Mode 5H	Mode 6H
243	1.937±0.070	0.466±0.028	4.80±0.11	-3.68±0.18
253	1.978±0.063	0.467±0.041	4.84±0.11	-3.707±0.067
263	2.001±0.029	0.468±0.033	4.868±0.088	-3.756±0.073
273	2.063±0.029	0.434±0.009	4.890±0.086	-3.795±0.050
283	2.121±0.029	0.388±0.017	4.903±0.067	-3.727±0.043
293	2.154±0.015	0.380±0.013	4.908±0.037	-3.528±0.020
298	2.173±0.064	0.379±0.014	4.908±0.038	-3.467±0.054
303	2.164±0.025	0.378±0.022	4.905±0.042	-3.389±0.037
313	2.223±0.026	0.354±0.024	4.893±0.070	-3.335±0.024
323	2.258±0.024	0.354±0.030	4.872±0.082	-3.354±0.050
333	2.264±0.032	0.341±0.024	4.84±0.11	-3.509±0.046
343	2.282±0.033	0.331±0.023	4.81±0.21	-3.616±0.050
353	2.335±0.050	0.326±0.018	4.76±0.17	-3.733±0.031
363	2.368±0.046	0.275±0.020	4.71±0.20	-3.857±0.031
373	2.363±0.044	0.177±0.020	4.64±0.13	-4.012±0.072
383	2.355±0.054	0.087±0.011	4.572±0.099	-4.143±0.071
393	2.347±0.050	0.018±0.024	4.49±0.16	-4.201±0.059

Table 6.3 $(1/W_o)(\partial W/\partial P)_{T,P=0}$ of the modes under hydrostatic pressure (10^{-11} Pa^{-1}) (Continued)

T (K)	Mode 7H	Mode 9H	Mode 10H	Mode 13H
243	3.982±0.040	1.149±0.028	4.75±0.18	2.754±0.092
253	4.055±0.030	1.233±0.026	4.80±0.15	2.71±0.10
263	4.080±0.031	1.269±0.024	4.85±0.14	2.851±0.029
273	4.140±0.031	1.394±0.032	4.897±0.071	2.853±0.023
283	4.248±0.028	1.491±0.033	4.946±0.074	2.758±0.036
293	4.348±0.014	1.548±0.011	4.995±0.077	2.782±0.023
298	4.386±0.017	1.631±0.008	5.020±0.047	2.818±0.015
303	4.417±0.019	1.664±0.007	5.044±0.085	2.744±0.019
313	4.490±0.028	1.683±0.008	5.094±0.088	2.758±0.024
323	4.571±0.025	1.750±0.009	5.143±0.059	2.699±0.022
333	4.663±0.053	1.801±0.004	5.192±0.094	2.603±0.035
343	4.735±0.059	1.873±0.012	5.241±0.082	2.521±0.047
353	4.759±0.034	1.949±0.017	5.291±0.090	2.384±0.033
363	4.836±0.040	2.044±0.013	5.34±0.10	2.312±0.034
373	4.905±0.059	2.117±0.024	5.39±0.14	2.114±0.012
383	4.963±0.070	2.139±0.029	5.44±0.15	2.075±0.057
393	5.086±0.065	2.235±0.035	5.49±0.17	2.229±0.046

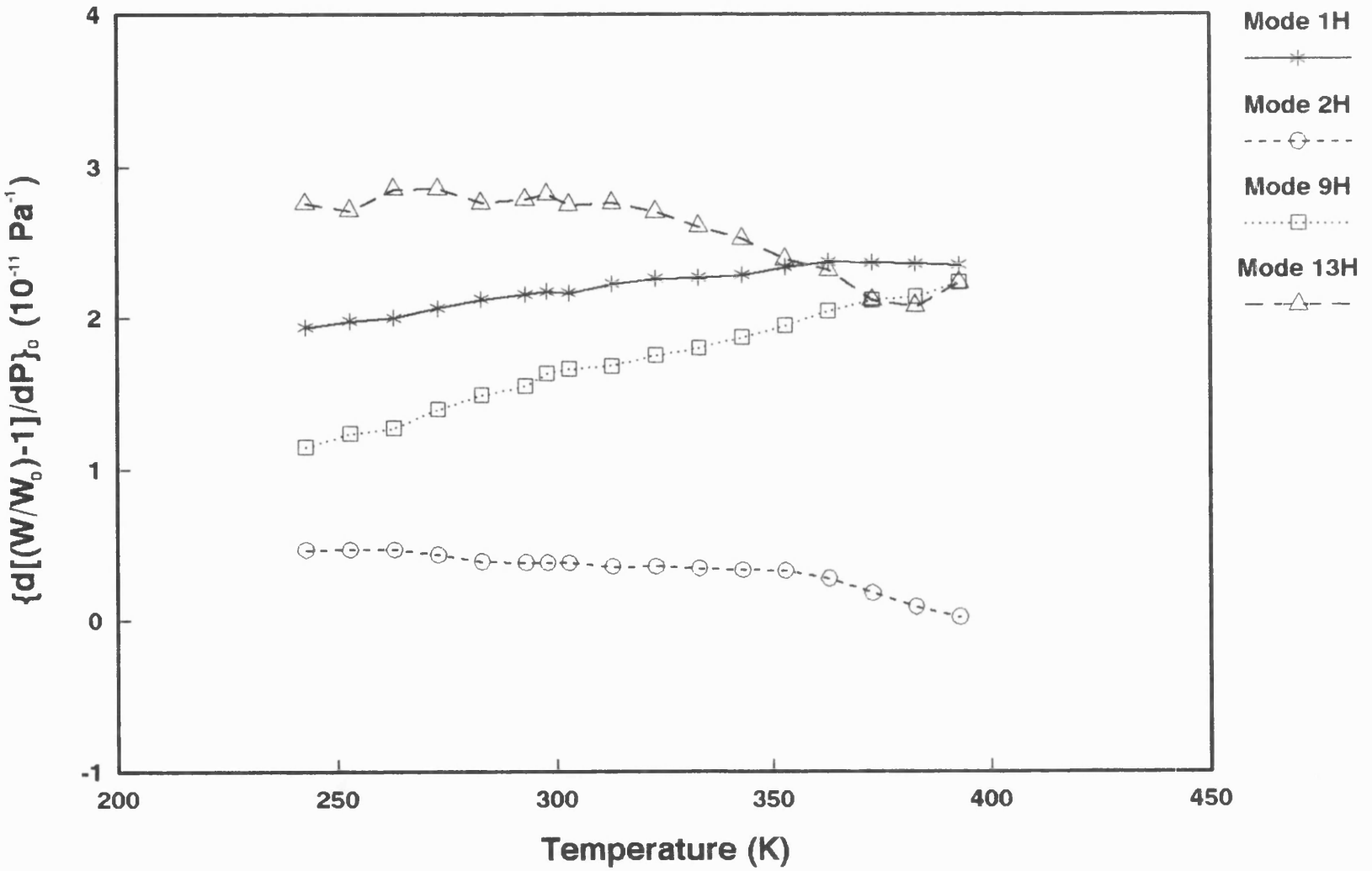

Fig. 6.1 (a) The temperature dependence of the hydrostatic pressure derivatives of the relative natural velocity.

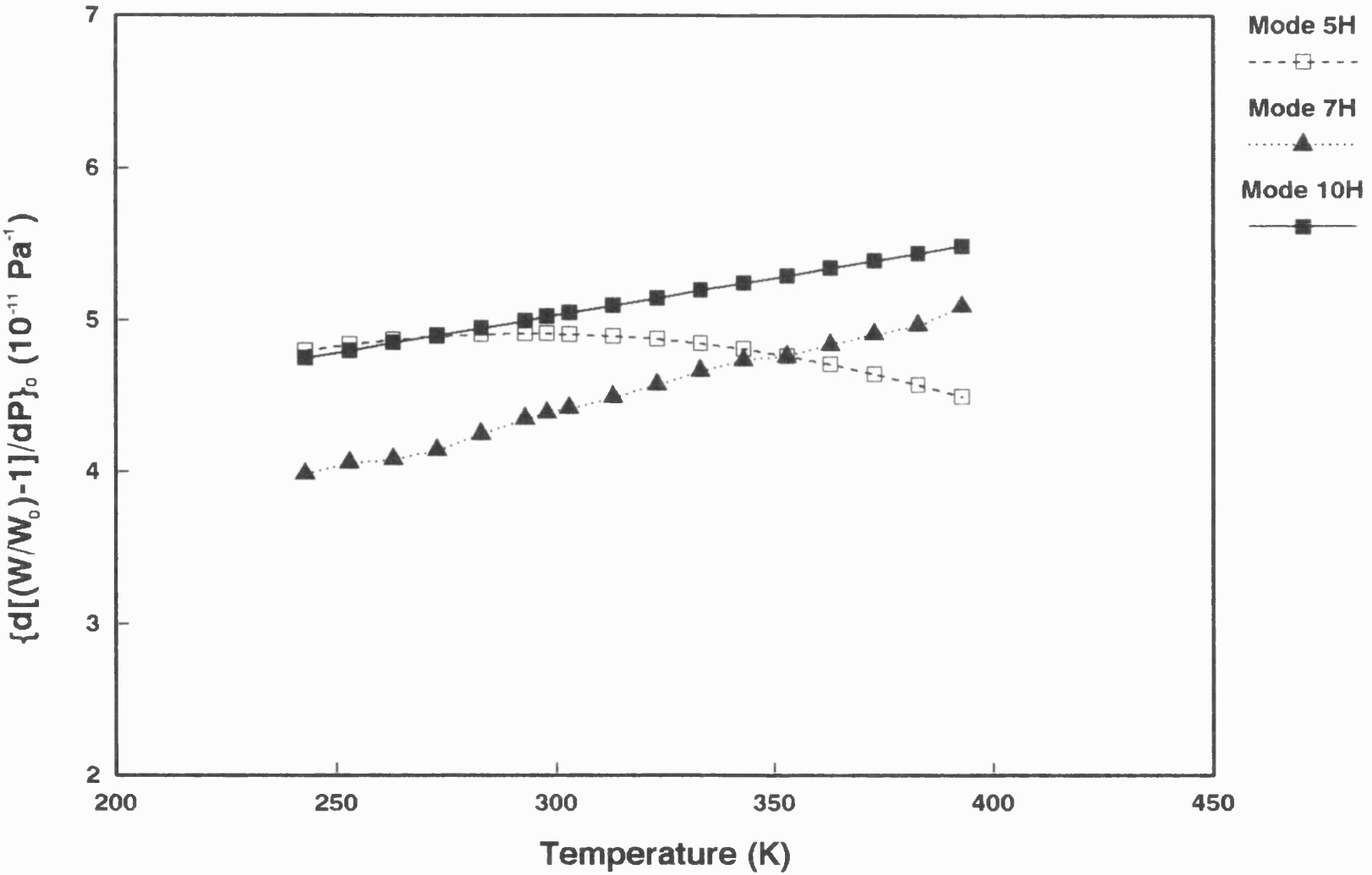

Fig. 6.1 (b) The temperature dependence of the hydrostatic pressure derivatives of the relative natural velocity.

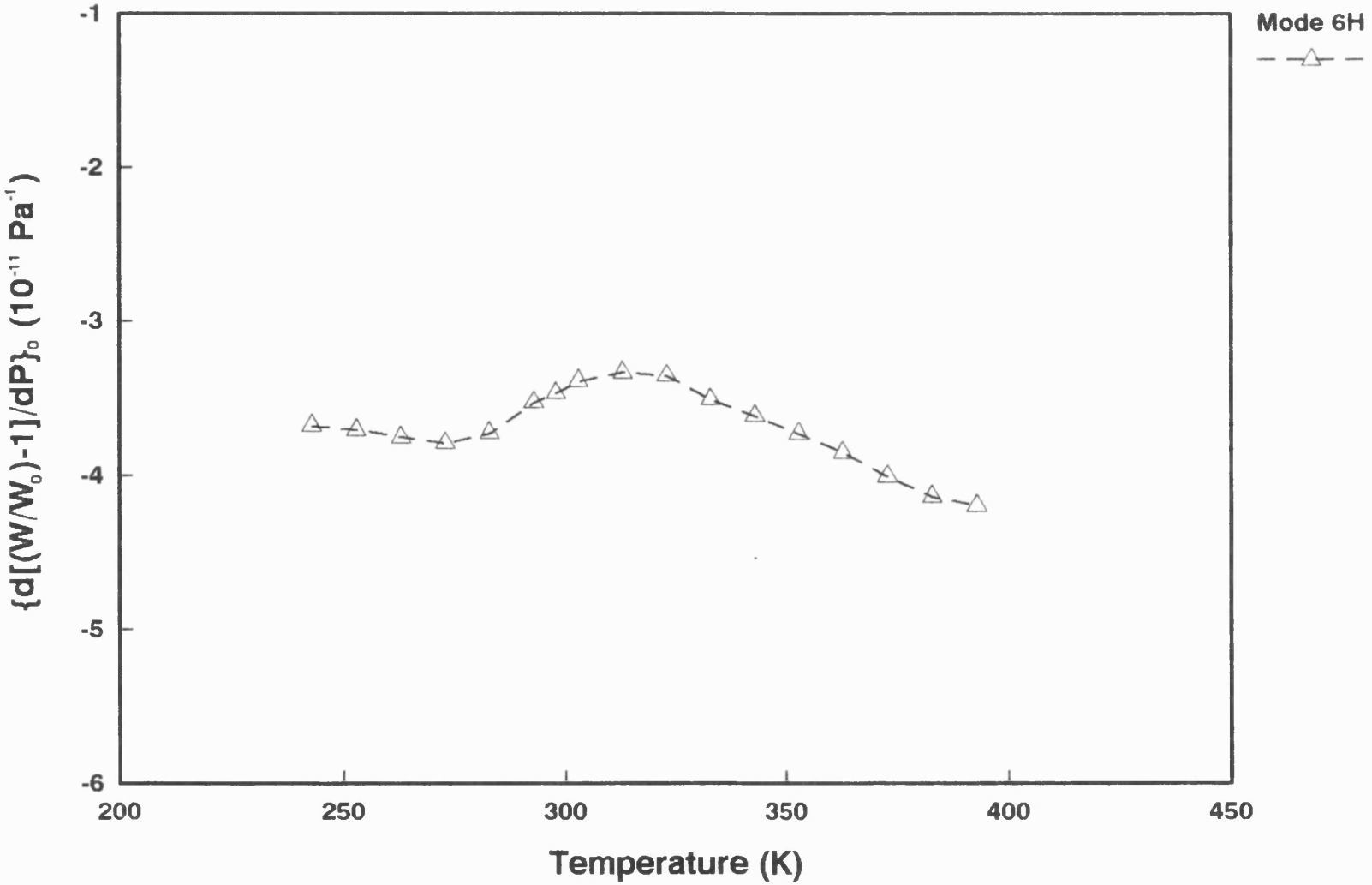

Fig. 6.1 (c) The temperature dependence of the hydrostatic pressure derivatives of the relative natural velocity.

Table 6.4 $(1/W_0)(\partial W/\partial P)_{T,P=0}$ at 298K (10^{-11} Pa^{-1})

Mode	Present work	McSkimin et al. (1965)	Mode	Present work	McSkimin et al. (1965)
1H	2.173±0.064	1.511	7H	4.386±0.017	4.507
2H	0.379±0.014	0.466	9H	1.631±0.008	**1.671
5H	4.908±0.038	3.956	10H	*5.020±0.047	2.190
6H	-3.467±0.054	-3.665	13H	*2.818±0.015	

* Measured on the left-handed quartz.

** Mode 8H.

The SOEC of VHPQ used in the determination of the $(\partial C_{IJ}/\partial P)_{T,P=0}$ are the weighted averages of the SOEC measured in this work and those given by James (1987) (Eq. 5.12). The weighting factors have been determined by the standard errors of the two groups of data. Let the standard errors measured in this work be designated by δ_W and those given by James (1987) be indicated by δ_J , The weighted average of the SOEC can be obtained by using the equation (Barford 1985)

$$\overline{C}_{IJ} = \frac{1}{\delta_W^{-2} + \delta_J^{-2}} \left(\frac{C_{IJ}^W}{\delta_W^2} + \frac{C_{IJ}^J}{\delta_J^2} \right) \quad , \tag{6.1}$$

where C_{IJ}^W are taken as the SOEC measured in this work and C_{IJ}^J are those given by James (1987). The standard errors of the weighted average of the SOEC can be obtained by using the equation

$$\delta^2 = \frac{\delta_W^2 \delta_J^2}{\delta_W^2 + \delta_J^2} \quad . \tag{6.2}$$

The real values of the weighted average of the SOEC are

$$C_{IJ} = \overline{C}_{IJ} + \delta \quad . \tag{6.3}$$

The bulk modulus B^S is calculated using the equation

$$B^S = \frac{[(C_{11}+C_{12})C_{33} - 2C_{13}^2]}{(C_{11}+C_{12}+2C_{33}-4C_{13})} \quad . \tag{6.4}$$

The data for C_{IJ} and B^S as functions of temperature are compiled in Table 6.5. In Table 6.6 the results at 298K have been compared with the C_{IJ} and B^S given by McSkimin (1962). Good agreement for most of the elastic constants and the bulk modulus is found, exceptions being C_{13} and C_{14}. The values of C_{14} given by McSkimin (1962) has a negative sign while that, calculated from our data, has a positive sign as is reported by Voigt (1910), Mason (1943), Atanasoff and Hart (1941) and James (1987) etc. The difference in the sign for C_{14} is due to the use of different conventions for piezoelectric crystals. In this work, the 1978 IEEE convention (IEEE 1978) has been used while the 1949 IRE convention (Standards on Piezoelectric Crystals 1949) was used by McSkimin (1962).

In the calculation of the direction cosines of particle displacements, the sign of C_{14} is crucial, since this determines the signs of the directional cosines β_1, β_2, γ_1 and γ_2 and the values of θ_1 and θ_2 (see Eqs. (5.1)-(5.8) in Section 5.4). The values of β_1 and γ_2 calculated in this work have opposite signs to those given by Thurston et al. (1966). This leads to a negative $(\partial C_{14}/\partial P)_{T,P=0}$ in our results while the value of McSkimin et al. (1965) is positive (Table 6.11).

The hydrostatic pressure derivatives of the SOEC have been determined by using a weighted least-squares-method (Pugh and Winslow 1966). The weights have been estimated from the standard errors of $(1/W_0)(\partial W/\partial P)_{T,P=0}$ of ultrasonic wave modes measured under hydrostatic pressure and are given in Table 6.7.

Table 6.5 C_{μ} (weighted average) and bulk modulus B^S

of VHPQ (10^{10} Pa)

T (K)	11 (±0.002)	13 (±0.005)	14 (±0.006)	33 (±0.002)
243	8.700	1.194	1.765	10.688
253	8.697	1.201	1.770	10.666
263	8.694	1.221	1.778	10.645
273	8.690	1.220	1.786	10.624
283	8.687	1.221	1.794	10.603
293	8.683	1.235	1.806	10.582
298	8.682	1.215	1.806	10.572
303	8.680	1.224	1.805	10.562
313	8.675	1.215	1.812	10.542
323	8.671	1.225	1.814	10.522
333	8.667	1.243	1.818	10.503
343	8.662	1.239	1.820	10.485
353	8.658	1.228	1.823	10.466
363	8.653	1.197	1.818	10.448
373	8.647	1.165	1.819	10.430
383	8.642	1.146	1.826	10.413
393	8.636	1.120	1.813	10.396

Table 6.5 C_{ij} (weighted average) and bulk modulus B^S

of VHPQ (10^{10} Pa) (Continued)

T (K)	44 (±0.005)	66 (±0.002)	B^S(±0.004)
243	5.876	3.940	3.758
253	5.868	3.948	3.753
263	5.859	3.956	3.752
273	5.850	3.963	3.742
283	5.841	3.971	3.732
293	5.831	3.978	3.725
298	5.826	3.982	3.714
303	5.821	3.985	3.715
313	5.811	3.992	3.702
323	5.801	3.999	3.696
333	5.790	4.006	3.693
343	5.779	4.013	3.682
353	5.768	4.019	3.668
363	5.756	4.026	3.651
373	5.744	4.032	3.630
383	5.731	4.039	3.611
393	5.719	4.046	3.599

Table 6.6 C_{IJ} and B^S at 298K (10^{10} Pa)

Source	11	13	14	33
WA	8.682±0.002	1.215±0.005	1.806±0.006	10.572±0.002
McSkimin (1962)	8.680	1.191	-1.904	10.575
Source	44	66	B^S	
WA	5.826±0.005	3.982±0.002	3.714±0.004	
McSkimin (1962)	5.820	3.988	3.741	

WA: Weighted average.

Table 6.7 Weights used for wave modes under hydrostatic pressure

Mode	1H	2H	5H	6H	7H	9H	10H	13H
Weight	0.7	0.9	0.4	0.7	0.8	1.0	0.4	0.7

Both the $(\partial C_{IJ}/\partial P)_{T,P=0}$, with and without contributions from piezoelectric effects, have been evaluated. To determine the $(\partial C_{IJ}/\partial P)_{T,P=0}$ with contributions from piezoelectric effects, the equations for the pressure derivatives of the thermodynamic SOEC (B_{IJ}^{st}) can be written into a set of (8×6) simultaneous equations which are formed from Eq. (2.170) for the eight modes measured under hydrostatic pressure:

$$\begin{pmatrix} a_{11} & a_{12} & a_{13} & a_{14} & a_{15} & a_{16} \\ a_{21} & a_{22} & a_{23} & a_{24} & a_{25} & a_{26} \\ a_{31} & a_{32} & a_{33} & a_{34} & a_{35} & a_{36} \\ a_{41} & a_{42} & a_{43} & a_{44} & a_{45} & a_{46} \\ a_{51} & a_{52} & a_{53} & a_{54} & a_{55} & a_{56} \\ a_{61} & a_{62} & a_{63} & a_{64} & a_{65} & a_{66} \\ a_{71} & a_{72} & a_{73} & a_{74} & a_{75} & a_{76} \\ a_{81} & a_{82} & a_{83} & a_{84} & a_{85} & a_{86} \end{pmatrix} \begin{pmatrix} B_{11}^{st} \\ B_{13}^{st} \\ B_{33}^{st} \\ B_{44}^{st} \\ B_{14}^{st} \\ B_{66}^{st} \end{pmatrix} = \begin{pmatrix} c_1 \\ c_2 \\ c_3 \\ c_4 \\ c_5 \\ c_6 \\ c_7 \\ c_8 \end{pmatrix} , \tag{6.5}$$

Here the coefficients a_{ij} can be obtained from the coefficients of B_{ij}^{st} in Eq. (2.168) and

$$c_i = (\rho_0 W_i^2)'_{P=0} + 1 + 2w_i F_{Hi} \qquad (i = 1, 2, \ldots, 8) \quad . \tag{6.6}$$

The subscript i represents a measured mode as follows:

i	1	2	3	4	5	6	7	8
Mode	1H	2H	5H	6H	7H	9H	10H	13H

The (8×6) simultaneous equations is then transformed to a set of (6×6) simultaneous equations, by applying the weighted least-squares-method (Pugh and Winslow 1966), as:

$$\begin{pmatrix} wa_1a_1 & wa_1a_2 & \ldots & wa_1a_6 \\ wa_1a_2 & wa_2a_2 & \ldots & wa_2a_6 \\ . & . & \ldots & . \\ . & . & \ldots & . \\ . & . & \ldots & . \\ wa_1a_6 & wa_2a_6 & \ldots & wa_6a_6 \end{pmatrix} \begin{pmatrix} B_{11}^{st} \\ B_{13}^{st} \\ B_{33}^{st} \\ B_{44}^{st} \\ B_{14}^{st} \\ B_{66}^{st} \end{pmatrix} = \begin{pmatrix} wca_1 \\ wca_2 \\ wca_3 \\ wca_4 \\ wca_5 \\ wca_6 \end{pmatrix} , \tag{6.7}$$

where

$$wa_i a_j = \sum_{n=1}^{8} w_n a_{ni} a_{nj} \quad , \qquad (i, j = 1, 2, \ldots, 6) \tag{6.8}$$

and

$$wca_i = \sum_{n=1}^{8} w_n c_n a_{ni} \quad , \qquad (i = 1,2,\ldots,6) \tag{6.9}$$

with w_i representing the weight of the i^{th} wave mode. By substituting the B_{IJ}^{si} solved from Eq. (6.6) into the equations given in Table 6.2, the pressure derivatives of the effective SOEC containing the contribution from piezoelectric effects can then be determined. To estimate the effects of the piezoelectricity on $(\partial C_{IJ}/\partial P)_{T,P=0}$, a set of (8×8) simultaneous equations can be set up in a similar manner as for the set of (8×6) simultaneous equations, with $[\partial(e_{11}^2/\varepsilon_{11}^{\eta})/\partial P]_{T,P=0}$ and $\{\partial[(e_{14}-e_{11})^2/(2\varepsilon_{11}^{\eta}+2\varepsilon_{33}^{\eta})]/\partial P\}_{T,P=0}$ as two added unknowns. The $(\partial C_{IJ}/\partial P)_{T,P=0}$ determined in this way do not contain the contributions from the piezoelectric effects.

The $(\partial C_{IJ}/\partial P)_{T,P=0}$ obtained for VHPQ are given in Tables 6.8, 6.9 and 6.10. The effect of crystal symmetry on piezoelectric and elastic properties of α-quartz precludes piezoelectric contributions to $(\partial C_{33}/\partial P)_{T,P=0}$ and $(\partial C_{44}/\partial P)_{T,P=0}$. The differences in $(\partial C_{44}/\partial P)_{T,P=0}$ between two groups of data given by Table 6.8 and Table 6.9 are due to the weighted least squares method used for two sets of the simultaneous equations mentioned above. The piezoelectric effects add positive contributions to $(\partial C_{11}/\partial P)_{T,P=0}$, $(\partial C_{13}/\partial P)_{T,P=0}$ and $(\partial C_{66}/\partial P)_{T,P=0}$, i.e. the effects accentuates the increase of C_{11}, C_{13} and C_{66} when VHPQ is subjected to a hydrostatic pressure. With rising temperature, all six independent pressure derivatives $(\partial C_{IJ}/\partial P)_{T,P=0}$, without contribution from piezoelectric effects, increase (Fig. 6.2 (a) and (b)). The piezoelectric effects change the behaviour of $(\partial C_{11}/\partial P)_{T,P=0}$, $(\partial C_{13}/\partial P)_{T,P=0}$ and $(\partial C_{66}/\partial P)_{T,P=0}$ as a function of temperature (Fig. 6.3 (a) (b)). This is due to $[\partial(e_{11}^2/\varepsilon_{11}^{\eta})/\partial P]_{T,P=0}$ which decreases sharply with increasing temperature above 310K (Fig. 6.4). By contrast, $\{\partial[(e_{14}-e_{11})^2/(2\varepsilon_{11}^{\eta}+2\varepsilon_{33}^{\eta})]/\partial P\}_{T,P=0}$ does not show any remarkable temperature dependence and only increases slightly over the temperatures range (Fig. 6.4).

Table 6.8 The hydrostatic pressure derivatives of the effective SOEC at zero pressure $(\partial C_{IJ}/\partial P)_{T,P=0}$ (with contributions from piezoelectric effects)

T (K)	11	12	13	66
243	3.32±0.12	10.13±0.43	5.49±0.73	-3.40±0.21
253	3.39±0.11	10.23±0.19	5.43±0.72	-3.42±0.08
263	3.42±0.05	10.35±0.18	5.45±0.57	-3.47±0.09
273	3.51±0.05	10.50±0.13	5.34±0.55	-3.49±0.06
283	3.61±0.05	10.49±0.11	5.30±0.45	-3.44±0.05
293	3.66±0.03	10.26±0.06	5.36±0.28	-3.30±0.03
298	3.69±0.11	10.19±0.17	5.28±0.30	-3.25±0.06
303	3.67±0.04	10.05±0.10	5.38±0.31	-3.19±0.04
313	3.77±0.05	10.07±0.08	5.44±0.46	-3.15±0.03
323	3.82±0.04	10.13±0.12	5.45±0.53	-3.15±0.06
333	3.81±0.06	10.33±0.12	5.42±0.68	-3.26±0.05
343	3.83±0.06	10.49±0.13	5.40±1.32	-3.33±0.06
353	3.91±0.09	10.70±0.11	5.46±1.04	-3.40±0.04
363	3.96±0.08	10.90±0.11	5.38±1.23	-3.47±0.04
373	3.94±0.08	11.10±0.18	5.41±0.81	-3.58±0.08
383	3.92±0.09	11.28±0.19	5.48±0.64	-3.68±0.08
393	3.89±0.09	11.32±0.16	5.28±0.98	-3.71±0.07

Table 6.8 The hydrostatic pressure derivatives of the effective SOEC at zero pressure $(\partial C_{IJ}/\partial P)_{T,P=0}$ (with contributions from piezoelectric effects) (Continued)

T (K)	33	44	14	
243	9.14±0.04	1.52±0.02	-2.85±0.05	
253	9.28±0.04	1.61±0.02	-2.79±0.04	
263	9.33±0.04	1.65±0.02	-2.83±0.04	
273	9.44±0.04	1.79±0.03	-2.75±0.04	
283	9.65±0.04	1.90±0.03	-2.61±0.03	
293	9.86±0.04	1.97±0.01	-2.48±0.02	
298	9.92±0.04	2.06±0.01	-2.41±0.02	
303	9.98±0.04	2.10±0.01	-2.33±0.02	
313	10.11±0.04	2.12±0.01	-2.27±0.03	
323	10.27±0.04	2.19±0.01	-2.21±0.03	
333	10.44±0.04	2.23±0.01	-2.20±0.04	
343	10.58±0.04	2.29±0.01	-2.16±0.08	
353	10.60±0.04	2.35±0.02	-2.11±0.07	
363	10.73±0.04	2.43±0.01	-2.06±0.08	
373	10.85±0.05	2.50±0.02	-1.99±0.05	
383	10.95±0.05	2.51±0.03	-1.98±0.04	
393	11.17±0.05	2.59±0.03	-1.97±0.06	

Table 6.9 The hydrostatic pressure derivatives of the effective SOEC at zero pressure $(\partial C_{IJ}/\partial P)_{T,P=0}$ (without contributions from piezoelectric effects)

T (K)	11	12	13	66
243	1.35±0.05	11.59±0.20	4.23±0.07	-5.12±0.09
253	1.49±0.10	11.64±0.11	4.21±0.05	-5.07±0.02
263	1.56±0.03	11.74±0.07	4.32±0.05	-5.09±0.03
273	1.82±0.04	11.77±0.06	4.35±0.05	-4.97±0.02
283	1.90±0.04	11.77±0.06	4.31±0.01	-4.93±0.02
293	1.76±0.03	11.69±0.03	4.31±0.06	-4.97±0.01
298	1.84±0.01	11.58±0.11	4.29±0.04	-4.87±0.03
303	1.77±0.04	11.49±0.05	4.32±0.06	-4.86±0.02
313	1.85±0.05	11.53±0.05	4.43±0.03	-4.84±0.01
323	2.09±0.04	11.44±0.05	4.53±0.04	-4.68±0.02
333	2.39±0.05	11.42±0.06	4.65±0.06	-4.51±0.01
343	2.73±0.07	11.32±0.11	4.80±0.18	-4.29±0.04
353	3.20±0.09	11.25±0.12	5.05±0.13	-4.02±0.04
363	3.64±0.09	11.14±0.13	5.17±0.16	-3.75±0.05
373	3.95±0.07	11.10±0.08	5.34±0.07	-3.58±0.02
383	4.15±0.08	11.11±0.10	5.58±0.03	-3.48±0.03
393	4.46±0.08	10.88±0.09	5.66±0.10	-3.21±0.02

Table 6.9 The hydrostatic pressure derivatives of the effective SOEC at zero pressure $(\partial C_{IJ}/\partial P)_{T,P=0}$ (without contributions from piezoelectric effects) (Continued)

T (K)	33	44	14	
243	9.14±0.03	1.40±0.05	-4.16±0.10	
253	9.28±0.03	1.50±0.04	-4.06±0.10	
263	9.33±0.03	1.54±0.03	-4.03±0.10	
273	9.44±0.03	1.69±0.03	-3.82±0.10	
283	9.65±0.03	1.80±0.03	-3.68±0.10	
293	9.86±0.03	1.87±0.02	-3.63±0.10	
298	9.92±0.04	1.96±0.02	-3.51±0.10	
303	9.98±0.04	2.00±0.02	-3.49±0.10	
313	10.11±0.04	2.02±0.02	-3.41±0.10	
323	10.27±0.04	2.09±0.03	-3.24±0.10	
333	10.44±0.04	2.15±0.04	-3.05±0.11	
343	10.58±0.04	2.23±0.07	-2.82±0.13	
353	10.60±0.04	2.32±0.05	-2.55±0.12	
363	10.73±0.04	2.42±0.06	-2.27±0.12	
373	10.85±0.04	2.50±0.04	-2.03±0.11	
383	10.95±0.04	2.52±0.04	-1.86±0.11	
393	11.17±0.04	2.62±0.05	-1.59±0.11	

Table 6.10 The hydrostatic pressure derivatives $(\partial e_i/\partial P)_{T,P=0}$ of the piezoelectric terms e_i at zero pressure

T (K)	$(\partial e_1/\partial P)_{T,P=0}$	$(\partial e_2/\partial P)_{T,P=0}$	T (K)	$(\partial e_1/\partial P)_{T,P=0}$	$(\partial e_2/\partial P)_{T,P=0}$
243	1.91±0.11	-0.47±0.15	323	1.687±0.030	-0.157±0.032
253	1.835±0.044	-0.48±0.17	333	1.382±0.029	-0.147±0.049
263	1.804±0.044	-0.358±0.043	343	1.066±0.033	-0.126±0.023
273	1.647±0.031	-0.283±0.032	353	0.689±0.025	-0.125±0.021
283	1.655±0.027	-0.283±0.061	363	0.306±0.026	-0.083±0.042
293	1.846±0.014	-0.233±0.044	373	-0.006±0.044	-0.100±0.038
298	1.797±0.035	-0.187±0.032	383	-0.223±0.044	-0.012±0.091
303	1.852±0.023	-0.234±0.037	393	-0.545±0.038	0.171±0.054
313	1.872±0.017	-0.175±0.039	298*	0.005	

* McSkimin et al. (1965).

$e_1 = e_{11}^2/\varepsilon_{11}^{\eta}$

$e_2 = (e_{11} - e_{14})^2/[2(\varepsilon_{11}^{\eta} + \varepsilon_{33}^{\eta})]$

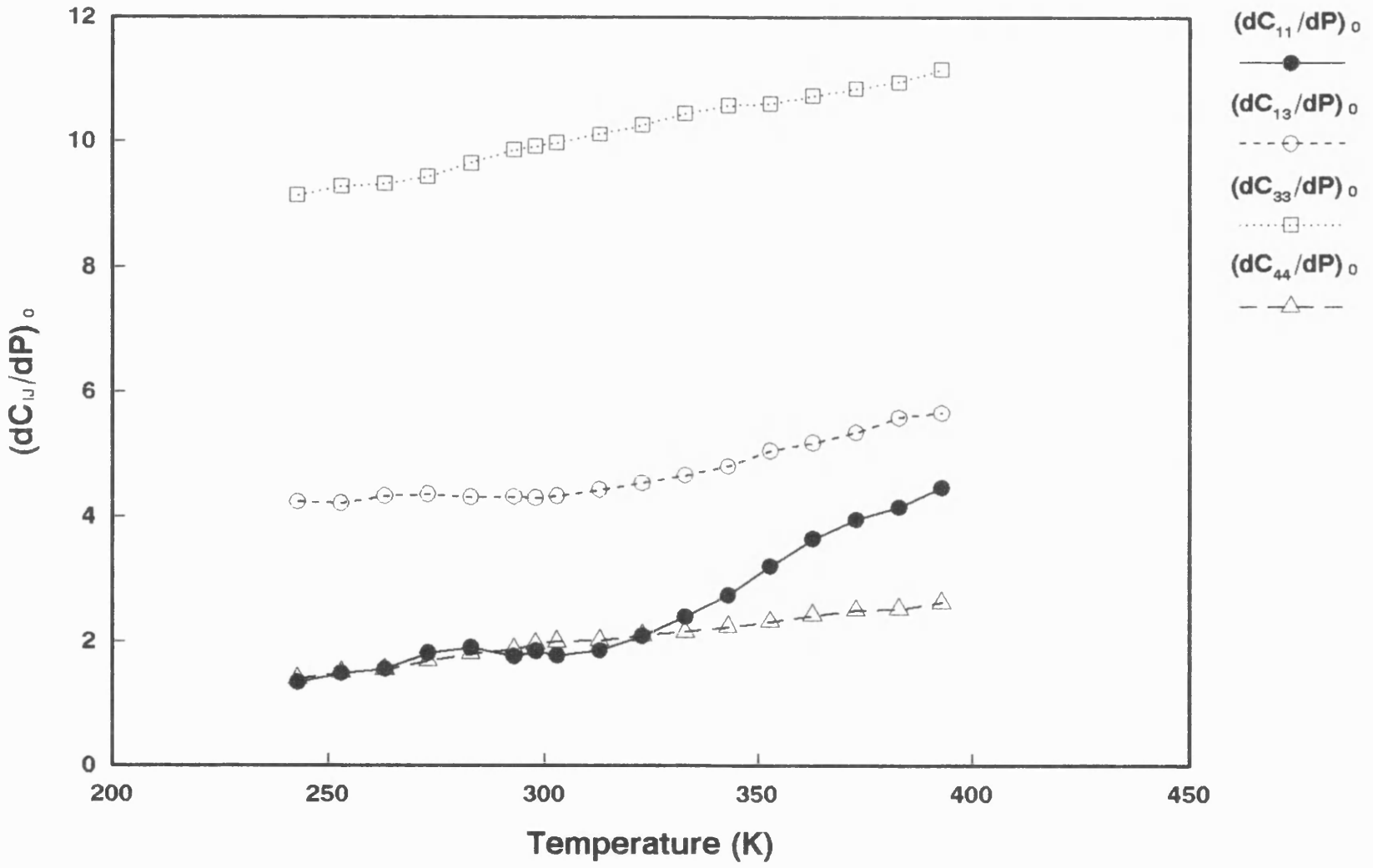

Fig. 6.2 (a) The temperature dependence of the pressure derivatives of elastic constants, without contribution from piezoelectric effects.

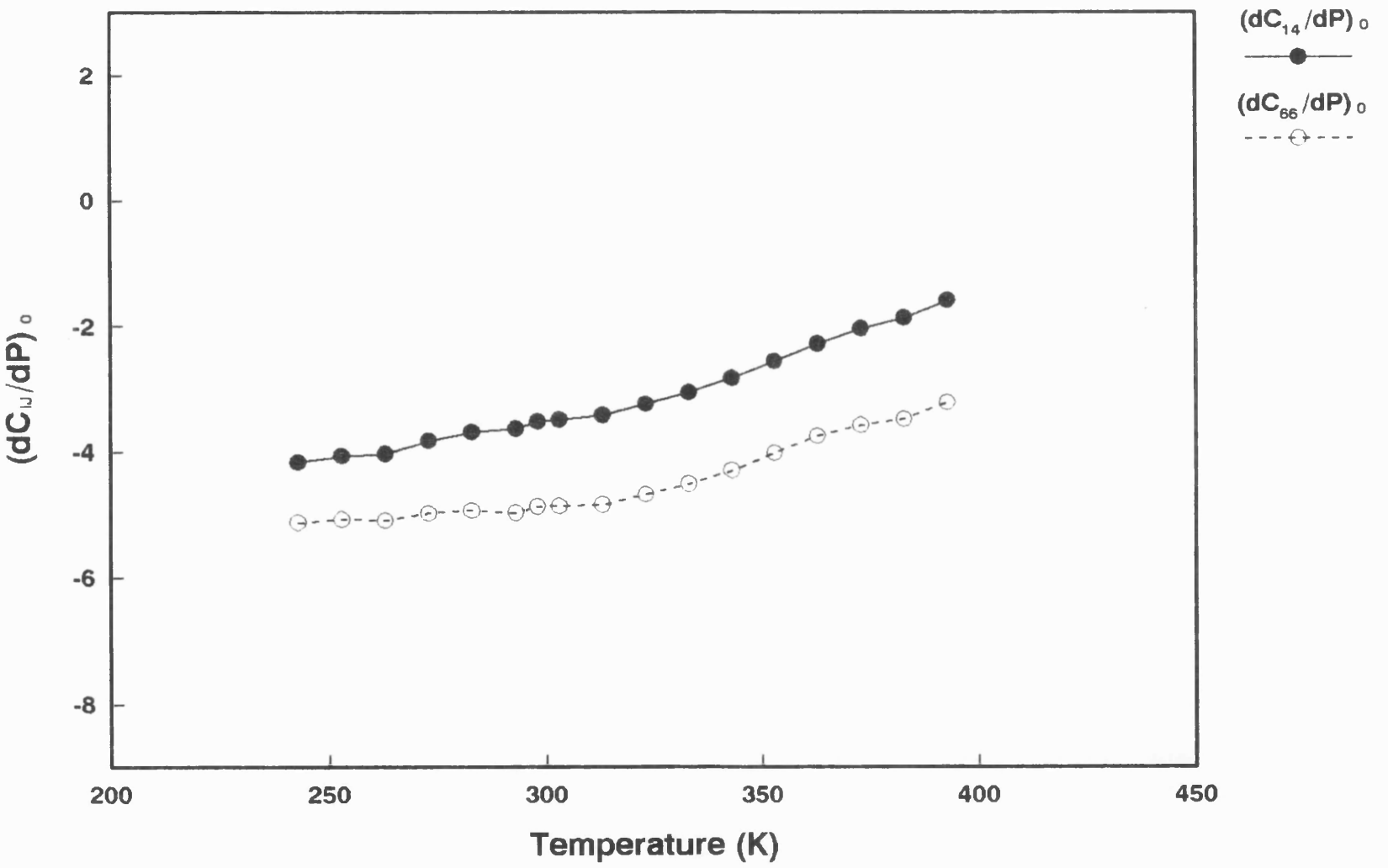

Fig. 6.2 (b) The temperature dependence of the pressure derivatives of elastic constants, without contribution from piezoelectric effects.

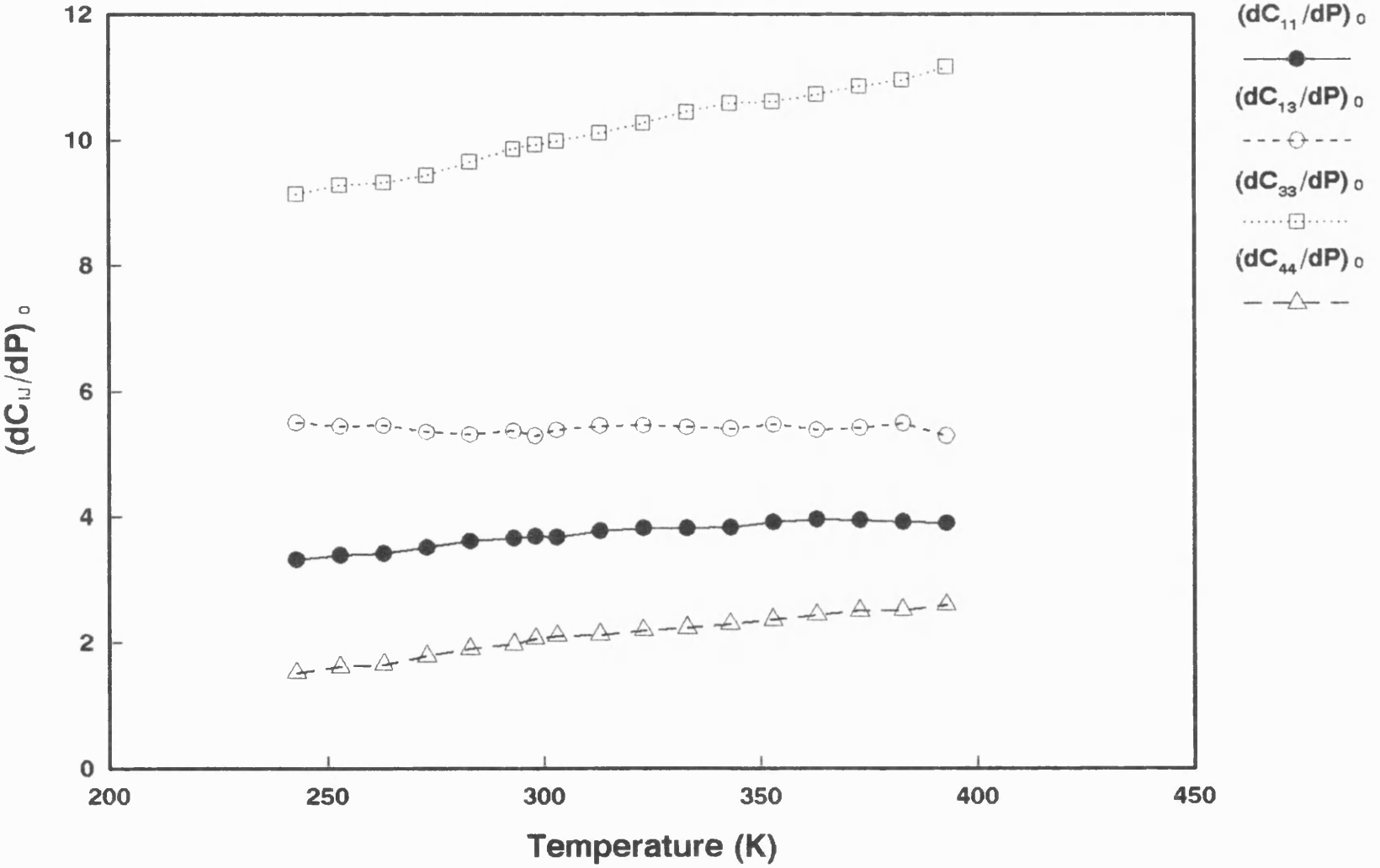

Fig. 6.3 (a) The temperature dependence of the pressure derivatives of elastic constants, with contribution from piezoelectric effects.

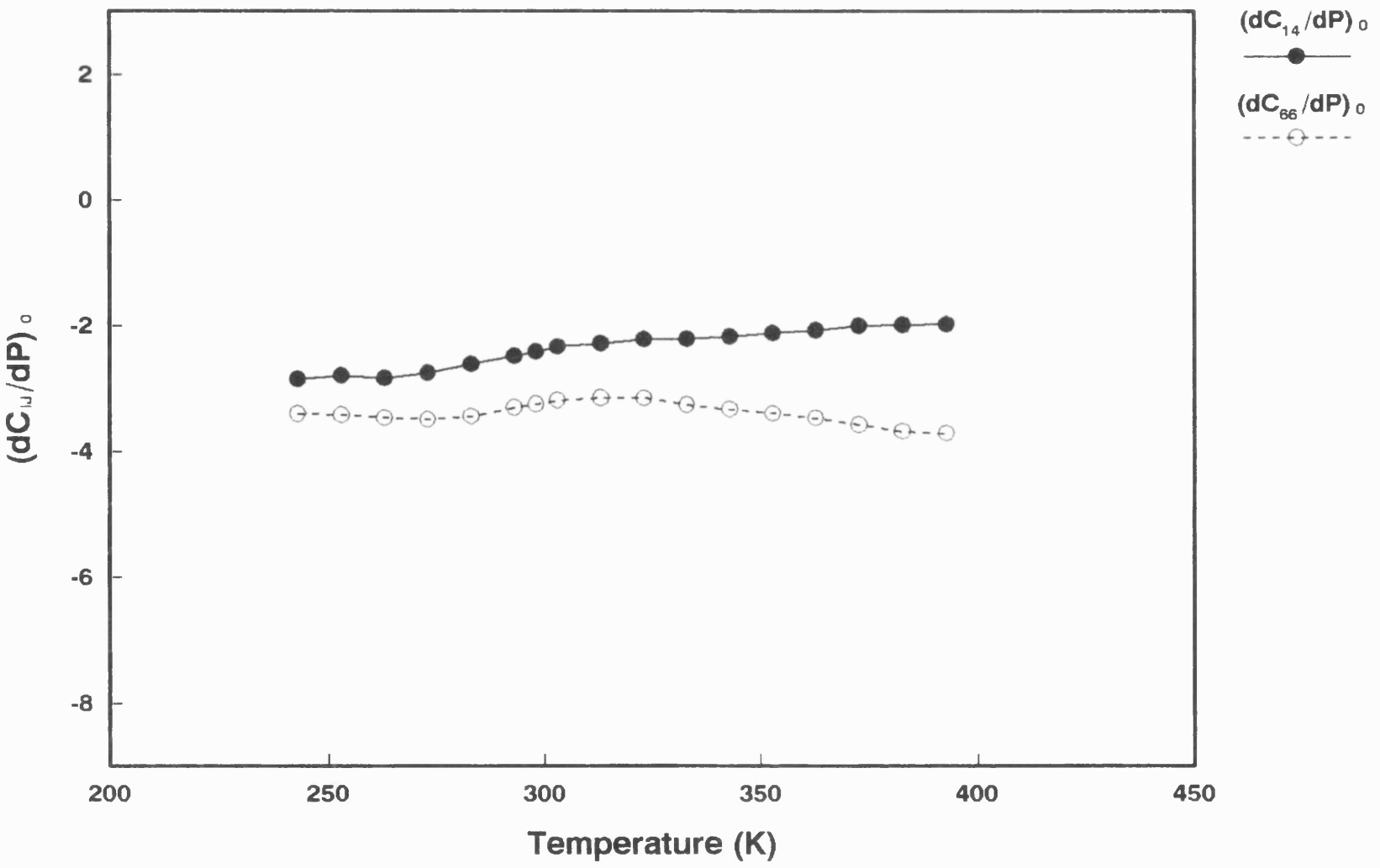

Fig. 6.3 (b) The temperature dependence of the pressure derivatives of elastic constants, with contribution from piezoelectric effects.

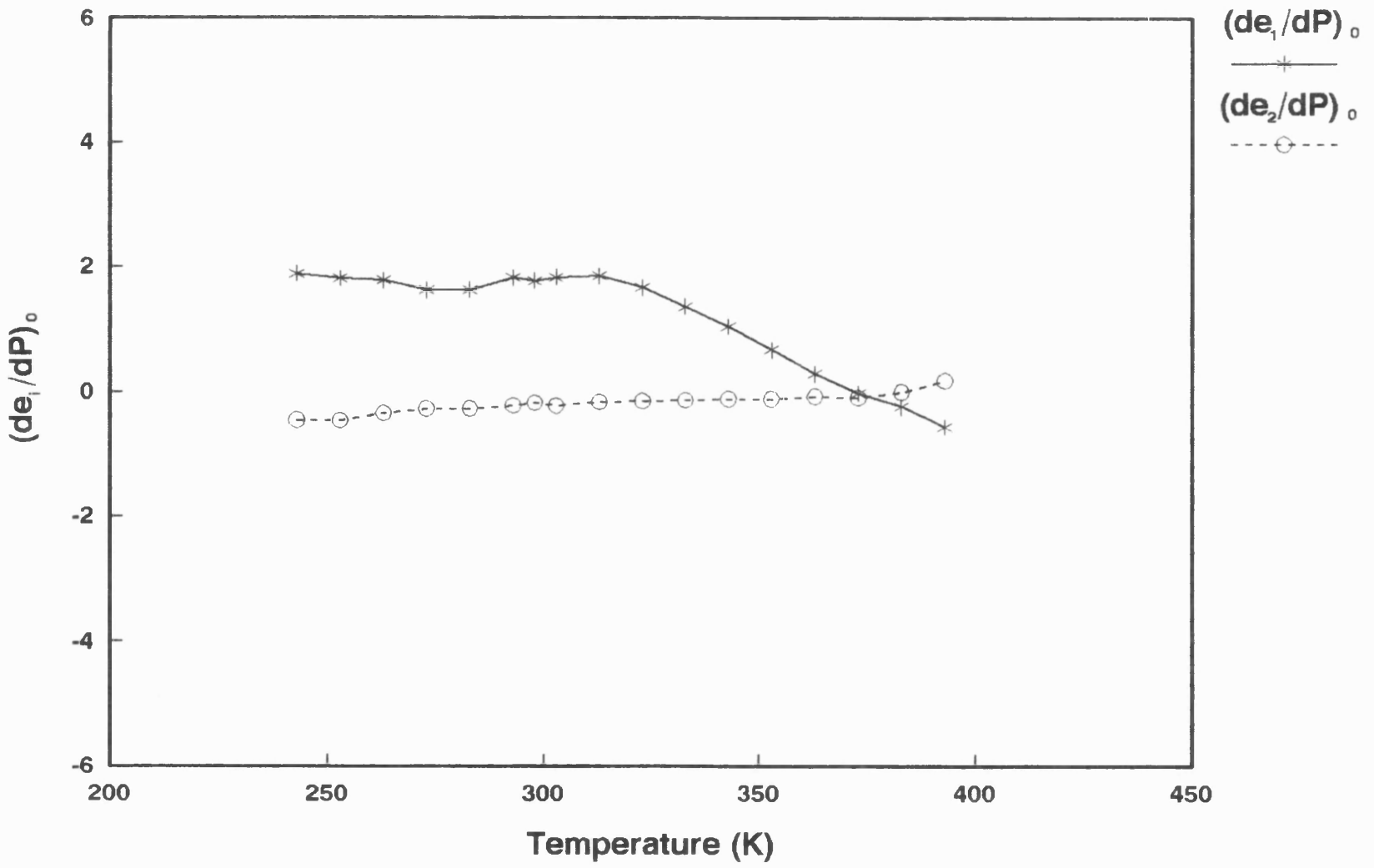

Fig. 6.4 The temperature dependence of the pressure derivatives of $(de_1/dP)_0$ and $(de_2/dP)_0$. $e_1 = e_{11}^2/\epsilon_{11}$, $e_2 = (e_{14}-e_{11})^2/(2\epsilon_{11}+2\epsilon_{33})$.

The $(\partial C_{IJ}/\partial P)_{T,P=0}$ at 298K are compared in Table 6.11 with those given by McSkimin et al. (1965). The values for the pressure derivatives $(\partial C_{IJ}/\partial P)_{T,P=0}$ which have not been adjusted for piezoelectric contributions are in reasonable agreement with the $(\partial C_{IJ}/\partial P)_{T,P=0}$ given by McSkimin et al. (1965); an exception is $(\partial C_{14}/\partial P)_{T,P=0}$ for which the absolute value of our data is much greater than that of McSkimin et al. (1965) (it is worth to repeating here that the difference in sign is due to a different choice of axial conventions). The value obtained for $[\partial(e_{11}^2/\varepsilon_{11}^\eta)/\partial P]_{T,P=0}$ at 298K is also greater than that quoted by McSkimin et al. (1965) (Table 6.10). The values of $[\partial(e_{11}^2/\varepsilon_{11}^\eta)/\partial P]_{T,P=0}$ measured here shows a stronger pressure dependence of the piezoelectric effects in VHPQ than in their material. By using an atomistic simulation method Wang et al. (1992) have calculated the pressure dependences of the SOEC of α-quartz at 0K and 300K respectively. The pressure derivatives of the SOEC as $P \rightarrow 0$ have been obtained by using a least-squares-fit method applied to calculated data from zero pressure to 0.5GPa. For comparison, the theoretically calculated $(\partial C_{IJ}/\partial P)_{T,P=0}$ at 300K are given in Table 6.11. All of the calculated $(\partial C_{IJ}/\partial P)_{T,P=0}$ are positive, except for the $(\partial C_{66}/\partial P)_{T,P=0}$ and $(\partial C_{14}/\partial P)_{T,P=0}$. Thus, the theoretical calculation confirms the experimental finding of a negative value for $(\partial C_{14}/\partial P)_{T,P=0}$ for VHPQ. The calculated values of $(\partial C_{11}/\partial P)_{T,P=0}$ and $(\partial C_{44}/\partial P)_{T,P=0}$ agree well with the measured data.

Table 6.11 Comparison of the values of $(\partial C_{IJ}/\partial P)_{T,P=0}$ at 298K*

Source	11	12	13	14
Data [1]	3.69±0.11	10.19±0.17	5.28±0.30	-2.41±0.02
Data [2]	1.84±0.01	11.58±0.11	4.29±0.04	-3.51±0.10
McSkimin et al. (1965)	3.28	8.66	5.97	1.93
Wang et al. (1992)	1.41±0.02	7.89±0.05	6.91±0.03	-1.98±0.01
Source	33	44	66	$(\partial B/\partial P)_{T,P=0}$
Data [1]	9.92±0.04	2.06±0.01	-3.25±0.06	6.50±0.20
Data [2]	9.92±0.04	1.96±0.02	-4.87±0.03	5.99±0.07
McSkimin et al. (1965)	10.84	2.66	-2.69	6.3
Wang et al. (1992)	15.39±0.03	1.75±0.03	-3.24±0.03	6.85±0.02

[1] With contributions from the piezoelectric effects; solved from a set of 8×6 simultaneous equations.

[2] Without contributions from the piezoelectric effects; solved from a set of 8×8 simultaneous equations.

*The data of Wang et al. (1992) have been determined at 300K.

The pressure derivatives of the bulk modulus $(\partial B/\partial P)_{T,P=0}$, both with and without contributions from piezoelectric effects, have been calculated by using the equation

$$\left(\frac{\partial B}{\partial P}\right)_{T,P=0} = \frac{[C'_{33}(C_{11}+C_{12})+C_{33}(C'_{11}+C'_{12})-4C_{13}C'_{13}]}{(C_{11}+C_{12}+2C_{33}-4C_{13})}$$

$$-\frac{[C_{33}(C_{11}+C_{12})-2C_{13}^2](C'_{11}+C'_{12}+2C'_{33}-4C'_{13})}{(C_{11}+C_{12}+2C_{33}-4C_{13})^2} \quad (6.10)$$

where

$$C'_{IJ} = (\partial C_{IJ}/\partial P)_{T,P=0} \quad . \quad (6.11)$$

The results are given in Table 6.12 and plotted in Fig. 6.5. The hydrostatic pressure derivative $(\partial B/\partial P)_{T,P=0}$ of the bulk modulus increases with rising temperature and is enhanced by the piezoelectric effects which become weaker as the temperature increases (Fig. 6.4). Compared with the value given by McSkimin et al. (1965) at 298K (Table 6.11), the value of $(\partial B/\partial P)_{T,P=0}$, including contributions form piezoelectric effects, is larger than that not including these. There is a significant enhancement of $(\partial B/\partial P)_{T,P=0}$ from the piezoelectric contributions. The values of $(\partial B/\partial P)_{T,P=0}$ calculated by the atomistic simulation (Wang et al. 1992) (Table 6.11) is in good agreement with the experimental work.

As mentioned in section 2.6, the values of the pressure derivatives for the thermodynamic SOEC, B_{IJ}, are significantly different from those for the effective SOEC $(\partial C_{IJ}/\partial P)_{T,P=0}$. In Tables 6.13 and 6.14 B_{IJ} are given as a function of temperature. They have been used in the determination of the TOEC of VHPQ. At 298K the B_{IJ} containing the contributions from piezoelectric effects are closer to the values given by Thurston et al. (1966) (Table 6.15).

Table 6.12 The hydrostatic pressure derivative $(\partial B/\partial P)_{T,P=0}$ of the bulk modulus at zero pressure

T (K)	$(\partial B/\partial P)_{T,P=0}$ [1]	$(\partial B/\partial P)_{T,P=0}$ [2]	T (K)	$(\partial B/\partial P)_{T,P=0}$ [1]	$(\partial B/\partial P)_{T,P=0}$ [2]
243	5.78±0.10	6.41±0.48	323	6.14±0.04	6.61±0.33
253	5.83±0.07	6.45±0.45	333	6.28±0.05	6.67±0.43
263	5.93±0.05	6.50±0.36	343	6.41±0.13	6.71±0.82
273	6.02±0.05	6.53±0.35	353	6.61±0.11	6.82±0.65
283	6.05±0.04	6.55±0.28	363	6.76±0.12	6.86±0.75
293	6.01±0.04	6.54±0.18	373	6.91±0.07	6.93±0.50
298	5.99±0.07	6.50±0.20	383	7.06±0.06	7.01±0.39
303	5.97±0.05	6.50±0.20	393	7.13±0.08	6.94±0.59
313	6.05±0.04	6.57±0.29			

[1] Without contributions from piezoelectric effects.

[2] With contributions from piezoelectric effects.

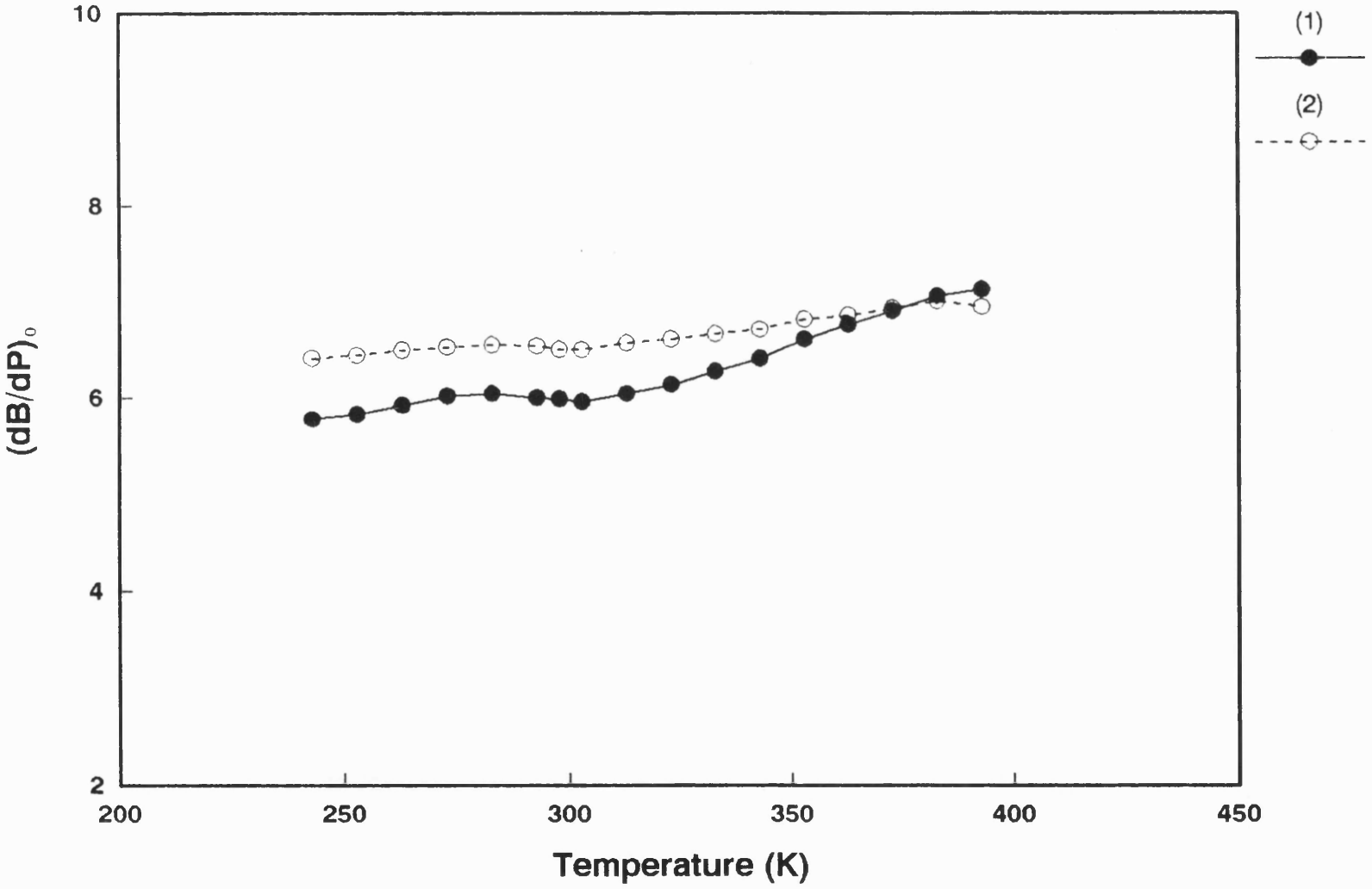

Fig. 6.5 The temperature dependence of the pressure derivative of bulk modulus: (1) without, (2) with contributions from piezoelectric effects.

Table 6.13 The hydrostatic pressure derivatives B_{ij} of the thermodynamic SOEC with contributions from piezoelectric effects

T (K)	B_{11}	B_{13}	B_{33}
243	5.39±0.12	4.58±0.73	10.363±0.036
253	5.46±0.11	4.52±0.72	10.503±0.036
263	5.497±0.051	4.54±0.57	10.537±0.036
273	5.598±0.052	4.43±0.55	10.646±0.037
283	5.699±0.051	4.39±0.45	10.853±0.037
293	5.756±0.030	4.45±0.28	11.044±0.037
298	5.79±0.11	4.37±0.30	11.112±0.037
303	5.774±0.045	4.46±0.31	11.165±0.038
313	5.876±0.047	4.53±0.46	11.301±0.039
323	5.929±0.044	4.53±0.53	11.445±0.039
333	5.929±0.057	4.51±0.68	11.608±0.043
343	5.951±0.059	4.5±1.3	11.737±0.045
353	6.035±0.087	4.5±1.0	11.763±0.041
363	6.084±0.080	4.5±1.2	11.901±0.043
373	6.072±0.077	4.50±0.81	12.029±0.046
383	6.051±0.093	4.57±0.64	12.134±0.048
393	6.025±0.086	4.37±0.98	12.361±0.048

Table 6.13 The hydrostatic pressure derivatives B_{ij} of the thermodynamic SOEC with contributions from piezoelectric effects (Continued)

T (K)	B_{14}	B_{44}	B_{66}
243	-2.67±0.45	2.945±0.023	-1.92±0.21
253	-2.62±0.45	3.037±0.021	-1.931±0.079
263	-2.65±0.35	3.074±0.020	-1.977±0.086
273	-2.58±0.34	3.208±0.026	-1.998±0.059
283	-2.43±0.27	3.318±0.027	-1.944±0.051
293	-2.30±0.17	3.393±0.011	-1.800±0.026
298	-2.23±0.18	3.485±0.010	-1.745±0.063
303	-2.15±0.19	3.524±0.009	-1.682±0.044
313	-2.09±0.28	3.545±0.010	-1.642±0.029
323	-2.03±0.33	3.609±0.011	-1.642±0.058
333	-2.02±0.42	3.646±0.009	-1.745±0.054
343	-1.98±0.82	3.708±0.013	-1.809±0.058
353	-1.93±0.65	3.772±0.016	-1.874±0.038
363	-1.88±0.77	3.857±0.014	-1.947±0.038
373	-1.81±0.50	3.921±0.022	-2.052±0.084
383	-1.79±0.39	3.933±0.026	-2.153±0.082
393	-1.78±0.61	4.019±0.030	-2.182±0.069

Table 6.14 The hydrostatic pressure derivatives B_{ij} of the thermodynamic SOEC without contributions from piezoelectric effects

T (K)	B_{11}	B_{13}	B_{33}
243	3.418±0.059	3.319±0.067	10.363±0.034
253	3.567±0.099	3.293±0.047	10.503±0.034
263	3.638±0.032	3.410±0.050	10.537±0.034
273	3.903±0.044	3.439±0.052	10.646±0.034
283	3.995±0.045	3.395±0.014	10.853±0.035
293	3.859±0.028	3.401±0.057	11.044±0.035
298	3.943±0.100	3.380±0.041	11.112±0.035
303	3.870±0.039	3.412±0.058	11.165±0.045
313	3.954±0.046	3.515±0.031	11.301±0.037
323	4.197±0.036	3.619±0.038	11.445±0.037
333	4.510±0.053	3.744±0.062	11.608±0.041
343	4.856±0.066	3.889±0.177	11.737±0.042
353	5.326±0.088	4.136±0.132	11.763±0.039
363	5.767±0.085	4.263±0.159	11.901±0.040
373	6.074±0.067	4.430±0.067	12.029±0.043
383	6.279±0.082	4.667±0.026	12.134±0.045
393	6.589±0.082	4.743±0.099	12.361±0.045

Table 6.14 (Continued)

T (K)	B_{14}	B_{44}	B_{66}
243	-3.991±0.029	2.827±0.046	-3.637±0.093
253	-3.892±0.038	2.924±0.040	-3.585±0.022
263	-3.853±0.026	2.964±0.033	-3.600±0.034
273	-3.647±0.028	3.109±0.033	-3.480±0.018
283	-3.506±0.021	3.220±0.028	-3.436±0.017
293	-3.451±0.014	3.285±0.016	-3.464±0.006
298	-3.332±0.005	3.380±0.016	-3.364±0.027
303	-3.307±0.014	3.416±0.017	-3.354±0.017
313	-3.233±0.026	3.437±0.024	-3.331±0.012
323	-3.055±0.027	3.513±0.029	-3.165±0.018
333	-2.867±0.037	3.568±0.036	-2.996±0.009
343	-2.639±0.076	3.648±0.069	-2.775±0.045
353	-2.370±0.060	3.734±0.054	-2.501±0.038
363	-2.089±0.071	3.839±0.064	-2.227±0.046
373	-1.849±0.041	3.922±0.044	-2.051±0.024
383	-1.672±0.028	3.945±0.036	-1.951±0.031
393	-1.401±0.052	4.049±0.053	-1.681±0.019

Table 6.15 The hydrostatic pressure derivatives B_{IJ} of the thermodynamic SOEC at 298K

Source	B_{11}	B_{13}	B_{33}
Data (1)	5.79±0.11	4.37±0.30	11.112±0.037
Data (2)	3.94±0.10	3.380±0.041	11.112±0.035
Thurston et al (1966)	5.358±0.030	5.050±0.042	12.079±0.043
Source	B_{14}	B_{44}	B_{66}
Data (1)	-2.23±0.18	3.485±0.010	-1.745±0.063
Data (2)	-3.332±0.005	3.380±0.016	-3.364±0.027
Thurston et al (1966)	1.731±0.014	4.081±0.014	-1.185±0.014

(1) With contributions from piezoelectric effects.

(2) Without contributions from piezoelectric effects.

6.3 The volume compression induced by application of hydrostatic pressure

Knowledge of the compression $V(P)/V_0$ (the ratio of the volume at an arbitrary pressure $V(P)$ to that at atmospheric pressure V_0) is useful in theoretical studies of the physical properties of a solid under pressure. Although the dependence of ultrasonic wave velocity with pressure can be measured with precision, the pressure range which can be applied in practice is limited. However, it has been shown that the bulk modulus and its pressure derivatives determined by low-pressure ultrasonic velocity measurements can be used to estimate compression at high pressure (Anderson 1966). This can be achieved using an extrapolation procedure based on the Murnaghan equation of state (Murnaghan 1944):

$$P = \frac{B_0^T}{B'^T_0}\left\{\left(\frac{V_0}{V(P)}\right)^{B'^T_0} - 1\right\} \quad . \tag{6.12}$$

This is may be written in the logarithmic form

$$\ln\left(\frac{V_0}{V(P)}\right) = \frac{1}{B'^T_0}\ln\left(\frac{B'^T_0}{B_0^T}P + 1\right) \quad , \tag{6.13}$$

where B_0^T and B'^T_0 are the isothermal bulk modulus and its pressure derivative at zero pressure respectively. The above equations are based on the assumption that the bulk modulus B has a linear relation with pressure. As shown by Anderson (1966), Eq. (6.13) describes well the compression of many solids.

Ultrasonic measurements give adiabatic moduli and so, in order to use this equation of state, it is necessary to transform the input data to isothermal moduli. The adiabatic and isothermal bulk moduli are related by

$$B_0^S = B_0^T(1 + \alpha\gamma T) \quad , \tag{6.14}$$

where α and γ are the volume thermal expansion coefficient and the thermal Grüneisen parameter respectively. The isothermal hydrostatic pressure derivative B'^{T}_{0} can be obtained by (Overton 1962, Anderson 1966)

$$B'^{T}_{0} = B'^{S}_{0} + T\alpha\gamma\left(\frac{B^{T}_{0}}{B^{S}_{0}}\right)\left[1 - \frac{2}{\alpha B^{T}_{0}}\left(\frac{\partial B^{T}}{\partial T}\right)_{P=0} - 2B'^{S}_{0}\right] + \left[T\alpha\gamma\left(\frac{B^{T}_{0}}{B^{S}_{0}}\right)\right]^{2}\left[B'^{S}_{0} - 1 - \frac{1}{\alpha^{2}}\left(\frac{\partial \alpha}{\partial T}\right)_{P=0}\right] \quad , \tag{6.15}$$

where $(\partial B^{T}/\partial T)_{P=0}$ is given by

$$\left(\frac{\partial B^{T}_{0}}{\partial T}\right)_{P} = \left(\frac{\partial B^{S}_{0}}{\partial T}\right)_{P}/(1+T\alpha\gamma) - \frac{B^{S}_{0}}{T}\frac{T\alpha\gamma}{[1+T\alpha\gamma]^{2}}\left\{1 + \frac{(\partial\alpha/\partial T)_{P}}{\alpha/T}\right\} \quad . \tag{6.16}$$

by taking $(\partial\gamma/\partial T)_{P} = 0$. If the temperature dependence of the thermal Grüneisen parameter γ is considered, the expression (6.16) has a correction term given by $(\partial\gamma/\partial T)_{P}$ and takes the form

$$\left(\frac{\partial B^{T}_{0}}{\partial T}\right)_{P} = \left(\frac{\partial B^{S}_{0}}{\partial T}\right)_{P}/(1+T\alpha\gamma) - \frac{B^{S}_{0}}{T}\frac{T\alpha\gamma}{[1+T\alpha\gamma]^{2}}\left\{1 + \frac{(\partial\alpha/\partial T)_{P}}{\alpha/T} + \frac{(\partial\gamma/\partial T)_{P}}{\gamma/T}\right\} \quad . \tag{6.17}$$

The compression of VHPQ has been calculated by using Eq. (6.13), the logarithmic form of Murnaghan equation of state. For VHPQ the volume thermal expansion coefficient is not available, hence the value for the standard synthetic quartz has been used, which has been determined from the thermal expansion tensors given by James (1987) (Eq. 5.8). The Grüneisen parameter γ used in these calculations has been calculated from

$$\gamma = \frac{\alpha B^{S}_{0}}{\rho_{0} C_{P}} \quad . \tag{6.18}$$

Here ρ_0 is the density of the VHPQ under atmospheric pressure and C_P is the specific heat at constant pressure. The values used for C_P has been estimated from an empirical equation given by Samsonov (1973) for α-quartz (Eq. 5.9). The temperature dependence

of the adiabatic bulk modulus $(\partial B^S/\partial T)_{P=0}$, calculated from the data given in Table 6.12, is in the form of a polynomial as a function of temperature T (in the unit of 10^{10} Pa K^{-1})

$$(\partial B^S/\partial T)_{P=0} = -7.818\times10^{-3} + 5.231\times10^{-5}T - 9.630\times10^{-8}T^2 \quad . \qquad (6.19)$$

The values of $(\partial\alpha/\partial T)_{P=0}$ has been estimated from the thermal expansion coefficient of standard synthetic quartz (James 1987) (Eq. 5.10), which can be expressed as

$$(\partial\alpha/\partial T)_{P=0} = 7.093 - 1.086\times10^{-2}(T-298) \qquad (10^{-8}K^{-1}) \quad . \qquad (6.20)$$

Insertion of data for B_0^S, α, γ, $(\partial\alpha/\partial T)_P$ and $(\partial B^S/\partial T)_{P=0}$ into Eq. (6.16) or Eq. (6.17) gives values of $(\partial B^T/\partial T)_{P=0}$. To estimate the effect of the temperature dependence of the thermal Grüneisen parameter γ, $(\partial B_0^T/\partial T)_{P=0}$ has been calculated respectively by using Eq. (6.16) and Eq. (6.17). The temperature derivative of the thermal Grüneisen parameter $(\partial\gamma/\partial T)_{P=0}$ can be obtained by differentiating Eq. (6.18)

$$\left(\frac{\partial\gamma}{\partial T}\right)_P = \frac{1}{\rho_0 C_P}\left[\alpha\left(\frac{\partial B^S}{\partial T}\right)_P + B_0^S\left(\frac{\partial\alpha}{\partial T}\right)_P\right] - \gamma\left[\frac{(\partial\rho/\partial T)_P}{C_P} + \frac{(\partial C_P/\partial T)_P}{\rho_0}\right] \quad . \qquad (6.21)$$

It has been demonstrated by calculation that the effect of the correction to $(\partial B^T/\partial T)_{P=0}$ of the term $(\partial\gamma/\partial T)_{P=0}$ is very small and does not cause any significant variation in the results of volume compression. The correction to $B'^T_0 (= \partial B_0^T/\partial P)$ from the term $(\partial B^T/\partial T)_P$ is also very small.

The volume compression of VHPQ at 243K, 298K, 333K and 393K is given in Fig. 6.6. The values for the relevant quantities at the four selected temperatures are given in Table 6.16. For comparison, the parameters corrected by using $(\partial\gamma/\partial T)_{P=0}$ are also listed in Table 6.16.

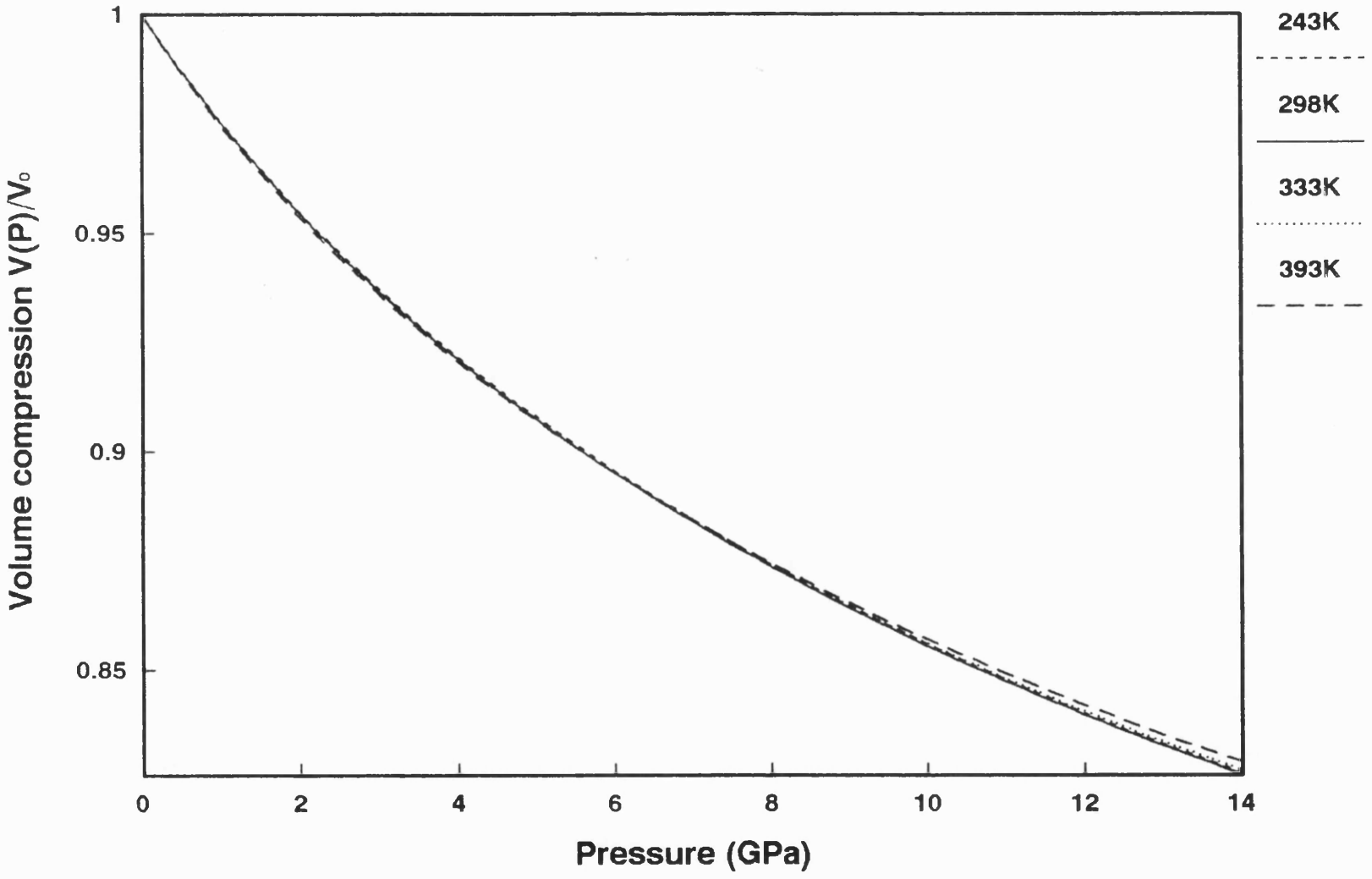

Fig. 6.6 The volume compression of VHPQ extrapolated to high pressure at 243K, 298K, 333K and 393K.

Table 6.16 The parameters used to calculate volume compression

T (K)	B_0^S (10^{10} Pa)	$(\partial B^S/\partial T)_{P=0}$ (10^7 PaK^{-1})	$(\partial B^S/\partial P)_{T,P=0}$	B_0^T (10^{10} Pa)	$(\partial B^T/\partial T)_{P=0}$ (10^7 PaK^{-1})
243	3.758	-0.745	6.415	3.741	-0.876
298	3.714	-0.723	6.541	3.695	-0.855
333	3.693	-1.012	6.665	3.659	-1.145
393	3.599	-2.057	6.950	3.559	-2.181

T (K)	α (10^{-6} K^{-1})	$(\partial\alpha/\partial T)_{P=0}$ (10^{-8} K^{-2})	γ	$(\partial\gamma/\partial T)_{P=0}$ (10^{-3} K^{-1})	$(\partial B^T/\partial P)_{T,P=0}$
243	30.958	7.690	0.727	-5.627	6.426
298	35.023	7.093	0.663	-2.844	6.506
333	37.439	6.713	0.649	-2.065	6.693
393	41.271	6.061	0.634	-1.553	7.118

The parameters with correction from $(\partial\gamma/\partial P)_{P=0}$

T (K)	$(\partial B^T/\partial T)_{P=0}$ (10^7 PaK^{-1})	$(\partial B^T/\partial P)_{T,P=0}$	T (K)	$(\partial B^T/\partial T)_{P=0}$ (10^7 PaK^{-1})	$(\partial B^T/\partial P)_{T,P=0}$
243	-0.718	6.411	333	-1.051	6.682
298	-0.746	6.494	393	-2.093	7.106

The parameters used by Anderson (1966) to calculate volume compression

T (K)	α (10^{-6} K^{-1})	$(\partial\alpha/\partial T)_{P=0}$ (10^{-8} K^{-2})	γ	B_0^S (10^{10} Pa)	$(\partial B^S/\partial T)_{P=0}$ (10^7 PaK^{-1})	$(\partial B^S/\partial P)_{T,P=0}$
298	35.6	6.1	0.746	3.741	-0.711	6.33

There is no significant difference between the compression at different temperatures when the pressure is low, but at high pressure differences do arise. The volume compression of VHPQ at 298K is compared in Fig. 6.7 with that of α-quartz measured by Bridgman (1948a and 1948b), Wackerle (1962), Jorgensen (1978), Levien et al. (1980), Hazen et al. (1989) and Glinnemann et al. (Chelikowsky et al. 1990). It is also compared with the compression of α-quartz computed by Anderson (1966) who used the values of B_0^S and $(\partial B_0^S/\partial P)_{P=0}$ determined by McSkimin et al. (1965). The parameters used by Anderson (1966) are also given in Table 6.16. Fig. 6.7 shows a very good agreement between the computation and most of the measurements and also with Anderson's calculated results. At high pressures, accurate measurement of the pressure is difficult. From Fig. 6.7 it can be seen that at high pressures, the data of the compression experimentally determined scatter around that estimated from the ultrasonic data.

On the microscopic scale a volume compression can occur in three ways, all of which are possible in α-quartz (Jorgensen 1978). These are: (i) a cooperative, rigid rotation of the linked tetrahedra; (ii) a distortion of the tetrahedra arising from bond-angle changes within the tetrahedra with bond lengths remaining constant; (iii) a decrease in bond length. Each SiO_4 tetrahedron has four Si-O bonds and six O-Si-O angles. The four oxygen corners are shared by neighbouring tetrahedra which are allowed to rotate or tilt. In general, when subjected to an applied pressure or a temperature change, the structure change of α-quartz includes a combination of tetrahedral distortion and tilting (Jorgensen 1978). However, because the neighbours of the tetrahedra are linked at the corners by much weaker forces than those which give rise to the tetrahedral structure (Grimm and Dorner 1974), a quartz lattice can be visualized as consisting of rigid SiO_4 tetrahedra units as long as an applied force is insufficient to cause the tetrahedra to distort significantly. Hence, changes of the dimensions of the unit cell induced by pressure and temperature in α-quartz can be explained as being dominated by a simultaneous tilt of tetrahedra around their two-fold axis (Grimm and Dorner 1974, Jorgensen 1978) within

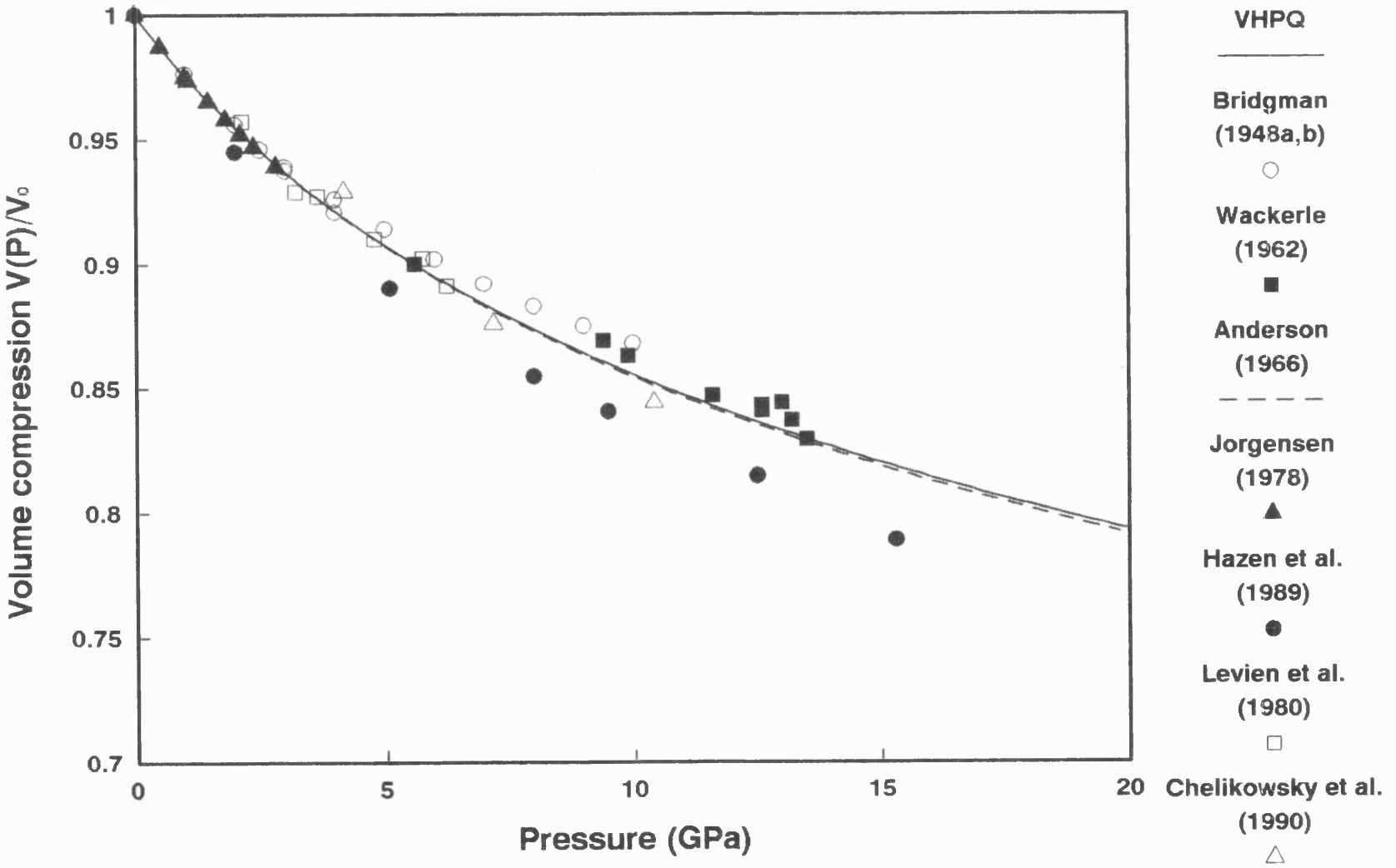

Fig. 6.7 The comparison of volume compression with other author's data at 298K.

the regime in which pressure is not very high. A tilt angle δ has been defined by Grimm and Dorner (1974). Jorgensen (1978) has shown from powder neutron diffraction measurements under high pressure that the tilt angle in α-quartz increases with increasing applied pressure. δ is equal to 15.9±4° at zero pressure and to 20.4±5° at 2.82GPa. Jorgensen's measurements have also indicated that the average Si-O bond distance remains constant over the pressure range from zero to 2.82GPa and the O-Si-O angle does not change significantly so as to cause any considerable distortion of the tetrahedra, thereby providing a confirmation of the validity of the rigid unit model in this pressure range. By contrast, Jorgensen's measurements show a considerable change in the Si-O-Si angle linking neighbouring tetrahedra when the pressure increases. The change in the Si-O-Si angle is attributed to the tetrahedra tilting. The tilt angle increases linearly with pressure from zero to 2.82GPa (Jorgensen 1978), which is consistent with the almost-linear pressure dependence of the volume compression in this range. Fig. 6.7 shows that at pressures up to 2.8GPa the volume compression for VHPQ is the same as that given by Jorgensen (1978) for less pure material, so his remarks apply equally to VHPQ. As pressure increases, the volume compression shows more curvature (Fig. 6.7). At high pressures, the tetrahedral distortion becomes more important. The decrease of the rate of volume compression at higher pressure may be partly due to the gradually increasing distortion of the SiO_4 tetrahedra. A dramatic increase in the SiO_4 tetrahedra distortion at pressures to 6GPa has been observed by Levien et al. (1980). Hazen et al. (1989) reported additional distortion at higher pressures (to 12.5GPa): the intra-tetrahedral Si-O bond distances differ from the one at atmospheric pressure by more than 0.02Å and O-Si-O intra-tetrahedral angles deviate by several degrees. When pressure is higher than 20GPa the distortion of the SiO_4 tetrahedra leads to a gradual transformation from the crystalline phase to an amorphous phase (Hemley et al. 1988).

6.4 Changes in the lattice parameters with hydrostatic pressure

The lattice parameters of a crystal change when hydrostatic pressure is applied. These changes in the lattice parameters can also be calculated from the pressure derivatives of the SOEC. In a similar way to Murnaghan's work (Murnaghan 1944) for the calculation of the volume compression, Thurston (1966) has derived an extrapolation to calculate the lattice parameter changes under high pressure by using the ultrasonic data measured at atmospheric pressure and assuming that the pressure derivative of the bulk modulus is a constant at a constant temperature. Let λ_i be the stretch along any crystal axis. Then at any given pressure P it can be expressed as (Thurston 1966):

$$\ln\lambda_i = \left(a_i + \frac{B_0^T y_{i0}}{B'^T_0}\right)P - \frac{(B_0^T)^2 y_{i0}}{(B'^T_0)^2}\ln\left(1 + \frac{PB'^T_0}{B_0^T}\right) \tag{6.22}$$

or

$$\lambda_i = e^{\left(a_i + B_0^T y_{i0}/B'^T_0\right)P}\left(\frac{B^T}{B_0^T}\right)^{-\left(B_0^T\right)^2 y_{i0}/\left(B'^T_0\right)^2} , \tag{6.23}$$

where B^T is the isothermal bulk modulus under arbitrary pressure and can be expressed as:

$$B^T = B_0^T + B'^T_0 P \quad . \tag{6.24}$$

The parameter a_i is the linear coefficient in a power series of the stretch

$$\lambda_i = 1 + a_i P + \frac{1}{2} b_i P^2 + \ldots \tag{6.25}$$

and is related to the second order compliances by (Thurston 1966)

$$a_i = -s_i^T = -(s_{i1}^T + s_{i2}^T + s_{i3}^T) \tag{6.26}$$

where the subscripts i (=1, 2, 3) indicate the crystal axes. The parameter y_{i0} contains the coefficient of the square term in the power series (6.25)

$$y_{i0} = b_i - a_i^2 \quad . \tag{6.27}$$

The coefficient b_i can be determined by using the pressure derivatives of the effective SOEC from ultrasonic measurements (Thurston 1966):

$$b_i = s_{i\lambda}^T s_{\mu}^T \left(\frac{\partial C_{\lambda\mu}}{\partial P} \right)_P + s_i^T \quad , \tag{6.28}$$

where the subscript λ and μ=1, 2, 3.

Trigonal crystals have two principle stretch directions: along crystal axes a (indicated by a subscript $\perp$) and c (indicated by a subscript $||$). Along the a axis the coefficients a_i and b_i of the series power (6.25) are

$$a_\perp = -(s_{11}^T + s_{12}^T + s_{13}^T) \quad , \tag{6.29}$$

$$b_\perp = (s_{11}^T + s_{12}^T + s_{13}^T)^2 + (s_{11}^T + s_{12}^T)Q_1 + s_{13}^T Q_3 \quad , \tag{6.30}$$

where

$$Q_1 = (s_{11}^T + s_{12}^T + s_{13}^T)\left[\left(\frac{\partial C_{11}}{\partial P} \right)_T + \left(\frac{\partial C_{12}}{\partial P} \right)_T \right] + (2s_{13}^T + s_{33}^T)\left(\frac{\partial C_{13}}{\partial P} \right)_T \quad , \tag{6.31}$$

$$Q_3 = 2(s_{11}^T + s_{12}^T + s_{13}^T)\left(\frac{\partial C_{13}}{\partial P} \right)_T + (2s_{13}^T + s_{33}^T)\left(\frac{\partial C_{33}}{\partial P} \right)_T \quad . \tag{6.32}$$

The parameter y_{i0} is

$$y_{\perp 0} = b_\perp - a_\perp^2 \quad . \tag{6.33}$$

Therefore, the stretch or compression along the a axis is

$$\frac{a}{a_0} = e^{\left(a_\perp + B_0^T y_{\perp 0}/B'^T_0\right)P} \left(\frac{B^T}{B_0^T} \right)^{-\left(B_0^T\right)^2 y_{\perp 0}/\left(B'^T_0\right)^2} \quad . \tag{6.34}$$

Along the c axis the coefficients a_i and b_i of the series power (6.25) are

$$a_{||} = -(2s_{13}^T + s_{33}^T) \quad , \tag{6.35}$$

$$b_{||} = (2s_{13}^T + s_{33}^T)^2 + 2s_{13}^T Q_1 + s_{33}^T Q_3 \quad . \tag{6.36}$$

The parameter y_{i0} is

$$y_{||} = b_{||} - a_{||}^2 \quad . \tag{6.37}$$

The stretch, or compression, along the c axis is

$$\frac{c}{c_0} = e^{\left(a_{||} + B_0^T y_{||0}/B'^T_0\right)P} \left(\frac{B^T}{B_0^T}\right)^{-\left(B_0^T\right)^2 y_{||0}/\left(B'^T_0\right)^2} \quad . \tag{6.38}$$

The coefficients $a_\perp$, $b_\perp$, $a_{||}$ and $b_{||}$ at 243K, 298K, 333K and 393K are listed in Table 6.17, for comparison, together with those used by Thurston (1966).

Table 6.17 The coefficients used in the calculation of linear compression

T (K)	$a_\perp$ (10^{-12} Pa^{-1})	$b_\perp$ (10^{-24} Pa^{-2})	$a_{||}$ (10^{-12} Pa^{-1})	$b_{||}$ (10^{-24} Pa^{-2})
243	-9.7707	0.1639	-7.2165	0.1105
298	-9.9387	0.1743	-7.2309	0.1169
333	-10.0425	0.1835	-7.2115	0.1260
393	-10.2926	0.2170	-7.4881	0.1554
The coefficients used by Thurston (1966)				
T (K)	$a_\perp$ (10^{-12} Pa^{-1})	$b_\perp$ (10^{-24} Pa^{-2})	$a_{||}$ (10^{-12} Pa^{-1})	$b_{||}$ (10^{-24} Pa^{-2})
298	-9.815	0.1631	-7.306	0.1575

The changes in the lattice parameters a/a_0 and c/c_0 at 243K, 298K, 333K and 393K are given in Fig. 6.8. The change along the lateral principal axis a is larger than that along the axial axis c . Both changes a/a_0 and c/c_0 at high pressures show a pronounced decrease with increasing temperature. Fig 6.9 ((a) and (b) gives a comparison of a/a_0 and c/c_0 computed in this work with those determined by other authors at 298K. The comparison is also given for the changes in the lattice parameters calculated by Thurston (1966) who used the data determined by McSkimin et al. (1965). Jorgensen (1978) has measured the changes in a/a_0 and c/c_0 up to 2.5GPa. There is good agreement of this measurement with the computed results (Fig. 6.9 (a) and (b)), as expected in that range. The computed a/a_0 fits well (Fig. 6.9 (a)) with those determined experimentally by Levien et al. (1980) and McWhan (1967) up to about 6GPa and 15GPa respectively and agrees with the results computed by Thurston (1966), except at high pressures. At higher pressures, McWhan's data show that the measured compression along the a axis is greater than the results obtained from the computations. The data measured by Hazen et al. (1989) show much greater changes in parameter a under hydrostatic pressure (Fig. 6.9 (a)). The deviation among the computed and measured c/c_0 results at high pressure is more pronounced (Fig. 6.9 (b)): our data for VHPQ show larger changes at high pressure than the measurements by McWhan (1967) and Hazen et al. (1989) on their materials while the computation of Thurston (1966) shows a smaller change and eventual saturation at high pressures. Hence, at high pressures the computation by our ultrasonic data measured at ambient pressure gives an overestimation on c/c_0 while the computation given by Thurston (1966) gives an under-estimation.

According to the discussion given in last section for the volume compression at high pressures the pressure induced changes in the lattice parameters can be attributed to the dominant role of the tilting of SiO_4 tetrahedra around their two-fold axis when pressure is not very high and to the gradually increasing distortion of the tetrahedra at higher

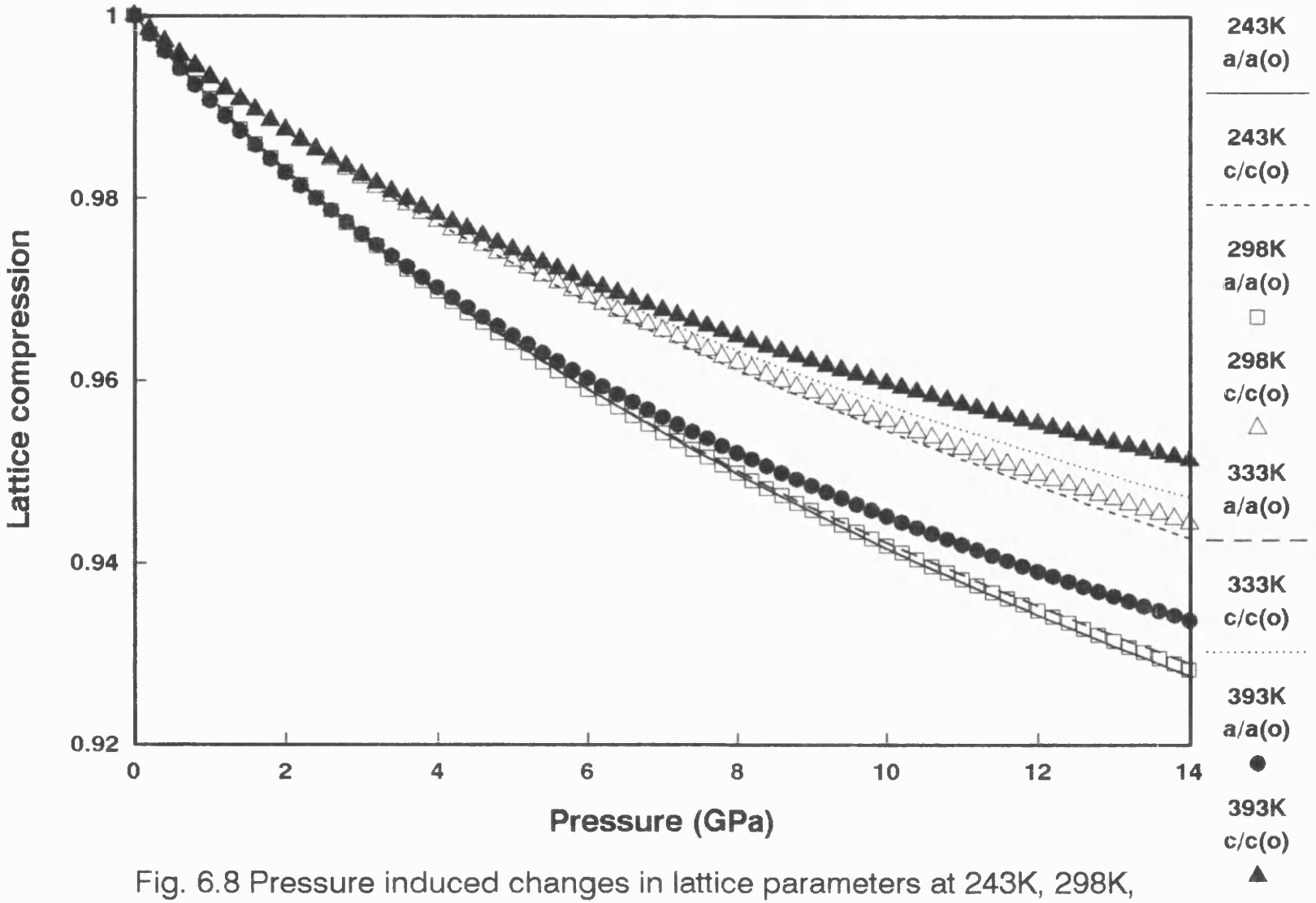

Fig. 6.8 Pressure induced changes in lattice parameters at 243K, 298K, 333K and 393K.

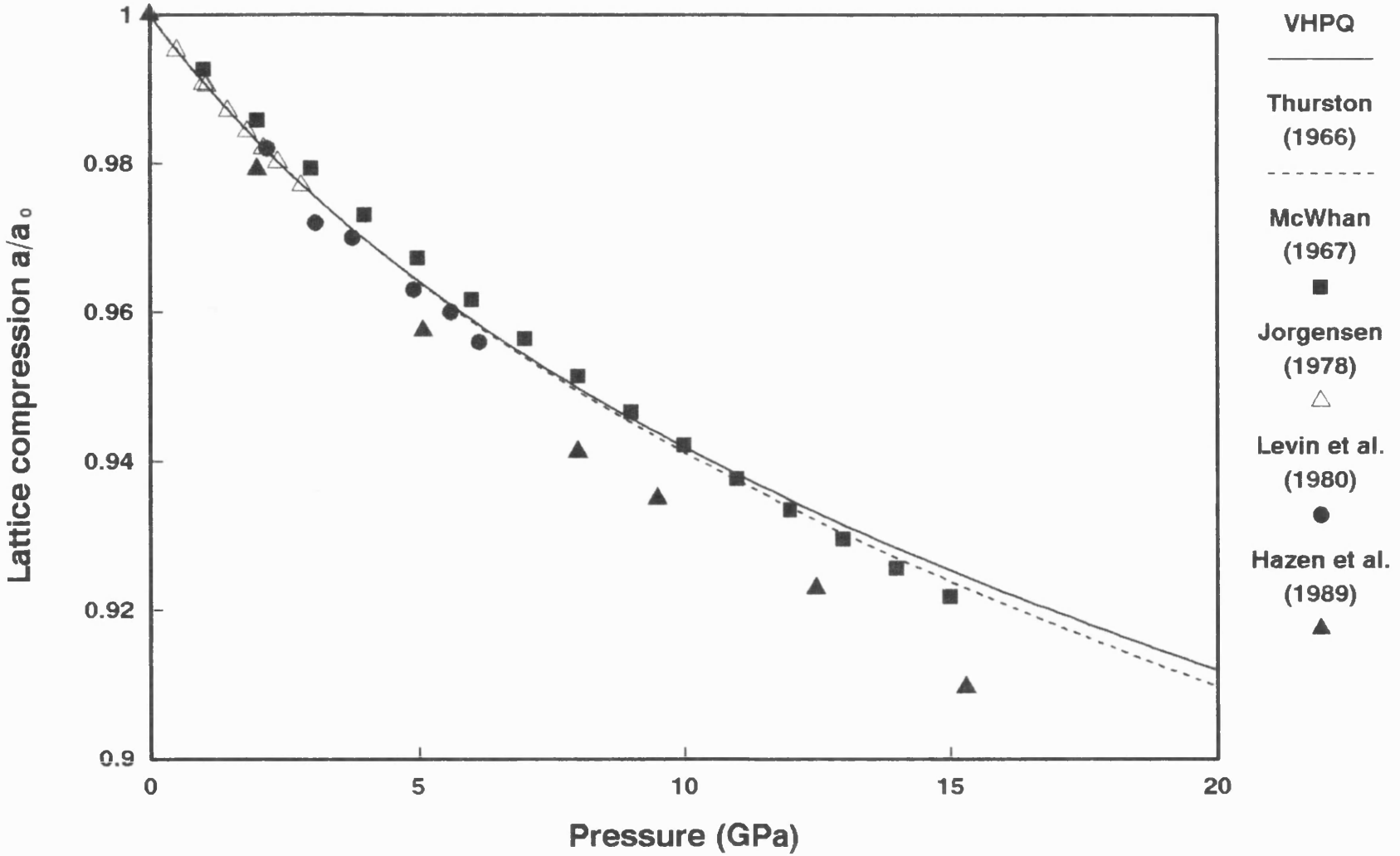

Fig. 6.9 (a) The comparison of changes in lattice parameter a induced by pressure at 298K.

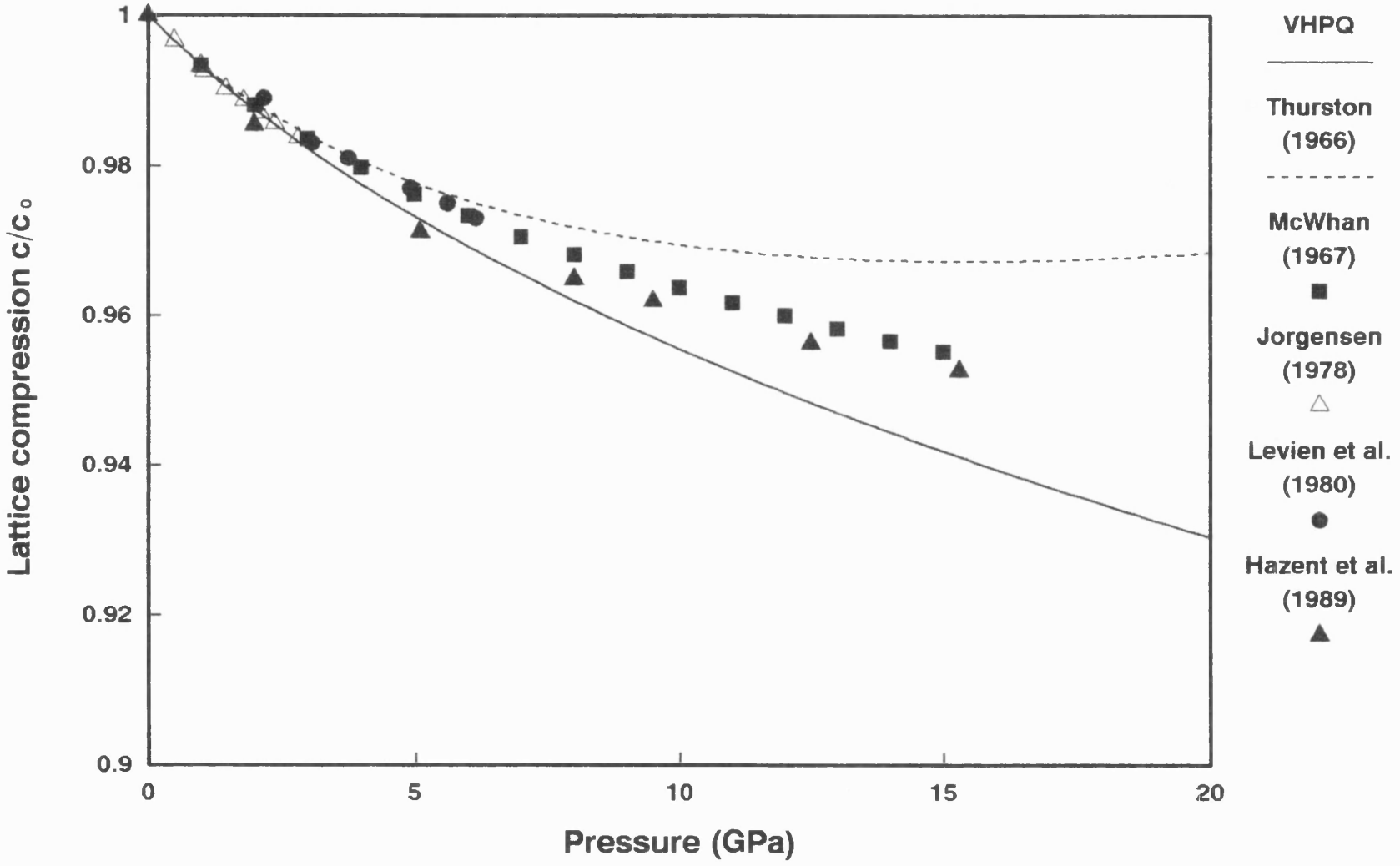

Fig. 6.9 (b) The comparison of changes in lattice parameter c induced by pressure at 298K.

pressures. The significant temperature dependences of the variations of the ratios a/a_0 and c/c_0 at high pressure (Fig. 6.9) indicate that the distortion of SiO_4 tetrahedra has stronger temperature dependence at higher pressure.

6.5 Negative $(\partial C_{IJ}/\partial P)_{T,P=0}$ and α-β phase transition

α-quartz transforms (Le Chatelier 1889) at 846K to β-quartz (space group $P6_422$ or $P6_222$). Light scattering showed that the transformation is first order and displacive (Shapiro and Cummins 1968, Shapiro et al. 1967). Since Raman and Nedungadi made their spectroscopic investigation of the structural phase transition in quartz (Raman and Nedungadi 1940), it has been suspected that the $\alpha-\beta$ transition was related to phonons. Using the harmonic approximation, Elcombe (1967) determined the eigenvectors of the long-wavelength normal modes and found that the eigenvector of the lowest symmetric mode is very similar to the displacements which occur during the $\alpha-\beta$ transition. It is confirmed by inelastic neutron scattering (Axe and Shirane 1970) that the long-wavelength mode is very structure dependent and intimately related to the $\alpha-\beta$ transition. Bauer et al. (1971) showed that the transition is driven by an optic phonon at the zone centre (q=0), which is very soft in the [ξ00] direction. There is only one irreducible representation for phonons in α-quartz with $\vec{q}$ in the [ξ00] direction so that one branch cannot cross another: as the optic branch softens it pushes down the transverse-acoustic phonon in that direction. This depressed acoustic branch has a slope ω/q equal to $(C_{66}/\rho)^{\frac{1}{2}}$. The experimental value of C_{66} for α-quartz is consistent with the calculated depression of this acoustic branch for wave vectors close to the zone centre (Bauer et al. 1971). The shear elastic stiffness C_{66} for α-quartz shows an anomalous increase with temperature (Atanasoff and Hart 1941) and $(\partial C_{66}/\partial P)_T$ has a negative value, features which identify acoustic-mode softening (Sidek et al. 1987). A decrease in an elastic constant under the influence of pressure can indicate incipient lattice instability because it corresponds to

a reduction in crystal stiffness for the associated acoustic-phonon mode (Chang and Barsch 1973). The finding of a negative pressure derivative for C_{66} indicates that even at room temperature there could be a degree of interaction between the soft optic phonon and the transverse-acoustic phonon in the same crystallographic direction leading to the anomalous behaviour of C_{66} with pressure and temperature.

The main contribution to the strain at the $\alpha-\beta$ transition is produced by rotation of the SiO_4 tetrahedra about their respective twofold axes (Höchli and Scott 1971) which comprises the displacement parameter in the α-quartz structure. Höchli and Scott (1971) showed that the elastic constant C_{14} in α-quartz is related to the displacement parameter x_0 by $C_{14}\sim x_0$ and their ultrasonic measurements show that near the transition temperature the elastic constant $C_{14}(T)$ behaves as the displacement parameter, as does the soft optic phonon frequency $\omega(T)$. It can be deduced from the above discussion that, although for α-quartz C_{14} is always coupled to other elastic constants in the relevant plane wave modes, the negative $(\partial C_{14}/\partial P)_T$ is also one of the results of the interaction between the soft optic phonons and the transverse-acoustic phonons in quartz.

6.6 Temperature dependences of the TOEC of VHPQ

6.6.1 Determination of the TOEC of VHPQ

The uniaxial pressure derivatives of the natural velocities of ultrasonic waves propagated in VHPQ from measurements are used together with the hydrostatic pressure derivatives B_{IJ} of the thermodynamic SOEC to determine the TOEC by using the equations given in section 2.5.4. The B_{IJ} are related to the TOEC, in tensor notation, by the equation:

$$B_{jrks} = -s^{T}_{iiuv} C_{uvjrks} \quad . \tag{6.39}$$

In matrix notation, Eq. (6.39) can be expanded for six independent B_{IJ} for rhombohedral (RI) crystals as follows (Thurston et al. 1965):

$$
\begin{aligned}
B_{11} &= -(s_1 C_{111} + s_1 C_{112} + s_3 C_{113}) \quad , \\
B_{13} &= -(s_1 C_{113} + s_1 C_{123} + s_3 C_{133}) \quad , \\
B_{33} &= -(2 s_1 C_{133} + s_3 C_{333}) \quad , \\
B_{44} &= -(s_1 C_{144} + s_1 C_{155} + s_3 C_{344}) \quad , \\
B_{14} &= -(s_1 C_{114} + s_1 C_{124} + s_3 C_{134}) \quad , \\
B_{66} &= -\frac{1}{2}(-s_1 C_{112} + s_3 C_{113} - s_3 C_{123} + s_1 C_{222}) \quad ,
\end{aligned}
\tag{6.40}
$$

where

$$
\begin{aligned}
s_1 &= s_{11}^T + s_{12}^T + s_{113}^T \quad , \\
s_3 &= 2 s_{13}^T + s_{33}^T \quad .
\end{aligned}
\tag{6.41}
$$

The wave modes which have been measured under uniaxial stress are 1A, 1B, 4B, 6A, 6B, 7A, 8A, 8B and 10B (the definitions of the modes have been given in Table 5.13), which were propagated in the same samples used in measurements under hydrostatic pressure. The uniaxial pressure derivatives of the natural velocities of the nine modes from 243K to 393K are given in Table 6.18. The pressure derivatives $(1/W_0)(\partial W/\partial P)_{T,P=0}$ of most modes become larger as the temperature increases (Fig. 6.10). The values of $(1/W_0)(\partial W/\partial P)_{T,P=0}$ for modes 7A and 6B increase linearly, while those for modes 1A and 8A show a bend at 343K and 300K respectively. Data for modes 1B and 8B show curvature; $(1/W_0)(\partial W/\partial P)_{T,P=0}$ for modes 4B, 6A and 10B do not change so much as those for other modes. $(1/W_0)(\partial W/\partial P)_{T,P=0}$ for mode 6A decreases as temperature is rising while that of mode 4B remains almost constant. There is a maximum at about 323K for mode 10B.

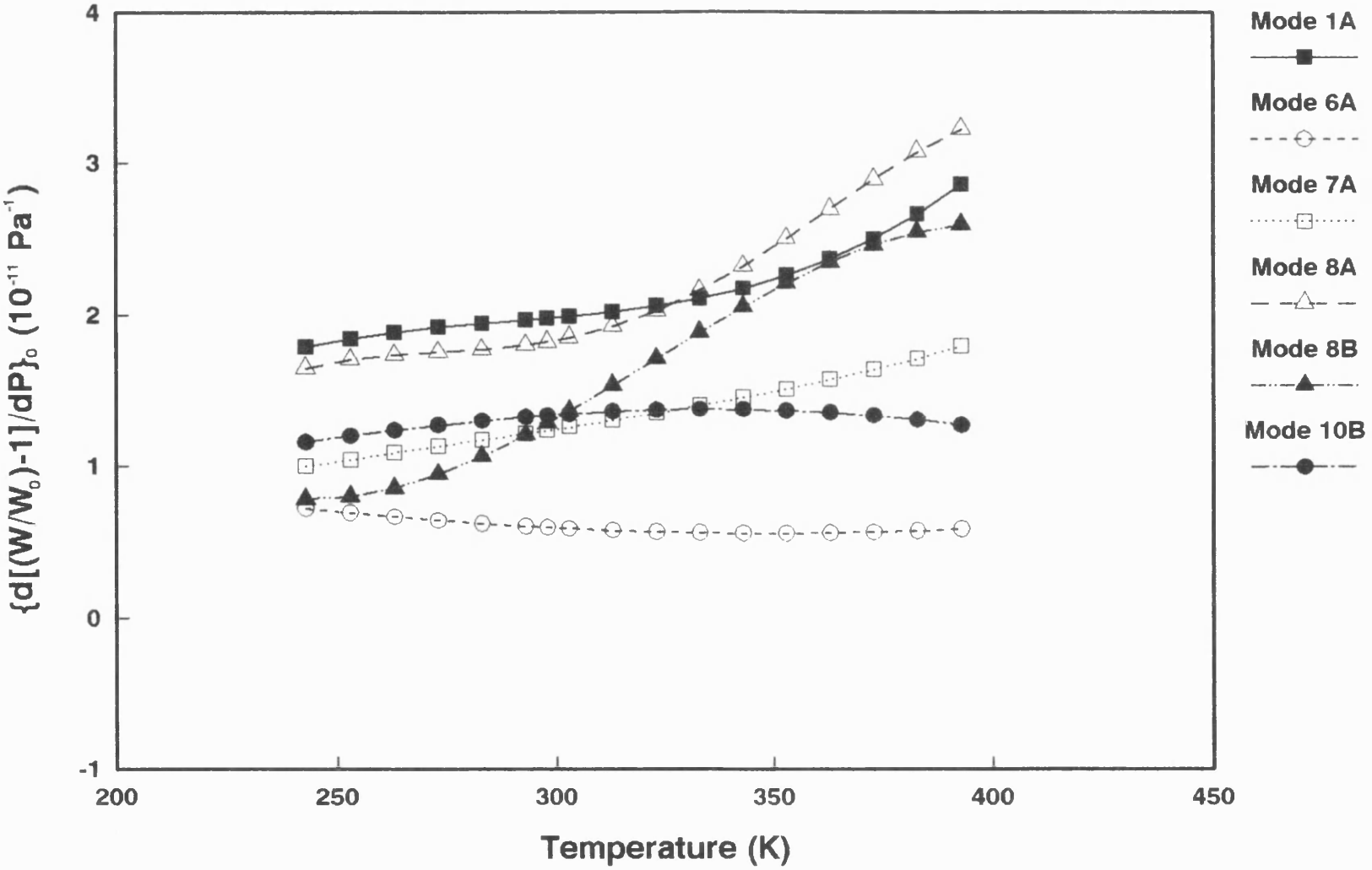

Fig. 6.10 (a) The temperature dependences of the uniaxial pressure derivatives of the relative natural velocity.

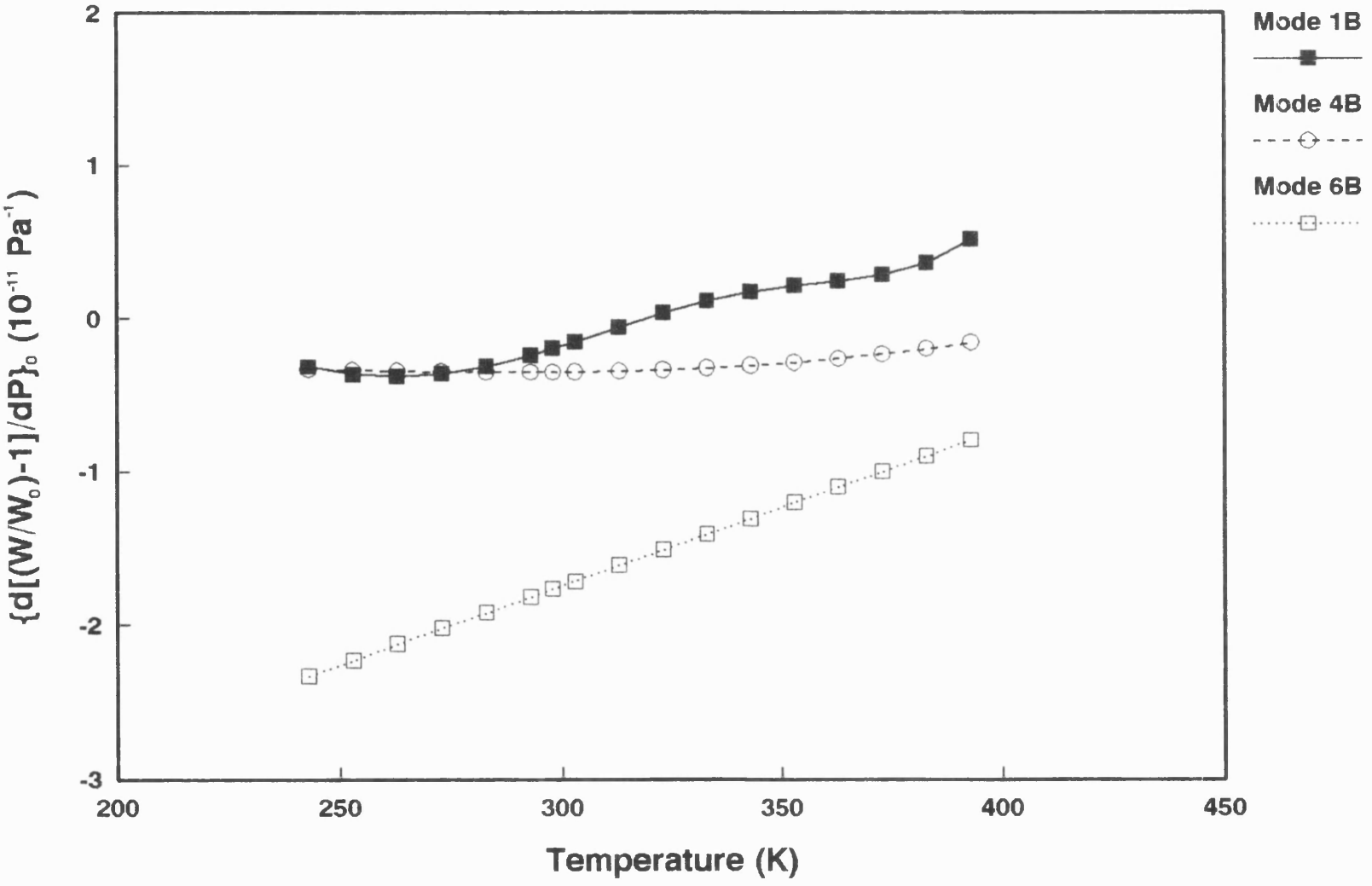

Fig. 6.10 (b) The temperature dependences of the uniaxial pressure derivatives of the relative natural velocity.

Table 6.18 Measured values for $(1/W_0)(\partial W/\partial P)_{T,P=0}$ of the ultrasonic modes under uniaxial stress (10^{-11} 1/Pa) (The mode nomenclature is given in Table 5.13)

T (K)	Mode 1A	Mode 1B	Mode 4B	Mode 6A
243	1.790±0.014	-0.314±0.008	-0.330±0.010	0.723±0.007
253	1.845±0.011	-0.362±0.005	-0.337±0.004	0.693±0.006
263	1.887±0.007	-0.377±0.005	-0.342±0.004	0.666±0.010
273	1.919±0.004	-0.359±0.004	-0.347±0.004	0.642±0.005
283	1.945±0.009	-0.311±0.004	-0.349±0.006	0.622±0.004
293	1.969±0.006	-0.238±0.004	-0.350±0.008	0.604±0.002
298	1.982±0.006	-0.195±0.003	-0.349±0.007	0.596±0.009
303	1.995±0.006	-0.149±0.005	-0.347±0.009	0.589±0.008
313	2.025±0.007	-0.054±0.005	-0.342±0.006	0.577±0.006
323	2.063±0.007	0.036±0.014	-0.334±0.004	0.567±0.007
333	2.113±0.004	0.115±0.010	-0.322±0.004	0.561±0.007
343	2.179±0.005	0.175±0.009	-0.306±0.004	0.558±0.012
353	2.264±0.004	0.217±0.011	-0.286±0.007	0.558±0.011
363	2.372±0.007	0.249±0.011	-0.261±0.006	0.560±0.010
373	2.506±0.007	0.287±0.013	-0.231±0.007	0.566±0.010
383	2.669±0.012	0.363±0.020	-0.196±0.007	0.574±0.009
393	2.866±0.028	0.522±0.023	-0.155±0.005	0.585±0.008

Table 6.18 (Continued)

T (K)	Mode 6B	Mode 7A	Mode 8A	Mode 8B
243	-2.328±0.012	1.001±0.006	1.650±0.026	0.785±0.016
253	-2.226±0.017	1.045±0.004	1.707±0.021	0.800±0.010
263	-2.124±0.008	1.088±0.004	1.735±0.013	0.856±0.007
273	-2.022±0.008	1.112±0.006	1.754±0.019	0.946±0.005
283	-1.919±0.010	1.173±0.007	1.772±0.014	1.065±0.005
293	-1.817±0.010	1.215±0.005	1.801±0.015	1.207±0.005
298	-1.766±0.014	1.237±0.009	1.823±0.020	1.285±0.008
303	-1.715±0.017	1.259±0.007	1.851±0.024	1.366±0.006
313	-1.613±0.013	1.305±0.011	1.926±0.019	1.537±0.016
323	-1.510±0.008	1.352±0.008	2.030±0.011	1.712±0.034
333	-1.408±0.012	1.402±0.011	2.164±0.011	1.888±0.010
343	-1.306±0.016	1.456±0.014	2.325±0.006	2.056±0.012
353	-1.204±0.035	1.513±0.010	2.507±0.010	2.213±0.006
363	-1.101±0.035	1.575±0.013	2.702±0.009	2.351±0.009
373	-0.999±0.034	1.642±0.017	2.899±0.008	2.465±0.021
383	-0.897±0.033	1.715±0.014	3.080±0.006	2.550±0.011
393	-0.795±0.033	1.794±0.020	3.228±0.012	2.598±0.007

Table 6.18 (Continued)

T (K)	Mode 10B	T(k)	Mode 10B	T(k)	Mode 10B
243	1.160±0.029	298	1.337±0.051	353	1.370±0.023
253	1.200±0.092	303	1.346±0.033	363	1.357±0.038
263	1.237±0.087	313	1.362±0.015	373	1.336±0.011
273	1.271±0.052	323	1.373±0.011	383	1.308±0.034
283	1.300±0.024	333	1.378±0.007	393	1.272±0.024
293	1.326±0.049	343	1.377±0.022		

Because sound wave propagation depends on the distribution of the strain field in solids, the effects of the uniaxial stress on the wave modes propagated in the samples are different from that of the hydrostatic pressure (Fig. 6.1 a-c). With increasing temperature, the values determined for $(1/W_0)(\partial W/\partial P)_{T,P=0}$ for modes 1A, 1B and 1H become larger, but for the modes under uniaxial stress $(1/W_0)(\partial W/\partial P)_{T,P=0}$ show some curvature and have different values. Modes 6A, 6B and 6H behave completely differently from one another; the hump shown by mode 6H does not appear in 6A and 6B. The linearity in $(1/W_0)(\partial W/\partial P)_{T,P=0}$ for mode 10H cannot be seen in mode 10B while $(1/W_0)(\partial W/\partial P)_{T,P=0}$ for modes 7A and 7H respond to temperature changes in a similar way except that their values are different from each other (Fig. 6.1b and 6.10a). Table 6.19 shows a comparison of the data with those given by Thurston et al. (1966) for a less purity α-quartz crystal at 298K. Agreement between the data can be seen for modes 1A, 1B, 4B, 6B and 7A. However there is no agreement for modes 6A, 8A, 8B and 10B.

Table 6.19 Comparison between the data obtained for $(1/W_0)(\partial W/\partial P)_{T,P=0}$ of the modes under uniaxial stress at 298K (10^{-11} Pa^{-1}) with the results of Thurston et al. (1966)

Mode	VHPQ	Thurston et al (1966)	Mode	VHPQ	Thurston et al (1966)
1A	1.982±0.006	2.219	7A	1.237±0.009	1.233
1B	-0.195±0.003	-0.377	8A	1.823±0.020	0.247
4B	-0.349±0.007	-0.246	8B	1.285±0.008	2.263
6A	0.596±0.009	0.087	10B	1.337±0.051	-1.806
6B	-1.766±0.014	-1.769			

In a similar way to that used in the analysis of the hydrostatic pressure data, a weight has been given to the value of $(1/W_0)(\partial W/\partial P)_{T,P=0}$ for each mode under uniaxial stress according to the standard error of the $(1/W_0)(\partial W/\partial P)_{T,P=0}$. These weighting factors are shown in the first row of Table 6.20.

Table 6.20 Weighting factors for $(1/W_0)(\partial W/\partial P)_{T,P=0}$ for ultrasonic modes under uniaxial stress

Mode	1A	1B	4B	6A	6B	7A	8A	8B	10B
w_i^s	0.86	0.88	1.00	0.42	0.39	0.69	0.47	0.65	0.28
w_i	0.69	0.70	0.80	0.34	0.31	0.55	0.38	0.52	0.22

w_i^s : Weighting factors determined from standard errors of $(1/W_0)(\partial W/\partial P)_{T,P=0}$.

w_i : Overall weighting factors determined by using Eq. (6.45).

The measured values of $(1/W_0)(\partial W/\partial P)_{T,P=0}$ for modes 1A, 1B, 6A and 6B include contributions from electromechanical effects, i.e. they are related to the second and third

order piezoelectric coefficients $e_{i\alpha}$ and e_{kJ} as well as to the electrostrictive coefficients l_{IJ} (the definitions of these coefficients are given in section 2.4). At present, the third order piezoelectric coefficients (TOPC) and electrostrictive coefficients are only available at room temperature in the published literature. It is not possible to eliminate the electromechanical effects at other temperatures. Hence, a modified form of Eq. (2.154) has been used

$$(\rho_0 W^2)'_{P=0} = -(\vec{N} \cdot \vec{M})^2 - 2wF_U - g_U \quad , \tag{6.42}$$

where

$$g_u = G_U + H_U = s^T_{abuv}(C_{uvjrks} + C^e_{uvjrks})M_a M_b N_j N_k U_r U_s \quad . \tag{6.43}$$

Other terms in Eq. (6.42) are the same as in Eq. (2.154). For convenience, Eq. (6.43) can be written as

$$g_u = s^T_{abuv} C_{uvjrks} M_a M_b N_j N_k U_r U_s \quad . \tag{6.44}$$

The matrix form of the tensor components C_{uvjrks} in Eq. (6.44) can be written as C_{IJK}. Here C_{IJK} are the TOEC including the contributions from piezoelectric effects. For the wave modes propagated under uniaxial stress, the relationship between g_u and C_{uvjrks} in Eq. (6.44) is the same as G_U in Table 5.14. The values of $-g_u$ for measured modes are listed in Table 6.21. Eq. (6.39) and (6.44), and the data given in Table 6.13 and 6.21, have been used to determine the TOEC with contributions from piezoelectric effects.

Table 6.21 The parameter -(g_{rr}) in Eqs. (6.43) and (6.44)

T (K)	Mode 1A	Mode 1B	Mode 4B	Mode 6A
243	3.908±0.018	0.218±0.011	1.899±0.014	2.686±0.005
253	4.008±0.014	0.131±0.006	1.887±0.005	2.663±0.004
263	4.085±0.009	0.099±0.006	1.875±0.005	2.642±0.006
273	4.145±0.005	0.131±0.006	1.866±0.006	2.622±0.003
283	4.195±0.012	0.218±0.006	1.860±0.009	2.605±0.003
293	4.240±0.008	0.345±0.005	1.857±0.011	2.587±0.002
298	4.261±0.008	0.426±0.004	1.859±0.010	2.582±0.006
303	4.287±0.008	0.506±0.007	1.862±0.012	2.578±0.005
313	4.342±0.009	0.676±0.006	1.871±0.009	2.568±0.004
323	4.416±0.010	0.835±0.017	1.887±0.005	2.563±0.005
333	4.511±0.005	0.969±0.013	1.910±0.006	2.561±0.004
343	4.633±0.006	1.076±0.012	1.939±0.005	2.561±0.007
353	4.786±0.005	1.153±0.014	1.977±0.010	2.562±0.007
363	4.982±0.009	1.215±0.014	2.026±0.009	2.569±0.006
373	5.222±0.009	1.289±0.016	2.082±0.009	2.577±0.006
383	5.511±0.016	1.426±0.025	2.146±0.010	2.583±0.005
393	5.870±0.035	1.714±0.029	2.226±0.008	2.603±0.005

Table 6.21 (Continued)

T (K)	Mode 6B	Mode 7A	Mode 8A	Mode 8B
243	-1.072±0.005	2.882±0.007	4.432±0.022	1.719±0.014
253	-0.988±0.004	2.969±0.010	4.495±0.018	1.739±0.008
263	-0.904±0.006	3.051±0.005	4.527±0.011	1.807±0.006
273	-0.818±0.003	3.135±0.005	4.542±0.016	1.915±0.005
283	-0.732±0.003	3.219±0.006	4.559±0.011	2.057±0.005
293	-0.644±0.002	3.300±0.006	4.589±0.013	2.227±0.004
298	-0.600±0.006	3.348±0.008	4.611±0.016	2.317±0.007
303	-0.560±0.005	3.390±0.010	4.640±0.020	2.412±0.005
313	-0.473±0.004	3.482±0.008	4.722±0.015	2.611±0.013
323	-0.390±0.005	3.574±0.005	4.837±0.010	2.817±0.028
333	-0.307±0.004	3.669±0.007	4.986±0.009	3.022±0.009
343	-0.222±0.007	3.777±0.010	5.164±0.006	3.217±0.010
353	-0.135±0.007	3.893±0.021	5.367±0.008	3.397±0.006
363	-0.050±0.006	4.025±0.021	5.582±0.007	3.552±0.008
373	0.038±0.006	4.166±0.021	5.798±0.007	3.681±0.017
383	0.128±0.005	4.315±0.020	5.996±0.006	3.776±0.009
393	0.212±0.005	4.479±0.020	6.152±0.010	3.826±0.006

Table 6.21 (Continued)

T (K)	Mode 10B	T(k)	Mode 10B	T(k)	Mode 10B
243	4.762±0.041	298	5.076±0.070	353	5.110±0.032
253	4.84±0.13	303	5.094±0.045	363	5.077±0.051
263	4.91±0.12	313	5.117±0.021	373	5.027±0.015
273	4.965±0.072	323	5.133±0.016	383	4.963±0.046
283	5.016±0.034	333	5.140±0.010	393	4.892±0.032
293	5.059±0.068	343	5.132±0.031		

The measurements to determine the effects of uniaxial stress are taken in a much smaller pressure range (0-0.3kbar) than the range (0-1.2kbar) in which measurements of the effects of hydrostatic pressure have been made. The accuracies of the data from the two types of measurement differ because the pressure derivatives $(1/W_0)(\partial W/\partial P)_{T,P=0}$ have been determined by the least squares fit to experimental data which have been obtained over widely different ranges of pressure. Hence, it is necessary to include in the analysis weighting factors for the modes measured under different pressure conditions. Let w_i be the weighting factors used to determine the TOEC. The weighting factors w_i for B_{IJ}, which are determined by measurements on the wave modes propagated under hydrostatic pressure, have been taken as 1. Let w_i^s be the factors determined by the standard error of $(1/W_0)(\partial W/\partial P)_{T,P=0}$ for mode i (the first row in Table 6.20). The weight w_i of the g_U of each mode propagated under uniaxial stress can be determined by

$$w_i = w_i^s \cdot w^l \quad , \tag{6.45}$$

where w^l is a relative weighting factor which represents the factor given to estimate the accuracy of measurements on the modes under uniaxial stress relative to those under hydrostatic pressure. w^l has been taken as 0.8. The values of w_i thus established for the modes propagated under uniaxial stress are listed in the second row of Table 6.20.

The combination of the six equations in Eq. (6.40) with the eight equations in Table 5.14 (excluding the equation for mode 1B, which is not independent from that of mode 4B) forms a set of 14×14 simultaneous equations

$$\begin{pmatrix} b_{1,1} & b_{1,2} & \cdots & b_{1,14} \\ b_{2,1} & b_{2,2} & \cdots & b_{2,14} \\ \cdot & \cdot & \cdots & \cdot \\ \cdot & \cdot & \cdots & \cdot \\ \cdot & \cdot & \cdots & \cdot \\ b_{14,1} & b_{14,2} & \cdots & b_{14,14} \end{pmatrix} \begin{pmatrix} X_1 \\ X_2 \\ \cdot \\ \cdot \\ \cdot \\ X_{14} \end{pmatrix} = \begin{pmatrix} C_1 \\ C_2 \\ \cdot \\ \cdot \\ \cdot \\ \cdot \\ C_{14} \end{pmatrix} \quad , \tag{6.46}$$

where the $b_{i,j}$ are the coefficients for the TOEC C_{IJK} in Eq. (6.40) and Table 5.14, X_i (i=1, 2, ..., 14) are the TOEC C_{111}, C_{112}, C_{113}, C_{114}, C_{123}, C_{124}, C_{133}, C_{134}, C_{144}, C_{155}, C_{222}, C_{333}, C_{344} and C_{444} respectively and C_i are B_{IJ} and $-g_U$ for the relevant modes. To introduce the weighting factors into Eq. (6.46), the weighted least squares method (Pugh and Winslow 1966) has been used in the same way as in section 6.2. Because the value of the determinant for the coefficient matrix in Eq. (6.46) is very small, the equations give a singular solution. To avoid this problem, Eq. (6.46) are divided into a few sets of simultaneous equations which have been written into a computer programme for the calculation of the TOEC.

All fourteen independent TOEC of VHPQ obtained in the temperature range from 243K to 393K are given in Table 6.22 and are plotted in Fig. 6.11 (a)-(e). C_{111}, C_{113}, C_{114}, C_{133}, C_{134}, C_{155} and C_{444} all have negative values, while C_{124}, C_{222} and C_{344} have positive values. The values of C_{112} and C_{123} vary from negative to positive, when the temperature increases. The TOEC show substantial temperature dependences. When the temperature is increased, C_{111}, C_{113}, C_{114}, C_{133}, C_{134}, C_{144} and C_{155} decrease while C_{112}, C_{123}, C_{124}, C_{133}, C_{222} and C_{344} increase. C_{444} shows a maximum at around 303K. Using the weighted sets for the data for different modes does not alter the values of the TOEC much. For the purpose of comparison, the TOEC when all the modes have the same weight have also been determined. Table 6.23 gives the fourteen TOEC determined with different weight sets at 298K. It can be seen that the different weight sets do not cause any significant changes in most of the TOEC. The largest change is in C_{123} the value of which changes by about 21%. Table 6.24 compares the TOEC of VHPQ at 298K with those given by Thurston et al. (1966) for α-quartz crystals. The TOEC given by Thurston et al. (1966) are in the frame of reference according to the IRE 1949 Standard for Piezoelectricity (Standards on Piezoelectric Crystals 1949). For convenience in the comparison, the TOEC given by Thurston et al. (1966) have been transformed into the reference frame according to the IEEE 1978 Standard for Piezoelectric Crystals (IEEE

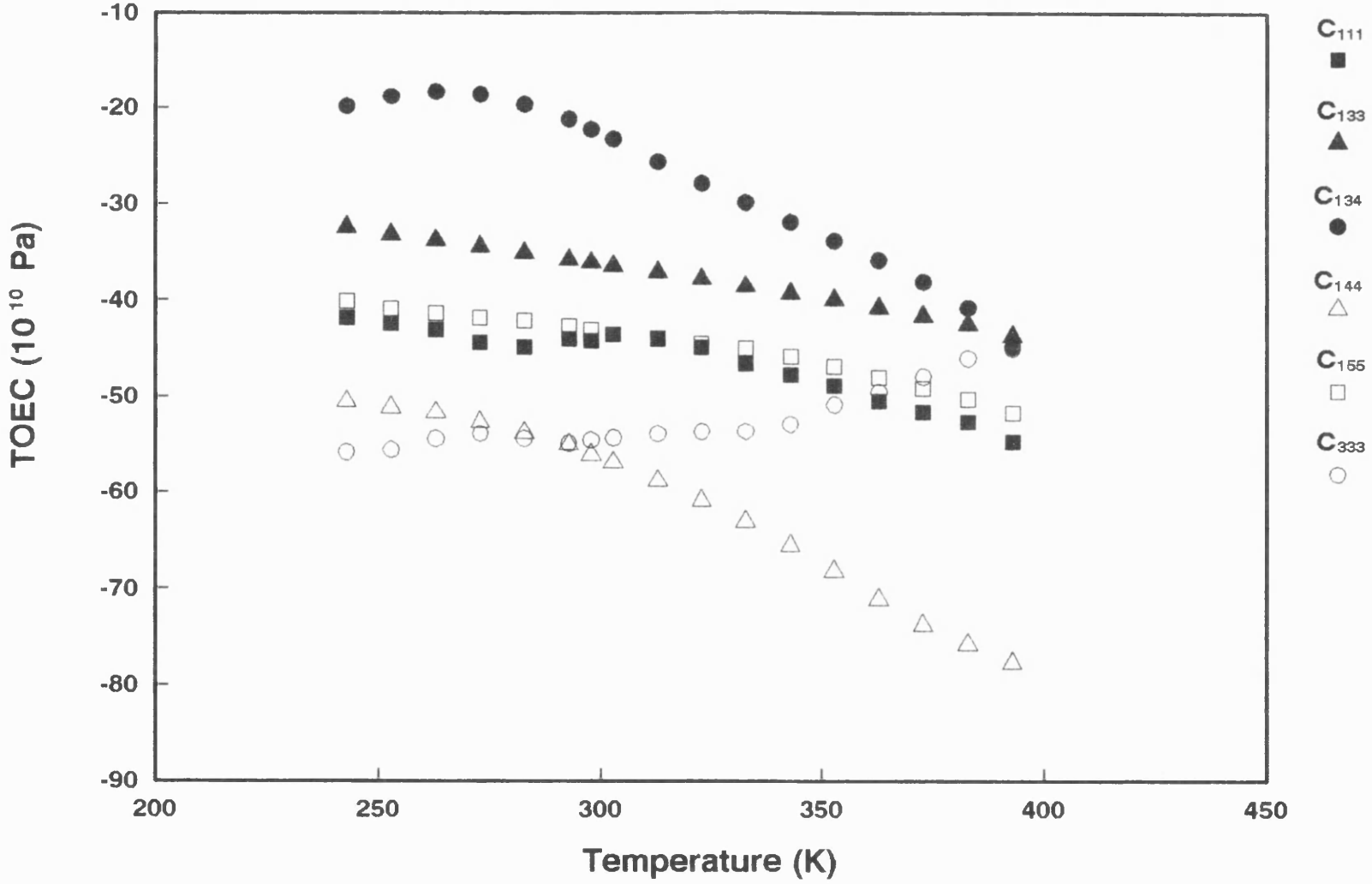

Fig. 6.11 (a) The temperature dependences of the third order elastic constants.

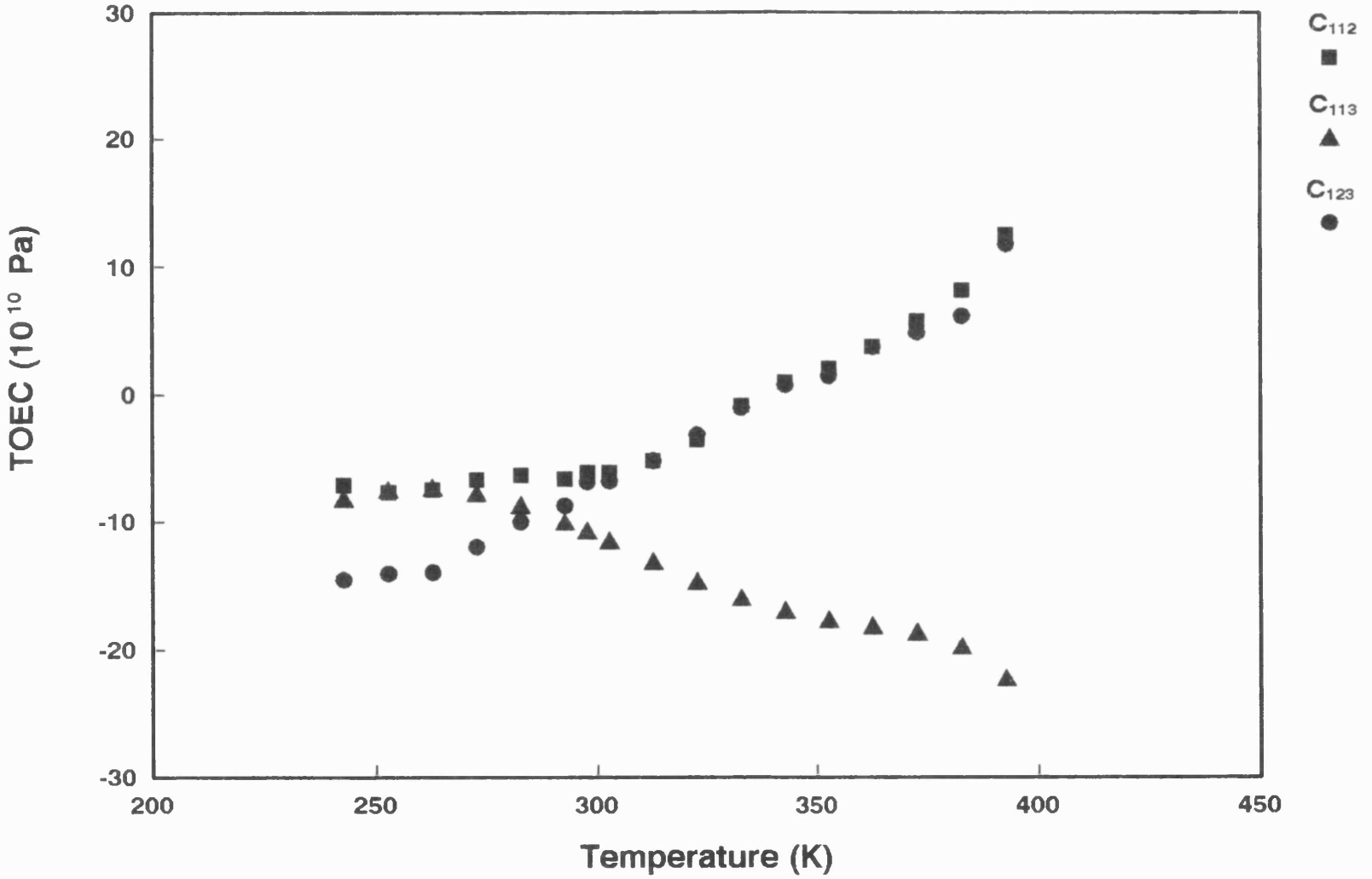

Fig. 6.11 (b) The temperature dependences of the third order elastic constants.

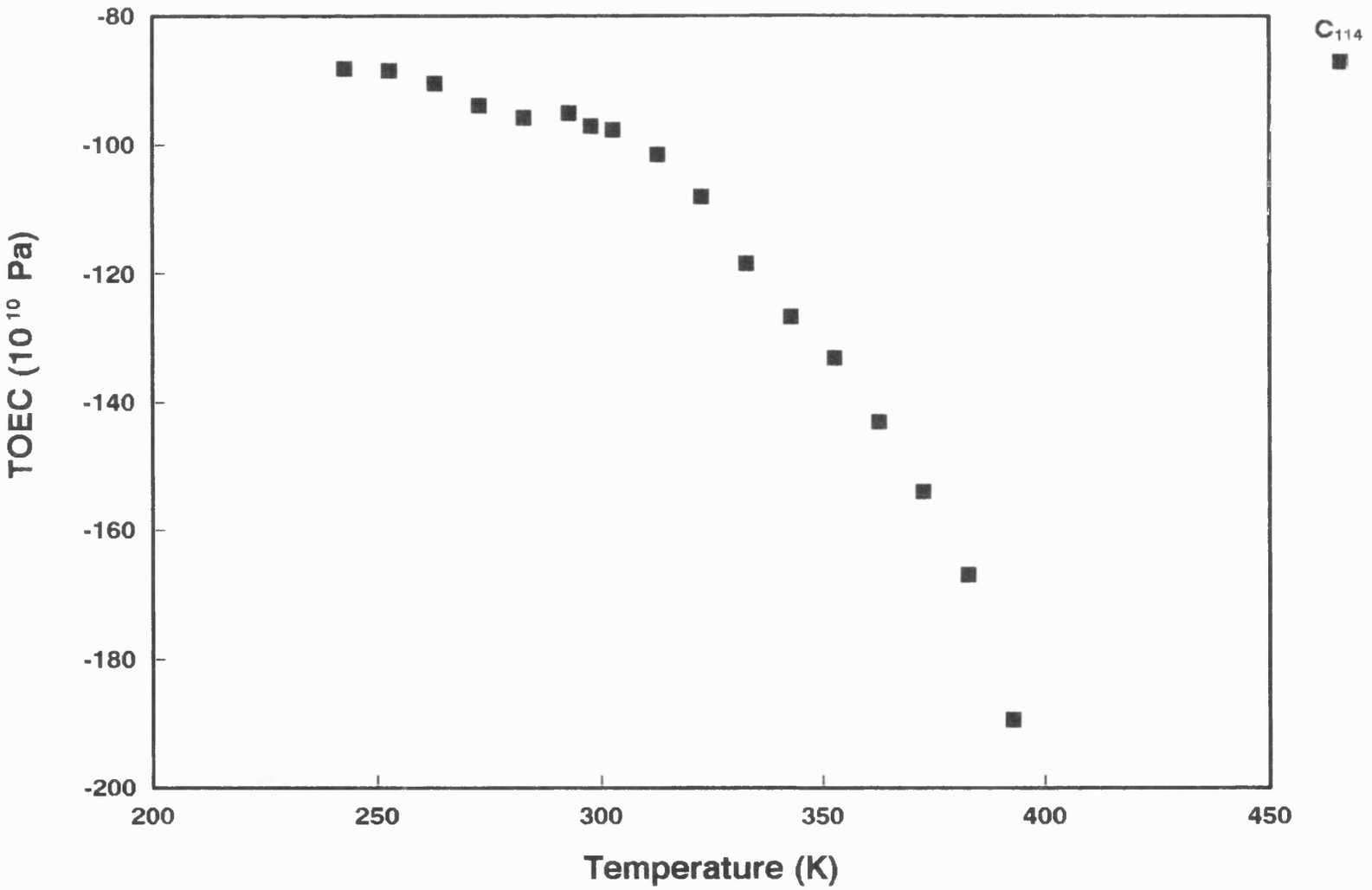

Fig. 6.11 (c) The temperature dependences of the third order elastic constants.

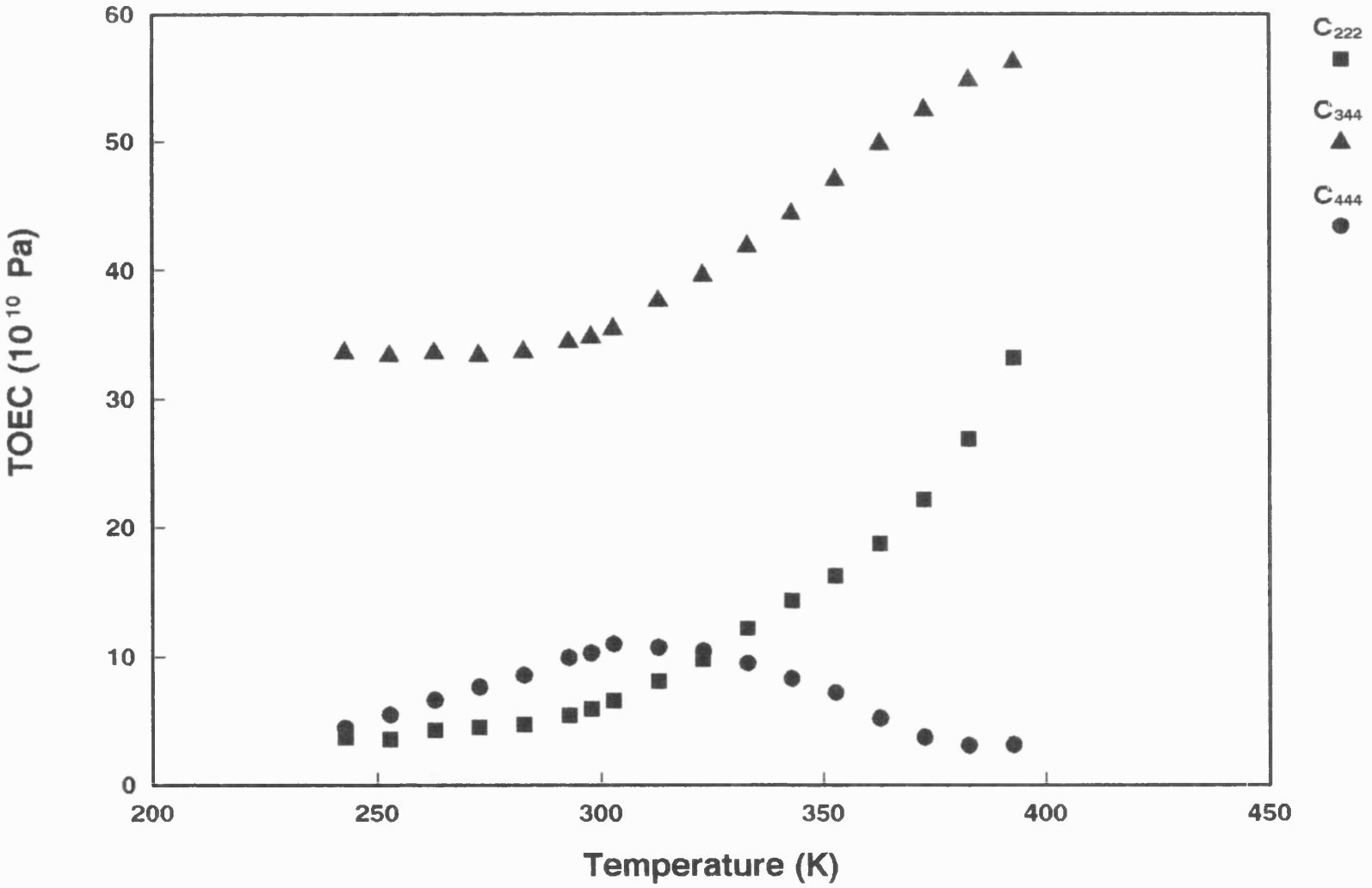

Fig. 6.11 (d) The temperature dependences of the third order elastic constants.

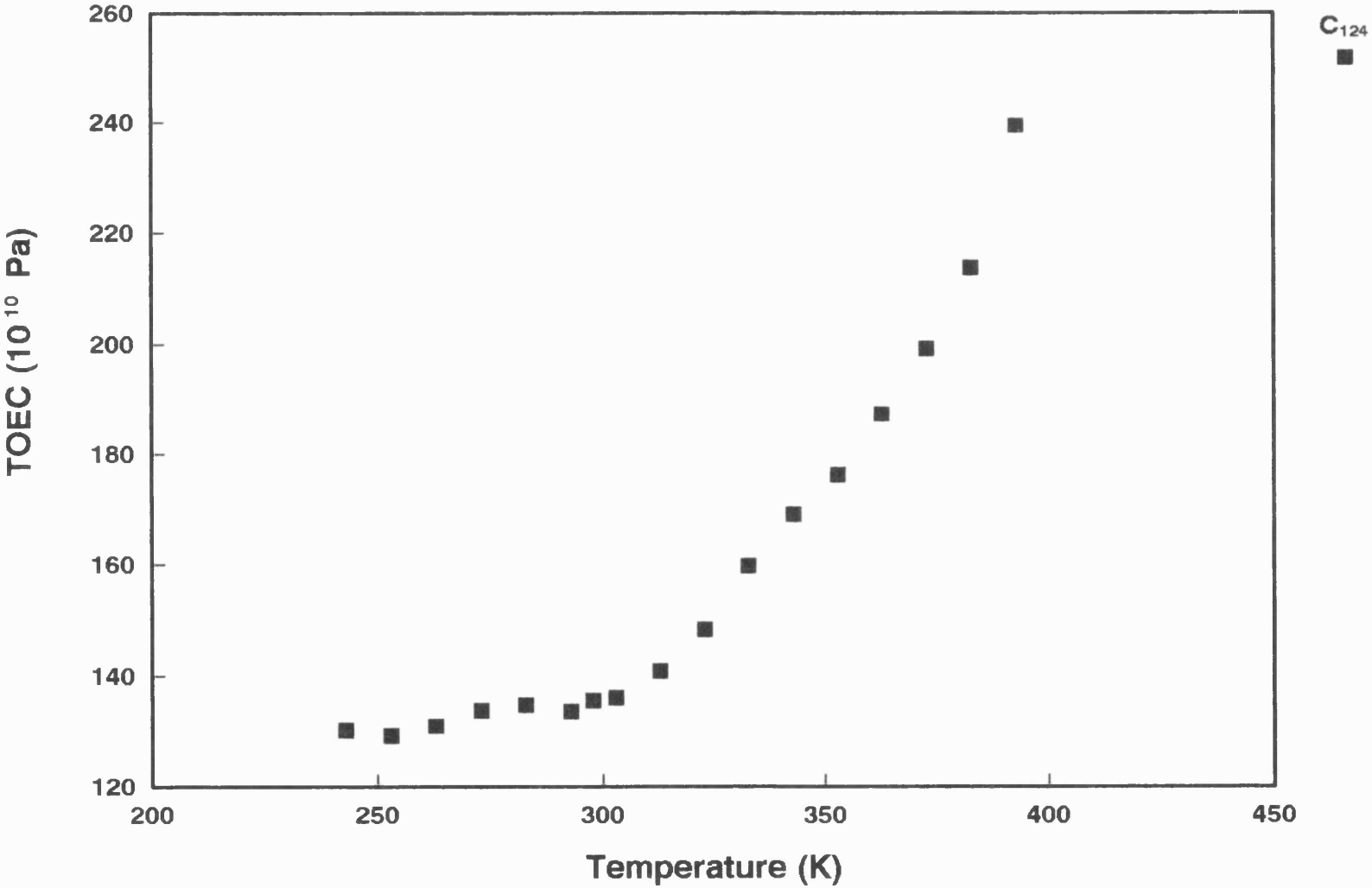

Fig. 6.11 (e) The temperature dependences of the third order elastic constants.

1978). There is almost no agreement between the two sets of data except for C_{133}. This large deviation is perhaps due to the different samples which have been used.

These calculated TOEC include the contributions from the piezoelectricity and the electrostrictivity. To estimate these contributions, the term H_U in Eq. (2.154), which includes the second and third order piezoelectric coefficients (SOPC and TOPC) and the electrostrictive coefficients, has been determined for the relevant wave modes by using the equations in Table 5.15. To do this the mean values of the SOPC, the TOPC and the electrostrictive coefficients in Table 5.17, 5.20 and 5.21 have been used in Eq. (2.156). The resultant values for H_U for the relevant modes are given in Table 6.25. The TOEC without contributions from piezoelectric and electrostrictive effects have then been determined at 293K by using the B_{IJ} in Table 6.14, H_U in Table 6.25 and the measured values of $(1/W_0)(\partial W/\partial P)_{T,P=0}$ given in Table 6.18. The TOEC without contributions from piezoelectric and electrostrictive effects are given in Table 6.26 to compare them with the TOEC including contributions from the piezoelectricity and the electrostrictivity. The largest differences occur in C_{111}, C_{112}, C_{113}, C_{114}, C_{123}, C_{124}, C_{222} and C_{444}. Such deviations are due to the large differences in B_{11}, B_{13}, B_{14} and B_{66} including and not including contributions from piezoelectric effects (Table 6.15).

Table 6.22 The TOEC with contributions from piezoelectric effects (10^{10} Pa)

T (K)	C_{111}	C_{112}	C_{113}	C_{114}
243	-41.8±1.5	-7.14±0.14	-8.41±0.11	-88.18±0.60
253	-42.4±1.2	-7.69±0.23	-7.69±0.13	-88.50±0.58
263	-43.07±0.28	-7.45±0.07	-7.53±0.04	-90.42±0.11
273	-44.37±0.29	-6.70±0.05	-7.95±0.06	-93.85±0.13
283	-44.88±0.25	-6.33±0.08	-8.88±0.04	-95.76±0.08
293	-44.00±0.12	-6.63±0.15	-10.21±0.02	-94.94±0.38
298	-44.17±0.18	-6.14±0.16	-10.89±0.13	-96.99±0.30
303	-43.5±1.1	-6.11±0.08	-11.66±0.02	-97.55±0.17
313	-43.99±0.18	-5.21±0.06	-13.30±0.01	-101.36±0.07
323	-44.87±0.22	-3.58±0.07	-14.88±0.16	-107.99±0.08
333	-46.54±0.36	-0.87±0.12	-16.19±0.10	-118.31±0.33
343	-47.75±0.57	1.02±0.22	-17.16±0.06	-126.65±0.61
353	-48.85±0.83	2.05±0.17	-17.88±0.07	-132.97±0.43
363	-50.46±0.59	3.78±0.48	-18.34±0.09	-143.0±1.4
373	-51.60±0.59	5.76±0.07	-18.83±0.13	-154.01±0.18
383	-52.66±0.77	8.17±0.05	-19.96±0.23	-166.87±0.23
393	-54.75±0.61	12.55±0.38	-22.46±0.28	-189.50±0.77

Table 6.22 (Continued)

T (K)	C_{123}	C_{124}	C_{133}	C_{134}
243	-14.55±0.03	130.19±0.63	-32.40±0.06	-19.83±0.14
253	-14.07±0.12	129.11±0.15	-33.14±0.02	-18.81±0.02
263	-13.96±0.02	130.91±0.13	-33.75±0.03	-18.28±0.10
273	-11.95±0.03	133.61±0.15	-34.35±0.05	-18.58±0.08
283	-9.98±0.02	134.70±0.04	-35.06±0.07	-19.61±0.08
293	-8.73±0.03	133.41±0.38	-35.76±0.03	-21.13±0.05
298	-6.88±0.02	135.54±0.30	-36.05±0.09	-22.20±0.04
303	-6.80±0.03	136.00±0.17	-36.40±0.07	-23.18±0.07
313	-5.22±0.06	140.87±0.04	-37.03±0.12	-25.55±0.07
323	-3.14±0.02	148.31±0.06	-37.75±0.08	-27.74±0.17
333	-1.02±0.05	159.80±0.30	-38.52±0.12	-29.75±0.15
343	0.80±0.31	169.09±0.28	-39.24±0.16	-31.79±0.19
353	1.50±0.17	176.17±0.29	-39.88±0.11	-33.73±0.18
363	3.73±0.25	187.2±1.4	-40.73±0.14	-35.75±0.20
373	4.87±0.04	199.20±0.20	-41.57±0.19	-38.00±0.19
383	6.16±0.03	213.77±0.19	-42.44±0.16	-40.73±0.27
393	11.82±0.10	239.43±0.78	-43.68±0.24	-44.82±0.33

Table 6.22 (Continued)

T (K)	C_{144}	C_{155}	C_{222}	C_{333}
243	-50.59±0.17	-40.09±0.21	3.71±0.58	-55.87±0.45
253	-51.22±0.12	-40.88±0.61	3.54±0.46	-55.63±0.46
263	-51.73±0.03	-41.34±0.58	4.30±0.11	-54.47±0.47
273	-52.69±0.09	-41.79±0.34	4.51±0.11	-53.93±0.45
283	-53.83±0.02	-42.15±0.16	4.73±0.10	-54.45±0.44
293	-55.05±0.07	-42.65±0.32	5.41±0.09	-54.94±0.47
298	-56.11±0.11	-43.09±0.33	5.90±0.42	-54.58±0.41
303	-56.94±0.14	-43.49±0.16	6.57±0.08	-54.37±0.45
313	-58.83±0.13	-43.92±0.04	8.06±0.08	-53.91±0.36
323	-60.90±0.22	-44.50±0.07	9.78±0.07	-53.69±0.45
333	-63.04±0.06	-45.00±0.10	12.16±0.11	-53.67±0.45
343	-65.56±0.15	-45.79±0.23	14.35±0.18	-52.91±0.37
353	-68.21±0.13	-46.85±0.22	16.26±0.29	-50.84±0.44
363	-71.14±0.15	-47.97±0.34	18.77±0.43	-49.53±0.37
373	-73.79±0.06	-49.16±0.15	22.19±0.22	-47.91±0.25
383	-75.78±0.10	-50.28±0.26	26.86±0.28	-45.99±0.43
393	-77.67±0.12	-51.72±0.23	33.22±0.32	-45.00±0.25

Table 6.22 (Continued)

T (K)	C_{344}	C_{444}		
243	33.58±0.40	4.47±0.79		
253	33.34±0.33	5.4±1.8		
263	33.56±0.34	6.6±1.7		
273	33.37±0.31	7.6±1.0		
283	33.66±0.27	8.55±0.52		
293	34.41±0.11	9.93±0.96		
298	34.80±0.04	10.3±1.0		
303	35.44±0.09	10.96±0.64		
313	37.61±0.16	10.70±0.34		
323	39.55±0.14	10.42±0.26		
333	41.85±0.36	9.45±0.34		
343	44.36±0.72	8.26±0.69		
353	47.03±0.57	7.16±0.65		
363	49.83±0.67	5.2±1.0		
373	52.47±0.43	3.71±0.43		
383	54.82±0.36	3.08±0.73		
393	56.20±0.55	3.15±0.69		

Table 6.23 Comparison of the TOEC (10^{10} Pa) at 298K obtained using different weighting factors

Data	C_{111}	C_{112}	C_{113}	C_{114}
[1]	-44.18	-6.64	-10.89	-97.01
[2]	-44.00	-6.63	-10.21	-94.94
Data	C_{123}	C_{124}	C_{133}	C_{134}
[1]	-6.88	135.56	-36.05	-22.20
[2]	-8.73	133.41	-35.76	-21.13
Data	C_{144}	C_{155}	C_{222}	C_{333}
[1]	-56.11	-43.09	5.91	-54.58
[2]	-55.05	-42.65	5.41	-54.94
Data	C_{344}	C_{444}		
[1]	34.80	10.27		
[2]	34.41	9.93		

[1] All weighting factors for the modes under uniaxial stress are 1.

[2] With the weighting factors given in the second row in Table 6.20.

Table 6.24 Comparison of the TOEC measured here with the results of Thurston et al. (1966) at 298K (10^{10} Pa)*

Data	C_{111}	C_{112}	C_{113}	C_{114}
[1]	-21.0±0.7	-34.5±0.6	1.2±0.6	16.3±0.5
[2]	-44.00±0.12	-6.63±0.15	-10.21±0.15	-94.94±0.38
Data	C_{123}	C_{124}	C_{133}	C_{134}
[1]	-29.4±0.5	1.5±0.4	-31.2±0.7	-0.2±0.4
[2]	-8.73±0.03	133.41±0.38	-35.76±0.03	-21.13±0.05
Data	C_{144}	C_{155}	C_{222}	C_{333}
[1]	-13.4±0.7	-20.0±0.8	-33.2±0.8	-81.5±1.8
[2]	-55.05±0.07	-42.65±0.32	5.41±0.09	-54.94±0.47
Data	C_{344}	C_{444}		
[1]	-11.0±0.7	27.6±1.7		
[2]	34.41±0.11	9.93±0.96		

[1] Thurston et al. (1966). The data have been transformed into the reference frame according to the IEEE 1978 Standard for Piezoelectric Crystals (IEEE 1978).

[2] Results of this work including the contribution from piezoelectric effects.

* The Error bars are for different samples.

Table 6.25 The parameter H_U in Eq. (2.156) at 293K (10^{10} Pa)

Mode	1A	1B	6A	6B
H_U	0.17±0.002	0.002±0.0003	0.005±0.002	-0.04±0.003

Table 6.26 Comparison of the TOEC with and without contributions from piezoelectric effects at 293K (10^{10} Pa)

Data	C_{111}	C_{112}	C_{113}	C_{114}
[1]	-7.19±0.22	-26.00±0.22	-7.89±0.23	-21.75±0.63
[2]	-44.00±0.12	-6.63±0.15	-10.21±0.15	-94.94±0.38
Data	C_{123}	C_{124}	C_{133}	C_{134}
[1]	-11.05±0.03	70.99±0.63	-35.76±0.04	-19.92±0.05
[2]	-8.73±0.03	133.41±0.38	-35.76±0.03	-21.13±0.05
Data	C_{144}	C_{155}	C_{222}	C_{333}
[1]	-54.98±0.39	-45.22±0.78	8.01±0.14	-54.94±0.45
[2]	-55.05±0.07	-42.65±0.32	5.41±0.09	-54.94±0.47
Data	C_{344}	C_{444}		
[1]	35.26±0.11	17.6±2.2		
[2]	34.41±0.11	9.93±0.96		

[1] Without contribution from piezoelectric effects.

[2] With contribution from piezoelectric effects.

6.6.2 Temperature coefficients of the SOEC and TOEC of VHPQ

In quartz device designs it is necessary to know the temperature coefficients of the relevant parameters. Let a parameter Ω has a value Ω_0 at some reference temperature T_0. Its value at an arbitrary temperature T is then given by

$$\Omega = \Omega_0(1 + T_\Omega^{(1)}\delta T + T_\Omega^{(2)}\delta T^2 + T_\Omega^{(3)}\delta T^3 + \cdots) \quad . \tag{6.47}$$

Here $\delta T = T - T_0$ and

$$T_\Omega^{(n)} = \frac{1}{n!\Omega_0}\left(\frac{\partial^n \Omega}{\partial T^n}\right)_{T=T_0} \tag{6.48}$$

are the n^{th} order temperature coefficients of the parameter Ω. For the SOEC of quartz most workers fit their data to a cubic approximation (as quoted by Brice (1985) and James (1987)).

In the present work the temperature coefficients of the SOEC (weighted average, see section 6.2) and the TOEC for VHPQ have been obtained by using a polynomial fit to the data given in Table 6.5 and 6.18. The reference temperature is set at 298K. Hence, the elastic coefficients have the form

$$C(T) = C_{298K}(1 + a_1\delta T + a_2\delta T^2 + a_3\delta T_3^3 + \cdots) \quad . \tag{6.49}$$

The values of the SOEC have been fitted to either a quadratic or a cubic approximation depending on the smoothness of the fit. The temperature coefficients of the SOEC are given in Table 6.26, where C_{IJ}^0 represents the C_{IJ} at 298K.

6.26 Temperature coefficients of the SOEC (weighted average)

	C_{11}	C_{13}	C_{14}
C_{IJ}^0 (Pa)	8.6816×10^{10}	1.2279×10^{10}	1.8041×10^{10}
a_1	-4.381×10^{-5}	3.841×10^{-4}	3.081×10^{-5}
a_2	-1.156×10^{-7}	-5.523×10^{-6}	-2.177×10^{-8}
a_3		-9.142×10^{-8}	-3.455×10^{-9}
	C_{33}	C_{44}	C_{66}
C_{IJ}^0 (Pa)	10.572×10^{10}	5.8265×10^{10}	3.9818×10^{10}
a_1	-1.910×10^{-4}	-1.693×10^{-4}	1.782×10^{-4}
a_2	1.660×10^{-7}	-2.646×10^{-7}	-1.771×10^{-7}
a_3	7.134×10^{-11}	1.224×10^{-10}	8.751×10^{-10}

Although many people have used a polynomial fit to third order for the data of SOEC, a polynomial to third order does not give a good fit for some data of the TOEC because those data do not lie on a smooth curve (Fig. 6.11 (a)-(e)). To get the temperature coefficients describing accurately the TOEC data, the fitting has been taken up to fifth order, and, to sixth order for some data of the TOEC. As a consequence, polynomials to different orders have been used to fit different TOEC tensor components C_{IJK}. Fig. 6.12 (a)-(h) compares the third order fitted curves with fifth or sixth order ones. For C_{111} (Fig. 6.12 (a)) and C_{113} (Fig. 6.12 (d)) a third order polynomial gives a better fit than higher orders. For C_{134} (Fig. 6.12 (b)) and C_{155} (Fig. 6.12 (c)) both third and fifth order polynomials fit accurately. For other TOEC tensor components the polynomial to fifth

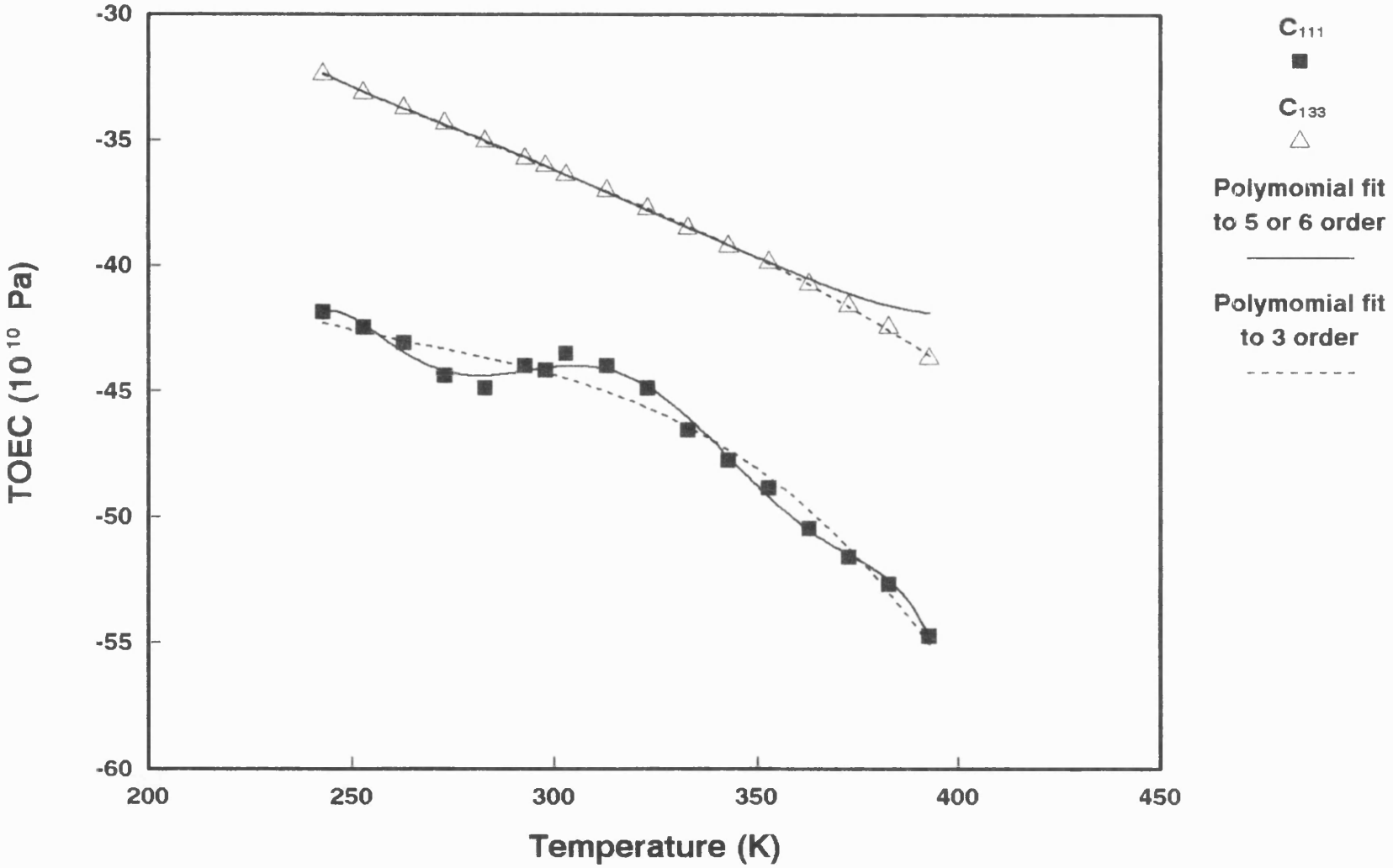

Fig. 6.12 (a) Polynomial fit to the third order elastic constants.

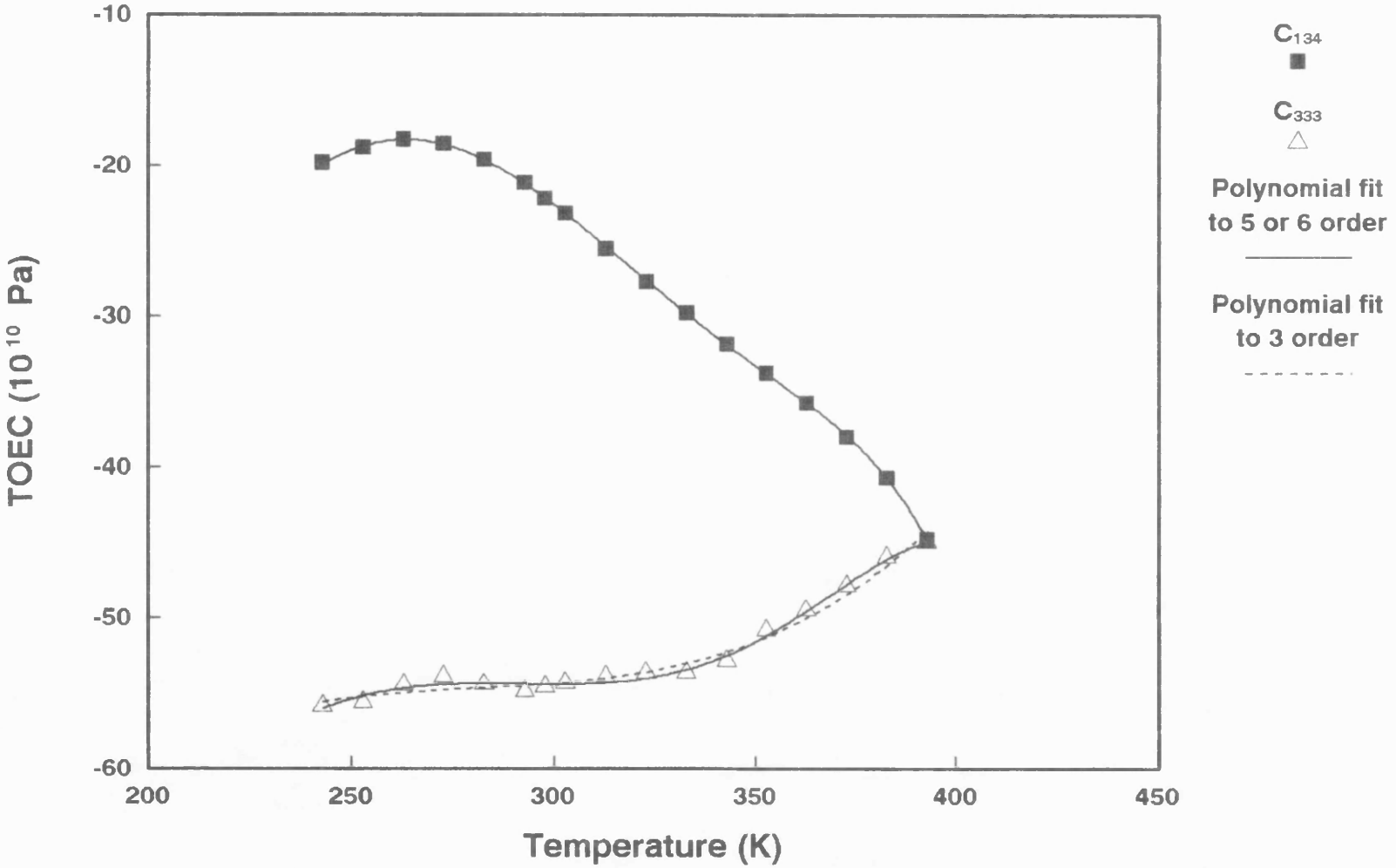

Fig. 6.12 (b) Polynomial fit to the third order elastic constants.

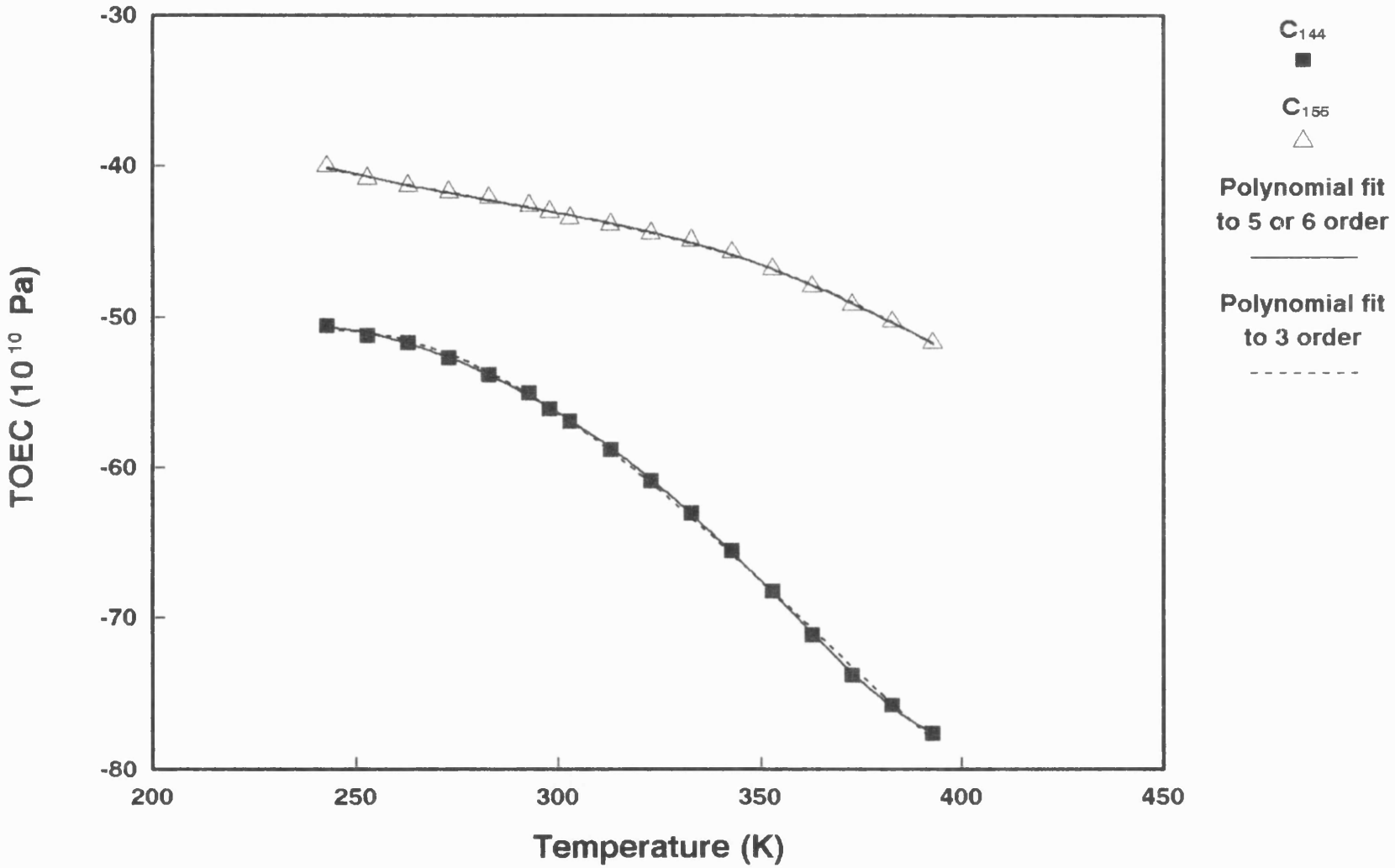

Fig. 6.12 (c) Polynomial fit to the third order elastic constants.

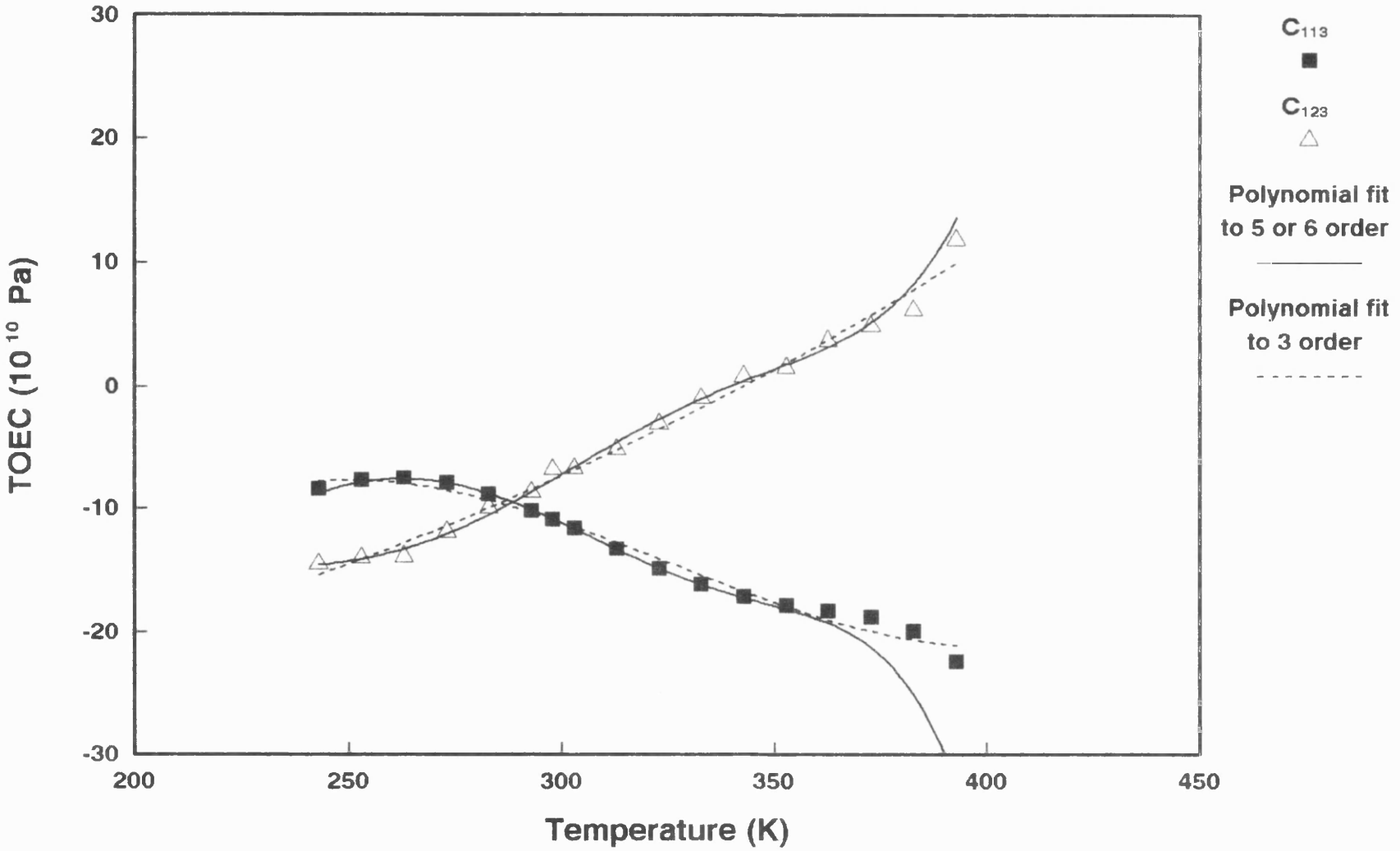

Fig. 6.12 (d) Polynomial fit to the third order elastic constants.

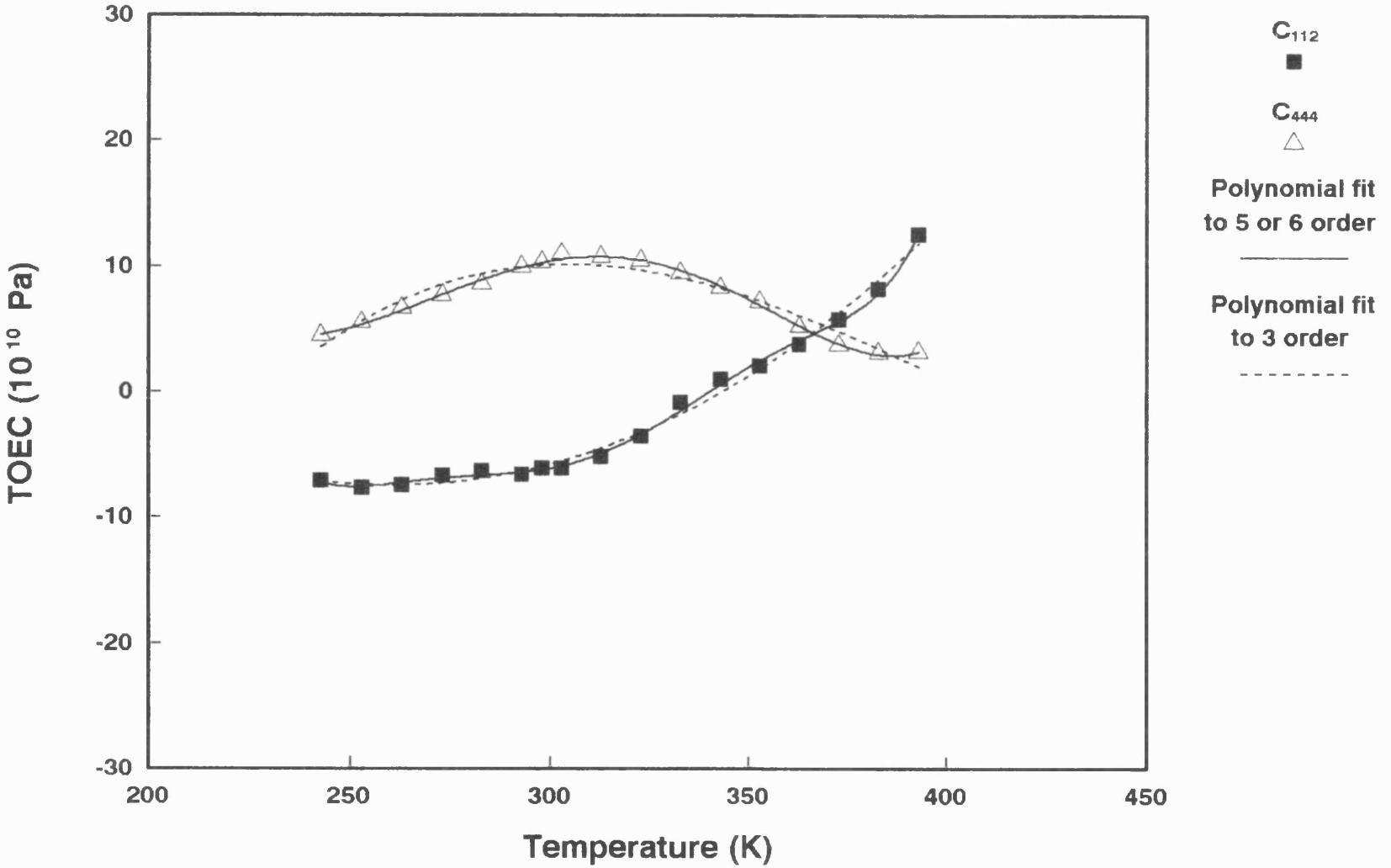

Fig. 6.12 (e) Polynomial fit to the third order elastic constants.

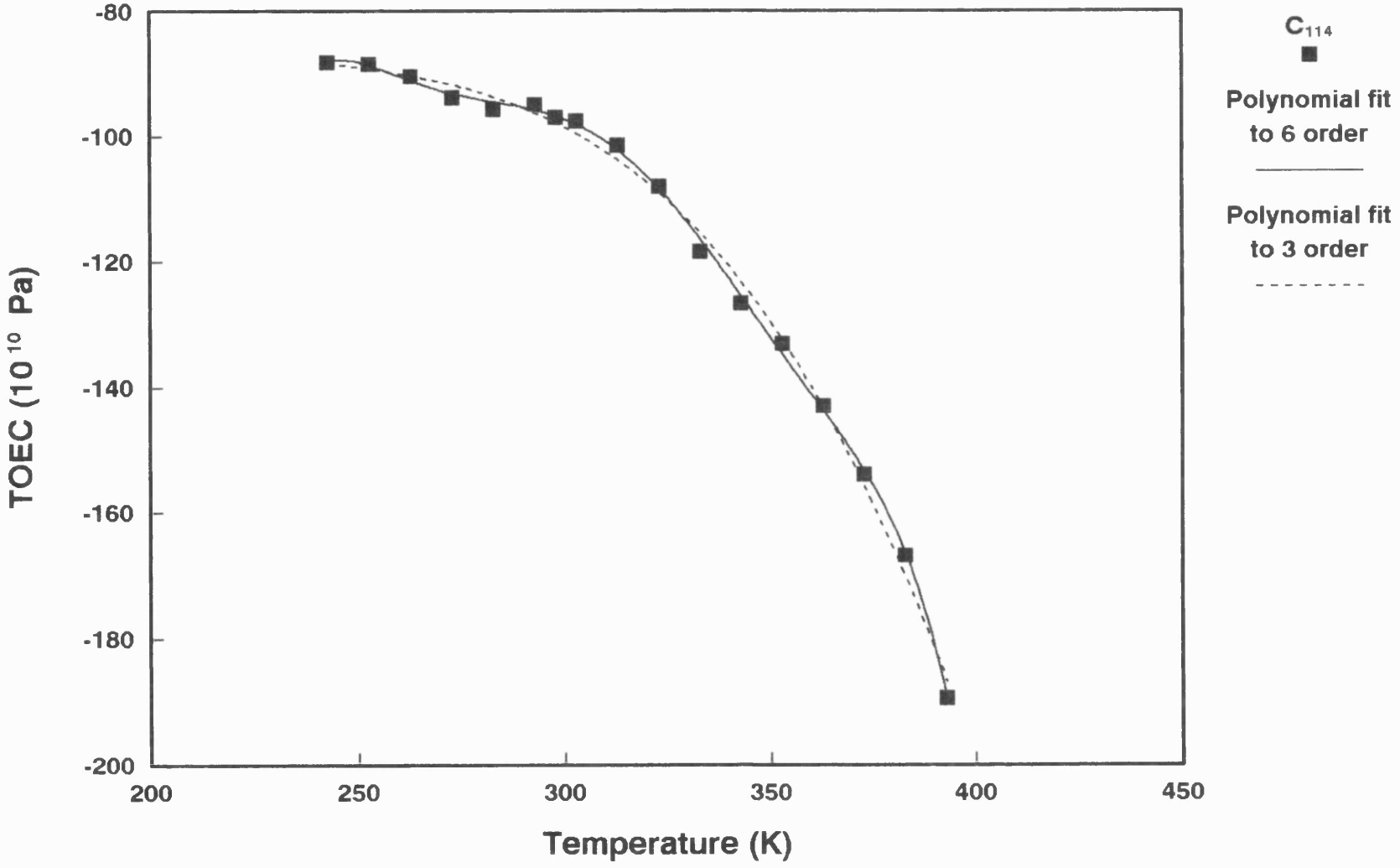

Fig. 6.12 (f) Polynomial fit to the third order elastic constants.

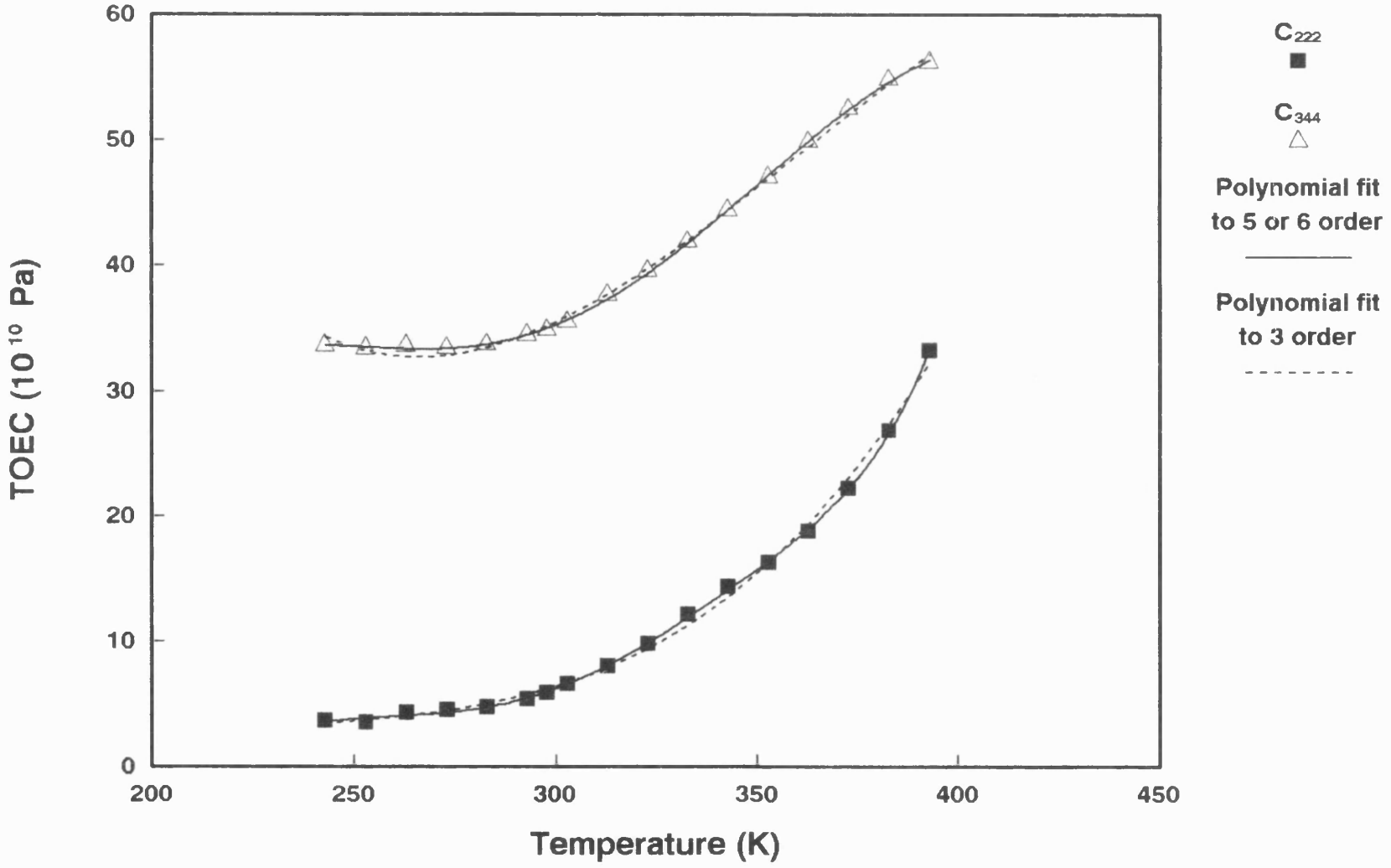

Fig. 6.12 (g) Polynomial fit to the third order elastic constans.

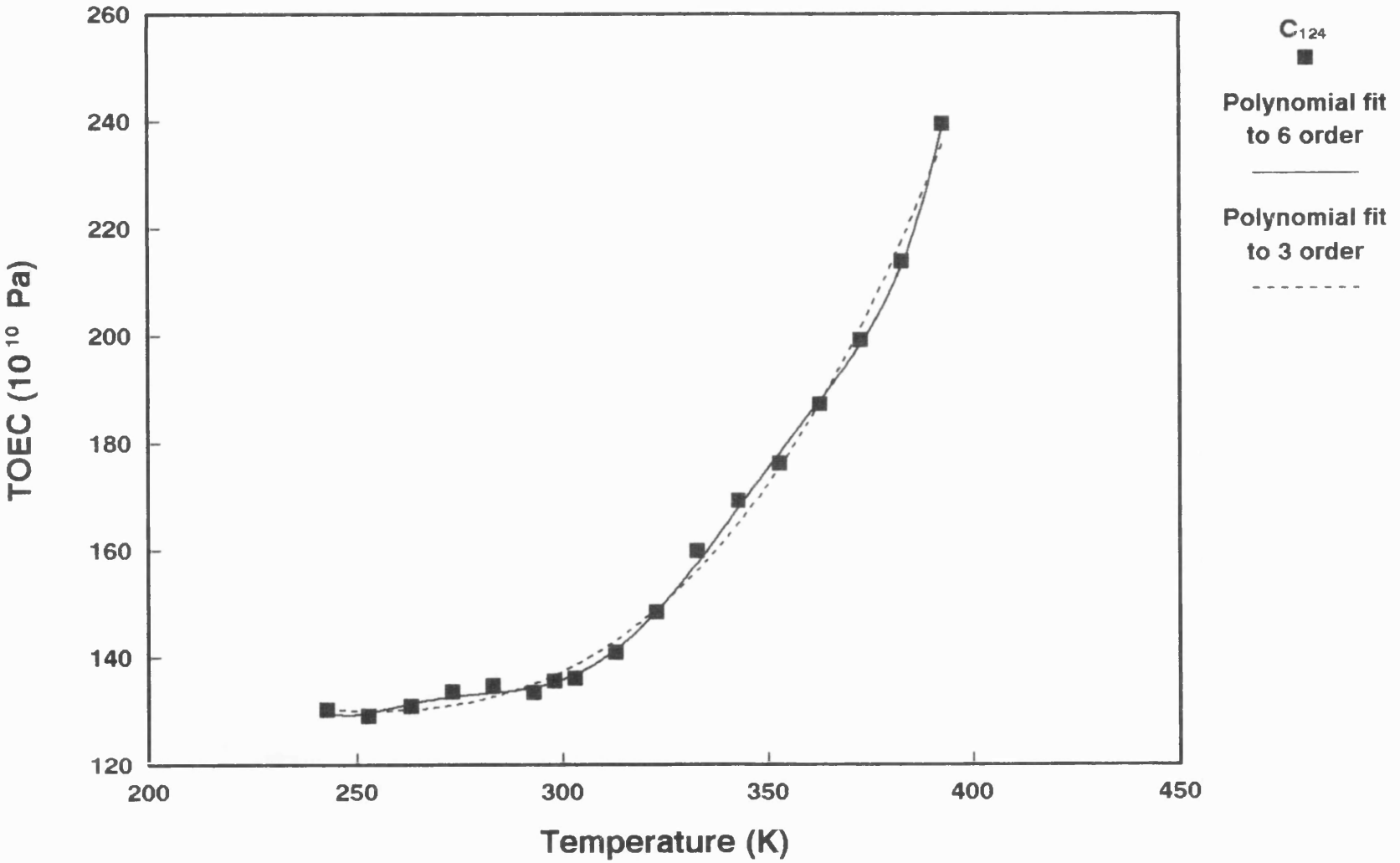

Fig. 6.12 (h) Polynomial fit to the third order elastic constants.

or sixth order give a better fit than the one to third order (Fig. 6.12 (a)-(h)). The temperature coefficients determined for the fourteen independent TOEC of VHPQ are tabulated in Table 6.27 , where C^0_{IJK} represents the C_{IJK} at 298K.

6.27 Temperature coefficients of the TOEC

	C_{111}	C_{112}	C_{113}
C^0_{IJK} (Pa)	-44.2600×10^{10}	-6.2233×10^{10}	-10.9340×10^{10}
a_1	1.005×10^{-3}	-8.324×10^{-3}	1.064×10^{-2}
a_2	8.288×10^{-6}	-3.214×10^{-4}	5.887×10^{-5}
a_3	8.605×10^{-8}	-5.449×10^{-6}	-7.129×10^{-7}
a_4		8.002×10^{-8}	
a_5		1.159×10^{-9}	
a_6		-1.382×10^{-11}	
	C_{114}	C_{123}	C_{124}
C^0_{IJK} (Pa)	-96.7665×10^{10}	-7.6350×10^{10}	135.4110×10^{10}
a_1	2.340×10^{-3}	-2.644×10^{-2}	1.767×10^{-3}
a_2	7.720×10^{-5}	-5.253×10^{-5}	7.099×10^{-5}
a_3	1.449×10^{-6}	3.188×10^{-6}	1.055×10^{-6}
a_4	-1.834×10^{-8}	7.715×10^{-10}	-1.585×10^{-8}
a_5	-2.547×10^{-10}	-2.970×10^{-10}	-1.874×10^{-10}
a_6	3.081×10^{-12}	-4.035×10^{-13}	2.447×10^{-12}

6.27 (Continue)

	C_{133}	C_{134}	C_{144}
C^0_{IJK} (Pa)	-36.0472×10^{10}	-22.1607×10^{10}	-56.0295×10^{10}
a_1	1.886×10^{-3}	7.148×10^{-3}	2.871×10^{-3}
a_2	2.292×10^{-6}	6.632×10^{-5}	2.085×10^{-5}
a_3	-1.885×10^{-8}	-3.603×10^{-7}	3.532×10^{-8}
a_4	-3.817×10^{-10}		-1.424×10^{-10}
a_5	7.562×10^{-12}		-1.214×10^{-11}
a_6	-6.789×10^{-14}		-4.613×10^{-17}
	C_{155}	C_{222}	C_{333}
C^0_{IJK} (Pa)	-43.0341×10^{10}	5.9997×10^{10}	-54.4064×10^{10}
a_1	1.210×10^{-3}	1.860×10^{-2}	4.899×10^{-5}
a_2	3.689×10^{-6}	3.204×10^{-4}	-5.196×10^{-6}
a_3	6.454×10^{-8}	-1.506×10^{-7}	-3.193×10^{-7}
a_4		-4.280×10^{-8}	-1.863×10^{-10}
a_5		1.427×10^{-10}	1.181×10^{-11}
a_6		3.273×10^{-12}	9.042×10^{-14}

6.27 (Continue)

	C_{344}	C_{444}	
C^0_{IJK} (Pa)	34.9859×10^{10}	10.2705×10^{10}	
a_1	3.441×10^{-3}	6.218×10^{-3}	
a_2	6.647×10^{-5}	-1.957×10^{-4}	
a_3	-9.330×10^{-9}	-1.576×10^{-6}	
a_4	-5.131×10^{-9}	1.617×10^{-8}	
a_5	1.400×10^{-11}	6.711×10^{-11}	
a_6	2.584×10^{-15}	1.043×10^{-19}	

Chapter 7 Lattice Vibrational Anharmonicity in α-Quartz

7.1 Introduction

The third order terms in the expansion of the lattice vibrational potential energy, which is characterised by the third order elastic constants (TOEC), lead to the anharmonicity in lattice vibrations. As consequences of the anharmonicity there appear thermal expansion, phonon-phonon interactions, etc in crystals. In this chapter, the experimentally determined TOEC and the pressure derivatives of the SOEC of VHPQ are used to obtain the relevant parameters for the thermal expansion of α-quartz. The acoustic mode and mean Grüneisen parameters of VHPQ in the long wavelength limit have been calculated as a function of acoustic mode propagation direction and temperature from the measured elastic constants and their pressure derivatives by using Eqs. (3.23)-(3.27). The Grüneisen parameters are presented in Section 7.2 together with a brief discussion of the thermal expansion property of α-quartz. The contributions of piezoelectric effects to these parameters are estimated and given in Section 7.3.

7.2. Long-wavelength acoustic mode Grüneisen parameters of VHPQ

Selected mode Grüneisen parameters as a function of acoustic wave propagation direction are given in Fig. 7.1 (a)-(d) at 243K, 303K, 353K, and 393K. As would be expected in a highly anisotropic crystal the values of the parameters are strongly dependent on the acoustic wave propagation direction. The substantial directional dependence of the acoustic mode Grüneisen parameters is consistent with the anisotropy shown by the linear thermal expansion coefficients (e.g. see James (1987)). In the absence of mode softening the elastic constants and the lattice vibrational frequencies

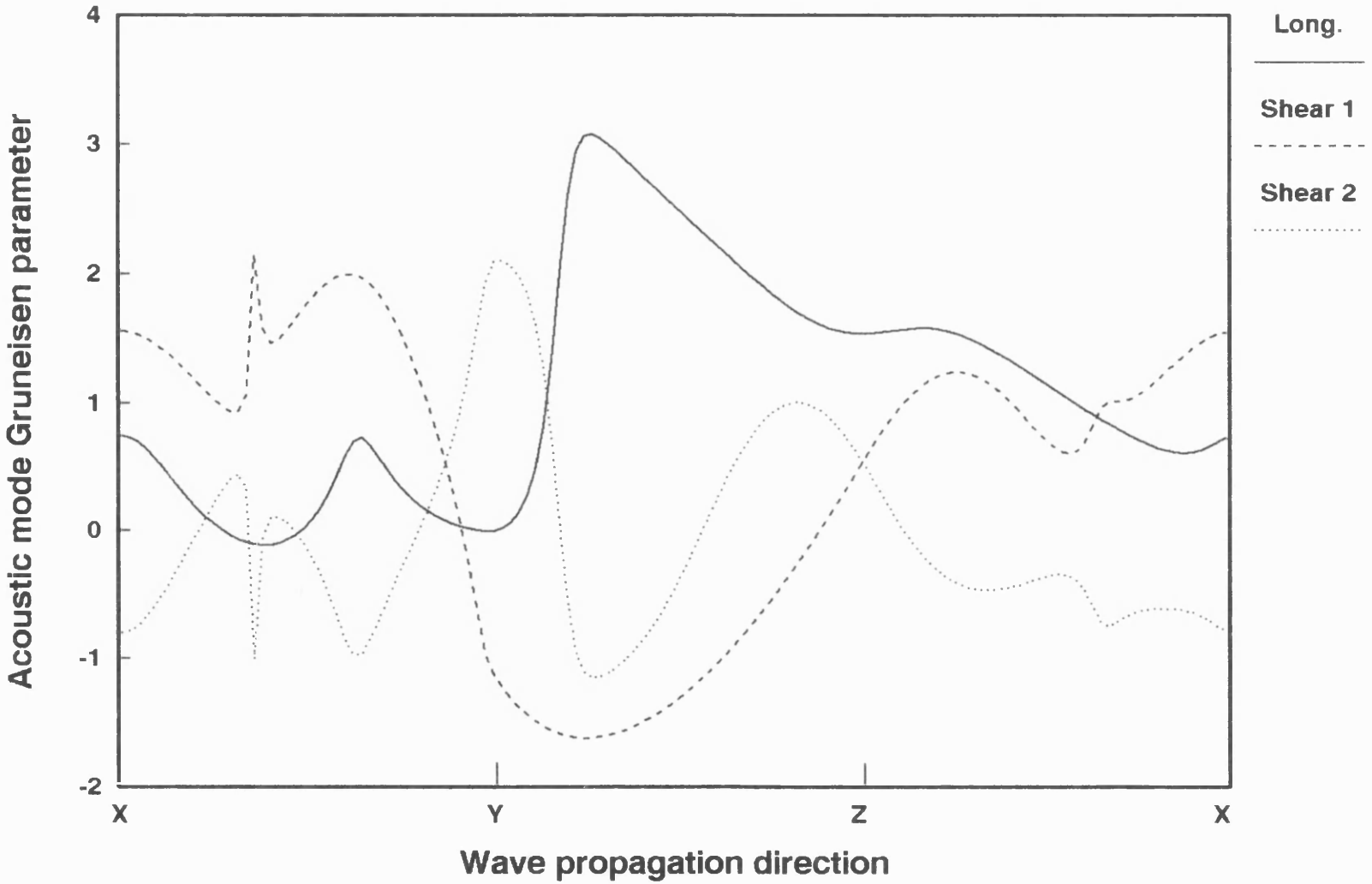

Fig. 7.1 (a) The acoustic mode Gruneisen parameters as a function of wave propagation direction at 243K.

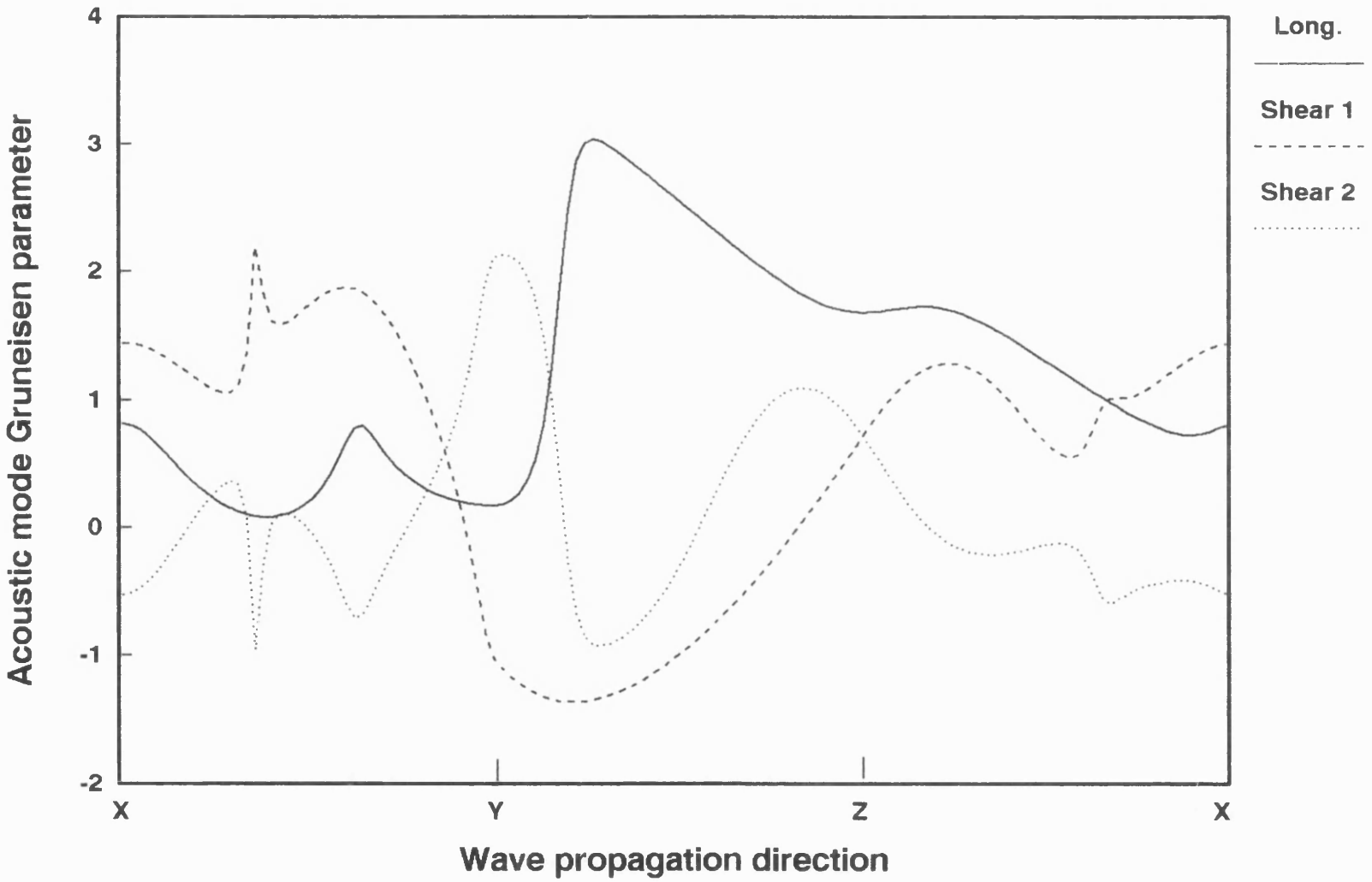

Fig. 7.1 (b) The acoustic mode Gruneisen parameters as a function of wave propagation direction at 303K.

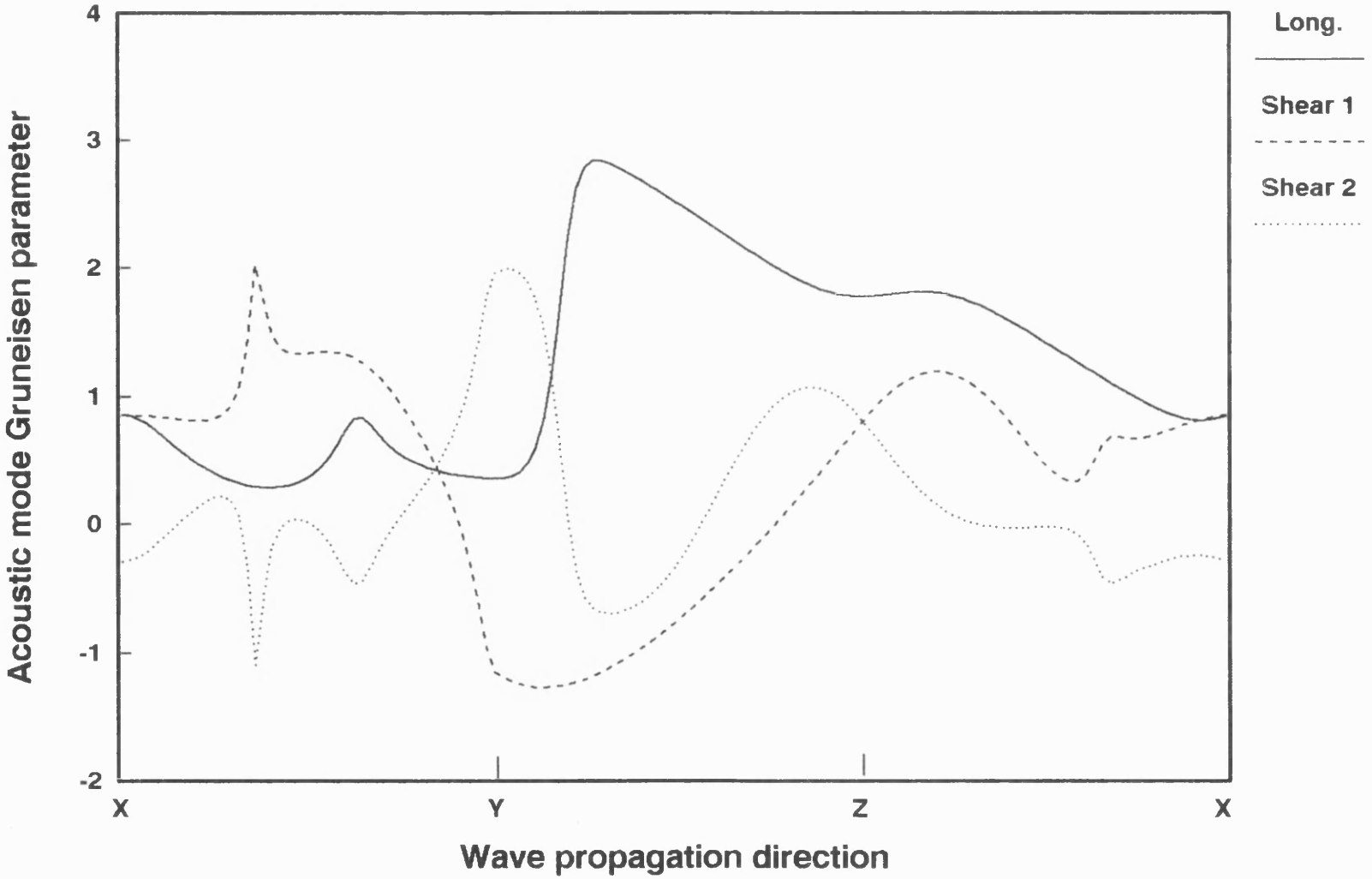

Fig. 7.1 (c) The acoustic mode Gruneisen parameters as a function of wave propagation direction at 353K.

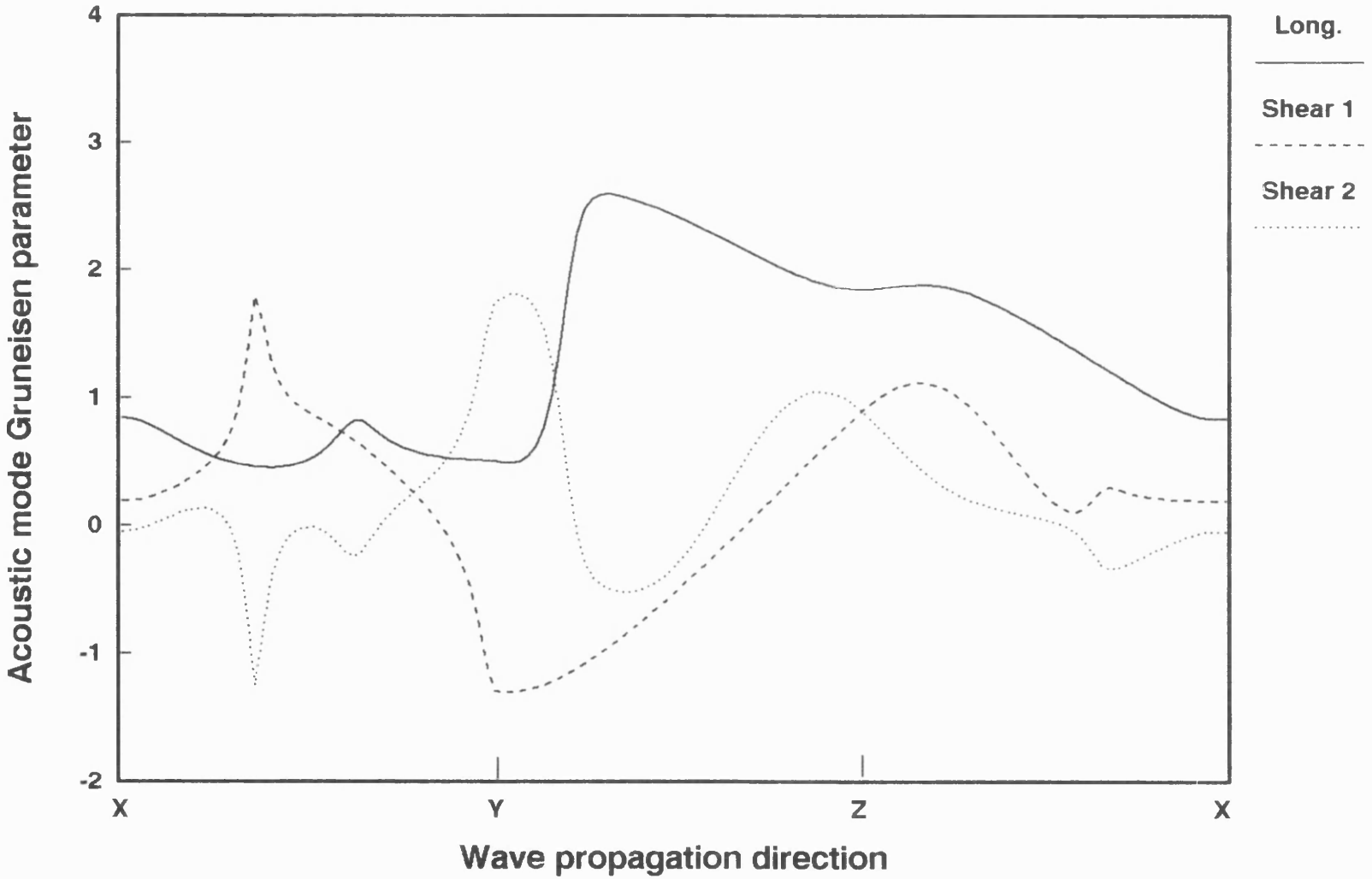

Fig. 7.1 (d) The acoustic mode Gruneisen parameters as a function of wave propagation direction at 393K.

increase under hydrostatic pressure, which raises the strain free energy, so that normally the mode Grüneisen parameters are positive. For quartz most values of the mode Grüneisen parameters are positive and lie in the usual range up to about 3. However many mode parameters on the two shear branches have negative values; these arise because $(\partial C_{66}/\partial P)_{T,P=0}$ and $(\partial C_{14}/\partial P)_{T,P=0}$ are negative throughout the whole temperature range. The behaviours of the mode parameters as a function of acoustic wave propagation direction can be affected by temperature variations. As temperature is increased the mode Grüneisen parameters in the two shear branches in Z-X plane and part of Y-Z plane become closer to each other and the longitudinal branch in X-Y and Z-X plane is lifted up relative to shear branches (Fig. 7.1 (a)-(d)).

The temperature dependences of the acoustic mode Grüneisen parameters of the modes propagated along the X-, Y- and Z-axes are shown in Fig. 7.2 (a), (b) and (c). The notations used to define the shear modes, which can be propagated along these three axes, are given in Table 7.1.

Table 7.1 Terminology used to define the shear acoustic mode Grüneisen parameters along the three major crystallographic axes

	X-axis			Y-axis			Z-axis		
Mode	U_1	U_2	U_3	U_1	U_2	U_3	U_1	U_2	U_3
Shear 1	0	β_2	$-\beta_1$	1	0	0	1	0	0
Shear 2	0	β_1	β_2	0	γ_1	γ_2	0	1	0

The direction cosines β_i and γ_i (i=1, 2) in Table 7.1 are defined as in Eqs. (5.2) and (5.3). The influence of the negative values of $(\partial C_{66}/\partial P)_{T,P=0}$ and $(\partial C_{14}/\partial P)_{T,P=0}$ can be seen in the findings that Grüneisen parameters for Shear 2 propagated along X-axis and Shear

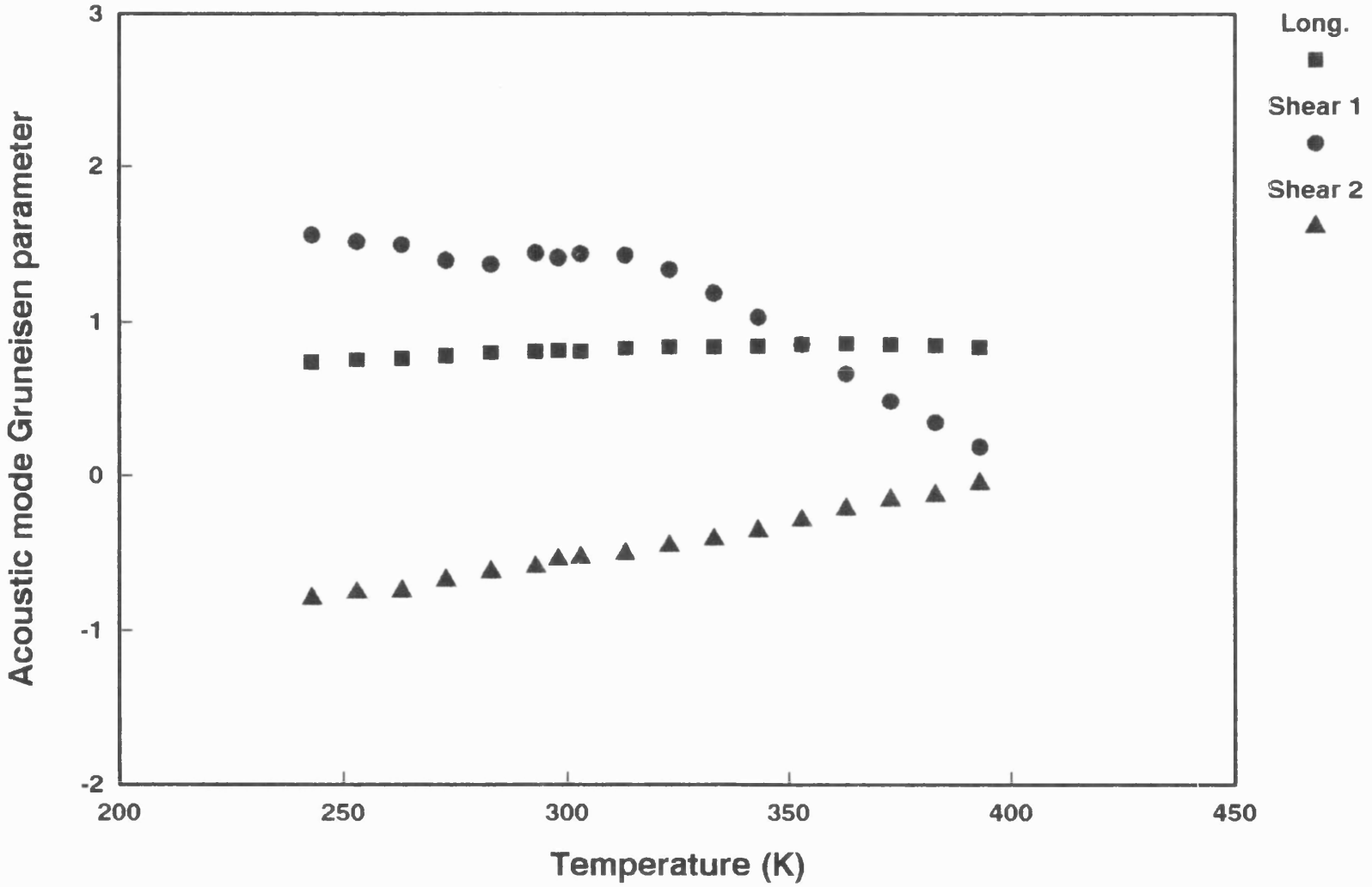

Fig. 7.2 (a) The temperature dependence of the acoustic mode Gruneisen parameter along the direction of X-axis.

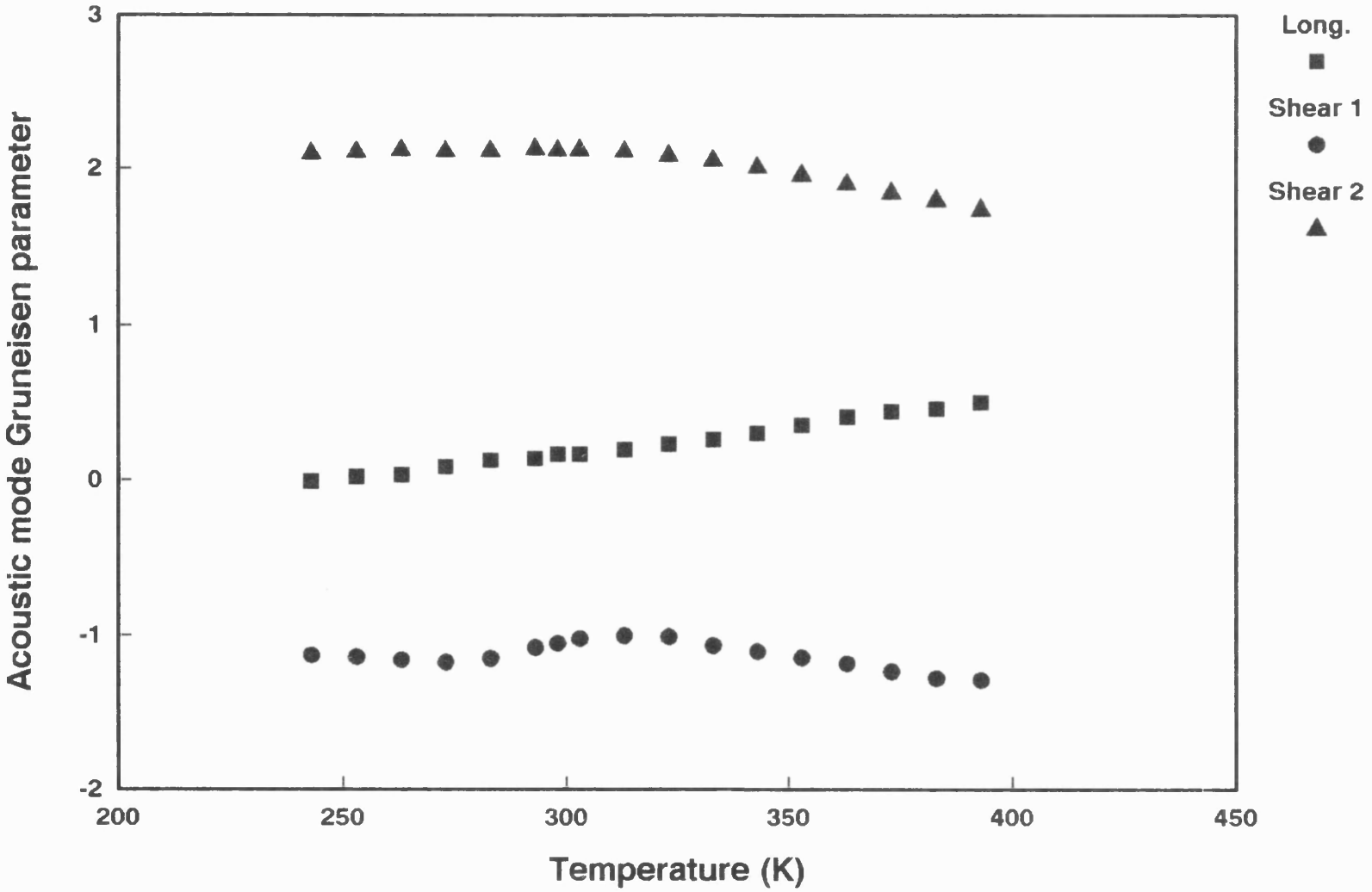

Fig. 7.2 (b) The temperature dependence of the acoustic mode Gruneisen parameter along the direction of Y-axis.

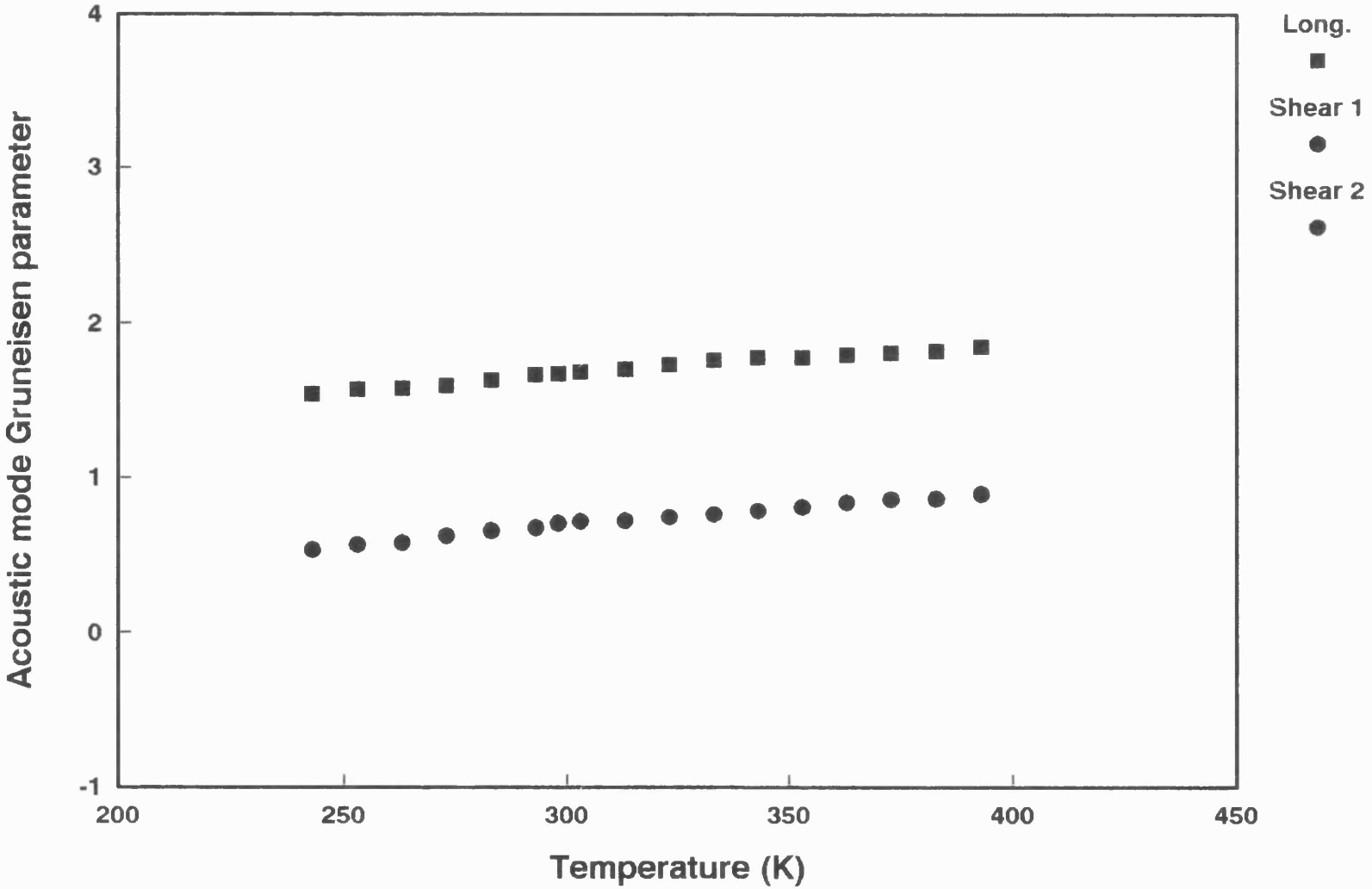

Fig. 7.2 (c) The temperature dependence of the acoustic mode Gruneisen parameter along the direction of Z-axis.

1 propagated along Y-axis have negative values ranging from -0.796 to -0.050 and -1.136 to -1.296, respectively. The values of the former include a contribution from $(\partial C_{14}/\partial P)_{T,P=0}$ while the values of the latter include a contribution from $(\partial C_{66}/\partial P)_{T,P=0}$ (see Eq. (3.23)). Most of the acoustic mode Grüneisen parameters show a marked temperature dependence. The values of all longitudinal modes propagated along the three axes increase almost linearly with increasing temperature (Fig. 7.2 (a)-(c)). Shear modes behave in a more complicated way. There is a sharp decrease starting at 323K in the value of the Grüneisen parameter for Shear 1 propagated along X-axis (Fig. 7.2 (a)). Below room temperature the value of Shear 2 along Y-axis is almost constant and then becomes smaller with increasing temperature (Fig. 7.2 (b)). A hump appears in the value of the Grüneisen parameter for Shear 1 along Y-axis at about 303K (Fig. 7.2 (b)). The Grüneisen parameter for other shear modes propagated along X- and Z-axes increase linearly when temperature is arising (Fig. 7.2 (a) and (c)).

In addition to being responsible for the nonlinear acoustic properties of a crystal under finite strain, the anharmonicity of lattice vibrations brings about thermal expansion. At a given temperature the expansion results from summation of the anharmonic effects of all the excited phonon modes rather than solely the acoustic modes at the long wavelength limit. The mean long wavelength acoustic mode Grüneisen parameter γ_H^l in the high temperature limit (H) has been calculated by using Eq. (3.23) and (3.55). The calculated γ_H^l is plotted in Fig. 7.3 together with the thermal Grüneisen parameter γ^{th} and the tensor components γ_{11}^{th} and γ_{33}^{th} given by Barron et al. (1982). As a summation of all long-wavelength acoustic mode Grüneisen parameters, γ_H^l does not change as sharply as some mode parameters from 243K to 393K (Fig. 7.1 (a)-(d) and 7.3). The value of γ_H^l increases to a maximum at about 313K and then decreases, ranging from 0.538 to 0.649. At moderate temperatures the tensor component γ_{11}^{th} is more sensitive to changes in temperature than the tensor component γ_{33}^{th} (Fig. 7.3). The observation that C_{11}/C_{33} is 0.81 at 243K and changes only slightly to 0.83 at 393K (Table 6.3) shows that elastically

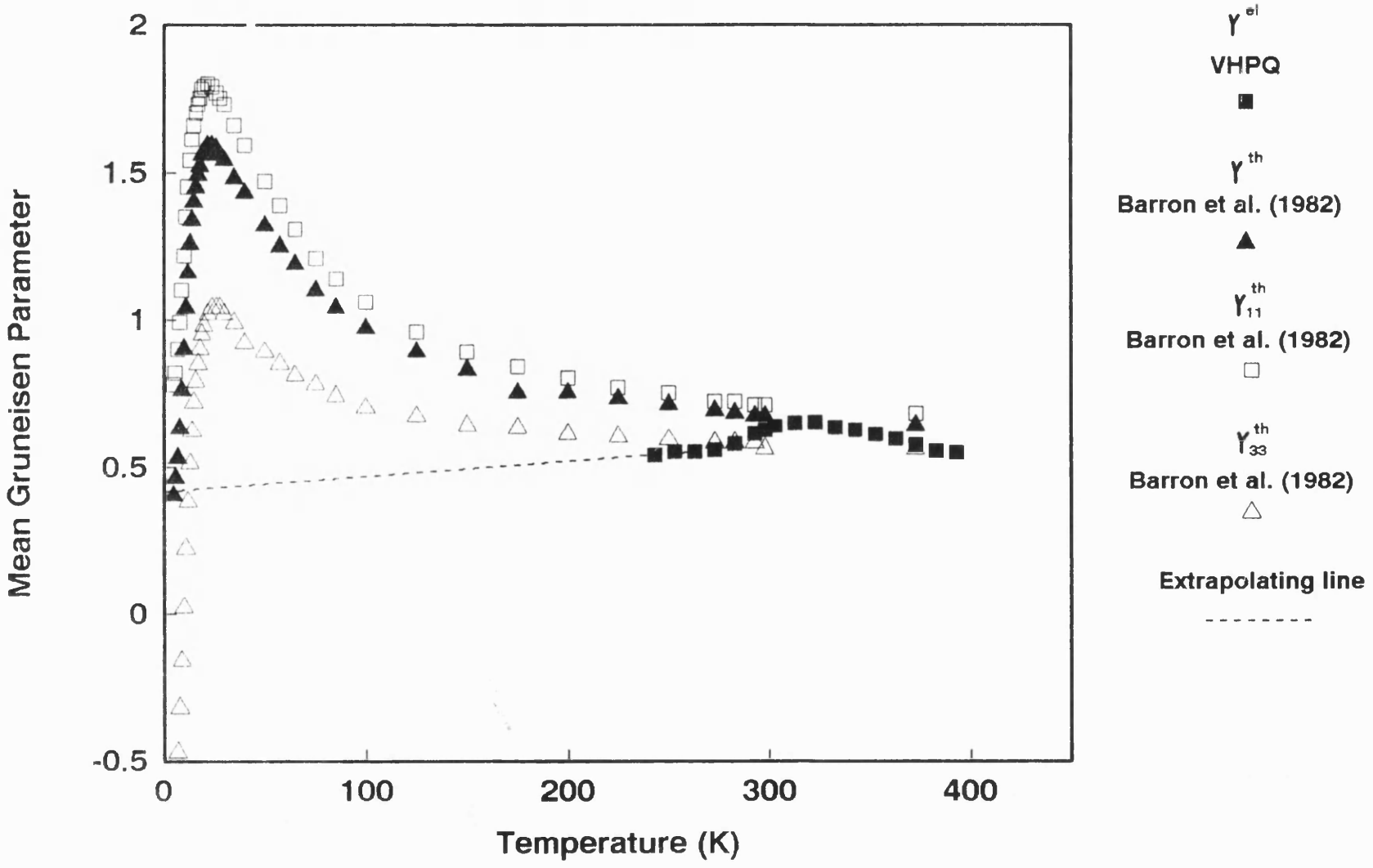

Fig. 7.3 The temperature dependence of mean Gruneisen parameters.

quartz is rather softer in the basal plane than in the direction of the threefold axis, and the anisotropy ($\alpha_{11} > \alpha_{33}$) of the thermal expansion tensor components evinces this. In this temperature range γ^{th} should be much influenced by optic mode contributions. Stress dependence measurements of Raman active mode frequencies (Tekippe et al. 1973, Grimsditch et al. 1977) reveal that lower frequency optic modes have large positive Grüneisen parameters. At low temperature ($T \ll \Theta_D$) the thermal expansion is mainly dominated by the acoustic vibration mode. The extrapolated temperature dependence of the mean acoustic Grüneisen parameter γ_H^l in high temperature limit (Fig. 7.3) shows that at low temperature (5K) the value of γ^l is nearly equal to that of γ^{th}, if γ^l decreases linearly with lowering temperature. The mean long wavelength acoustic mode Grüneisen parameter γ_L^l and the tensor components γ_{L11}^l and γ_{L33}^l in the low temperature limit (L) have been calculated by using Eq. (3.34)-(3.54) and the TOEC for VHPQ at 243K (Table 6.22). The calculated γ_{L11}^l , γ_{L33}^l and γ_L^l are listed in Table 7.2 and are compared with the thermal Grüneisen parameter γ^{th} and the tensor components γ_{11}^{th} and γ_{33}^{th} calculated by Barron et al. (1982) from the measured data of thermal expansion coefficients and the specific heat at 5K.

Table 7.2 The acoustic and thermal Grüneisen parameters of α-quartz at low temperature

VHPQ			Barron et al. (1982) (5K)		
γ_{L11}^l	γ_{L33}^l	γ_L^l	γ_{11}^{th}	γ_{33}^{th}	γ^{th}
0.54	-0.62	0.46	0.78	-0.64	0.40

The results in Table 7.2 indicate that at very low temperature, the long wavelength acoustic modes dominate the vibrational anharmonicity of the crystal. As the temperature is lowered the negative values of the Grüneisen parameters for some acoustic modes

cause the value of the thermal Grüneisen parameter γ^{th} and the tensor components γ^{th}_{11} and γ^{th}_{33} to decrease until γ^{th}_{33} become negative (see Fig. 7.3 and Table 7.2). The contributions α^{el}_{11}, α^{el}_{33} and α^{el} of long wavelength acoustic modes to the thermal expansion coefficients at low temperature have been calculated, by using Eqs. (3.32), (3.33) and (3.31) and the smoothed value of 0.074 for the measured C_P at 5K (Barron et al. 1982). The coefficients α^{el}_{11}, α^{el}_{33} and α^{el} are given in Table 7.3, compared with the smoothed values of the measured thermal expansion coefficients at 5K.

Table 7.3 The thermal expansion coefficients of α-quartz at low temperature (in the units of 10^{-8} K^{-1})

VHPQ			Barron et al. (1982) (5K)		
α^{el}_{11}	α^{el}_{33}	α^{el}	α_{11}	α_{33}	α
0.13	-0.14	0.12	0.18	-0.16	0.20

The close similarity between the values of the two groups of the thermal coefficients in Table 7.3 confirms that at very low temperature the thermal expansion is mainly dominated by the low frequency modes in acoustic branches. The negative value of the thermal expansion tensor component α_{33} is a consequence of long wavelength acoustic modes softening along the threefold axis. As temperature increases, more higher frequency acoustic modes contribute and add positive values to the thermal expansion, due to the dispersion effects in the acoustic branches (Barron et al. 1982), so that the thermal Grüneisen parameters, and therefore thermal expansion coefficients, increase rapidly (Fig. 7.3). A lattice dynamic modelling study for the thermal expansion of α-quartz (Barron and Pasternak 1986) indicates that the negative value of the tensor component α_{33} at very low temperature (below 5K) arises from the contribution of the lattice vibrational effects on the bond between two atoms. A negative contribution to

the thermal expansion is obtained when the bonded atoms are forced to displace relatively in a direction perpendicular to the bond direction or in a way to cause a rotation in the bond direction (Barron and Pasternak 1987).

7.3 Piezoelectric contributions to the acoustic mode Grüneisen parameters

In the calculation of the acoustic mode Grüneisen parameters the piezoelectric coefficients e_{11} and e_{14} and the hydrostatic pressure derivative $[\partial(e_1^2/\varepsilon_{11}^\eta)/\partial P]_{T,P=0}$ contribute in three aspects: (i) e_{11} and e_{14} appear in the coefficients λ_{ij} of the Christoffel equations which are used to determine the unit vector of the direction of particle displacements:

$$\alpha_j\lambda_{ij} = \alpha_i\rho v^2 \quad , \qquad (i,j = 1, 2, 3) \tag{7.1}$$

where α_i are direction cosines of the particle displacements, ρ is the density of a material measured and v is wave velocity, (ii) $[\partial(e_1^2/\varepsilon_{11}^\eta)/\partial P]_{T,P=0}$ plays a part in Eq. (3.23), (iii) e_{11} and e_{14} occur in Eq. (3.24). If the terms containing the piezoelectric coefficients and their pressure derivatives are taken off, Eq. (3.23) and (3.24) can be written as:

$$
{}_H\gamma(p,\vec{N}) = -\frac{B^T}{2w}\{1 + 2w[s_1(U_1^2 + U_2^2) + s_3U_3^2]
$$

$$
-\left[\left(\frac{\partial C_{11}^{ef}}{\partial P}\right)_T + 1 + (2s_1 - s_3)C_{11}^{S,E}\right](N_1U_1 + N_2U_2)^2
$$

$$
-\left[\left(\frac{\partial C_{66}^{ef}}{\partial P}\right)_T + 1 + (2s_1 - s_3)C_{66}^{S,E}\right](N_1U_2 - N_2U_1)^2
$$

$$
-\left[\left(\frac{\partial C_{33}^{ef}}{\partial P}\right)_T + 1 + (3s_3 - 2s_1)C_{33}^{S,E}\right]N_3^2U_3^2
$$

$$
-\left[\left(\frac{\partial C_{44}^{ef}}{\partial P}\right)_T + 1 + s_3C_{44}^{S,E}\right][(N_2U_3 + N_3U_2)^2 + (N_1U_3 + N_3U_1)^2]
$$

$$
-2\left[\left(\frac{\partial C_{13}^{ef}}{\partial P}\right)_T - 1 + s_3C_{13}^{S,E}\right](N_1U_1 + N_2U_2)N_3U_3
$$

$$
-2\left[\left(\frac{\partial C_{14}^{ef}}{\partial P}\right)_T + s_1C_{14}^{S,E}\right][(N_1^2 - N_2^2)U_2U_3 + (U_1^2 - U_2^2)N_2N_3
$$

$$
+ 2N_1U_1(N_2U_3 + N_3U_2)]\} \quad , \tag{7.2}
$$

where

$$
w = C_{11}^{S,E}(N_1U_1 + N_2U_2)^2 + C_{66}^{S,E}(N_1U_2 - N_2U_1)^2
$$

$$
+C_{33}^{S,E}N_3^2U_3^2 + C_{44}^{S,E}[(N_2U_3 + N_3U_2)^2 + (N_1U_3 + N_3U_1)^2]
$$

$$
+2C_{13}^{S,E}(N_1N_3U_1U_3 + N_2N_3U_2U_3)
$$

$$
+2C_{14}^{S,E}[(N_1^2 - N_2^2)U_2U_3 + N_2N_3(U_1^2 - U_2^2) + 2N_1U_1(N_2U_3 + N_3U_2)] \quad . \tag{7.3}
$$

Eqs. (7.2) and (7.3) are the form required for non-piezoelectric materials. The contributions of the piezoelectric effects to the acoustic mode Grüneisen parameters of VHPQ can be estimated by comparing the results calculated without considering the piezoelectric effects with those calculated by using equations including piezoelectric coefficients and their pressure derivatives. This process provides information of the effects of piezoelectricity on the vibrational anharmonicity of VHPQ crystals. There is no contribution from piezoelectric effects to the Grüneisen parameters of the acoustic

modes along Z axis; hence the values of these parameters are the same as those given in Fig. 7.2 (c). The acoustic mode Grüneisen parameters along two crystallographic axes, X and Y, calculated by using Eq. (7.2) and (7.3) are plotted in Fig. 7.4 (a) and (b). For comparison, the acoustic mode Grüneisen parameters including the piezoelectric contributions are included in the figures. Below 363K the piezoelectric contributions add positive values to the acoustic mode parameters along X- and Y-axes. Above 373K the values of these parameters are lowered due to the negative values of $[\partial(e_{11}^2/\varepsilon_{11}^\eta)/\partial P]_{T,P=0}$ (Table 6.10). The piezoelectric contributions to the modes Shear 2 along both X- and Y-axes are much less than those to the other modes along these two axes (Fig. 7.4 (a) and (b)). Fig 7.5 (a)-(f) shows that there how the other modes are affected by piezoelectric contributions. The modes which are most affected by the piezoelectric effects are those propagated in X-Y plane. Below 343K, for the acoustic shear modes lying in the wave propagation directions from $\phi = 20°$ to $\phi = 50°$ in X-Y plane the dependence of the Grüneisen parameters, not including the piezoelectric contributions, upon wave propagation direction is totally unlike that for the parameters including the piezoelectric contributions (Fig. 7.5 (a)-(d) and Fig. 7.2 (a)-(d)). As temperature increases the wave propagation direction dependence of the Grüneisen parameters for the shear modes in X-Y plane changes more than for the other modes. The values of the Grüneisen parameters of these shear modes change gradually with increasing temperature (Fig. 7.5 (a)-(d)) and eventually, when $T > 333K$, take a similar form to the case where the piezoelectric contributions are considered (Fig. 7.5 (e)-(g) and Fig. 7.2 (a)-(d)). The Grüneisen parameters of the other modes except for these shear modes are also temperature dependent, but they do not show substantial changes when the piezoelectric contributions are excluded. Differences caused by the exclusion of the piezoelectric contribution are also found in the wave propagation direction dependences of the Grüneisen parameters of other modes, for instance, for the shear modes lying in the direction from $\phi = 0°$ to $\phi = 20°$ in X-Y plane and the shear modes

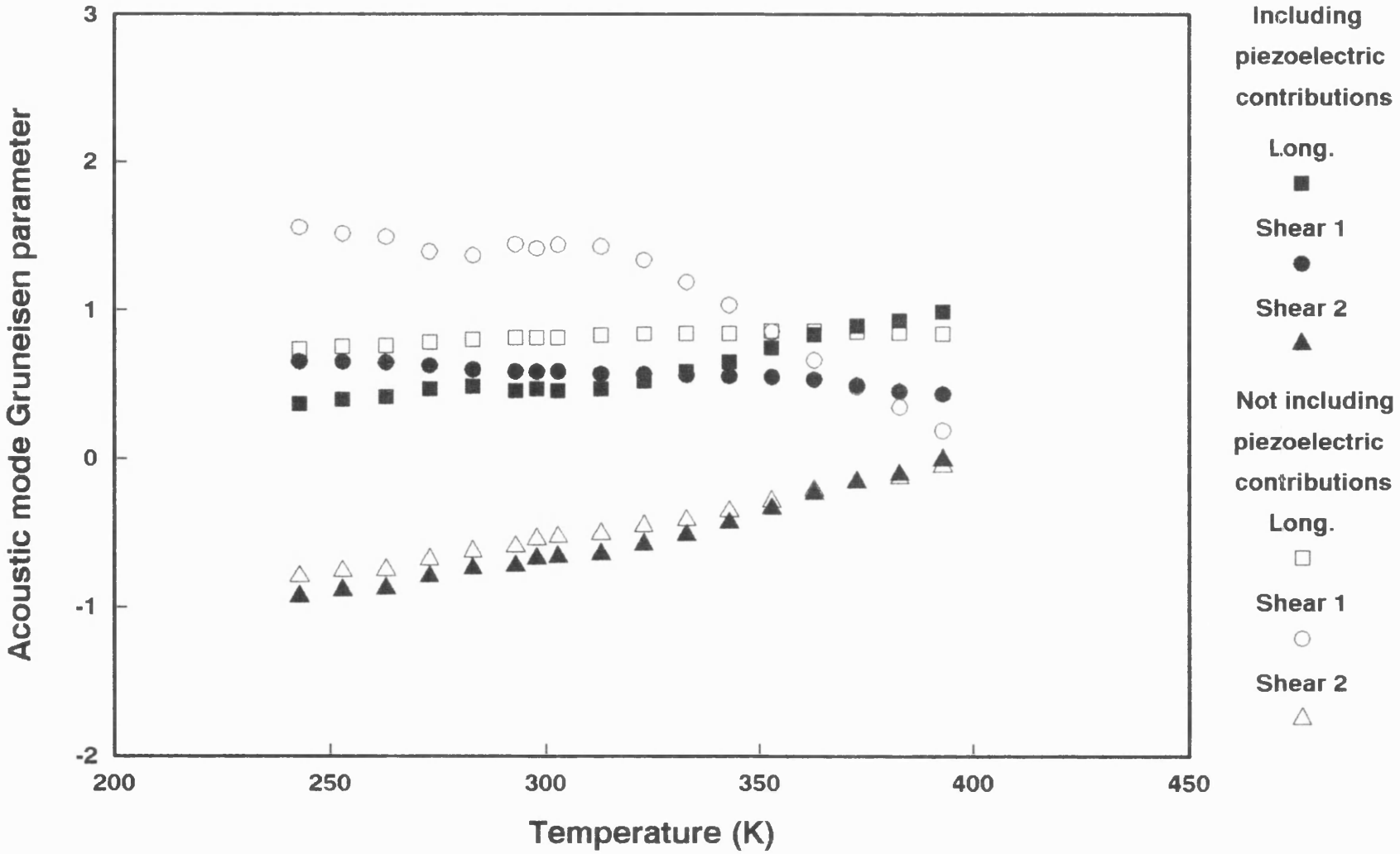

Fig. 7.4 (a) The temperature dependence of the acoustic mode Gruneisen parameter along the direction of X-axis, including and not including piezoelectric effects.

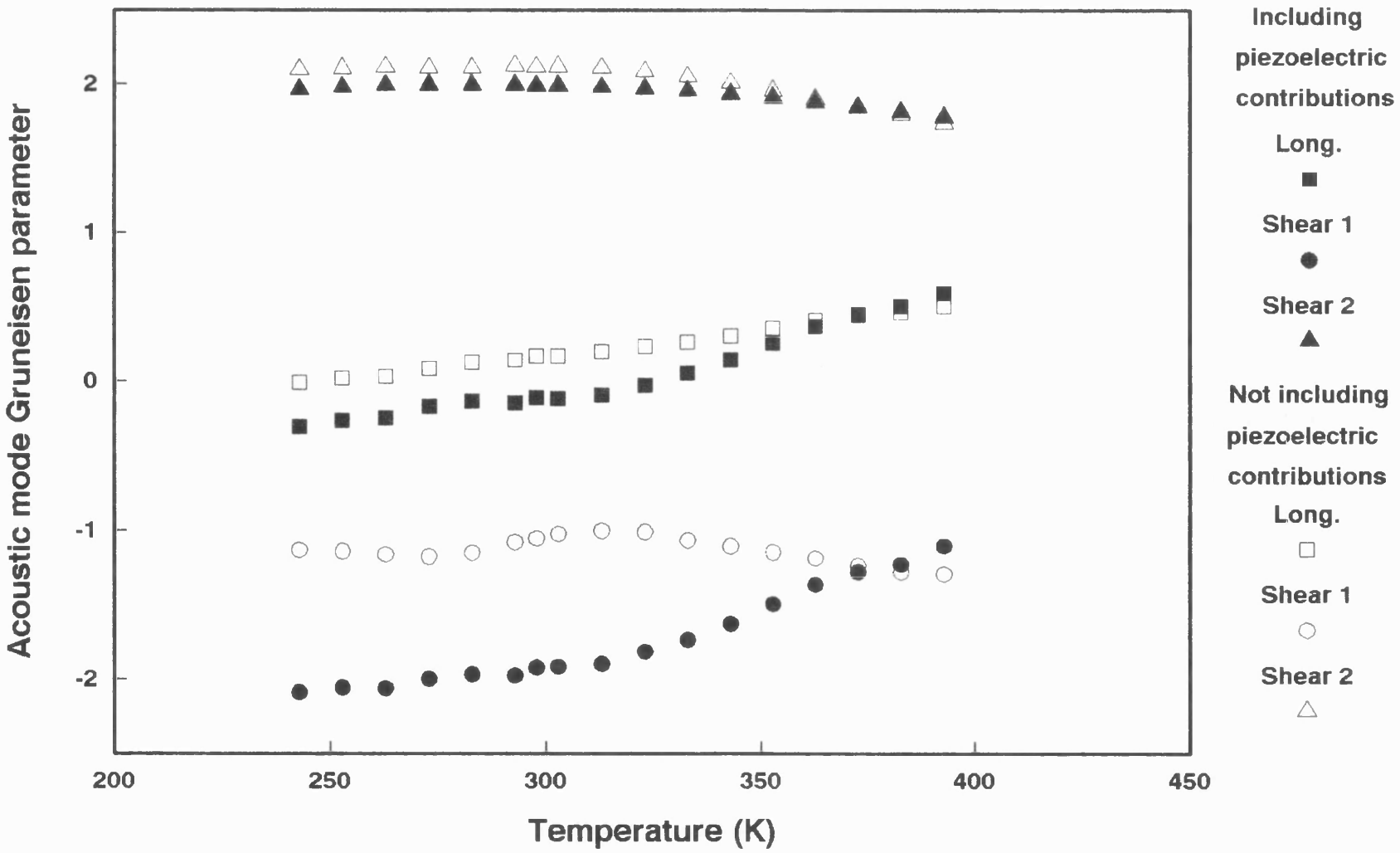

Fig. 7.4 (b) The temperature dependence of the acoustic mode Gruneisen parameter along the direction of Y-axis, including and not including piezoelectric effects.

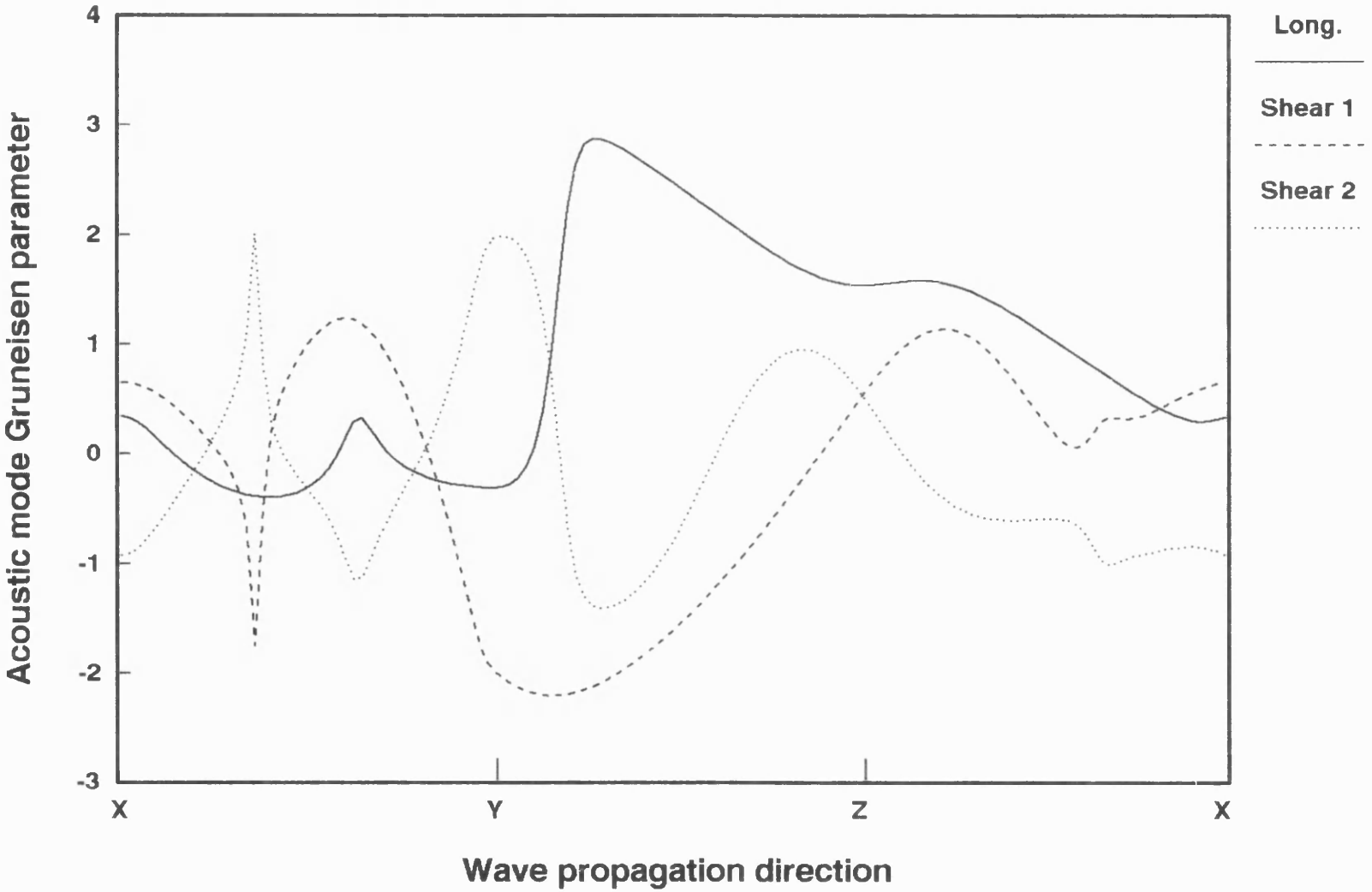

Fig. 7.5 (a) The acoustic mode Gruneisen parameters as a function of wave propagation direction at 243K, not including piezoelectric effects.

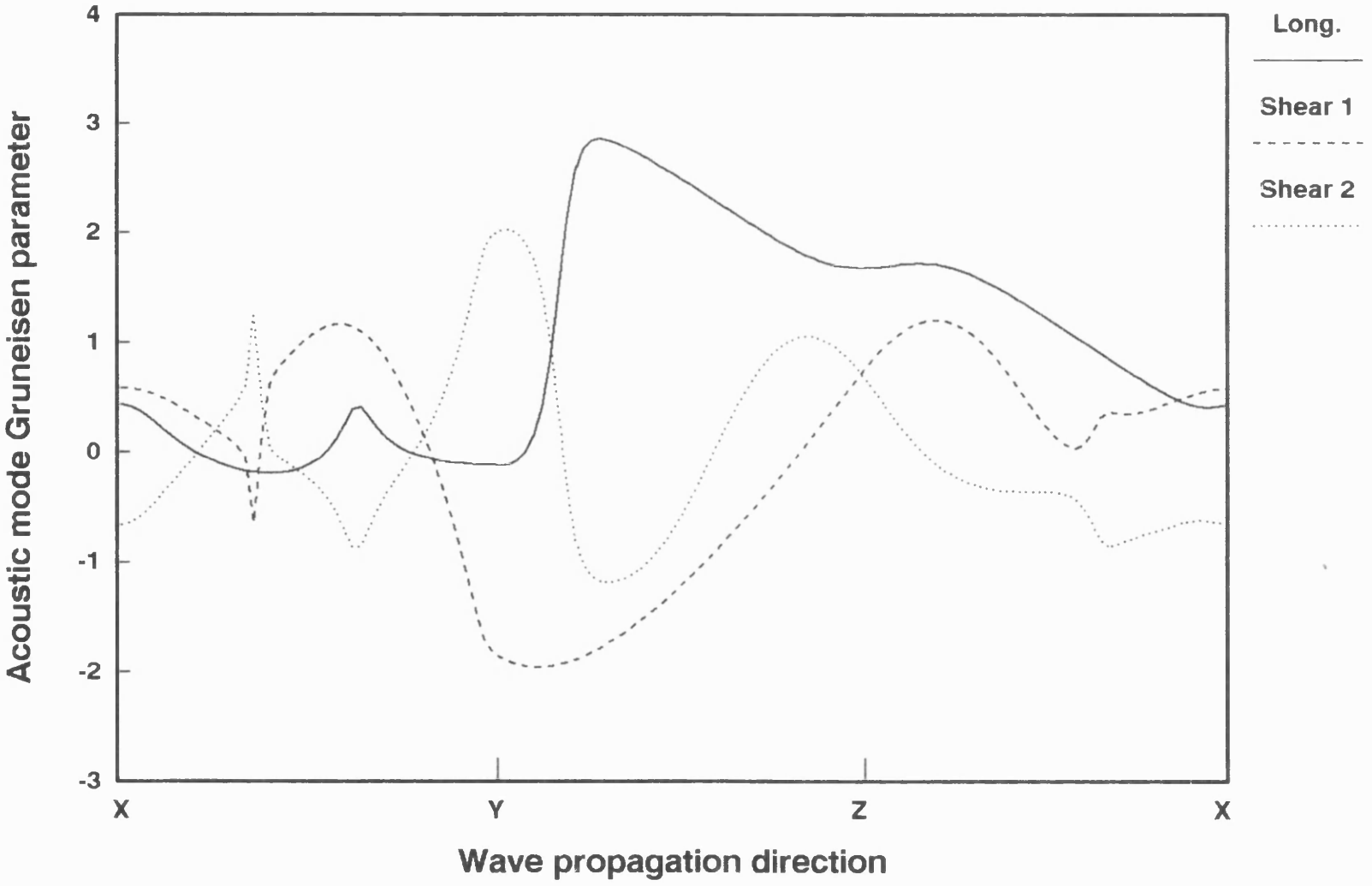

Fig. 7.5 (b) The acoustic mode Gruneisen parameters as a function of wave propagation direction at 303K, not including piezoelectric effects.

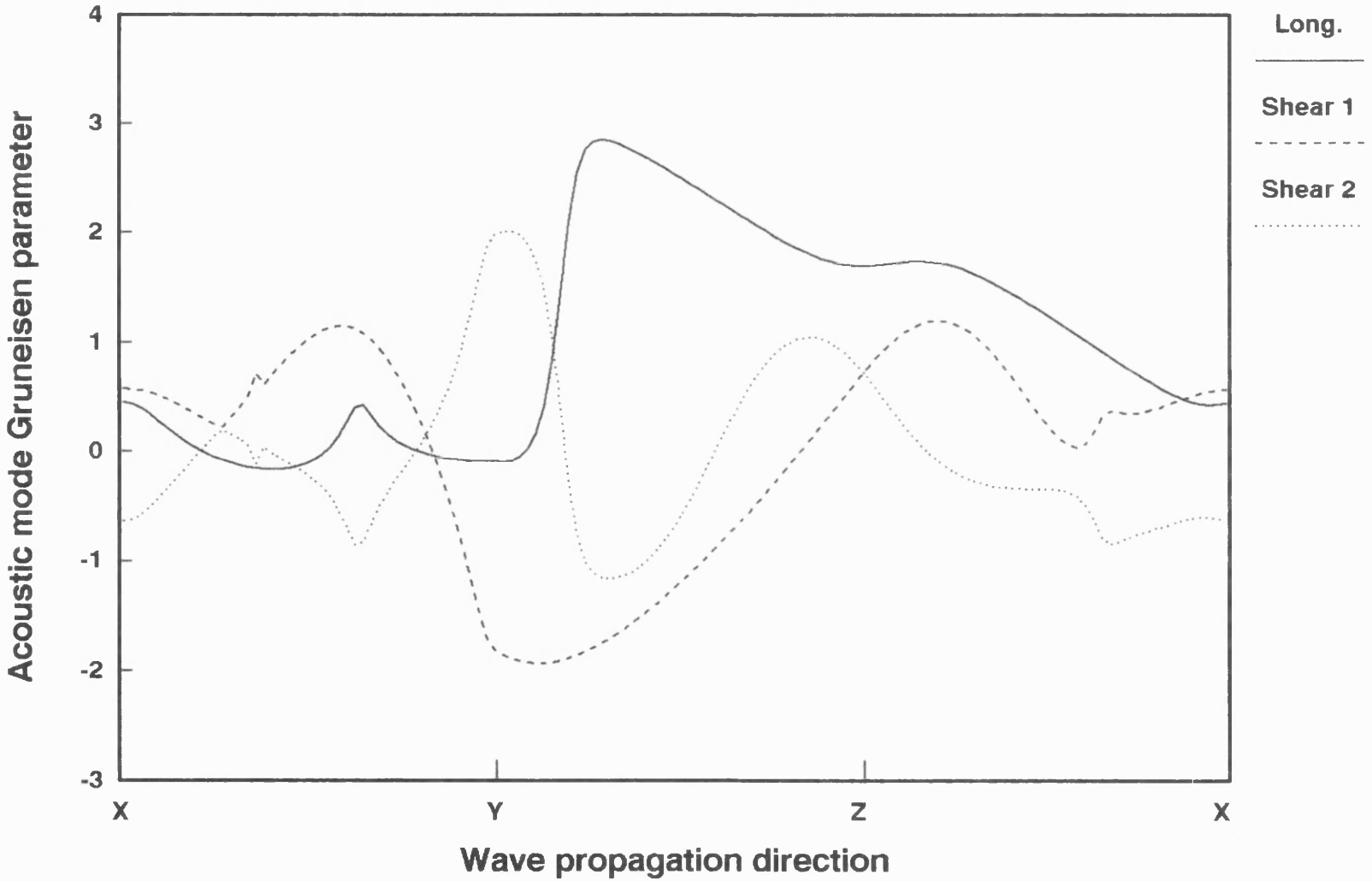

Fig. 7.5 (c) The acoustic mode Gruneisen parameters as a function of wave propagation direction at 313K, not including piezoelectric effects.

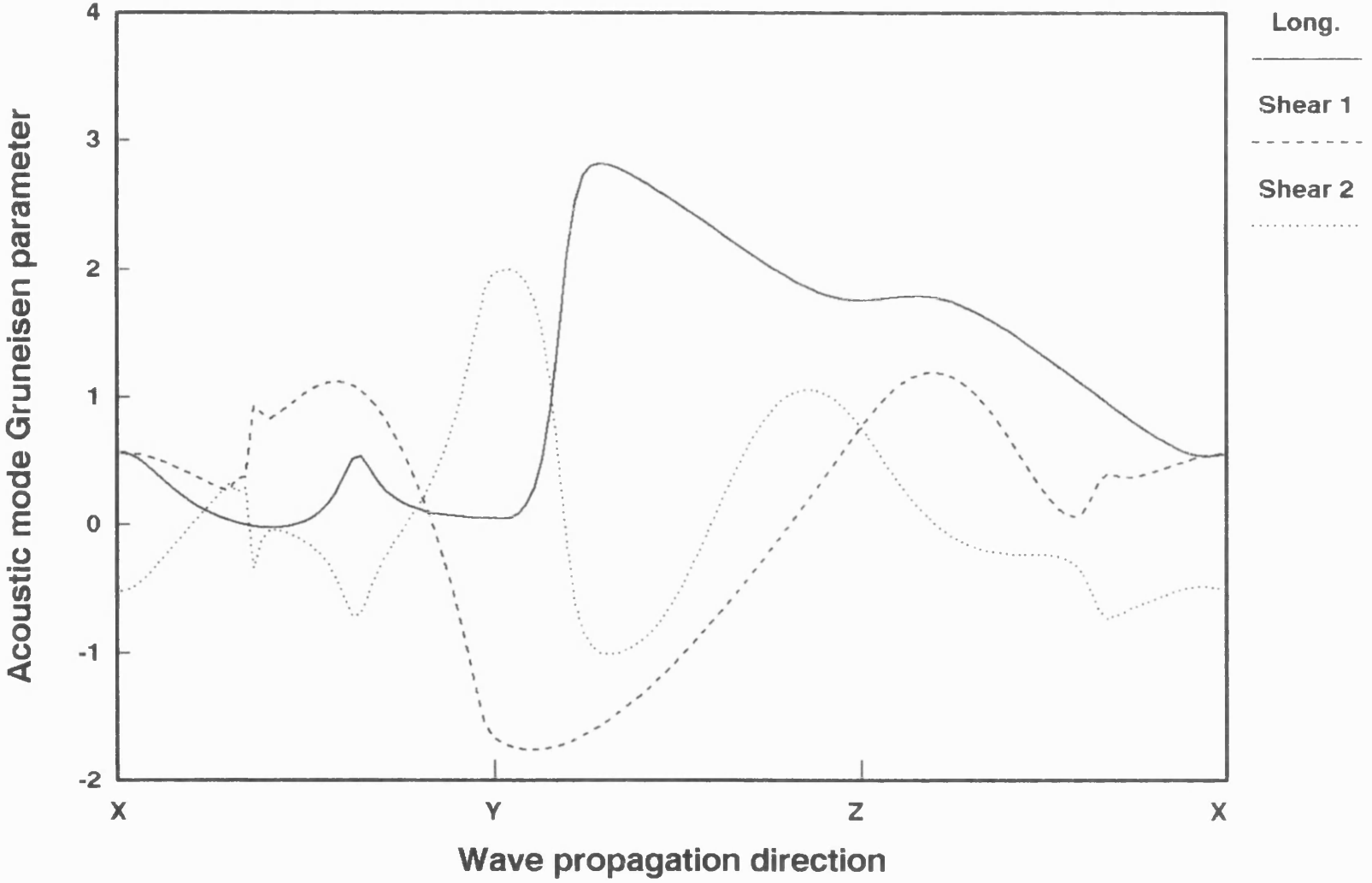

Fig. 7.5 (d) The acoustic mode Gruneisen parameters as a function of wave propagation direction at 333K, not including piezoelectric effects.

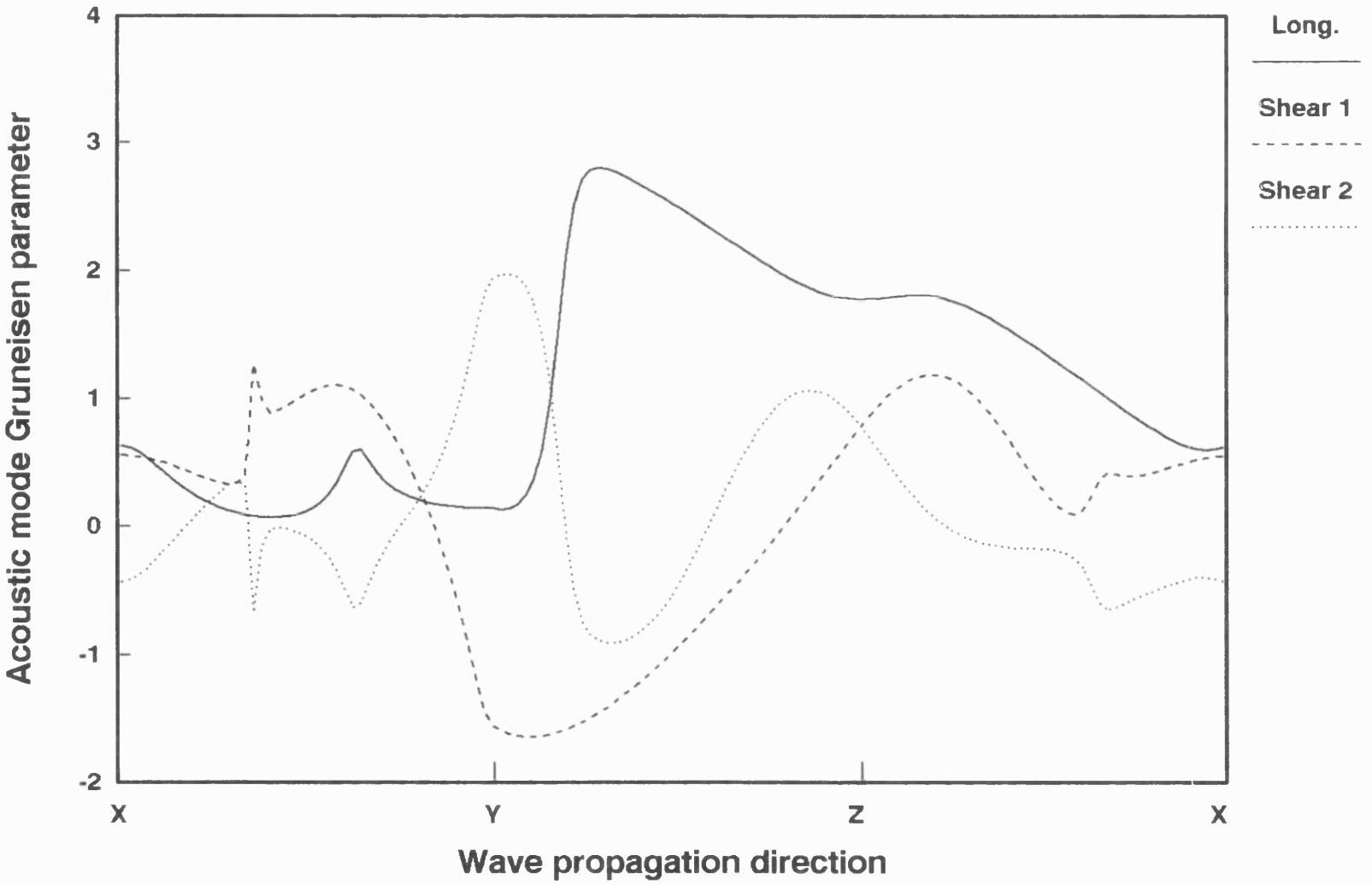

Fig. 7.5 (e) The acoustic mode Gruneisen parameters as a function of wave propagation direction at 343K, not including piezoelectric effects.

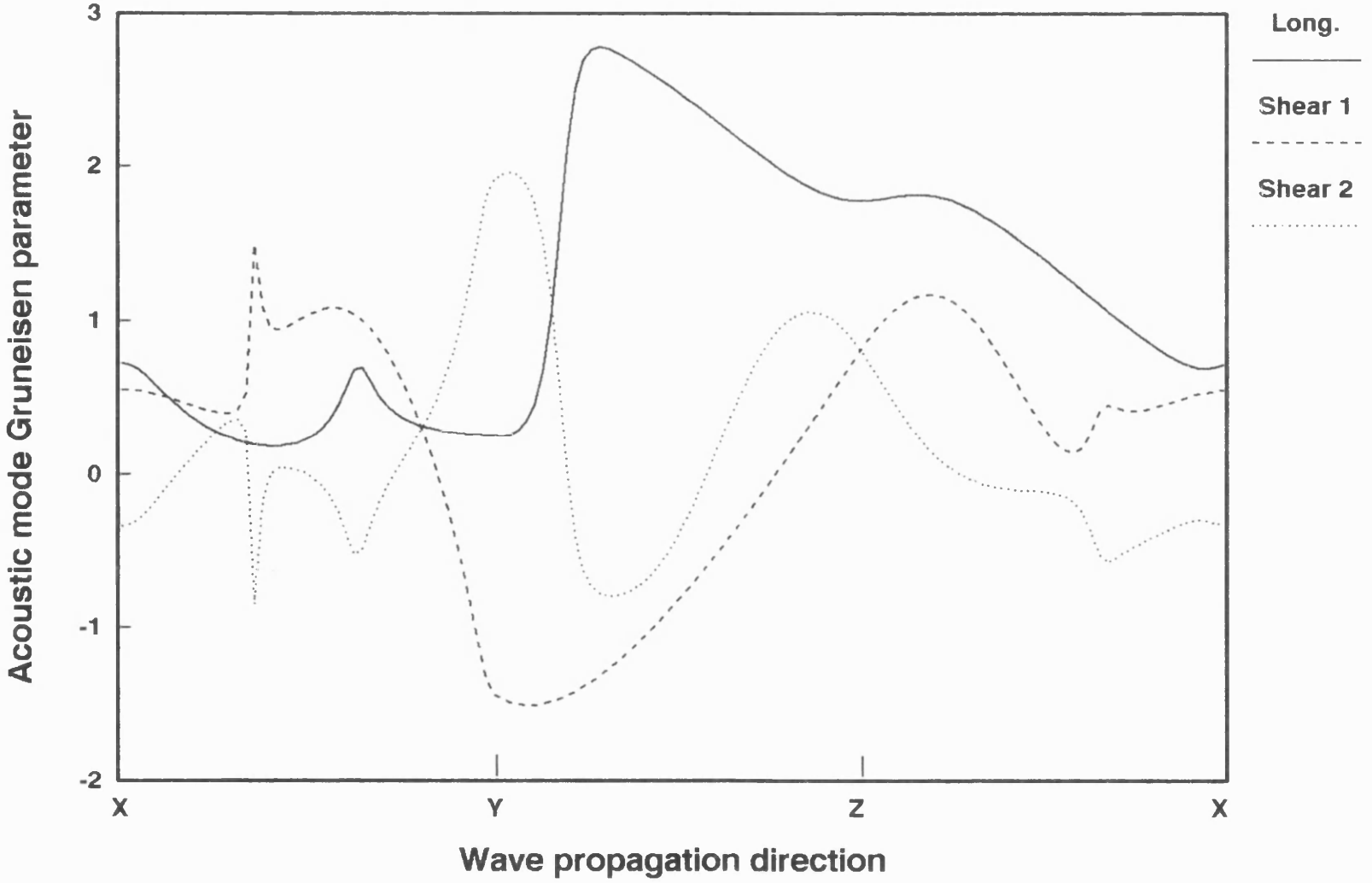

Fig. 7.5 (f) The acoustic mode Gruneisen parameters as a function of wave propagation direction at 353K, not including piezoelectric effects.

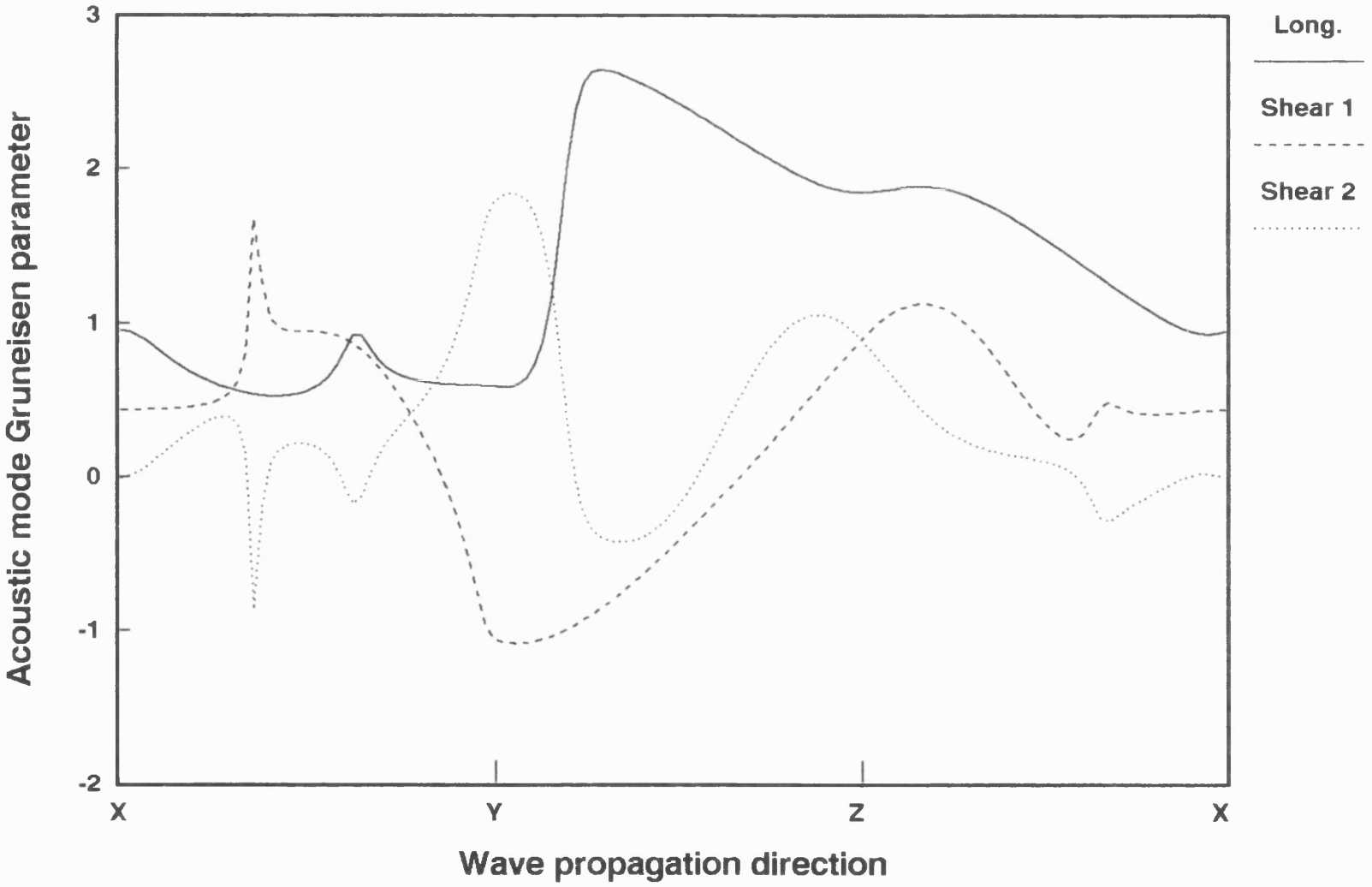

Fig. 7.5 (g) The acoustic mode Gruneisen parameters as a function of wave propagation direction at 393K, not including piezoelectric effects.

in Z-X plane. For these modes, the relative difference of values of the Grüneisen parameters are smaller than the ones in which piezoelectric contributions are included (Fig. 7.5 (e)-(g) and Fig. 7.2 (a)-(d)).

When the piezoelectric contribution is excluded, the value of the mean long wavelength acoustic mode Grüneisen parameter γ^l as a function of temperature is also changed. The values of the γ^l, including and not including piezoelectric contributions, are given in Table 7.4. In Table 7.4 the notation $\gamma^l_{p\epsilon}$ indicates the mean long wavelength acoustic mode Grüneisen parameters including piezoelectric contributions. Below 373K. the piezoelectric contributions enhance the lattice vibrational anharmonicity and add the positive values to the γ^l. Above 373K, the value of the pressure derivative $[\partial(e_1^2/\varepsilon_{11}^\eta)/\partial P]_{T,P=0}$, the main part of the contribution, becomes negative and reduces the value of γ^l. In conclusion, piezoelectric contributions affect considerably the lattice vibrational anharmonicity of α-quartz.

Table 7.4 Comparison of the mean long wavelength acoustic mode Grüneisen parameters including (γ_{pe}^{l}) and not including (γ^{l}) piezoelectric contributions

T (K)	γ_{pe}^{l}	γ^{l}	T (K)	γ_{pe}^{l}	γ^{l}
243	0.54	0.22	323	0.65	0.38
253	0.55	0.25	333	0.63	0.41
263	0.55	0.25	343	0.62	0.45
273	0.56	0.29	353	0.61	0.50
283	0.58	0.31	363	0.59	0.55
293	0.61	0.31	373	0.57	0.58
298	0.62	0.33	383	0.55	0.59
303	0.64	0.34	393	0.55	0.63
313	0.65	0.34			

Chapter 8 Conclusion

The properties of α-quartz found in the present study can be summarized as follows:

1. The fourteen independent third order elastic constants (TOEC) of VHPQ change markedly with temperature from 243K to 393K. C_{113} , C_{114} , C_{133} , C_{134} , C_{155} and C_{444} all have negative values, while C_{124} , C_{222} and C_{344} have positive values. When the temperature increases the values of C_{112} and C_{123} vary from negative to positive. When the temperature is increased, C_{111} , C_{113} , C_{114} , C_{133} , C_{134} , C_{144} and C_{155} decrease while C_{112} , C_{123} , C_{124} , C_{133} , C_{222} and C_{344} increase. C_{444} shows a maximum at around 303K.

2. The hydrostatic pressure derivatives $(\partial C_{IJ}/\partial P)_{T,P=0}$ of the SOEC which are combinations of the TOEC of VHPQ increase approximately linearly with temperature when the contributions from piezoelectric effects are deducted. The temperature dependences of the $(\partial C_{11}/\partial P)_{T,P=0}$, $(\partial C_{13}/\partial P)_{T,P=0}$ and $(\partial C_{66}/\partial P)_{T,P=0}$ are considerably affected by the contributions from piezoelectric effects.

3. The values of volume compression and pressure-induced changes in the lattice parameter a extrapolated up to high pressure at 298K by a computational procedure, using the pressure derivatives of the bulk modulus and of the SOEC determined for zero pressure, agree well with data measured by other scientists. The calculated values of the pressure induced changes in the lattice parameter c give an overestimation at high pressure when compared with experimental data. The calculated values of the volume compression and of the pressure-induced changes in lattice parameters extrapolated to high pressure show significant temperature dependence only at very high pressures (above about 8GPa). Under those high pressures the values of the compressions decrease,

when temperature increases.

4. Negative values of the pressure derivatives $(\partial C_{14}/\partial P)_{T,P=0}$ and $(\partial C_{66}/\partial P)_{T,P=0}$ have been related to soft phonon modes and order parameters which induce the $\alpha-\beta$ phase transformation which occurs at 846K and may be a precursor of the structural instability which results in the phase transformation.

5. The highly unsymmetrical crystal structure of the α-quartz is reflected by the dependences of the long wavelength acoustic mode Grüneisen parameters on wave propagation direction. The lattice vibrational anharmonicity is strongly temperature dependent from 243K to 393K. The long wavelength acoustic modes Grüneisen parameters and the mean acoustic Grüneisen parameter, and hence their contributions to thermal expansion coefficient, are temperature dependent. At low temperature the values of elastic thermal expansion tensor components which counter the contributions of the long wavelength acoustic mode Grüneisen parameters are approximately equal to measured thermal expansion tensor components, a verification of the dominant role of the long wavelength acoustic phonon modes in thermal expansion at low temperature.

6. The piezoelectric effects provide significant contributions to nonlinear elastic properties and vibrational anharmonicity. The values of most of the TOEC and the hydrostatic pressure derivatives $(\partial C_{IJ}/\partial P)_{P=0}$ change remarkably when the contributions of the piezoelectric effects are deducted. The temperature dependence of the mean long wavelength acoustic mode Grüneisen parameter is affected significantly by the behaviour of the hydrostatic pressure derivative of the piezoelectric term $e_{11}^2/\varepsilon_{11}^\eta$.

REFERENCES

Adam, W., Tichy, J., and Kittinger, E., J. Appl. Phys. **64**, 2556 (1988).

Altman H.E. and Beyer R.T., J. Acoust. Sco. Am. **59**, 545 (1976).

Anderson O.L., J. Phys. Chem. Solids, **27**, 547 (1966).

Atanasoff J.V. and Hart P.J., Phys. Rev. **59**, 85 (1941).

Aubry S. and Pick R., J. de Phys. **32**, 657 (1971).

Axe J.D. and Shirane G., Phys. Rev. B **1**, 342 (1970).

Auld B.A., "Acoustic Fields and Waves in Solids" Vol. 1, (John Wiley & Sons, New York, 1973).

Barford N.C., "Experimental Measurements: Presision, Error and Truth", 2ed (John Wiley & Sons, Chichester, 1985).

Barron T.H.K., Collins J.G. and White G.K., Adv. Phys. **29**, 609 (1980).

Barron T.H.K., Collins J.F., Smith T.W. and White G.K., J. Phys. C**15**, 4311 (1982).

Barron T.H.K. and Pasternak A., J. Phys. C**20**, 215 (1987).

Bauer K.H.W., Jagodzinski H., Dorner B. and Grimm H., Phys. Stat. Sol. (b) **48**, 437 (1971).

Bechmann R., Phys. Rev. **110**, 1060 (1958).

Bechmann R., Ballato A.D. and Lukaszek T.J., Proc. IRE **50**, 1812 (1962).

Born M. and Oppenheimer J., Ann. Phys. **84**, 457 (1927).

Born M. and Huang K., "Dynamical Theory of Crystal Lattice" (Clarendon Press, Oxford, 1954).

Bottom V.E., J. Appl. Phys. **43**, 1493 (1972).

Bottom V.E., "Introduction to Quartz Crystal Unit Design" (Van Nostrand Reinhold company, New York, 1982).

Brassington M.P., PhD Thesis, University of Bath, 1982.

Brassington M.P. and Saunders G.A., Proc. R. Soc. Lond. **A387**, 289 (1982).

Breazeale M.A., Cantrell,Jr. J.H. and Heyman J.S., "Ultrasonic Wave Velocity and Attenuation Measurements", in "Methods of Experimental Physics (Volume 19): Ultrasonics", ed. by P.D. Edmonds (Academic Press, London, 1981).

Brendel R., J. Appl. Phys. **55**, 608 (1984).

Brice J.C., J. Mater. Sci. **15**, 161 (1980).

Brice J.C., Rev. Mod. Phys., **57**, 105 (1985).

Bridgman P.W., Proc. Am. Acad. Arts Sci. **76**, 55 (1948a).

Bridgman P.W., Proc. Am. Acad. Arts Sci. **76**, 71 (1948b).

Brüesch P., "Phonons: Theory and Experiments I (Lattice Dynamics and Methods of Interatomic Forces)" (Springer-Verlag, Berlin, 1982).

Brugger K., Phys, Rev. **133**, A1611 (1964).

Brugger K., Phys, Rev. **137**, A1826 (1965a).

Brugger K., J. Appl. Phys. **36**, 759 (1965b).

Brugger K. and Fritz T.C., Phys, Rev. **157**, 524 (1967).

Cady W.G., "Piezoelectricity: An Introduction to the Theory and Applications of Electromechanical Phenomena in Crystals" (McGraw-Hill Book Company, Inc., 1946).

Cady W.G., "Piezoelectricity: An Introduction to the Theory and Applications of Electromechanical Phenomena in Crystals", Vol. 1 (Dover Publications, Inc., New York, 1964).

Chang E. and Barsch G.R., J. Phys. Chem. Solids **34**, 1543 (1973).

Chelikowsky J.R., King,Jr. H.E., Troullier N., José Luís Martins and Glinnemann J., Phys. Rev. Let. **65**, 3309 (1990).

Cho Y. and Yamanouchi K., J. Appl. Phys. **61**, 875 (1987).

Croxall D.F., Christie I.R.A., Isherwood B.J. and Todd A.G., Proc. 36th Ann. Freq. control Symp., 62 (1982).

Davies G.F. and O'Connell R.J., "High Presssure Research Applications in Geophysics", ed. M.H. Maghnam and S.I. Akimoto (Academic Press, New York, 1977).

Dieulesaint E. and Royer D., "Elastic Waves in Solids: Applications to Signal Processing", (John Wiley & Sons, Chichester, 1980).

Elcombe M.M., Proc. Phys. Soc. **91**, 947 (1967).

Evans R. C., "An Introduction to Crystal Chemistry", 2nd Ed., (Cambridge University Press, Cambridge, 1966).

Fedorov A.F., "Theory of Elastic Waves in Crystals", trans. J.E. Bradley (Plenum Press,

New York, 1968).

Fleury P.A., "Phase Transitions - 1973" (Proseedings of the Conference on Phase Transitions and Their Applications in Materials Since, University Park, Pennsylvania, May 23-25, 1973), editors: H.K. Henisch, R. Roy and L.E. Cross (Pergamon Press, New York, 1973).

Fowles R., Geophys. Res. **72**, 5729 (1967).

Gaganipain J.J. and Besson, R., "Nonlinear Effects in Piezoelectric Quartz Crystals", "Physical Acoustics" vol. XI, editor: W.P. Mason and R.N. Thurston (Academic Press, London, 1975).

Gagnepain J.J., Proc. 35th Ann. Freq. control Symp., 14 (1981).

Gerlich D. and Breazeale M.A., J. Appl. Phys. **68**, 5119 (1990).

Glinnemann et al., in J.R. Chelikowsky, H.E. King, Jr., N. Troullier, José Luís Martins and J. Glinnemann, Phys. Rev. Let. **65**, 3309 (1990).

Graham R.A., Phys. Rev. B **6**, 4779 (1972).

Gray D.E., "The American Institute of Physics Handbook" (McGraw-Hill, New York, 1972).

Grimsditch M.H., Ramdas A.K., Rodriguez S. and Telippe V.J., Phys. Rev. B**15**, 5869 (1977).

Grimm H. and Dornner B., J. Phys. Chem. Solids **36**, 407 (1975).

Hazen R.M., Finger L.W., Hemley R.J. and Mao H.K., Solid State Commun. **72**, 507 (1989).

Hemley R.J., Jephcoat A.P., Mao H.K., Ming L.C. and Manghnani M.H., Nature (London) **334**, 52 (1988).

Höchli U.T. and Scott J.F., Phys. Rev. Letters **26**, 1627 (1971).

Holder J., Rev. Sci. Instr. **41**, 1355 (1970).

Hruska C.K. and Kazda V., Czech. J. Phys. B **18**, 500 (1968).

Hrusk, C.K., J. Appl. Phys. **61**, 1127 (1987).

Hrusk, C.K., J. Appl. Phys. **66**, 1071 (1989).

Hruska C.K., IEEE Trans. Ultrasonics, Ferroelectrics Freq. Contr. **37**, 329 (1990a).

Hruska C.K., The 4th European Frequency and time Forum Neuchâtel, 295 (1990b).

Hruska C.K. and Brendel R., J.Appl. Phys. **65**, 715 (1989).

IEEE Standard on Piezoelectricity, ANSI/IEEE Std **176** (The Institute of Electrical and Electronics Engineers, Inc., New York, 1978).

Ikeda T., "Fundamentals of Piezoelectricity", (Oxford University Press, Oxford, 1990).

James B.J., PhD Thesis, Roya Hollway and Bedford New College, University of London, 1987.

James B.J., private communication, 1989.

James B.J., private communication, 1990.

Jorgensen J.D., J. Appl. Phys. **49**, 547 (1978).

Kharusi M.S. and Rarnell G.W., J. Acoust. Soc. Am. **48**, 665 (1970).

Kittinger E., Ultrasonics **15**, 30 (1977).

Kittinger E., Tichy, J. and Friedel, W., J. Appl. Phys. **60**, 1465 (1986).

Koga I., Aruga M. and Yoshinaka Y., Phys. Rev. **109**, 1467 (1958).

Kusters J.A., Proc. 24th Ann. Freq. control Symp., 46 (1970).

Laudise R.A. and Barns R.L., IEEE Trans. Ultrasonics, Ferroelectrics Freq. Contr. **35**, 277 (1988).

Le Chatelier, C.R. Acad. Sci. (Paris) 1889.

Leibfried G. and Ludwig W., in "Solid State Physics: Advances in Research and Applications" Vol. 12, Ed. F. Seitz and D. Turubull (Academic Press, New York, 1961).

Levien L., Prewitt C.T., and Weidner D.J., Am. Mineral. **65**, 920 (1980).

Linchnowski A.J., Ph.D. Thsis, University of Durham, 1975.

Ljamov, V.E., J. Acoust. Soc. Am. **52**, 199 (1971).

Ludanov A.G., Fotchenkov A.A. and Yakovlev L.A., Akust. Zh. **22**, 612 (1976) [Sov. Phys.-Acoust. **22**, 343 (1976)].

Mason W.P., Bell Syst. T. J., **22**, 178 (1943).

Mason W.P., Bell Syst. T. J., **30**, 366 (1951).

Mason W.P., "Physical Acoustic and the Properties of Solids" (D. Van Nostrand Company, Inc., Princeton, 1958).

Maugin G.A., "Nonlinear Electromechanical Effects and Applications", vol.1 of "Series in Theoretical and Applied Mechanics", editor: R.K.T. Hsieh (World Scientific, Singapore, 1985).

May J.E., Jr., IRE Natl. Conv. Rec. **6**, Pt. 2, 134 (1958).

McMahon, D.H., J. Acoust. Soc. Am. **44**, 1007 (1968).

McSkimin H.J., J. Acoust. Soc. Am. **33**, 12 (1961).

McSkimin H.J. and Andreatch P. Jr., J. Acoust. Soc. Am. **34**, 609 (1962).

McSkimin H.J., J. Acoust. Soc. Am. **34**, 1271 (1962).

McSkimin H.J., Andreatch P. Jr. and Thurston R.N., J. Appl. Phys. **36**, 1624 (1965).

McWhan D.B., J. Appl. Phys., **38**, 347 (1967).

Megaw H.D., "Crystal Structures: A working Approach" (W.B. Saunders Company, Philadelphia, 1973).

Miklowitz J., "The Theory of Elastic Waves and Waveguids" (North-Holland, 1980).

Murnaghan F.D., Proc. Nat. Acad. Sci. USA, **30**, 244 (1944).

Nakagawa, Y., Yamanouchi, K. and Shibayama, K., J. Appl. Phys. **44**, 3969 (1973).

Nelson D.F., J. Acoust. Soc. Am. **63**, 1738 (1978).

Nelson D.F., "Electric, Optic and Acoustic Interaction in Dielectrics" (Willy, New York, 1979).

O'Donnell M., Busse L.J. and Miller J.G., "1. Piezoelectric Transducers" in "Methods of Experimental Physics: Volume 19 Ultrasonics", Ed. by P.D. Edmonds (Academic Press, Inc. (London) Ltd., London, 1981).

Overton W.C., J. Chem. Phys. **37**, 116 (1962).

Papadakis E.P., J. Appl. Phys. **35**, 1474 (1964).

Papadakis E.P., J. Acoust. Soc. Am. **40**, 863 (1966).

Papadakis E.P., J. Acoust. Soc. Am. **42**, 1045 (1967).

Perrier A. and de Mandrot R., Mém. Société vaudoise sci. nat. Vol. 1, pp.333-363, 1922-1924; abst. in Arch. sci. phys. nat., Vol. 4, pp.367-369, 1922.

Press W.H., Flannery B.P., Teukolsky S.A. and Vetterling W.T., "Numerical Recipes: The art of Scientific Computing" (Cambridge University Press, Cambridge, 1986).

Pugh E.M. and Winslow G.H., "The analysis of Physical Measurements" (Addison-Wesley, Reading, 1966).

Raman C.V. and Nedungadi T.M.K., Nature (London) **145**, 147 (1940).

Rao C. N. and Rao K.J., "Phase Transitions in Solids: An Approach to the Study of the Chemistry and Physics of Solids" (McGraw-Hill Inc., 1978).

Reider G.A., Kittinger E. and Tichy J., J. Appl. Phys. **53**, 8716 (1982).

Reissland J.A. Discuss. Faraday Soc. **40**, 123 (1966).

Samsonov G.V., "The Oxide Handbook" (IFI/Plenum, New York, 1973).

Shapiro S.M., O'Shea D.C. and Cummins H.Z., Phys. Rev. Lett. **19**, 361 (1967).

Shapiro S.M. and Cummins H.Z., Phys. Rev. Lett. **21**, 1578 (1968).

Shevel'ko M.M. and Yakovlev L.A., Sov. Phys.-Acoust. **23**, 187 (1977).

Sidek H.A.A., Saunders G.A., Wang Hong, Xu Bin and Han jianru, Phys. Rev. B **36**, 7612, (1987).

Slater J.C., "Introduction to Chemical Physics" (McGraw-Hill Book Company, Inc., New York, 1939).

Smith J.V., "Geometrical and Structural Crystallography" (John Wiley & Sons, New York, 1982).

Sosman R.B., "The Phases of Silica" (Rutgers Uinversity Press, New Brunswick, 1965).

"Standards on Piezoelectric Crystals, 1949", Proceedings of the I.R.E. **37**, 1378 (1949).

Tekippe V.J., Ramdas A.K., and Rodriguez S., Phys. Rev. B**8**, 706, (1973).

Thurston R.N., in "Physical Acoustics", Ed. W.P. Mason, Vol. 1A, 1 (Academic Press Inc., New York, 1964).

Thurston R.N. and Brugger K., Phys. Rev. **133**, A1604 (1964).

Thurston R.N., Proc. IEEE **53**, 1320 (1965a).

Thurston R.N., J. Acoust. Soc. Am. **37**, 348 (1965b).

Thurston R.N., J. Acoust. Soc. Am. **41**, 1093 (1966).

Thurston R.N., McSkimin H.J. and Andreatch P. Jr., J. Appl. Phys. **37**, 267 (1966).

Thurston R.N., "Waves in Solids", in "Encyclopedia of Physics" Vol. VIa/4, Ed. S. Flügge and C. Truesdell (Springer-Verlag, Berlin, 1974).

Touloukian Y.S., "Thermophysical Properties of High Temperature Materials" (Mac-Millan, London, 1967).

Toupin R.A., Int. J. Engng. Sci. **1**, 101 (1963).

Truesdell, C. and Toupin, R., "Handbych der Physik" Vol. III/1, edited by S. Flügge (Springger-Verlag, Berlin, 1960).

Tu Hailin, PhD Thesis, University of Bath, 1983.

Voigt W., "Lehrbuch der Krisallphysik", 1st Ed., pp.752-753 (B.G. Toubner, Leipzig, 1910).

Wackerle J., J. Appl. Phys. **33**, 922 (1962).

Wang Q. G.A. Saunders E.F. Lambson, P. Tschaufeser, S.C. Parker and B.J. James, Phys. Rev. B **45**, 10242 (1992).

Weast R.C., "Handbook of Chemistry and Physics" (Chemical Rubber Company, Cleveland, 1964).

Williams J. and Lamb J., J. Acoust. Soc. Am. **30**, 308 (1958).

White G.K., Cryogenics **4**, 2 (1964).

Yogurtcu Y.K., PhD Thesis, University of Bath, 1980.

Zeller R.C. and Pohl R.O., Phys. Rev. B **4**, 2029 (1971).

Appendix A

Computer Programme: MAOE.FOR

This programme computes the third order elastic constants (TOEC) as well as the hydrostatic pressure derivatives, $(\partial C_{IJ}/\partial P)_{T,P=0}$ and B_{IJ}, of the effective and thermodynamic second order elastic constants (SOEC) respectively in the temperature range from 243K to 393K for α-quartz which has trigonal symmetry (class 32). The input data are the SOEC, the quantities $e_1 = e_{11}^2/\varepsilon_{11}^\eta$ and $e_2 = (e_{14} - e_{11})^2/(2\varepsilon_{11}^\eta + 2\varepsilon_{33}^\eta)$, the hydrostatic pressure derivatives $[\partial(\rho_0 W^2)/\partial P]_{T,P=0}$ for the modes under hydrostatic or uniaxial pressure. These data are obtained from the measurements of ultrasonic waves carried out in this work. The TOEC, $(\partial C_{IJ}/\partial P)_{T,P=0}$ and B_{IJ} both with and without the contributions from piezoelectric effects are calculated by using the weighted least-square-method (Pugh and Winslow 1966). The simultaneous equations involved in the computation are solved using the LU decomposition method which is performed by the subroutines LUBKSB and LUDCMP (Press et al. 1986). The programme, written in FORTRAN 77, has been operated in a Viglen IV/25 (486) PC with the aid of the Microsoft FORTRAN Compiler V5.0. The primary variables used are:

c(i,j) (i=1,7 and j=1,17)	SOEC,
ep(1,j) (j=1,17)	$e_{11}^2/\varepsilon_{11}^\eta$,
ep(2,j) (j=1,17)	$(e_{14} - e_{11})^2/(2\varepsilon_{11}^\eta + 2\varepsilon_{33}^\eta)$,
w(i,j) (i=1,8 and j=1,17)	$[\partial(\rho_0 W^2)/\partial P]_{T,P=0}$ for the modes under hydrostatic pressure,

ud(i,j) (i=1,9 and j=1,17)	$[\partial(\rho_0 W^2)/\partial P]_{T,P=0}$ for the modes under uniaxial pressure,
cb(i,k) (i=1,6 and j=1,17)	B_{IJ} without contributions from piezoelectric effects,
pb(i,j) (i=1,6 and j=1,17)	B_{IJ} with contributions from piezoelectric effects,
cp(i,j) (i=1,7 and j=1,17)	$(\partial C_{IJ}/\partial P)_{T,P=0}$ without contributions from piezoelectric effects,
pcp(i,j) (i=1,7 and j=1,17)	$(\partial C_{IJ}/\partial P)_{T,P=0}$ with contributions from piezoelectric effects,
de(i,k) (i=1,2 and j=1,17)	$(\partial e_1/\partial P)_{T,P=0}$ and $(\partial e_2/\partial P)_{T,P=0}$
toep(i,j) (i=1,14 and j=1,17) ...	TOEC with contributions from piezoelectric effects,
toe(i) (i=1,14)	TOEC without contributions from piezoelectric effects.

```
c    The program for the calculation of Bij, dCij/dP and TOEC of
c    a-quartz from weighted {d(W/Wo-1)/dP]o
c    c(1)=C11, c(2)=C12, c(3)=C33, c(4)=C44, c(5)=C14,
c    c(6)=C66, c(7)=C13, d-standard error
c    ep(1,17)-e1,ep(2,17)-e2
     common /wei/ wm(8)
     common /uwim/ uwm(9)
     integer wgc
c    set weights for all modes
     data wm/0.7,0.9,0.4,0.7,0.8,1.,0.4,0.7/
     data uwm/0.69,0.7,0.8,0.34,0.31,0.55,0.38,0.52,0.22/

     print*,'  Calculation of Bij, dCij/dP and TOEC'
     print*,'  by using weighed average {d[(W/Wo)-1]/dP}o'
     print*,'          for  quartz crystal          '
     print*,' '
     print*,'              Q. Wang'
     print*,'            School of physics'
     print*,'            University of Bath'
     print*,'               June 1992'
     print*,' '

     print*,'1. Calculate TOEC with weights'
     print*,'2. Calculate TOEC with equal weights (=1)'
     read(5,*) wgc
     if (wgc.eq.2) then
      do i=1,9
       uwm(i)=1.
      end do
     end if
     call load
     do 50 k=1,17
      call set(k)
      call selm(k)
      call dcp(k)
      call pebij(k)
      call uni(k)
      call toecp(k)
      if (k.eq.6) then
        call conp
        call toec(k,wgc)
      end if
      call trans(k)
50    continue
     call save(wgc)
     stop
     end

     subroutine load
c    load data
     common /ang/ al(2,17),be(2,17),ga(2,17)
     common /cij/ c(7,17),csd(7,17)
     common /cpie/ ee(2,17),esd(2,17)
     common /temp/ t(17)
     common /dev/ w(8,17)
```

```
      common /udwp/ ud(9,17)
      character*10  fl(20),fn(10),fm(10)
      open (7,file='wcij.d')
      do 51 j=1,17
       read(7,*) t(j),c(1,j),c(2,j),c(3,j)
       read(7,*) c(4,j),c(5,j),c(6,j),c(7,j)
51    continue
      close (7)
c     (de*Wo2)' of each mode
      do 54 i=1,8
       fl(i)='cwd .d'
       fn(i)='du .d'
       write(fl(i)(4:4),'(i1)') i
       write(fn(i)(3:3),'(i1)') i
       open (7,file=fl(i))
       open (8,file=fn(i))
       do 53 j=1,17
        read(7,*) t(j),w(i,j)
        read(8,*) t(j),ud(i,j)
53     continue
       close (7)
       close (8)
54    continue
      fn(1)='du9.d'
      open (8,file=fn(1))
      do 55 j=1,17
       read(8,*) t(j),ud(9,j)
55    continue
      close (8)
      do 57 i=1,2
c      gamma
       fl(i)='al .d'
c      beta
       fn(i)='bl .d'
c      theta
       fm(i)='cl .d'
       write(fl(i)(3:3),'(i1)') i
       write(fn(i)(3:3),'(i1)') i
       write(fm(i)(3:3),'(i1)') i
       open (7,file=fl(i))
       open (8,file=fn(i))
       open (9,file=fm(i))
       do 56 j=1,17
        read(7,*) t(j),be(i,j)
        read(8,*) t(j),al(i,j)
        read(9,*) t(j),ga(i,j)
56     continue
       close (7)
       close (8)
       close (9)
57    continue
      open (7,file='ep.d')
      do 59 j=1,17
       read(7,*) t(j)
```

```
      do 58 i=1,2
       read(7,*) ee(i,j),esd(i,j)
58     continue
59    continue
      close (7)
      return
      end

      subroutine set(k)
c     Calculate the coefficients and parameters used the program
c     ex1--(2*thermal expansion coef. along X-axis)*1E5
c     ex2--(thermal expansion coef. along Z-axis)*1E5
c     cp--specific heat Cp;de--density
c     ts--isothermal s;ts(8)-s1;ts(9)--s3
c     al--beta,be--gamma,ga--theta
      common /comp/ ts(9)
      common /ec/ vn(10)
      common /ang/ al(2,17),be(2,17),ga(2,17)
      common /cij/ c(7,17),csd(7,17)
      common /cpie/ ee(2,17),esd(2,17)
      common /temp/ t(17)
      common /cofac/ ap,bp
      common /rbulk/ bs(17)
      real s(7)
      real de,dt
      double precision cf,cp,th1,th2,ex1,ex2
      dt=t(k)-298.
c     Integrals of thermal expansion coefficients
      th1=2.*(1.377*dt+1.303D-3*dt**2-6.329D-7*dt**3)*1.D-5
      th2=(0.7483*dt+9.405D-4*dt**2-5.44D-7*dt**3)*1.D-5
c     Thermal expansion correction of dencity
      de=2648.38/(1.+th1+th2)
c     Specific heat
      cp=(47.0118+3.4358D-2*t(k)-1.131D6/t(k)**2)/60.0118*1.D3
c     Adiabatic sij transformed from Cij
      ap=c(3,k)*(c(1,k)+c(2,k))-2.*c(7,k)**2
      bp=c(4,k)*(c(1,k)-c(2,k))-2.*c(5,k)**2
      s(1)=0.5*(c(3,k)/ap+c(4,k)/bp)
      s(2)=0.5*(c(3,k)/ap-c(4,k)/bp)
      s(3)=(c(1,k)+c(2,k))/ap
      s(4)=(c(1,k)-c(2,k))/bp
      s(5)=-c(5,k)/bp
      s(6)=2.*(s(1)-s(2))
      s(7)=-c(7,k)/ap
c     Thermal expansion coefficients
      ex1=(1.377+2.*1.303D-3*dt-3.*6.329D-7*dt**2)
      ex2=(0.7483+2.*9.405D-4*dt-3.*5.44D-7*dt**2)
c     Isothermal sij
      cf=t(k)/de/cp
      ts(1)=s(1)+cf*ex1**2
      ts(2)=s(2)+cf*ex1**2
      ts(3)=s(3)+cf*ex2**2
      ts(4)=s(4)
      ts(5)=s(5)
```

```
      ts(6)=s(6)
      ts(7)=s(7)+cf*ex1*ex2
c     ts(8)=s1, ts(9)=s3
      ts(8)=ts(1)+ts(2)+ts(7)
      ts(9)=2.*ts(7)+ts(3)
c     (density*W**2)o of each mode
      vn(1)=c(1,k)+ee(1,k)
      vn(2)=0.5*(c(6,k)+c(4,k)-sqrt((c(6,k)-c(4,k))**2+4.*c(5,k)**2))
      vn(3)=0.5*(c(1,k)+c(4,k)-sqrt((c(1,k)-c(4,k))**2+4.*c(5,k)**2))
      vn(4)=c(6,k)+ee(1,k)
      vn(5)=c(3,k)
      vn(6)=c(4,k)
      vn(7)=0.5*(0.5*(c(1,k)+c(3,k))+c(4,k)-c(5,k)
     &+sqrt(0.25*(c(1,k)-c(3,k)-2.*c(5,k))**2+(c(7,k)
     &+c(4,k)-c(5,k))**2))
      vn(8)=0.5*(c(6,k)+c(4,k))-c(5,k)+ee(2,k)
      vn(9)=0.5*(c(1,k)+c(4,k)+sqrt((c(1,k)-c(4,k))**2+4.*c(5,k)**2))
      bs(k)=((c(1,k)+c(2,k))*c(3,k)-2.*c(7,k)**2)/(c(1,k)+c(2,k)
     $+2.*c(3,k)-4.*c(7,k))
46    return
      end

      subroutine matmul (a,np,lp,v,mp,pr)
c     Matrix multiplication
c     n--limit on matrix dimensions,np--row dimension of matrix a
c     mp--dimension of the column of matrix a and the row of
c     matrix v; pr--product matrix
      dimension a(np,lp),v(lp,mp),pr(np,mp)
      real pr
      integer np,mp
c     matrix multiplication
c     i is ranged from 1 to the number of rows of matric a
      do 34 i=1,np
c     j is ranged from 1 to the number of columns of matrix v
      do 34 j=1,mp
       sum=0
c     k is renged from 1 to number of columns of matrix a
       do 35 k=1,lp
c     Add a(i,k)*v(k,j) to sum
        sum=sum+a(i,k)*v(k,j)
35     continue
c     Set pr(i,j) equal to sum
       pr(i,j)=sum
34    continue
      return
      end

      subroutine selm(k)
c     Set the values of the elements for matrices used to solve Bij
c     al--beta,be--gamma,ga--theta
      common /red/ eb(8,8)
      common /comp/ ts(9)
      common /mb/ ec(8,8),ewm(17)
      common /wei/ wm(8)
```

```
      common /ec/ vn(10)
      common /coa/ ea(8,8),em(8)
      common /ang/ al(2,17),be(2,17),ga(2,17)
      common /dev/ w(8,17)
      common /norma/ ano(8,8)
      real s(8)
c     Set all elements equal to zero
      do 37 i=1,8
       do 36 j=1,8
        ea(i,j)=0.
        eb(i,j)=0.
        ec(i,j)=0.
36     continue
       em(i)=0.
       ewm(i)=0.
37     continue
c     Set values for matrix ea
      ea(1,1)=1.
      ea(1,7)=1.
      ea(2,4)=al(2,k)**2
      ea(2,5)=2.*al(1,k)*al(2,k)
      ea(2,6)=al(1,k)**2
      ea(3,1)=be(1,k)**2
      ea(3,4)=be(2,k)**2
      ea(3,5)=-2.*be(1,k)*be(2,k)
      ea(4,6)=1.
      ea(4,7)=1.
      ea(5,3)=1.
      ea(6,4)=1.
      ea(7,1)=ga(1,k)**2/2.
      ea(7,2)=ga(1,k)*ga(2,k)
      ea(7,3)=ga(2,k)**2/2.
      ea(7,4)=(1.+2.*ga(1,k)*ga(2,k))/2.
      ea(7,5)=-(ga(1,k)**2+ga(1,k)*ga(2,k))
      ea(8,4)=0.5
      ea(8,5)=-1.
      ea(8,6)=0.5
      ea(8,8)=1.
c     Set elements of matrix em
      s(1)=ts(8)
      s(2)=al(1,k)**2*ts(8)+al(2,k)**2*ts(9)
      s(3)=be(1,k)**2*ts(8)+be(2,k)**2*ts(9)
      s(4)=ts(8)
      s(5)=ts(9)
      s(6)=ts(8)
      s(7)=ga(1,k)**2*ts(8)+ga(2,k)**2*ts(9)
      s(8)=ts(8)
      do 38 i=1,8
       em(i)=1.+vn(i)*s(i)+w(i,k)
38     continue
c     em(i) in the old order, i.e. em(1)--mode 1,
c     em(2)--mode 2, em(3)--mode 5, em(4)--mode 6
c     em(5)--mode 7, em(6)--mode 9, em(7)--mode 10
c     em(8)--mode 13
```

```
c    Set matrix eb;eb(ij)=wm(j)*ea(ij)
     do 29 i=1,8
      do 29 j=1,8
       eb(i,j)=wm(j)*ea(j,i)
29    continue
c    Calculate elements of the weighted simultaneous equations
     call matmul (eb,8,8,ea,8,ec)
     call matmul (eb,8,8,em,1,ewm)
     do 39 i=1,8
      do 39 j=1,8
       ano(i,j)=ec(i,j)
39    continue
c    solve Bij
     call LUDCMP(ano,8,8,INDEX,D)
     call LUBKSB(ano,8,8,INDEX,ewm)
45    return
     end

     subroutine dcp(k)
c    Calculate the dCij/dP without piezoelectric contributions
c    cp(i,k)=dCij/dP:1--11,2--13,3-33,4--44,5--14,6--66,7--12
     common /dcijp/ cp(7,17)
     common /comp/ ts(9)
     common /mb/ ec(8,8),ewm(17)
     common /codc/ cs(9)
     common /cij/ c(7,17),csd(7,17)
     cs(1)=-1.+(ts(9)-2.*ts(8))*c(1,k)
     cs(2)=1.-ts(9)*c(7,k)
     cs(3)=-1.+(2.*ts(8)-3.*ts(9))*c(3,k)
     cs(4)=-1.-ts(9)*c(4,k)
     cs(5)=-ts(8)*c(5,k)
     cs(6)=-1.+(ts(9)-2.*ts(8))*c(6,k)
     do 41 i=1,6
      cp(i,k)=ewm(i)+cs(i)
41    continue
     cp(7,k)=cp(1,k)-2.*cp(6,k)
     return
     end

     subroutine pebij(k)
c    Calculate the Bij and dCij/dP with contributions from the
c    piezoelectric effects for hydrostatic modes
c    pb-Bij,pcp-dCij/dP
     common /pbij/ pb(7,17)
     common /pdcij/ pcp(7,17)
     common /red/ eb(8,8)
     common /mb/ ec(8,8),ewm(17)
     common /ec/ vn(10)
     common /coa/ ea(8,8),em(8)
     common /codc/ cs(9)
     common /pect/ pwm(6)
     real pc(6,6),peb(6,8)
     do 42 i=1,6
      do 42 j=1,8
```

```
      peb(i,j)=eb(i,j)
42    continue
      do 43 i=1,6
       do 43 j=1,6
        pc(i,j)=ec(i,j)
43    continue
      call matmul (peb,6,8,em,1,pwm)
      call LUDCMP(pc,6,6,INDEX,D)
      call LUBKSB(pc,6,6,INDEX,pwm)
c     Transfer calculated Bij
      do 44 i=1,6
       pb(i,k)=pwm(i)
       pcp(i,k)=pwm(i)+cs(i)
44    continue
      pcp(7,k)=pcp(1,k)-2.*pcp(6,k)
      return
      end

      subroutine uni(k)
c     Calculate the G(U) (-ewm(9+)) for eight modes (uniaxial)
c     ewm(9)-(-G1A),ewm(10)-(-G1B)...ewm(16)-(-G8B)
c     vn(9)-(de*W**2) of mode 4, (de*W**2) of mode 8=vn(6)
      common /ec/ vn(10)
      common /cij/ c(7,17),csd(7,17)
      common /mb/ ec(8,8),ewm(17)
      common /comp/ ts(9)
      common /ang/ al(2,17),be(2,17),ga(2,17)
      common /udwp/ ud(9,17)
      common /unic/ fu(9),uw(9),wn(9)
      fu(1)=ts(2)
      fu(2)=ts(7)
      fu(3)=be(2,k)**2*ts(7)+be(1,k)*ts(3)
      fu(4)=ts(1)
      fu(5)=ts(7)
      fu(6)=ts(7)
      fu(7)=ts(1)
      fu(8)=ts(2)
      fu(9)=0.5*(ts(7)+ga(1,k)**2*(ts(1)+ts(5))+ga(2,k)**2*ts(3)
     $+ga(1,k)*ga(2,k)*(ts(4)+ts(5)))
      wn(1)=vn(1)
      wn(2)=vn(1)
      wn(3)=vn(9)
      wn(4)=vn(4)
      wn(5)=vn(4)
      wn(6)=vn(5)
      wn(7)=vn(6)
      wn(8)=vn(6)
      wn(9)=vn(7)
      do 45 i=1,9
       uw(i)=2.*wn(i)*ud(i,k)*0.1
       ewm(8+i)=1.+2.*wn(i)*fu(i)+uw(i)
45    continue
      return
      end
```

```
      subroutine conp
c     Calculate the contribution of the piezolectric effects to
c     the d(de*W**2)/dP for modes in both hydrostatic and uniaxial
c     measurements
      common /ed/ e1(2),di(2)
      real ep(8),esc(8),sh3(5),sh4(5),sh6(5)
      common /comp/ ts(9)
      common /tpie/ ah(8)
      character*5 pc
      data e1 /0.172, 0.04/, di /39.16, 40.93/
      open(7,file='topc.d')
      do 44 i=1,8
       read(7,*) ep(i)
44    continue
      close (7)
      open(7,file='esc.d')
      do 45 i=1,8
       read(7,*) esc(i)
       esc(i)=esc(i)*8.8542
45    continue
      close (7)
c     e1(i)-e(ij):1-11,2-14;di(i)-pesilon:di(1)-11,d(i)-33
c     ep(i)-e(ijk):1-111,2-113,3-114,4-122,5-124,6-144,7-315,8-134
c     esc(i)-l(ij):1-11,2-12,3-13,4-14,5-31,6-33,7-41,8-44
c     ah(i)-H(H,U):1-1H,2-6H,3-13H,4-1A,5-1B,6-6A,7-6B
      ah(1)=((ts(8)*(ep(1)-ep(4))+2.*ts(9)*ep(2))*e1(1)/di(1)
     $-(ts(8)*(esc(1)+esc(2))+ts(9)*esc(3))*(e1(1)/di(1))**2)*1.0e2
      ah(2)=ah(1)
      sh3(1)=(ts(8)*(ep(1)-ep(4)-2.*ep(3)-2.*ep(5))+ts(9)*(ep(2)
     $-ep(8)))*(e1(1)-e1(2))/(di(1)+di(2))
      sh3(2)=0.5*(ts(8)*(esc(1)+esc(2)+2.*esc(5))+ts(9)*(esc(3)
     $+esc(6)))*((e1(1)-e1(2))/(di(1)+di(2)))**2
      ah(3)=(sh3(1)-sh3(2))*1.0e2
      sh4(1)=((2.*ts(2)-ts(1))*ep(1)-ts(2)*ep(4)-2.*ts(5)*ep(6))
     $*e1(1)/di(1)
      sh4(2)=(ts(2)*esc(1)+ts(1)*esc(2)+ts(7)*esc(3)
     $-ts(5)*esc(4))*(e1(1)/di(1))**2
      ah(4)=(sh4(1)-sh4(2))*1.0e2
      ah(5)=(ts(7)*(ep(1)-ep(4))*e1(1)/di(1)
     $-(ts(7)*(esc(1)+esc(2))+ts(3)*esc(3))*(e1(1)/di(1))**2)*1.0e2
      sh6(1)=(0.25*(ts(1)-3.*ts(2))*ep(1)+0.25*(3.*ts(1)-ts(2))*ep(4)
     $-ts(7)*ep(2)+0.5*ts(5)*(ep(3)-ep(5)))*e1(1)/di(1)
      sh6(2)=(ts(2)*esc(1)+ts(1)*esc(2)+ts(7)*esc(3)-ts(5)*esc(4))
     $*(e1(1)/di(1))**2
      ah(6)=(sh6(1)-sh6(2))*1.0e2
      ah(7)=(0.5*(-ts(7)*ep(1)+ts(7)*ep(4)-2.*ts(3)*ep(2))*e1(1)/di(1)
     $-(ts(7)*(esc(1)+esc(2))+ts(3)*esc(3))*(e1(1)/di(1))**2)*1.0e2
      pc='ah .d'
      open(7,file='pecon.d')
      do i=1,7
       write(pc(3:3),'(i1)') i
       write(7,*) pc,ah(i)
      end do
```

```
      close(7)
      return
      end

      subroutine toecp(k)
c     Calculate the TOEC with contributions from the piezoelectrcic
c     effects
      common /comp/ ts(9)
      common /ang/ al(2,17),be(2,17),ga(2,17)
      common /mb/ ec(8,8),ewm(17)
      common /petoec/ toep(14,17)
      common /uwim/ uwm(9)
      common /pect/ pwm(6)
      common /tcf/ ea(14)
      common /tco/ to(3,17)
      real ta(5,5),we(2),twm(15),c(2),ww(5)
      real coe(5),aa(2,2),ab(2,2),ac(2,2),wc(2)
      real A,B,E,tb(5,5),tc(5,5),cc(5),wi(3),da(3,3),db(3,3)
      real dc(3,3),dd(3),dm(3),dz(3)
      real c133,c333,c113,c344,c134,c123
      real c111,c112,c114,c124,c222
      aa(1,1)=-2.*ts(8)
      aa(1,2)=-ts(9)
      aa(2,1)=ts(1)+ts(2)
      aa(2,2)=ts(7)
      ab(1,1)=aa(1,1)
      ab(1,2)=uwm(6)*aa(2,1)
      ab(2,1)=aa(1,2)
      ab(2,2)=uwm(6)*aa(2,2)
      call matmul (ab,2,2,aa,2,ac)
      c(1)=pwm(3)
      c(2)=-ewm(14)
      call matmul (ab,2,2,c,1,wc)
      call LUDCMP(ac,2,2,INDEX,D)
      call LUBKSB(ac,2,2,INDEX,wc)
      twm(7)=wc(1)
      twm(10)=wc(2)
      c133=wc(1)
      c333=wc(2)
      we(1)=1.
      we(2)=uwm(2)
      aa(1,1)=-ts(8)
      aa(1,2)=-ts(9)
      aa(2,1)=ts(7)
      aa(2,2)=ts(3)
      do 65 i=1,2
       do 65 j=1,2
        ab(i,j)=we(j)*aa(j,i)
65    continue
      c(1)=pwm(1)
      c(2)=-ewm(10)
c     Calculate elements of the weighted simultaneous equations
      call matmul (ab,2,2,aa,2,ac)
      call matmul (ab,2,2,c,1,wc)
```

```
      call LUDCMP(ac,2,2,INDEX,D)
      call LUBKSB(ac,2,2,INDEX,wc)
      twm(3)=wc(2)
      c113=wc(2)
      A=wc(1)
      we(1)=1.
      we(2)=0.45
      aa(1,1)=-ts(1)
      aa(1,2)=-ts(3)
      aa(2,1)=ts(1)+ts(2)
      aa(2,2)=2.*ts(7)
      do i=1,2
       do j=1,2
        ab(i,j)=we(j)*aa(j,i)
       end do
      end do
      c(1)=pwm(4)
      c(2)=-ewm(15)-ewm(16)
c     Calculate elements of the weighted simultaneous equations
      call matmul (ab,2,2,aa,2,ac)
      call matmul (ab,2,2,c,1,wc)
      call LUDCMP(ac,2,2,INDEX,D)
      call LUBKSB(ac,2,2,INDEX,wc)
      twm(11)=wc(2)
      c344=wc(2)
      E=wc(1)
      we(1)=1.
      we(2)=uwm(3)
      aa(1,1)=-ts(8)
      aa(1,2)=-ts(9)
      aa(2,1)=2.*be(1,k)*be(2,k)*ts(7)
      aa(2,2)=2.*be(1,k)*be(2,k)*ts(3)
      do i=1,2
       do j=1,2
        ab(i,j)=we(j)*aa(j,i)
       end do
      end do
      c(1)=pwm(5)
      c(2)=-ewm(11)-be(2,k)**2*ewm(10)-be(1,k)**2*(ts(7)*E
     $+ts(3)*c344)
c     Calculate elements of the weighted simultaneous equations
      call matmul (ab,2,2,aa,2,ac)
      call matmul (ab,2,2,c,1,wc)
      call LUDCMP(ac,2,2,INDEX,D)
      call LUBKSB(ac,2,2,INDEX,wc)
      twm(8)=wc(2)
      c134=wc(2)
      B=wc(1)
      twm(5)=-(pwm(2)+ts(8)*c113+ts(9)*c133)/ts(8)
      c123=twm(5)
      ww(1)=uwm(1)
      ww(2)=uwm(4)
      ww(3)=1.
      ww(4)=1.
```

```
      ww(5)=1.
      do i=1,5
       do j=1,5
        ta(i,j)=0.
       end do
      end do
      ta(1,1)=ts(2)
      ta(1,2)=ts(1)
      ta(1,3)=-ts(5)
      ta(2,1)=-0.25*ts(6)
      ta(2,2)=0.5*(ts(1)+ts(2))
      ta(2,4)=ts(5)
      ta(2,5)=0.25*(3.*ts(1)-ts(2))
      ta(3,1)=0.5*ts(8)
      ta(3,2)=-0.5*ts(8)
      ta(4,1)=1.
      ta(4,2)=1.
      ta(5,3)=1.
      ta(5,4)=1.
      do i=1,5
       do j=1,5
        tb(i,j)=ww(j)*ta(j,i)
       end do
      end do
      coe(1)=-ewm(9)-ts(7)*c113
      coe(2)=-ewm(12)-0.5*ts(7)*(c113-c123)
      coe(3)=pwm(6)+0.5*ts(9)*(c113-c123)
      coe(4)=A
      coe(5)=B
c     Calculate elements of the weighted simultaneous equations
      call matmul (tb,5,5,ta,5,tc)
      call matmul (tb,5,5,coe,1,cc)
      call LUDCMP(tc,5,5,INDEX,D)
      call LUBKSB(tc,5,5,INDEX,cc)
      c111=cc(1)
      c112=cc(2)
      c114=cc(3)
      c124=cc(4)
      c222=cc(5)
      twm(1)=cc(1)
      twm(2)=cc(2)
      twm(4)=cc(3)
      twm(6)=cc(4)
      twm(9)=cc(5)
      ea(1)=0.25*ga(1,k)**2*(ts(2)+ts(7)-ts(5))
      ea(2)=ea(1)
      ea(3)=0.25*ga(1,k)**2*(ts(7)+ts(3))-0.5*ga(1,k)*ga(2,k)*(ts(1)
     $+ts(7)+ts(5))
      ea(4)=-0.5*ga(1,k)*ga(2,k)*(ts(1)+ts(7)+ts(5))-0.5*ga(1,k)**2
     $*(2.*ts(1)+2.*ts(7)+ts(5)-ts(4))
      ea(5)=0.5*ga(1,k)*ga(2,k)*(ts(2)+ts(7)-ts(5))
      ea(6)=(ga(1,k)**2+ga(1,k)*ga(2,k))*(-ts(1)+0.5*ts(2)-0.5*ts(7))
     $+0.5*ga(1,k)**2*(ts(4)-2.*ts(5))-3.*ga(1,k)*ga(2,k)*ts(5)/2.
      ea(7)=0.25*ga(2,k)**2*(ts(1)+ts(2)+2.*ts(7))+0.5*ga(1,k)
```

```
     $*ga(2,k)*(ts(7)+ts(3))
      ea(8)=-0.25*(ga(2,k)**2+ga(1,k)*ga(2,k))*ts(6)
     $-(0.5*ga(1,k)*ga(2,k)+ga(2,k)**2)*ts(5)+0.5*ga(1,k)*ga(2,k)
     $*ts(4)-0.5*(ga(1,k)**2+ga(1,k)*ga(2,k))*(ts(7)+ts(3))
      ea(9)=0.25*(1.+2.*ga(1,k)*ga(2,k))*(ts(2)+ts(7)-ts(5))
      ea(10)=0.25*(1.+2.*ga(1,k)*ga(2,k))*(ts(1)+ts(7))
     $+0.25*(ga(2,k)**2-ga(1,k)**2)*ts(5)-0.5*(ga(1,k)*ga(2,k)
     $+ga(1,k)**2)*ts(4)
      ea(11)=ga(1,k)**2*(ts(6)/8.+ts(6)/2.)
      ea(12)=0.25*ga(2,k)**2*(ts(7)+ts(3))
      ea(13)=0.25*(1.+2.*ga(1,k)*ga(2,k))*(ts(7)+ts(3))
     $-0.5*(ga(2,k)**2+ga(1,k)*ga(2,k))*(ts(5)+ts(4))
      ea(14)=-0.25*(1.+2.*ga(1,k)*ga(2,k))*(ts(5)+ts(4))
      wi(1)=uwm(9)
      wi(2)=uwm(7)
      wi(3)=1.
      da(1,1)=ea(9)
      da(1,2)=ea(10)
      da(1,3)=ea(14)
      da(2,1)=ts(2)
      da(2,2)=ts(1)
      da(2,3)=-ts(5)
      da(3,1)=1.
      da(3,2)=1.
      da(3,2)=-0.5*ts(8)
      do i=1,3
       do j=1,3
        db(i,j)=wi(j)*da(j,i)
       end do
      end do
      dz(1)=-ea(1)*c111-ea(2)*c112-ea(3)*c113-ea(4)*c114
      dz(2)=-ea(5)*c123-ea(6)*c124-ea(7)*c133-ea(8)*c134
      dz(3)=-ea(11)*c222-ea(12)*c333-ea(13)*c344
      dd(1)=-ewm(17)+dz(1)+dz(2)+dz(3)
      dd(2)=-ewm(15)-ts(7)*c344
      dd(3)=E
c     Calculate elements of the weighted simultaneous equations
      call matmul (db,3,3,da,3,dc)
      call matmul (db,3,3,dd,1,dm)
      call LUDCMP(dc,3,3,INDEX,D)
      call LUBKSB(dc,3,3,INDEX,dm)
      twm(12)=dm(1)
      twm(13)=dm(2)
      twm(14)=dm(3)
      twm(1)=c111
      twm(2)=c112
      twm(3)=c113
      do 70 i=1,14
       toep(i,k)=twm(i)
70    continue
      to(1,k)=A
      to(2,k)=B
```

```
      to(3,k)=E
      return
      end

      subroutine toec(k,wgc)
c     Calculate the TOEC without contributions from the piezoelectrcic
c     effects at room temperature (293K)
      common /comp/ ts(9)
      common /ang/ al(2,17),be(2,17),ga(2,17)
      common /mb/ ec(8,8),ewm(17)
      common /tpie/ ah(8)
      common /uwim/ uwm(9)
      common /pect/ pwm(6)
      common /tcf/ ea(14)
      real dc(3,3),dd(3),dm(3),dz(3),da(3,3),db(3,3)
      real ta(5,5),we(2),twm(12),c(2),ww(5),wi(3)
      real coe(5),aa(2,2),ab(2,2),ac(2,2),wc(2)
      real A,B,E,tb(5,5),tc(5,5),cc(5)
      real toe(14)
      real c133,c333,c113,c344,c123,c134
      real c111,c112,c114,c124,c222
      character*5 cijk(14)
      integer wgc
      data cijk/'C111','C112','C113','C114','C123','C124','C133',
     $'C134','C222','C333','C344','C144','C155','C444'/
      aa(1,1)=-2.*ts(8)
      aa(1,2)=-ts(9)
      aa(2,1)=ts(1)+ts(2)
      aa(2,2)=ts(7)
      ab(1,1)=aa(1,1)
      ab(1,2)=0.55*aa(2,1)
      ab(2,1)=aa(1,2)
      ab(2,2)=0.55*aa(2,2)
      call matmul (ab,2,2,aa,2,ac)
      c(1)=ewm(3)
      c(2)=-ewm(14)
      call matmul (ab,2,2,c,1,wc)
      call LUDCMP(ac,2,2,INDEX,D)
      call LUBKSB(ac,2,2,INDEX,wc)
      twm(7)=wc(1)
      twm(10)=wc(2)
      c133=wc(1)
      c333=wc(2)
      we(1)=1.
      we(2)=uwm(2)
      aa(1,1)=-ts(8)
      aa(1,2)=-ts(9)
      aa(2,1)=ts(7)
      aa(2,2)=ts(3)
      do 65 i=1,2
       do 65 j=1,2
        ab(i,j)=we(j)*aa(j,i)
65    continue
      c(1)=ewm(1)
```

```
      c(2)=-ewm(10)+0.002
c     Calculate elements of the weighted simultaneous equations
      call matmul (ab,2,2,aa,2,ac)
      call matmul (ab,2,2,c,1,wc)
      call LUDCMP(ac,2,2,INDEX,D)
      call LUBKSB(ac,2,2,INDEX,wc)
      twm(3)=wc(2)
      c113=wc(2)
      A=wc(1)
      we(1)=1.
      we(2)=0.45
      aa(1,1)=-ts(1)
      aa(1,2)=-ts(3)
      aa(2,1)=ts(1)+ts(2)
      aa(2,2)=2.*ts(7)
      do i=1,2
       do j=1,2
        ab(i,j)=we(j)*aa(j,i)
       end do
      end do
      c(1)=ewm(4)
      c(2)=-ewm(15)-ewm(16)
c     Calculate elements of the weighted simultaneous equations
      call matmul (ab,2,2,aa,2,ac)
      call matmul (ab,2,2,c,1,wc)
      call LUDCMP(ac,2,2,INDEX,D)
      call LUBKSB(ac,2,2,INDEX,wc)
      twm(11)=wc(2)
      c344=wc(2)
      E=wc(1)
      we(1)=1.
      we(2)=uwm(3)
      aa(1,1)=-ts(8)
      aa(1,2)=-ts(9)
      aa(2,1)=2.*be(1,k)*be(2,k)*ts(7)
      aa(2,2)=2.*be(1,k)*be(2,k)*ts(3)
      do i=1,2
       do j=1,2
        ab(i,j)=we(j)*aa(j,i)
       end do
      end do
      c(1)=ewm(5)
      c(2)=-ewm(11)-be(2,k)**2*ewm(10)-be(1,k)**2*(ts(7)*E
     $+ts(3)*c344)
c     Calculate elements of the weighted simultaneous equations
      call matmul (ab,2,2,aa,2,ac)
      call matmul (ab,2,2,c,1,wc)
      call LUDCMP(ac,2,2,INDEX,D)
      call LUBKSB(ac,2,2,INDEX,wc)
      twm(8)=wc(2)
      c134=wc(2)
      B=wc(1)
      twm(5)=-(pwm(2)+ts(8)*c113+ts(9)*c133)/ts(8)
      c123=twm(5)
```

```
      ww(1)=uwm(1)
      ww(2)=uwm(4)
      ww(3)=1.
      ww(4)=1.
      ww(5)=1.
      do i=1,5
       do j=1,5
        ta(i,j)=0.
       end do
      end do
      ta(1,1)=ts(2)
      ta(1,2)=ts(1)
      ta(1,3)=-ts(5)
      ta(2,1)=-0.25*ts(6)
      ta(2,2)=0.25*(ts(1)+ts(2))
      ta(2,4)=ts(5)
      ta(2,5)=0.25*(3.*ts(1)-ts(2))
      ta(3,2)=0.5*ts(8)
      ta(3,5)=-0.5*ts(8)
      ta(4,1)=1.
      ta(4,2)=1.
      ta(5,3)=1.
      ta(5,4)=1.
      do i=1,5
       do j=1,5
        tb(i,j)=ww(j)*ta(j,i)
       end do
      end do
      coe(1)=-ewm(9)-ts(7)*c113+0.14
      coe(2)=-ewm(12)-0.5*ts(7)*(c113-c123)+0.005
      coe(3)=pwm(6)+0.5*ts(9)*(c113-c123)
      coe(4)=A
      coe(5)=B
c     Calculate elements of the weighted simultaneous equations
      call matmul (tb,5,5,ta,5,tc)
      call matmul (tb,5,5,coe,1,cc)
      call LUDCMP(tc,5,5,INDEX,D)
      call LUBKSB(tc,5,5,INDEX,cc)
      c111=cc(1)
      c112=cc(2)
      c114=cc(3)
      c124=cc(4)
      c222=cc(5)
      twm(1)=cc(1)
      twm(2)=cc(2)
      twm(4)=cc(3)
      twm(6)=cc(4)
      twm(9)=cc(5)
      ea(1)=0.25*ga(1,k)**2*(ts(2)+ts(7)-ts(5))
      ea(2)=ea(1)
      ea(3)=0.25*ga(1,k)**2*(ts(7)+ts(3))-0.5*ga(1,k)*ga(2,k)*(ts(1)
     $+ts(7)+ts(5))
      ea(4)=-0.5*ga(1,k)*ga(2,k)*(ts(1)+ts(7)+ts(5))-0.5*ga(1,k)**2
     $*(2.*ts(1)+2.*ts(7)+ts(5)-ts(4))
```

```
      toe(i)=twm(i)
74    continue
      if (wgc.eq.2) then
       open (7,file='nwrtoec.d')
      else
       open (7,file='rtoec.d')
      end if
      do 75 i=1,14
       write (7,*) cijk(i),toe(i)
75    continue
      close (7)
      return
      end

      subroutine trans(k)
c     ewm(i)=Bij:ewm(1)=B11,ewm(2)=B13,ewm(3)=B33,ewm(4)=B44,
c     ewm(5)=B14,ewm(6)=B66
c     ewm(7)=d(e1)/dP,ewm(8)=d(e2/dP)
      common /mb/ ec(8,8),ewm(17)
      common /bij/ cb(6,17),erb(6,17)
      common /dpe/ de(2,17),sdep(2,17)
      common /emat/ dem(8),dewm(17)
      common /unig/ ug(9,17),dug(9,17)
      common /comp/ ts(9)
      common /thers/ ths(9,17)
c     Transfer calculated Bij
      do 102 i=1,6
       cb(i,k)=ewm(i)
102   continue
c     Transfer calculated d(e(i))/dP
      do 103 i=1,2
       de(i,k)=ewm(6+i)
103   continue
c     transfer G(U) for uniaxial modes
      do 104 i=1,9
       ug(i,k)=ewm(8+i)
104   continue
      do 105 i=1,9
       ths(i,k)=ts(i)
105   continue
      return
      end

      subroutine save(wgc)
      common /swam/ scc(8,17)
      common /temp/ t(17)
      common /bij/ cb(6,17),erb(6,17)
      common /dpe/ de(2,17),sdep(2,17)
      common /dcijp/ cp(7,17)
      common /pbij/ pb(7,17)
      common /pdcij/ pcp(7,17)
      common /petoec/ toep(14,17)
      common /unig/ ug(9,17),dug(9,17)
      common /sdcij/ dcp(7,17)
```

```
      ea(5)=0.5*ga(1,k)*ga(2,k)*(ts(2)+ts(7)-ts(5))
      ea(6)=(ga(1,k)**2+ga(1,k)*ga(2,k))*(-ts(1)+0.5*ts(2)-0.5*ts(7))
     $+0.5*ga(1,k)**2*(ts(4)-2.*ts(5))-3.*ga(1,k)*ga(2,k)*ts(5)/2.
      ea(7)=0.25*ga(2,k)**2*(ts(1)+ts(2)+2.*ts(7))+0.5*ga(1,k)
     $*ga(2,k)*(ts(7)+ts(3))
      ea(8)=-0.25*(ga(2,k)**2+ga(1,k)*ga(2,k))*ts(6)
     $-(0.5*ga(1,k)*ga(2,k)+ga(2,k)**2)*ts(5)+0.5*ga(1,k)*ga(2,k)
     $*ts(4)-0.5*(ga(1,k)**2+ga(1,k)*ga(2,k))*(ts(7)+ts(3))
      ea(9)=0.25*(1.+2.*ga(1,k)*ga(2,k))*(ts(2)+ts(7)-ts(5))
      ea(10)=0.25*(1.+2.*ga(1,k)*ga(2,k))*(ts(1)+ts(7))
     $+0.25*(ga(2,k)**2-ga(1,k)**2)*ts(5)-0.5*(ga(1,k)*ga(2,k)
     $+ga(1,k)**2)*ts(4)
      ea(11)=ga(1,k)**2*(ts(6)/8.+ts(6)/2.)
      ea(12)=0.25*ga(2,k)**2*(ts(7)+ts(3))
      ea(13)=0.25*(1.+2.*ga(1,k)*ga(2,k))*(ts(7)+ts(3))
     $-0.5*(ga(2,k)**2+ga(1,k)*ga(2,k))*(ts(5)+ts(4))
      ea(14)=-0.25*(1.+2.*ga(1,k)*ga(2,k))*(ts(5)+ts(4))
      wi(1)=uwm(9)
      wi(2)=uwm(7)
      wi(3)=1.
      da(1,1)=ea(9)
      da(1,2)=ea(10)
      da(1,3)=ea(14)
      da(2,1)=ts(2)
      da(2,2)=ts(1)
      da(2,3)=-ts(5)
      da(3,1)=1.
      da(3,2)=1.
      da(3,2)=-0.5*ts(8)
      do i=1,3
       do j=1,3
        db(i,j)=wi(j)*da(j,i)
       end do
      end do
      dz(1)=-ea(1)*c111-ea(2)*c112-ea(3)*c113-ea(4)*c114
      dz(2)=-ea(5)*c123-ea(6)*c124-ea(7)*c133-ea(8)*c134
      dz(3)=-ea(11)*c222-ea(12)*c333-ea(13)*c344
      dd(1)=-ewm(17)+dz(1)+dz(2)+dz(3)
      dd(2)=-ewm(15)-ts(7)*c344
      dd(3)=E
c     Calculate elements of the weighted simultaneous equations
      call matmul (db,3,3,da,3,dc)
      call matmul (db,3,3,dd,1,dm)
      call LUDCMP(dc,3,3,INDEX,D)
      call LUBKSB(dc,3,3,INDEX,dm)
      twm(12)=dm(1)
      twm(13)=dm(2)
      twm(14)=dm(3)
      twm(1)=c111
      twm(2)=c112
      twm(3)=c113
      twm(4)=c114
      twm(6)=c124
  102 do 74 i=1,14
```

```
      common /bulk/ dbup(17)
      common /pbulk/ pdbup(17)
      common /rbulk/ bs(17)
      common /thers/ ths(9,17)
      common /tco/ to(3,17)
      character*10  fl,fn,fm
      integer wgc
      do 107 i=1,6
       fl='whb .d'
       write(fl(4:4),'(i1)') i
c     Save Bij without contribution from the piezoelectric effects
       open (7,file=fl)
       do 108 k=1,17
        write(7,*)t(k),cb(i,k)
108    continue
      close (7)
107   continue
c     save de(i)/dP
      do 110 i=1,2
       fn='wdpe .d'
       write(fn(5:5),'(i1)') i
       open (7,file=fn)
       do 109 k=1,17
        write (7,*)t(k),de(i,k)
109    continue
      close (7)
110   continue
c     save dCij/dP without contribution from the piezoelectric effects
      do 112 i=1,7
       fl='dc .d'
       write(fl(3:3),'(i1)') i
       open (7,file=fl)
       do 111 j=1,17
        write(7,*) t(j),cp(i,j)
111    continue
      close (7)
112   continue
c     save Bij and dCij/dP with contribution from the piezoelectric
c     effects
      do 114 i=1,7
       fl='pd .d'
       write(fl(3:3),'(i1)') i
       open(7,file=fl)
       do 113 j=1,17
        write(7,*) t(j),pcp(i,j)
113    continue
      close (7)
114   continue
      do 116 i=1,6
       fn='pebij .d'
       write(fn(6:6),'(i1)') i
       open(7,file=fn)
       do 115 j=1,17
        write(7,*) t(j),pb(i,j)
```

```
115   continue
      close (7)
116   continue
c     save G(U) for uniaxial modes
      do 118 i=1,9
       fl='gu .d'
       write(fl(3:3),'(i1)') i
       open(7,file=fl)
       do 117 j=1,17
        write(7,*)t(j),ug(i,j)
117    continue
      close (7)
118   continue
c     save TOEC with contributions from piezoelectric effects
      do 120 i=1,14
       fl='ptoec  .d'
       if (wgc.eq.2) then
         fl='nwtoec  .d'
       end if
       write(fl(6:7),'(i2.2)') i
       open (7,file=fl)
       do 119 j=1,17
        write(7,*) t(j),toep(i,j)
119    continue
      close (7)
120   continue
      fl='dbulk.d'
      fm='pdbulk.d'
      open (7,file=fl)
      open (8,file=fm)
      do 121 j=1,17
       write(7,*) t(j),dbup(j)
       write(8,*) t(j),pdbup(j)
121   continue
      close (7)
      close (8)
      fl='bulk.d'
      open (7,file=fl)
      do 122 j=1,17
       write(7,*) t(j),bs(j)
122   continue
      close (7)
c     save isothermal stiffnesses
      do 124 i=1,9
       fl='ts .d'
       write(fl(3:3),'(i1)') i
       open (7,file=fl)
       do 123 j=1,17
        write(7,*) t(j), ths(i,j)
123    continue
      close (7)
124   continue
      do i=1,3
       fl='tcoe .d'
```

```
      write(fl(5:5),'(i1)') i
      open(7,file=fl)
      do j=1,17
       write(7,*) t(j),to(i,j)
      end do
      close(7)
     end do
     return
     end

     SUBROUTINE LUBKSB(A,N,NP,INDX,B)
     DIMENSION A(NP,NP),INDX(N),B(N)
     II=0
     DO 22 I=1,N
      LL=INDX(I)
      SUM=B(LL)
      B(LL)=B(I)
      IF (II.NE.0)THEN
       DO 21 J=II,I-1
        SUM=SUM-A(I,J)*B(J)
21      CONTINUE
      ELSE IF (SUM.NE.0.) THEN
       II=I
      ENDIF
      B(I)=SUM
22    CONTINUE
     DO 24 I=N,1,-1
      SUM=B(I)
      IF(I.LT.N)THEN
       DO 23 J=I+1,N
        SUM=SUM-A(I,J)*B(J)
23      CONTINUE
      ENDIF
      B(I)=SUM/A(I,I)
24    CONTINUE
     RETURN
     END

     SUBROUTINE LUDCMP(A,N,NP,INDX,D)
     PARAMETER (NMAX=100,TINY=1.0E-20)
     DIMENSION A(NP,NP),INDX(N),VV(NMAX)
     D=1.
     DO 12 I=1,N
      AAMAX=0.
      DO 11 J=1,N
       IF (ABS(A(I,J)).GT.AAMAX) AAMAX=ABS(A(I,J))
11     CONTINUE
      IF (AAMAX.EQ.0.) PAUSE 'Singular matrix.'
      VV(I)=1./AAMAX
12    CONTINUE
     DO 19 J=1,N
      IF (J.GT.1) THEN
       DO 14 I=1,J-1
        SUM=A(I,J)
```

```
        IF (I.GT.1)THEN
          DO 13 K=1,I-1
            SUM=SUM-A(I,K)*A(K,J)
13          CONTINUE
          A(I,J)=SUM
        ENDIF
14      CONTINUE
      ENDIF
      AAMAX=0.
      DO 16 I=J,N
        SUM=A(I,J)
        IF (J.GT.1)THEN
          DO 15 K=1,J-1
            SUM=SUM-A(I,K)*A(K,J)
15          CONTINUE
          A(I,J)=SUM
        ENDIF
        DUM=VV(I)*ABS(SUM)
        IF (DUM.GE.AAMAX) THEN
          IMAX=I
          AAMAX=DUM
        ENDIF
16      CONTINUE
      IF (J.NE.IMAX)THEN
        DO 17 K=1,N
          DUM=A(IMAX,K)
          A(IMAX,K)=A(J,K)
          A(J,K)=DUM
17        CONTINUE
        D=-D
        VV(IMAX)=VV(J)
      ENDIF
      INDX(J)=IMAX
      IF(J.NE.N)THEN
        IF(A(J,J).EQ.0.)A(J,J)=TINY
        DUM=1./A(J,J)
        DO 18 I=J+1,N
          A(I,J)=A(I,J)*DUM
18        CONTINUE
      ENDIF
19    CONTINUE
    IF(A(N,N).EQ.0.)A(N,N)=TINY
    RETURN
    END
```

Appendix B

Computer Programme: MQCOMP.FOR

This programme is employed to compute the volume compression and pressure-induced changes in lattice parameters, which are extrapolated up 20GPa, for α-quartz crystals at selected temperatures. The volume compression is calculated using Murnaghan's equation of state (Murnaghan 1944), Eq. (6.13). The pressure-induced changes in the lattice parameters are computed using Thurston's method (Eq. (6.23)) (Thurston 1966). The input data are the SOEC and the hydrostatic pressure derivatives $(\partial C_{IJ}/\partial P)_{T,P=0}$ with and without the contributions from piezoelectric effects. The other parameters, such as the thermal expansion coefficient α, the bulk modulus B , the hydrostatic pressure derivatives of the bulk modulus, the thermal Grüneisen parameters γ, specific heat at constant pressure C_P, density and the temperature derivatives of α, B and γ are given or calculated in the programme. The programme, written in FORTRAN 77, has been operated in a Viglen IV (486) PC with the aid of the Microsoft FORTRAN Compiler V5.0. The primary variables used are:

c(i,j) (i=1,7 and j=1,17)	SOEC,
cp(i,j) (i=1,7 and j=1,17)	$(\partial C_{IJ}/\partial P)_{T,P=0}$ without contributions from piezoelectric effects,
pcp(i,j) (i=1,7 and j=1,17)	$(\partial C_{IJ}/\partial P)_{T,P=0}$ with contributions from piezoelectric effects,
al	α,

ga	γ,
bps	B,
p	pressure,
comp	volume compression,
ca(1,k)	pressure-induced changes in the lattice parameter a,
ca(2,k)	pressure-induced changes in the lattice parameter c .

```
c    The programme for the calculation of the ratioes
c    V(P)/Vo and l(P)/lo for quartz as a function of T
c    The temperature range is 243K to 393K
     character*10 fn1,sp
     common /pre/ p(150)
     common /comp/ ts(9)
     common /coe/ ai(2),bi(2)
     common /lap/ ca(2,101)
     common /bsp/ bps(17)
     common comp(3,150)
     common gcom(3,150)
     common /tem/ it(17)
     dimension cb(3,101),cc(3,101)
     integer T,ht
     common /int/ m
     data bps/6.41,6.45,6.50,6.53,6.55,6.54,6.50,6.50,6.57,
    $6.61,6.66,6.71,6.82,6.86,6.93,7.01,6.95/
     data it/243,253,263,273,283,293,298,303,313,323,333,
    $343,353,363,373,383,393/
     L=0
     write(6,65)
     write(6,*)' CALCULATION OF VOLUME COMPRESSION AND'
     write(6,*)'  CHANGES OF LATTICE PARTAMETERS FOR'
     write(6,*)'  QUARTZ CRYSTAL TO HIGH PRESSURE'
     write(6,*)'        BY EXTRAPOLATION'
     write(6,65)
     write(6,*)'        Qingxian Wang'
     write(6,*)'        Solid State Physics'
     write(6,*)'        School of Physics'
     write(6,*)'        University of Bath'
     write(6,*)'          March 1992'
     write(6,65)
65   format(//' ')
     print*, '    The pressure range is 0-20 GPa'
     print*, '    The temperature range is 243-393 K.'
     print*,'Press key "a" and "Enter" to continue'
     read(5,81) sp
81   format(A1)
     if (sp.eq.'a') then
      goto 69
     end if
69   write(6,65)
     print*,'  1. Calculate volume compression V(P)/Vo--P'
     print*,'       (by Murnaghan equation)'
     print*,'  2. Calculate change of lattice parameters'
     print*,'       (by Thurston equation)'
     write(6,65)
     read(5,*) m
     if (m.eq.2) then
     call load
     end if
     write(6,65)
     write(6,*)' 1. Calculation at one temperature point'
     write(6,*)' 2. At three temperature points'
```

```
      read(5,*) H
      if (H.eq.2) then
       if (m.eq.2) then
        do 74 i=1,3
         print*,'Input the temperature (K)'
         read(5,*) T
         call set(T)
         call lat(pbt,T,ht)
         do 74 k=1,101
          cb(i,k)=ca(1,k)
          cc(i,k)=ca(2,k)
74       continue
        print*,' Input filename to save l(P)/lo--P'
        read(5,*)fn1
        open(13,file=fn1)
        do 75 k=1,101
         write(13,*)10.*p(k),cb(1,k),cb(2,k),cb(3,k),
     $cc(1,k),cc(2,k),cc(3,k)
75       continue
        close(13)
       elseif (m.eq.1) then
        call more
        goto 58
       end if
      elseif (H.eq.1) then
       goto 42
      end if
42    print*,'Input the temperature (K)'
      read(5,*) T
      call cal(T,1,pbt)
      if (m.eq.2) then
       call set(T)
       call lat(pbt,T,ht)
      end if
c     SAVE RESULTS
      if (m.eq.2) then
       goto 67
      end if
64    print*,'          Save V(P)/Vo-P'
      print*,'  1. Save V(P)/Vo-P without (d(gamma)/dT)p'
      print*,'  2. Save V(P)/Vo-P with (d(gamma)/dT)p'
      print*,'  3. Stop'
      read(5,*) L
      if (L.eq.3) then
       goto 58
      else
       goto 62
      end if
67    if (ht.eq.1)goto 58
      print*,'  Save l(P)/lo-P'
62    print*,'    Input filename'
      read(5,56) fn1
56    format(A10)
c     SAVE RESULTS
```

```
      open (13,FILE=fn1)
      if (m.eq.2) then
        goto 53
      end if
      if (L.eq.2) then
        goto 52
      else
        goto 53
      end if
53    do 57 i=1,101
      if (m.eq.2) then
        goto 68
      end if
      write(13,*) 10.*p(i),comp(1,i)
      goto 57
68    write(13,*) 10.*p(i),ca(1,i),ca(2,i)
57    CONTINUE
      goto 55
52    do 59 i=1,101
      write(13,*) 10.*p(i),gcom(1,i)
59    CONTINUE
55    close(13)
      L=0
      if (m.eq.2) then
        goto 58
      end if
      goto 64
58    m=0
      STOP
      END

      subroutine cal(T,K,pbt)
c     calculate the compression
      common /int/ m
      common /bsp/ bps(17)
      common /pre/ p(150)
      common comp(3,150)
      common gcom(3,150)
      common /tem/ it(17)
      integer T,kt
      real de,dt,bt,agt
      double precision al,cf,cp,th1,th2,ex1,ex2,ga,bs
      double precision dbs,dal,dbt,dgt,cdbt,det,dcp,cpbt
      do 67 i=1,17
      kt=T-it(i)
      if (kt.eq.0) then
        b=bps(i)
      end if
67    continue
c     calculations
c     ex1--thermal expansion coef. along X-axis
c     ex2--thermal expansion coef. along Z-axis
c     cp--specific heat Cp;de--density,dgt-(d(gamma)/dT)p
c     det--d(density)/dT,dcp-(dCp/dT)p
```

```
      dt=float(T)-298.
c     thermal expansion correction
      th1=2.*(1.377*dt+1.303D-3*dt**2-6.329D-7*dt**3)*1.D-5
      th2=(0.7483*dt+9.405D-4*dt**2-5.44D-7*dt**3)*1.D-5
c     Correction of density for thermal expansion
      de=2648.38/(1.+th1+th2)
c     specific heat and its temperature derivative
      cp=(47.0118+3.4358D-2*(dt+298.)-1.131D6/(dt+298.)**2)
     & /60.0118*1.D3
      dcp=(3.4358D-2+2.*1.131D6/(dt+298.)**3)/60.0118*1.D3
c     thermal expansion coefficient tensors
      ex1=(1.377+2.*1.303D-3*dt-3.*6.329D-7*dt**2)*1.D-5
      ex2=(0.7483+2.*9.405D-4*dt-3.*5.44D-7*dt**2)*1.D-5
c     volume thetrmal expansion coefficient and its temperature
c     derivatives
      al=2.*ex1+ex2
      dal=(2.*(2.*1.303D-3-2.*3.*6.329D-7*dt)+2.*9.405D-4
     $ -2.*3.*5.44D-7*dt)*1.D-5
c     temperature derivatives of density
      det=-de*dal/(1.+al)**2
c     a parameter
      cf=al/de/cp*1.D10
c     isentropic bulk modulus and its temperature derivative
      bs=4.5773-7.8184D-3*(dt+298.)+2.6156D-5*(dt+298.)**2
     $-3.2105D-8*(dt+298.)**3
      dbs=-7.8184D-3+2.*2.6256D-5*(dt+298.)-3.*3.2105D-8*(dt+298.)**2
c     Gruneisen parameter and its temperature derivative
      ga=cf*bs
      dgt=((bs*dal+al*dbs)*1.D10/de/cp-(det/de+dcp/cp)/ga)
c     a parameter
      agt=al*ga*(dt+298.)
c     isothermal bulk modulus and its temperature derivative with or
c     without d(gamma)/dT
      bt=bs/(1.+agt)
      dbt=dbs/(1.+agt)-bs*al*ga*(1.+dal*(dt+298.)/al)/(1.+agt)**2
      cdbt=dbs/(1.+agt)-bs*al*ga*(1.+dal*(dt+298.)/al
     $ +dgt*(dt+298.)/ga)/(1.+agt)**2
c     pressure derivative of isothermal bulk modulus without d(gamma)
c     correction
      pbt=b+agt*bt/bs*(1.-2.*dbt/al/bt-2.*b)+(agt*bt/bs)**2
     $ *(b-1.-dal/al**2)
      if (m.eq.2) then
        goto 78
      end if
c     pressure derivative of isothermal bulk modulus with
c     d(gamma) correction term
      cpbt=b+agt*bt/bs*(1.-2.*cdbt/al/bt-2.*b)+(agt*bt/bs)**2
     $ *(b-1.-dal/al**2)
      do 68 i=1,101
c     calculate pressure
      p(i)=0.01*(2.*float(i)-2)
c     calculate compression with d(gamma) correction
      comp(K,i)=exp(-(log(pbt*p(i)/bt+1.))/pbt)
c     calculate compression without d(gamma) correction
```

```
68     gcom(K,i)=exp(-(log(cpbt*p(i)/bt+1.))/cpbt)
c    print out the paramters
     print*,'  At',T,' K'
     write(6,71)dal*1E8
71   format(2X,'Temp. deriv. of vol. therm. expan. coef.=',F8.4,
    $ ' 1E-8 1/K')
     write(6,70)bt,dbs*1.E4
70   format(2X,'Bt=',F8.4,' 10Gpa',2X,'(dBs/dT)p=',F8.4,' 1E+6 Pa/K')
     write(6,69)dbt*1.E4,ga,pbt
69   format(2X,'(dBt/dT)p=',F8.4,' 1E+6Pa/K',2X,'th. gamma=',F8.4/
    $ 2X,'(dBt/dP)o=',F8.4)
     write(6,72)dgt*1.E3,cdbt*1.E4
72   format(2X,'(d(gamma)/dT)p=',F8.4,' 1E-3',2X,'cor. (dBt/dT)p=',F8.4,
    $ '  1E+6Pa/K')
     write(6,73)cpbt
73   format(2X,'cor. (dBt/dP)o=',F8.4/)
78   return
     end

     subroutine more
c    calculate the compression at three temperatures
     integer T
     common /pre/ p(150)
     common /bsp/ bps(17)
     common comp(3,150)
     common gcom(3,150)
     common /tem/ it(17)
     dimension ht(3)
     character*10 fn1
     do 54 i=1,3
     print*,'Input the temperature (K)'
     read(5,*) ht(i)
54   continue
     do 45,K=1,3
     T=ht(K)
     call cal(T,K,pbt)
45   continue
311  print*,'          Save V(P)/Vo-P'
     print*,'  1. Save V(P)/Vo-P without (d(gamma)/dT)p'
     print*,'  2. Save V(P)/Vo-P with (d(gamma)/dT)p'
     print*,'  3. Stop'
     read(5,*) L
     if (L.eq.3) then
       goto 307
     else
       goto 315
     end if
315  print*,'       Input filename'
     read(5,310) fn1
310  format(A10)
c    SAVE RESULTS
     open (13,FILE=fn1)
     if (L.eq.2) then
       goto 302
```

```
      else
        goto 303
      end if
303   do 301 i=1,101
      write(13,*) 10.*p(i),comp(1,i),comp(2,i),comp(3,i)
301   CONTINUE
      goto 305
302   do 304 i=1,101
      write(13,*) 10.*p(i),gcom(1,i),gcom(2,i),gcom(3,i)
304   CONTINUE
305   close(13)
      goto 311
307   return
      end

      subroutine lat(pbt,T,ht)
c     calculate the compression of lattice paramters
      common /pre/ p(150)
      common /comp/ ts(9)
      common /coe/ ai(2),bi(2)
      common /lap/ ca(2,101)
      common /dcij/ dc(10)
      common /dcijp/ cp(7,17)
      common /pdcij/ pcp(7,17)
      common /sdcij/ dcp(7,17)
      common /spdbc/ dpcp(7,17)
      common /tem/ it(17)
      dimension yi(2),bp(101),ex(2),ax(2,101)
      real bo,q1,q2,pbt,cc(2,101)
      integer T,nm,ht
      do i=1,17
       if (T.eq.it(i)) then
         l=i
       end if
      end do
      write(6,1)
      print*,'   Calculate the changes of lattice prameters'
      write(6,1)
      print*,' 1. With contribution from piezoelectric effects'
      print*,' 2. Without contribution from piezoelectric effects'
      write(6,1)
1     format(//' ')
      read(5,*) nm
      if (nm.eq.1) then
        do i=1,7
         dc(i)=cp(i,l)
        end do
        goto 55
      else if (nm.eq.2) then
        do i=1,7
         dc(i)=pcp(i,l)
        end do
      end if
55    ai(1)=-ts(8)
```

```
      ai(2)=-ts(9)
      q1=ts(8)*(dc(1)+dc(7))+ts(9)*dc(2)
      q2=2.*ts(8)*dc(2)+ts(9)*dc(3)
      bi(1)=ai(1)**2+(ts(1)+ts(2))*q1+ts(7)*q2
      bi(2)=ai(2)**2+2.*ts(7)*q1+ts(3)*q2
      bo=-1./(2.*ai(1)+ai(2))
      do 241 i=1,2
       yi(i)=bi(i)-ai(i)**2
       ex(i)=-bo**2*yi(i)/pbt**2
       do 241 k=1,101
        p(k)=0.01*(2.*float(k)-2)
        bp(k)=bo+pbt*p(k)
        ax(i,k)=(ai(i)+bo*yi(i)/pbt)*p(k)
        ca(i,k)=(bp(k)/bo)**ex(i)*exp(ax(i,k))
241   continue
      print*,'Calculate l/l(o) by using the data of Thurston?'
      print*,'1. Yes'
      print*,'2. No'
      read(5,*) ht
      if(ht.eq.2)goto 243
      ai(1)=-0.9815
      ai(2)=-0.7306
      bi(1)=16.31
      bi(2)=17.75
      bo=0.3712
      pbt=6.33
      do i=1,2
       yi(i)=bi(i)-ai(i)**2
       ex(i)=-bo**2*yi(i)/pbt**2
       do k=1,101
       p(k)=0.01*(2.*float(k)-2)
       bp(k)=bo+pbt*p(k)/10.
       ax(i,k)=(ai(i)+bo*yi(i)/pbt)*p(k)/10.
       cc(i,k)=(bp(k)/bo)**ex(i)*exp(ax(i,k))
       end do
      end do
      open (7,file='thurlc.d')
      do i=1,101
       write(7,*) 10.*p(i),cc(1,i),cc(2,i)
      end do
      close (7)
243   return
      end

      subroutine set(T)
c     calculate the elastic constants and the direction cosines
c     ex1--2*thermal expansion coef. along X-axis
c     ex2--thermal expansion coef. along Z-axis
c     cp--specific heat Cp;de--density
c     w1=(de*W^2)1,w2=(de*W^2)2,w3=(de*W^2)5,w4=(de*W^2)6,
c     w5=(de*W^2)7,w6=(de*W^2)9,w7=(de*W^2)10,
c     w8=(de*W^2)12,
c     ts--isothermal s;ts(8)-s1;ts(9)--s3
      common /comp/ ts(9)
```

```
      common /cij/ c(7,17),csd(7,17)
      common /tem/ it(17)
      real s(7)
      real ap,bp,de,dt
      double precision cf,cp,th1,th2,ex1,ex2
      integer T
      do i=1,17
       if (T.eq.it(i)) then
         k=i
       end if
      end do
      dt=float(T)-298.
c     thermal expansion correction
      th1=2.*(1.377*dt+1.303D-3*dt**2-6.329D-7*dt**3)*1.D-5
      th2=(0.7483*dt+9.405D-4*dt**2-5.44D-7*dt**3)*1.D-5
      de=2648.38/(1.+th1+th2)
      cp=(47.0118+3.4358D-2*(dt+298.)-1.131D6/(dt+298.)**2)
     &/60.0118*1.D3
      ex1=(1.377+2.*1.303D-3*dt-3.*6.329D-7*dt**2)*1.D-5
      ex2=(0.7483+2.*9.405D-4*dt-3.*5.44D-7*dt**2)*1.D-5
      cf=(dt+298.)/de/cp*1.D10
      ap=c(3,k)*(c(1,k)+c(2,k))-2.*c(7,k)**2
      bp=c(4,k)*(c(1,k)-c(2,k))-2.*c(5,k)**2
      s(1)=(c(3,k)/ap+c(4,k)/bp)/2.
      s(2)=(c(3,k)/ap-c(4,k)/bp)/2.
      s(3)=(c(1,k)+c(2,k))/ap
      s(4)=(c(1,k)-c(2,k))/bp
      s(5)=-c(5,k)/bp
      s(6)=2.*(s(1)-s(2))
      s(7)=-c(7,k)/ap
      ts(1)=s(1)+cf*ex1**2
      ts(2)=s(2)+cf*ex1**2
      ts(3)=s(3)+cf*ex2**2
      ts(4)=s(4)
      ts(5)=s(5)
      ts(6)=s(6)
      ts(7)=s(7)+cf*ex1*ex2
      ts(8)=ts(1)+ts(2)+ts(7)
      ts(9)=2.*ts(7)+ts(3)
      return
      end


      subroutine load
c     load data
      common /cij/ c(7,17),csd(7,17)
      common /dcijp/ cp(7,17)
      common /pdcij/ pcp(7,17)
      common /sdcij/ dcp(7,17)
      common /spdbc/ dpcp(7,17)
      real t(17)
      character*10  fl,fm
c     load weighted SOEC c(1,j),...,c(7,j):C11,C12,C33,C44,C14,C66,C13
      open (7,file='wcij.d')
```

```
      do j=1,17
       read(7,*) t(j),c(1,j),c(2,j),c(3,j)
       read(7,*) c(4,j),c(5,j),c(6,j),c(7,j)
      end do
      close (7)
c     load the standard errors of SOEC
      open (7,file='csd.d')
      do j=1,17
       read(7,*) t(j),csd(1,j),csd(2,j),csd(3,j)
       read(7,*) csd(4,j),csd(5,j),csd(6,j),csd(7,j)
      end do
      close (7)
c     load dCij/dP without contribution from the piezoelectric effects
c     and their standard errors
      do i=1,7
       fl='dc .d'
       fm='dcer .d'
       write(fl(3:3),'(i1)') i
       write(fm(5:5),'(i1)') i
       open (7,file=fl)
       open (8,file=fm)
       do j=1,17
        read(7,*) t(j),cp(i,j)
        read(8,*) t(j),dcp(i,j)
       end do
       close (7)
       close (8)
      end do
c     load dCij/dP with contribution from the piezoelectric
c     effects and their standard errors
      do i=1,7
       fl='pd .d'
       fm='pder .d'
       write(fl(3:3),'(i1)') i
       write(fm(5:5),'(i1)') i
       open(7,file=fl)
       open(8,file=fm)
       do j=1,17
        read(7,*) t(j),pcp(i,j)
        read(8,*) t(j),dpcp(i,j)
       end do
       close (7)
       close (8)
      end do
      return
      end
```

Appendix C

Computer Programme: QGRU.FOR

This programme is for the computation of the long wavelength acoustic mode Grüneisen parameters and the mean acoustic mode Grüneisen parameter for α-quartz crystal from 243K to 393K. The mode Grüneisen parameters both with and without contributions from piezoelectric effects are computed in the X-Y, Y-Z and Z-X planes using Eqs. (3.23) and (7.2), respectively. The mean Grüneisen parameters in the high and low temperature limit are calculated using Eqs. (3.54) and (3.55) respectively. The input data are the SOEC, the second order piezoelectric coefficients e_{11} and e_{14}, the hydrostatic pressure derivatives $(\partial C_{IJ}/\partial P)_{T,P=0}$ not including the contributions from piezoelectric effects and the hydrostatic pressure derivative $[\partial(e_{11}^2/\varepsilon_{11}^{\eta})/\partial P]_{T,P=0}$. The other parameters, such as the thermal expansion tensors α_{11} and α_{33} , the dielectric constants ε_{11}^{η} and ε_{33}^{η}, specific heat C_P and density are given in the programme. The programme is employed to solve the Christoffel equations (Eq. (7.1)) for the three polarization vectors $\vec{V}$ correspond to the three normal vibrational modes associated with the wave propagation direction $\vec{N}$. The polarization vector $\vec{V}$ is then used together with the ultrasonic data to compute the Grüneisen parameters. The eigenvalues and eigenvectors of Eq. (7.1) are solved by using the Jacobi method (Press et al. 1986), employing the subroutine JACOBI (Press et al. 1986). The computational process is repeated in intervals of 1° in the angles θ and ϕ. The programme, written in FORTRAN 77, has been operated in a Viglen IV (486) PC with the aid of the Microsoft FORTRAN Compiler V5.0. The primary variables used are:

C11,C12,C66,C33,C44,

C13,C14 ..... SOEC,

E11,E14 ..... the second order piezoelectric coefficients,

DC(1)=DC11,DC(2)=DC66,

DC(3)=DC33,DC(4)=DC44, ... $(\partial C_{IJ}/\partial P)_{T,P=0}$ without contributions

DC(5)=DC13,DC(6)=DC14 from piezoelectric effects,

FP(1) ..... $[\partial(e_{11}^2/\varepsilon_{11}^{\eta})/\partial P]_{T,P=0}$,

PHI ..... ϕ,

THETA ..... θ,

CS ..... γ_L ,

SB ..... γ_{S1} ,

BC ..... γ_{S2} ,

IG ..... γ^{I}.

```
C    THE INPUT DATA ARE THE IOTHERMAL ELASTIC COMPLIANCES,
C    SAMPLE DENSITY AND THE HYDROSTATIC PRESSURE DERIVATIVES
C    OF THE EFFECTIVE ISENTROPIC SOEC DC(1)=DC11,DC(2)=DC66,
c    DC(3)=DC33,DC(4)=DC44,DC(5)=DC13,DC(6)=DC14

     CHARACTER*10 FN,FM,FL
     COMMON /TSIJ/ S11,S66,S33,S44,S13,S14
     COMMON /CEIJ/ C11,C12,C66,C33,C44,C13,C14,E11,E14
     COMMON /DP/ DC(6),FP(6)
     COMMON /RES/ CS,SB,BA,P1,P2,P3
     COMMON /DENS/ DE
     COMMON /DIAE/ EP1,EP3
     COMMON /WEI/ VP
     INTEGER PHI,NC,CHO,LIM
     COMMON /ANG/ THETA,PHI
     COMMON /ICE/ CHO,LIM
     REAL s(7),T,ap,bp,DT,ANGLE,IG,PI,QQI,O,X,P,SW
     DOUBLE PRECISION EP1,EP3,ce1,ce2,ex1,ex2,cf

     WRITE(6,65)
     PRINT*,'   CALCULATE ACOUSTIC MODE AND MEAN GRUNEISEN'
     PRINT*,'  PARAMETERS FOR VERY HIGH PURITY QUARTZ CRYSTALS'
     WRITE(6,65)
     PRINT*,'          QINGXIAN WANG'
     PRINT*,'          SCHOOL OF PHYSICS'
     PRINT*,'          UNIVERSITY OF BATH'
     PRINT*,'          SEPTEMBER  1992 '
64   WRITE(6,65)
65   FORMAT(//' ')
     PRINT*,'1. With contribution from piezoelectric effects'
     PRINT*,'2. Without contribution from piezoelectric effects'
     PRINT*,'3. Quit'
     READ(5,*) CHO
     IF (CHO .EQ. 3) GOTO 70
C    FILES FOR MODE GAMMAS IN THREE PLANES
     FN='qzx  .d'
     FM='qyz  .d'
     FL='qxy  .d'
     IF (CHO .EQ. 2) THEN
     FN='nzx  .d'
     FM='nyz  .d'
     FL='nxy  .d'
     END IF

C    FILES FOR MODE GAMMAS ALONG X-, Y- AND Z-AXES
     IF (CHO .EQ. 2) THEN
      OPEN (16,FILE='NGX.D')
      OPEN (17,FILE='NGY.D')
      OPEN (18,FILE='NGZ.D')
      GOTO 66
     END IF
```

```
      OPEN (16,FILE='MGX.D')
      OPEN (17,FILE='MGY.D')
      OPEN (18,FILE='MGZ.D')

63    WRITE(6,65)
      PRINT*,'  Clculation of mean gamma:'
      PRINT*,'  1. In low temperature limit'
      PRINT*,'  2. In high temperature limit'
      READ(5,*) LIM
C     FILE FOR MEAN GAMMA
66    IF (CHO .EQ. 2) THEN
      IF (LIM .EQ. 1) THEN
        OPEN(19,FILE='LQNG.D')
      ELSE IF (LIM .EQ. 2) THEN
        OPEN(19,FILE='HQNG.D')
      END IF
        GOTO 67
      END IF
      IF (LIM .EQ. 1) THEN
        OPEN(19,FILE='LQMG.D')
      ELSE IF (LIM .EQ. 2) THEN
        OPEN(19,FILE='HQMG.D')
      END IF

C     FILE OF INPUT DATA
67    OPEN(20,FILE='qgd.d')
      DO 1 K=1,17
      READ(20,*)T,C11,C12,C33,C44,C14,C66,C13
      READ(20,*)DC(1),DC(2),DC(3),DC(4),DC(5),DC(6)
      READ(20,*)E11,E14,FP(1)
      FP(2)=FP(1)
      DO 3 I=3,6
      FP(I)=0
 3    CONTINUE
      PRINT*,T
C     EP=DIELECTRIC CONSTANTS AT CONSTANT STRAIN
      DT=T-293.
      ce1=2.*(1.377*dt+1.303D-3*dt**2-6.329D-7*dt**3)*1.D-5
      ce2=(0.7483*dt+9.405D-4*dt**2-5.44D-7*dt**3)*1.D-5
      de=2648.38/(1.+ce1+ce2)
      cp=(47.0118+3.4358D-2*(dt+298.)-1.131D6/(dt+298.)**2)
     & /60.0118*1.D3
      ex1=(1.377+2.*1.303D-3*dt-3.*6.329D-7*dt**2)
      ex2=(0.7483+2.*9.405D-4*dt-3.*5.44D-7*dt**2)
      cf=(dt+298.)/de/cp
      EP1=(3.916D-1)*(1.+DT*1.47D-5+DT**2*1.45D-8-DT**3*2.10D-11)
      EP3=4.10395D-1*(1.+DT*1.88D-5+DT**2*3.29D-8-DT**3*1.92D-10)
      ap=c33*(c11+c12)-2.*c13**2
      bp=c44*(c11-c12)-2.*c14**2
      s(1)=(c33/ap+c44/bp)/2.
      s(2)=(c33/ap-c44/bp)/2.
      s(3)=(c11+c12)/ap
```

```
      s(4)=(c11-c12)/bp
      s(5)=-c14/bp
      s(6)=2.*(s(1)-s(2))
      s(7)=-c13/ap
      s11=s(1)+cf*ex1**2
      s33=s(3)+cf*ex2**2
      s44=s(4)
      s14=s(5)
      s66=s(6)
      s13=s(7)+cf*ex1*ex2

      PRINT*,'Calculate mode Gruneisen parameters'
C     CALCULATE MODE GAMMA IN X-Y PLANE
      WRITE(FL(4:5),'(I2.2)') K
      OPEN(21,FILE=FL)
      DO I=1,91
       PHI=I-1
       THETA=90.
       CALL PDS
       CALL CAL
C      SAVE RESULTS
       WRITE(21,*) PHI,CS,SB,BA
       IF (PHI .EQ. 0) THEN
         WRITE(16,*) T,CS,SB,BA
       ELSE IF (PHI .EQ. 90) THEN
         WRITE(17,*) T,CS,SB,BA
       END IF
      END DO
      CLOSE(21)
C     CALCULATE MODE GAMMA IN Y-Z PLANE
      WRITE(FM(4:5),'(I2.2)') K
      OPEN(21,FILE=FM)
      DO I=1,91
       PHI=90
       THETA=REAL(91-I)
       CALL PDS
       CALL CAL
C      SAVE RESULTS
       WRITE(21,*) INT(THETA),CS,SB,BA
       IF (I .EQ. 91) THEN
         WRITE(18,*) T,CS,SB,BA
       END IF
      END DO
      CLOSE(21)

C     CALCULATE MODE GAMMA IN Z-X PLANE
      WRITE(FN(4:5),'(I2.2)') K
      OPEN(21,FILE=FN)
      DO I=1,91
       PHI=0
       THETA=REAL(I-1)
       CALL PDS
       CALL CAL
```

```
C    SAVE RESULTS
     WRITE(21,*) INT(THETA),CS,SB,BA
     END DO
     CLOSE(21)

     PRINT*,'Calculate mean Gruneisen parameters'
C    CALCULATE MEAN GRUNEISEN PARAMETER
     ANGLE=1.
     PI=3.14159
     X=ANGLE*PI/180.
     X2=X*X
C    MATRIX FOR CALCULATE VELOCITY AND POLARIZATION VECTORS
     SUMG=0.
     SW=0.
     NC=0
     P=X/2.
 203 QQI=2.*PI*COS(P)/3.
     O=-X/2.
 204 O=O+X
     IF (O.GT.QQI) GO TO 210
     CALL DCC(P,O)
     NC=NC+1
     CALL CAL
     SUMG=SUMG+CS+SB+BA
     IF (LIM .EQ. 1) SW=SW+VP
     GOTO 204
210  P=P+X
     IF (P.GT.(PI/2)) GO TO 205
     GO TO 203
205  WRITE(6,206)NC
206  FORMAT('  No. of poi.=',I4)
     CONST=X*X/(PI*2.)
     IG=SUMG*CONST
     IF (LIM .EQ. 1) IG=IG/SW/CONST
C    SAVE RESULTS
     WRITE(19,*) T,IG

1    CONTINUE
     CLOSE(16)
     CLOSE(17)
     CLOSE(18)
     CLOSE(19)
     CLOSE(20)

     GOTO 64
70   STOP
     END


     SUBROUTINE PDS
     REAL BN,AN,N1,N2,N3
     INTEGER PHI
     COMMON /ANG/ THETA,PHI
     COMMON /DICOS/ N1,N2,N3,U1,U2,U3
```

```
      AN=THETA/57.29598
      BN=REAL(PHI)/57.29598
      N3=(COS(AN))
      N2=(SIN(AN))*(SIN(BN))
      N1=(SIN(AN))*(COS(BN))
      RETURN
      END

      SUBROUTINE CAL
      COMMON /TSIJ/ S11,S66,S33,S44,S13,S14
      COMMON /CEIJ/ C11,C12,C66,C33,C44,C13,C14,E11,E14
      COMMON /DP/ DC(6),FP(6)
      COMMON /DICOS/ N1,N2,N3,U1,U2,U3
      COMMON /OUT/ W,BU,SV,TO
      COMMON /RES/ CS,SB,BA,P1,P2,P3
      COMMON /DENS/ DE
      COMMON /DIAE/ EP1,EP3
      COMMON /ICE/ CHO,LIM
      COMMON /WEI/ VP
      DOUBLE PRECISION EP1,EP3
      REAL L11,L22,L33,L12,L23,L31,V1,V2,V3,N1,N2,N3
      DIMENSION A(3,3),D(3),V(3,3)
      INTEGER NROT,CHO
C     MATRIX FOR CALCULATE VELOCITY AND POLARIZATION VECTORS
      IF (CHO .EQ. 2) THEN
        L11=(N1**2)*C11+(N2**2)*C66+(N3**2)*C44+2.*N2*N3*C14
        L22=N1**2*C66+N2**2*C11+N3**2*C44-2.*N2*N3*C14
        L33=(N1**2+N2**2)*C44+N3**2*C33
        L12=2*N1*N3*C14+0.5*N1*N2*(2*C11-3*C66)
        L23=(N1**2-N2**2)*C14+N2*N3*(C13+C44)
        L31=N1*N3*(C44+C13)+2*N1*N2*C14
        GOTO 11
      END IF
      L11=(N1**2)*C11+(N2**2)*C66+(N3**2)*C44+2.*N2*N3*C14
     & +(((N1**2-N2**2)*E11-E14*N2*N3)**2)/
     & (EP1*(N1**2+N2**2)+EP3*N3**2)
      L22=N1**2*C66+N2**2*C11+N3**2*C44-2.*N2*N3*C14
     & +((-2.*E11*N1*N2+E14*N1*N3)**2)/(EP1*(N1**2+N2**2)
     & +EP3*N3**2)
      L33=(N1**2+N2**2)*C44+N3**2*C33
      L12=2*N1*N3*C14+0.5*N1*N2*(2*C11-3*C66)
     & +((N1**2-N2**2)*E11-N2*N3*E14)*((-2.)*N1*N2*E11
     & +N1*N3*E14)/(EP1*(N1**2+N2**2)+EP3*N3**2)
      L23=(N1**2-N2**2)*C14+N2*N3*(C13+C44)
      L31=N1*N3*(C44+C13)+2*N1*N2*C14
11    A(1,1)=L11
      A(1,2)=L12
      A(2,2)=L22
      A(1,3)=L31
      A(2,3)=L23
      A(3,3)=L33
      A(2,1)=A(1,2)
      A(3,1)=A(1,3)
      A(3,2)=A(2,3)
```

```
C    CALCULATE THE EIGENVECTORS OF VELOCITY
     CALL JACOBI (A,3,3,D,V,NROT)
C    CALCULATE THE VELOCITIES FROM THE EIGENVALUES
     V1=SQRT(ABS(D(1))/DE)
     V2=SQRT(ABS(D(2))/DE)
     V3=SQRT(ABS(D(3))/DE)
     U1=V(1,1)
     U2=V(2,1)
     U3=V(3,1)
C    CALCULATE HYDROSTATIC GRUNEISEN PARAMETERS
     CALL GRU
     CS=-(BU/(2.*W))*(1.+2.*W*SV+TO)
     IF (LIM .EQ. 1) THEN
      CS=CS*V1**(-3)
     END IF
     P1=CS
     U1=V(1,2)
     U2=V(2,2)
     U3=V(3,2)
     CALL GRU
     SB=-(BU/(2.*W))*(1.+2.*W*SV+TO)
     IF (LIM .EQ. 1) THEN
      SB=SB*V2**(-3)
     END IF
     P2=SB
     U1=V(1,3)
     U2=V(2,3)
     U3=V(3,3)
     CALL GRU
     BA=-(BU/(2.*W))*(1.+2.*W*SV+TO)
     IF (LIM .EQ. 1) THEN
      BA=BA*V3**(-3/2)
      VP=V1**(-3)+V2**(-3)+V3**(-3)
     END IF
     P3=BA
     RETURN
     END

     SUBROUTINE GRU
     DIMENSION PER(6),Q(10),SP(6)
     REAL SV,S1,S3,W,S12,N1,N2,N3
     COMMON /TSIJ/ S11,S66,S33,S44,S13,S14
     COMMON /CEIJ/ C11,C12,C66,C33,C44,C13,C14,E11,E14
     COMMON /DP/ DC(6),FP(6)
     COMMON /DICOS/ N1,N2,N3,U1,U2,U3
     COMMON /OUT/ W,BU,SV,TO
     COMMON /DIAE/ EP1,EP3
     COMMON /ICE/ CHO,LIM
     DOUBLE PRECISION EP1,EP3
     INTEGER CHO
     S12=S11-0.5*S66
     S1=S11+S12+S13
     S3=2.*S13+S33
     BU=1./(2.*(S11+S12+2*S13)+S33)
```

```
      Q(1)=(N1*U1+N2*U2)**2
      Q(2)=(N1*U2-N2*U1)**2
      Q(3)=N3**2*U3**2
      Q(4)=(N2*U3+N3*U2)**2+(N3*U1+N1*U3)**2
      Q(5)=2.*(N1*U1+N2*U2)*N3*U3
      Q(6)=2.*((N1**2-N2**2)*U2*U3+N2*N3*(U1**2-U2**2)
     & +2.*N1*U1*(N2*U3+N3*U2))
      Q(7)=(N1**2-N2**2)*U1-2.*N1*N2*U2
      Q(8)=N1*N3*U2-N2*N3*U1
      SV=S1*(U1**2+U2**2)+S3*U3**2
      SP(1)=1.+(2.*S1-S3)*C11
      SP(2)=1.+(2.*S1-S3)*C66
      SP(3)=1.+(3.*S3-2.*S1)*C33
      SP(4)=1.+S3*C44
      SP(5)=-1.+S3*C13
      SP(6)=S1*C14
      TO=0.
      DO 29 I=1,6
      PER(I)=0.
   29 CONTINUE
      DO 31 I=1,6
      IF (CHO .EQ. 2) THEN
        PER(I)=-(DC(I)+SP(I))
        GOTO 31
      END IF
      PER(I)=-(DC(I)+FP(I)+SP(I))
   31 CONTINUE
      DO 32 I=1,6
      TO=TO+PER(I)*Q(I)
   32 CONTINUE
      IF (CHO .EQ. 2) THEN
        W=C11*Q(1)+C66*Q(2)+C33*Q(3)+C44*Q(4)
     &  +C13*Q(5)+C14*Q(6)
        GOTO 33
      END IF
      W=C11*Q(1)+C66*Q(2)+C33*Q(3)+C44*Q(4)
     & +C13*Q(5)+C14*Q(6)+((E11*Q(7)+E14*Q(8))**2)/
     & ((N1**2+N2**2)*EP1+EP3*N3**2)
   33  RETURN
      END

      SUBROUTINE DCC(P,O)
      REAL PI,AT,N1,N2,N3
      COMMON /DICOS/ N1,N2,N3,U1,U2,U3
      PI=3.14159
      AT=O*COS(P)
      AT=AT+2.*PI/3.
      N1=COS(P)*COS(AT)
      N2=COS(P)*SIN(AT)
      N3=SIN(P)
      RETURN
      END
```

```
      SUBROUTINE JACOBI(A,N,NP,D,V,NROT)
      PARAMETER (NMAX=100)
      DIMENSION A(NP,NP),D(NP),V(NP,NP),B(NMAX),Z(NMAX)
      DO 12 IP=1,N
       DO 11 IQ=1,N
        V(IP,IQ)=0.
11     CONTINUE
       V(IP,IP)=1.
12    CONTINUE
      DO 13 IP=1,N
       B(IP)=A(IP,IP)
       D(IP)=B(IP)
       Z(IP)=0.
13    CONTINUE
      NROT=0
      DO 24 I=1,50
       SM=0.
       DO 15 IP=1,N-1
        DO 14 IQ=IP+1,N
         SM=SM+ABS(A(IP,IQ))
14      CONTINUE
15     CONTINUE
      IF(SM.EQ.0.)RETURN
      IF(I.LT.4)THEN
       TRESH=0.2*SM/N**2
       ELSE
       TRESH=0.
      ENDIF
      DO 22 IP=1,N-1
       DO 21 IQ=IP+1,N
        G=100.*ABS(A(IP,IQ))
        IF((I.GT.4).AND.(ABS(D(IP))+G.EQ.ABS(D(IP)))
     *       .AND.(ABS(D(IQ))+G.EQ.ABS(D(IQ))))THEN
         A(IP,IQ)=0.
        ELSE IF(ABS(A(IP,IQ)).GT.TRESH)THEN
         H=D(IQ)-D(IP)
         IF(ABS(H)+G.EQ.ABS(H))THEN
          T=A(IP,IQ)/H
         ELSE
          THETA=0.5*H/A(IP,IQ)
          T=1./(ABS(THETA)+SQRT(1.+THETA**2))
          IF(THETA.LT.0.)T=-T
         ENDIF
         C=1./SQRT(1+T**2)
         S=T*C
         TAU=S/(1.+C)
         H=T*A(IP,IQ)
         Z(IP)=Z(IP)-H
         Z(IQ)=Z(IQ)+H
         D(IP)=D(IP)-H
         D(IQ)=D(IQ)+H
         A(IP,IQ)=0.
         DO 16 J=1,IP-1
          G=A(J,IP)
```

```
        H=A(J,IQ)
        A(J,IP)=G-S*(H+G*TAU)
        A(J,IQ)=H+S*(G-H*TAU)
16      CONTINUE
       DO 17 J=IP+1,IQ-1
        G=A(IP,J)
        H=A(J,IQ)
        A(IP,J)=G-S*(H+G*TAU)
        A(J,IQ)=H+S*(G-H*TAU)
17      CONTINUE
       DO 18 J=IQ+1,N
        G=A(IP,J)
        H=A(IQ,J)
        A(IP,J)=G-S*(H+G*TAU)
        A(IQ,J)=H+S*(G-H*TAU)
18      CONTINUE
       DO 19 J=1,N
        G=V(J,IP)
        H=V(J,IQ)
        V(J,IP)=G-S*(H+G*TAU)
        V(J,IQ)=H+S*(G-H*TAU)
19      CONTINUE
       NROT=NROT+1
      ENDIF
21     CONTINUE
22    CONTINUE
     DO 23 IP=1,N
      B(IP)=B(IP)+Z(IP)
      D(IP)=B(IP)
      Z(IP)=0.
23    CONTINUE
24    CONTINUE
    PAUSE '50 iterations should never happen'
    RETURN
    END
```

Appendix D

Computer Programme: QAGP.FOR

This programme is for the computation of the long wavelength acoustic Grüneisen parameters γ_{11}^{el} and γ_{33}^{el} for α-quartz crystal from 243K to 393K for the parameters including contributions from piezoelectric effects and also at 293K for the parameters not including these contributions, using Eqs. (3.34) and (3.35) respectively. The method used in this programme for the computation is basically the same as the programme QGRU.FOR. The input data are the SOEC, the second order piezoelectric coefficients $e_{11}^2/\varepsilon_{11}^{\eta}$ and $(e_{14}-e_{11})^2/(2\varepsilon_{11}^{\eta}+2\varepsilon_{33}^{\eta})$, the third order elastic constants (TOEC) both with and without the contributions from piezoelectric effects. The TOEC not including the contributions from the piezoelectric effects are only available at 293K. The integration step is 1° in angles θ and ϕ. The programme, written in FORTRAN 77, has been operated in a Viglen IV (486) PC by virtue of the Microsoft FORTRAN Compiler V5.0. The primary variables used are:

c(i,j) (i=1,7;j=1,17)	SOEC,
ee(1,j) (j=1,17)	$e_{11}^2/\varepsilon_{11}^{\eta}$,
ee(2,j) (j=1,17)	$(e_{14}-e_{11})^2/(2\varepsilon_{11}^{\eta}+2\varepsilon_{33}^{\eta})$,
ct(i,j) (i=1,7;j=1,17)	TOEC,
PHI	ϕ,
THETA	θ,
ag(1,k) (k=1,17)	γ_{11}^{el},

ag(1,k) (k=1,17) ..... γ_{33}^{el} .

```
c    The programme for the calculation of the axial Gruneisen
c    parameters of very high purity quartz crystals as a
c    function of T
c    s1,..->sij,
c    ud1..->(den*W^2)'for hydro. pres.; al, be and ga are
c    special direction consines for Ui.c1..->cij
c    The temperature range is 243K to 393K, 17 steps
c    Unit:w(i)--1E10 pa;ct(i,k)(i.e.TOEC)--1E10 Pa

     character*10 fn(3)
     common /temp/ t(17)
     common /saxg/ ag(3,17)
     integer ch,run,wcg,lim

700  write(6,65)
     write(6,*)'   CALCULATION OF THE AXIAL GRUNEISEN PARAMETERS'
     write(6,*)'                OF QUARTZ'
     write(6,65)
     write(6,*)'          Qingxian Wang'
     write(6,*)'          Solid State Physics'
     write(6,*)'          School of Physics'
     write(6,*)'          University of Bath'
     write(6,*)'          September 1992'
     write(6,65)
65   FORMAT(//' ')

40   print*,'1. With piezoelectric effects'
     print*,'2. Without piezoelectric effects'
     print*,'3. By using Thurston and McSkimin (s) results'
     read(5,*) ch

     write(6,65)
     print*,'1. Use TOEC calculated with weights'
     print*,'2. Use TOEC calculated with equal weights (=1)'
     read (5,*) wcg

     write(6,65)
     print*,'1. In low temperature limit'
     print*,'2. In high temperature limit'
     read (5,*) lim

     if (ch.eq.1) then
      call load(wcg)
      run=17
     else if (ch.eq.2) then
      call load(wcg)
      call wep
      run=1
     else if (ch.eq.3) then
     call tmd
     run=1
     end if
```

```
      do 1 K=1,run
      print*,t(k)
      call set(K)
      call axgru(K,ch,lim)
    1 continue
c     SAVE RESULTS
      if (ch.eq.1) then
       fn(1)='qagu.d'
       fn(2)='qcgu.d'
       fn(3)='qmgu.d'
      else if (ch.eq.2) then
       fn(1)='npqagu.d'
       fn(2)='npqcgu.d'
       fn(3)='npqmgu.d'
      else if (ch.eq.3) then
       fn(1)='tmqagu.d'
       fn(2)='tmqcgu.d'
       fn(3)='tmqmgu.d'
      end if
  671 do 673 i=1,3
      open (13,FILE=fn(i))
      do 675 k=1,run
       write(13,*) t(k),ag(i,k)
  675 continue
      close(13)
  673 continue
  676 print*,'The calculation has finished'
      stop
      end

      subroutine load(wcg)
c     load data
      common /cij/ c(7,17)
      common /cpie/ ee(2,17),esd(2,17)
      common /temp/ t(17)
      common /toec/ ct(14,17)
      real pt(14,17)
      integer wcg
      character*10 fl(20)
      open (7,file='wcij.d')
c     load Cij
      do j=1,17
       read(7,*) t(j),c(1,j),c(2,j),c(3,j)
       read(7,*) c(4,j),c(5,j),c(6,j),c(7,j)
      end do
      close (7)
c     load e(i) (i=1,2)
      open (7,file='ep.d')
      do j=1,17
       read(7,*) t(j)
       do i=1,2
        read(7,*) ee(i,j),esd(i,j)
```

```
      end do
     end do
     close (7)
c    load Cijk
     do i=1,14
      if (wcg.eq.1) then
        fl(i)='ptoec  .d'
      else if (wcg.eq.2) then
        fl(i)='nwtoec  .d'
      end if
      write(fl(i)(6:7),'(i2.2)') i
      open (7,file=fl(i))
      do j=1,17
       read(7,*) t(j),pt(i,j)
      end do
      close (7)
     end do
c    reorder the variables for Cijk
     do i=1,8
      do j=1,17
       ct(i,j)=pt(i,j)
      end do
     end do
     do i=9,10
      do j=1,17
       ct(i,j)=pt(i+3,j)
      end do
     end do
     do i=11,13
      do j=1,17
       ct(i,j)=pt(i-2,j)
      end do
     end do
     do i=1,17
      ct(14,i)=pt(14,i)
     end do
     return
     end

     subroutine wep
     common /temp/ t(17)
     common /cij/ c(7,17)
     common /toec/ ct(14,17)
     do i=1,17
      t(i)=0.
     end do
     t(1)=298.
     do i=1,14
      do j=1,17
       ct(i,j)=0.
      end do
     end do
     open (7,file='rtoec.d')
     do i=1,14
```

```
 read(7,*) ct(i,1)
end do
close (7)
return
end

subroutine tmd
common /temp/ t(17)
common /cij/ c(7,17)
common /toec/ ct(14,17)
do i=1,17
 t(i)=0.
end do
t(1)=298.
c(1,1)=8.68+0.077
c(2,1)=0.704
c(7,1)=1.191
c(5,1)=-1.804
c(3,1)=10.575
c(4,1)=5.82
c(6,1)=3.988+0.077
ct(1,1)=-21.
ct(2,1)=-34.5
ct(3,1)=1.2
ct(4,1)=-16.3
ct(5,1)=-29.4
ct(6,1)=-1.5
ct(7,1)=-31.2
ct(8,1)=0.2
ct(9,1)=-13.4
ct(10,1)=-20.
ct(11,1)=-33.2
ct(12,1)=-81.5
ct(13,1)=-11.
ct(14,1)=-27.6
return
end

subroutine set(K)
c    calculate the isothermal sij
c    ex1--2*thermal expansion coef. along X-axis
c    ex2--thermal expansion coef. along Z-axis
c    cp--specific heat Cp;de--density
c    ts--isothermal s;ts(8)-s1;ts(9)--s3
common /comp/ ts(9)
common /pie/ ee(2,17)
common /cij/ c(7,17)
common /temp/ t(17)
common /den/ de
real s(7)
real ap,bp,de,dt
double precision cf,cp,th1,th2,ex1,ex2
dt=t(k)-298.
c    thermal expansion correction
th1=2.*(1.377*dt+1.303D-3*dt**2-6.329D-7*dt**3)*1.D-5
```

```
th2=(0.7483*dt+9.405D-4*dt**2-5.44D-7*dt**3)*1.D-5
de=2648.38/(1.+th1+th2)
cp=(47.0118+3.4358D-2*(dt+298.)-1.131D6/(dt+298.)**2)
& /60.0118*1.D3
ex1=(1.377+2.*1.303D-3*dt-3.*6.329D-7*dt**2)*1.D-5
ex2=(0.7483+2.*9.405D-4*dt-3.*5.44D-7*dt**2)*1.D-5
cf=(dt+298.)/de/cp*1.D10
ap=c(3,k)*(c(1,k)+c(2,k))-2.*c(7,k)**2
bp=c(4,k)*(c(1,k)-c(2,k))-2.*c(5,k)**2
s(1)=(c(3,k)/ap+c(4,k)/bp)/2.
s(2)=(c(3,k)/ap-c(4,k)/bp)/2.
s(3)=(c(1,k)+c(2,k))/ap
s(4)=(c(1,k)-c(2,k))/bp
s(5)=-c(5,k)/bp
s(6)=2.*(s(1)-s(2))
s(7)=-c(7,k)/ap
ts(1)=s(1)+cf*ex1**2
ts(2)=s(2)+cf*ex1**2
ts(3)=s(3)+cf*ex2**2
ts(4)=s(4)
ts(5)=s(5)
ts(6)=s(6)
ts(7)=s(7)+cf*ex1*ex2
ts(8)=ts(1)+ts(2)+ts(7)
ts(9)=2.*ts(7)+ts(3)
return
end

SUBROUTINE AXGRU(K,ch,lim)
PARAMETER (PI=3.14159)
REAL L11,L22,L33,L12,L23,L31,V1,V2,V3
REAL DT,CS,SB,BA,QQI,O,N1,N2,N3
common /saxg/ ag(3,17)
common /axg/ vg,pg
common /ddc/ U1,U2,U3
common /toec/ ct(14,17)
common /cij/ c(7,17)
common /temp/ t(17)
common /pie/ ee(2,17)
common /comp/ ts(9)
common /sst/ C11,C66,C33,C44,C13,C14,E11,E14
common /den/ de
REAL GP1,GP2,GP3,P,vw
DIMENSION A(3,3),D(3),V(3,3)
DIMENSION SUMG(2)
DOUBLE PRECISION EP1,EP3
integer ch
dt=t(k)-298.
c11=c(1,k)
c33=c(3,k)
c44=c(4,k)
c14=c(5,k)
c66=c(6,k)
c13=c(7,k)
```

```
      if(ch.ne.1)goto 211
      EP1=(3.916D-1)*(1.+DT*(1.47D-5)+(DT**2)*(1.45D-8)
     & -(DT**3)*(2.10D-11))
      EP3=(4.10395E-1)*(1.+DT*(1.88D-5)+(DT**2)*(3.29D-8)
     & -(DT**3)*(1.92D-10))
      e11=sqrt(ee(1,k)*ep1)
      e14=-(e11-sqrt(2.*(ep1+ep3)*ee(2,k)))
c     The integration step (or angle) is 1 degree
211   X=1.*PI/180.
      X2=X*X
c     ELEMENT OF SOLID ANGLE=X2
CC    MATRIX FOR CALCULATE VELOCITY AND POLARIZATION
VECTORS
      SUMG(1)=0.
      SUMG(2)=0.
      vw=0.
      NC=0
      P=X/2.
 203  QQI=2.*PI/3.
      O=-X/2.
 204  O=O+X
      IF (O.GT.QQI) GO TO 210
      N1=COS(P)*COS(O)
      N2=COS(P)*SIN(O)
      N3=SIN(P)
      NC=NC+1
      if (ch.ne.1) then
        L11=(N1**2)*C11+(N2**2)*C66+(N3**2)*C44+2.*N2*N3*C14
        L22=(N1**2)*C66+(N2**2)*C11+(N3**2)*C44-2.*N2*N3*C14
        L33=((N1**2)+N2**2)*C44+(N3**2)*C33
        L12=2*N1*N3*C14+0.5*N1*N2*(2*C11-3*C66)
        L23=((N1**2)-(N2**2))*C14+N2*N3*(C13+C44)
        L31=N1*N3*(C44+C13)+2*N1*N2*C14
        goto 212
      end if
      L11=(N1**2)*C11+(N2**2)*C66+(N3**2)*C44+2.*N2*N3*C14
     & +((((N1**2)-(N2**2))*E11-E14*N2*N3)**2)/
     & (EP1*((N1**2)+(N2**2))+EP3*(N3**2))
      L22=(N1**2)*C66+(N2**2)*C11+(N3**2)*C44-2.*N2*N3*C14
     & +((-2.*E11*N1*N2+E14*N1*N3)**2)/(EP1*((N1**2)+(N2**2))
     & +EP3*(N3**2))
      L33=((N1**2)+N2**2)*C44+(N3**2)*C33
      L12=2*N1*N3*C14+0.5*N1*N2*(2*C11-3*C66)
     & +(((N1**2)-(N2**2))*E11-N2*N3*E14)*((-2.)*N1*N2*E11
     & +N1*N3*E14)/(EP1*((N1**2)+(N2**2))+(EP3)*(N3**2))
      L23=((N1**2)-(N2**2))*C14+N2*N3*(C13+C44)
      L31=N1*N3*(C44+C13)+2*N1*N2*C14
212   A(1,1)=L11
      A(1,2)=L12
      A(2,2)=L22
      A(1,3)=L31
      A(2,3)=L23
      A(3,3)=L33
      A(2,1)=A(1,2)
```

```
      A(3,1)=A(1,3)
      A(3,2)=A(2,3)
CC    CALCULATE THE EIGENVECTORS OF VELOCITY
      CALL JACOBI (A,3,3,D,V,NROT)
CC    CALCULATE THE VELOCITIES FROM THE EIGENVALUES
      V1=SQRT(ABS(D(1))/DE)
      V2=SQRT(ABS(D(2))/DE)
      V3=SQRT(ABS(D(3))/DE)
      U1=V(1,1)
      U2=V(2,1)
      U3=V(3,1)
CC    CALCULATE HYDROSTATIC GRUNEISEN PARAMETERS
      CALL GRU(K,EP1,EP3,N1,N2,N3,ch)
      GP1=vg
      CS=pg
      if (lim.eq.1) then
       GP1=GP1*V1**(-3/2)
       CS=CS*V1**(-3/2)
      end if
      U1=V(1,2)
      U2=V(2,2)
      U3=V(3,2)
      CALL GRU(K,EP1,EP3,N1,N2,N3,ch)
      GP2=vg
      SB=pg
      if (lim.eq.1) then
       GP2=GP2*V2**(-3/2)
       SB=SB*V2**(-3/2)
      end if
      U1=V(1,3)
      U2=V(2,3)
      U3=V(3,3)
      CALL GRU(K,EP1,EP3,N1,N2,N3,ch)
      GP3=vg
      BA=pg
      if (lim.eq.1) then
       GP3=GP3*V3**(-3/2)
       BA=BA*V3**(-3/2)
      end if
      SUMG(1)=SUMG(1)+(GP1+GP2+GP3)*COS(P)
      SUMG(2)=SUMG(2)+(CS+SB+BA)*COS(P)
      vw=vw+V1**(-3/2)+V2**(-3/2)+V3**(-3/2)
      GOTO 204
210   P=P+X
      IF (P.GT.(PI/2.)) GO TO 205
      GO TO 203
205   WRITE(6,206)NC
206   FORMAT('  No. of poi.=',I6)
      CONST=X*X/(PI*2.)
      ag(1,k)=SUMG(1)*CONST
      ag(2,k)=SUMG(2)*CONST
      if (lim.eq.1) then
       ag(1,k)=ag(1,k)/vw/const
       ag(2,k)=ag(2,k)/vw/const
```

```
      end if
      ag(3,k)=2.*ag(1,k)+ag(2,k)
      return
      END

      SUBROUTINE GRU(K,EP1,EP3,N1,N2,N3,ch)
      DIMENSION PER(6),Q(10),SG(6),FP(6),SP(6)
      common /axg/ vg,pg
      common /ddc/ U1,U2,U3
      common /toec/ ct(14,17)
      common /comp/ ts(9)
      REAL BU,S1,W,S2,C12,pr,vr,N1,N2,N3
      common /sst/ C11,C66,C33,C44,C13,C14,E11,E14
      double precision EP1,EP3
      integer ch
      C12=C11-2.*C66
      BU=((C11+C12)*C33-2.*C13**2)/(C11+C12+2.*C33-4.*C13)
      Q(1)=(N1*U1+N2*U2)**2
      Q(2)=(N1*U2-N2*U1)**2
      Q(3)=(N3**2)*(U3**2)
      Q(4)=(N2*U3+N3*U2)**2+(N3*U1+N1*U3)**2
      Q(5)=2.*(N1*U1+N2*U2)*N3*U3
      Q(6)=2.*((N1**2-N2**2)*U2*U3+N2*N3*(U1**2-U2**2)
     & +2.*N1*U1*(N2*U3+N3*U2))
      Q(7)=(N1**2-N2**2)*U1-2.*N1*N2*U2
      Q(8)=N2*(N1*U3-N3*U1)+N1*(N3*U2-N2*U3)
      S1=(ts(1)+ts(2))*(U1**2+U2**2)+2.*ts(7)*U3**2
      S2=ts(7)*(U1**2+U2**2)+ts(3)*U3**2
      SP(1)=ct(1,K)+ct(2,K)
      SP(2)=(-ct(2,K)+ct(11,K))/2.
      SP(3)=2.*ct(7,K)
      SP(4)=ct(9,K)+ct(10,K)
      SP(5)=ct(3,K)+ct(5,K)
      SP(6)=ct(4,K)+ct(6,K)
      FP(1)=ct(3,K)
      FP(2)=(ct(3,K)-ct(5,K))/2.
      FP(3)=ct(12,K)
      FP(4)=ct(13,K)
      FP(5)=ct(7,K)
      FP(6)=ct(8,K)
      vr=0.
      pr=0.
      DO 31 I=1,6
      SG(I)=(ts(1)+ts(2))*SP(I)+2.*ts(7)*FP(I)
      PER(I)=ts(7)*SP(I)+ts(3)*FP(I)
      vr=vr+SG(I)*Q(I)
      pr=pr+PER(I)*Q(I)
31    CONTINUE
      if (ch.ne.1) then
        W=11*Q(1)+C66*Q(2)+C33*Q(3)+C44*Q(4)
     & +C13*Q(5)+C14*Q(6)
        goto 32
      end if
      W=11*Q(1)+C66*Q(2)+C33*Q(3)+C44*Q(4)
```

```
     & +C13*Q(5)+C14*Q(6)+((E11*Q(7)+E14*Q(8))**2)/
     & ((N1**2+N2**2)*EP1+EP3*(N3**2))
32    vg=-BU*(N1**2+N2**2+2.*W*S1+vr)/4./W
      pg=-BU*(N3**2+2.*W*S2+pr)/2./W
      RETURN
      END

      SUBROUTINE JACOBI(A,N,NP,D,V,NROT)
      PARAMETER (NMAX=100)
      DIMENSION A(NP,NP),D(NP),V(NP,NP),B(NMAX),Z(NMAX)
      DO 12 IP=1,N
       DO 11 IQ=1,N
        V(IP,IQ)=0.
11     CONTINUE
       V(IP,IP)=1.
12    CONTINUE
      DO 13 IP=1,N
       B(IP)=A(IP,IP)
       D(IP)=B(IP)
       Z(IP)=0.
13    CONTINUE
      NROT=0
      DO 24 I=1,50
      SM=0.
      DO 15 IP=1,N-1
       DO 14 IQ=IP+1,N
        SM=SM+ABS(A(IP,IQ))
14     CONTINUE
15    CONTINUE
      IF(SM.EQ.0.)RETURN
      IF(I.LT.4)THEN
       TRESH=0.2*SM/N**2
      ELSE
       TRESH=0.
      ENDIF
      DO 22 IP=1,N-1
       DO 21 IQ=IP+1,N
        G=100.*ABS(A(IP,IQ))
        IF((I.GT.4).AND.(ABS(D(IP))+G.EQ.ABS(D(IP)))
     *       .AND.(ABS(D(IQ))+G.EQ.ABS(D(IQ))))THEN
         A(IP,IQ)=0.
        ELSE IF(ABS(A(IP,IQ)).GT.TRESH)THEN
         H=D(IQ)-D(IP)
         IF(ABS(H)+G.EQ.ABS(H))THEN
          T=A(IP,IQ)/H
         ELSE
          THETA=0.5*H/A(IP,IQ)
          T=1./(ABS(THETA)+SQRT(1.+THETA**2))
          IF(THETA.LT.0.)T=-T
         ENDIF
         C=1./SQRT(1+T**2)
         S=T*C
         TAU=S/(1.+C)
         H=T*A(IP,IQ)
```

```
      Z(IP)=Z(IP)-H
      Z(IQ)=Z(IQ)+H
      D(IP)=D(IP)-H
      D(IQ)=D(IQ)+H
      A(IP,IQ)=0.
      DO 16 J=1,IP-1
       G=A(J,IP)
       H=A(J,IQ)
       A(J,IP)=G-S*(H+G*TAU)
       A(J,IQ)=H+S*(G-H*TAU)
16     CONTINUE
      DO 17 J=IP+1,IQ-1
       G=A(IP,J)
       H=A(J,IQ)
       A(IP,J)=G-S*(H+G*TAU)
       A(J,IQ)=H+S*(G-H*TAU)
17     CONTINUE
      DO 18 J=IQ+1,N
       G=A(IP,J)
       H=A(IQ,J)
       A(IP,J)=G-S*(H+G*TAU)
       A(IQ,J)=H+S*(G-H*TAU)
18     CONTINUE
      DO 19 J=1,N
       G=V(J,IP)
       H=V(J,IQ)
       V(J,IP)=G-S*(H+G*TAU)
       V(J,IQ)=H+S*(G-H*TAU)
19     CONTINUE
      NROT=NROT+1
     ENDIF
21    CONTINUE
22   CONTINUE
     DO 23 IP=1,N
      B(IP)=B(IP)+Z(IP)
      D(IP)=B(IP)
      Z(IP)=0.
23    CONTINUE
24   CONTINUE
     PAUSE '50 iterations should never happen'
     RETURN
     END
```

PUBLICATIONS

1. **An Ultrasonic Study of Superconducting and Non-superconducting $GdBa_2Cu_3O_{7-X}$**

   D.P. Almond, Qingxian Wang, J. Freestone, E.F. Lambson, B.Chapman and G.A. Saunders.

   J. Phys.: Condens. Matter **1**, 6853-6864, 1989.

2. **Elastic and Anelastic Effects in the Orthorhombic and Tetragonal Forms of $GdBa_2Cu_3O_{7-X}$ as A Function of Pressure and Temperature**

   M. Cankurtaran, G.A. Saunders, D.P. Almond, A. Al-Kheffaji, J. Freestone, Qingxian Wang and E.F. Lambson.

   Physics and Material Science of High Temperature Superconductors, edited by R. Kossowsky, S. Methfessel and D. Wohlleben, Kluwer Academic Publishers, Dordrecht (1990) pages 627-637.

3. **The Elastic Behaviour of Natural Single Crystals of the High-Spin Compound MnS_2**

   G.A. Saunders, Wang Qingxian, E.F. Lambson, N. Lodge, D. Paine and W. Hönle.

   J. Phys.: Condens. Matter **2**, 3713-3721, 1990.

4. **Elastic and Anelastic Properties of Rare Earth Phosphate Glasses**

   G. Carini, M. Cutroni, G. Dángelo, M. Federico, G. Galli, G. Tripodo, G.A. Saunders and Wang Qingxian.

   J. Non-Crystalline Solids **121**, 288-293, 1990.

5. **Vibrational Anharmonicity of Vitreous Samarium Phosphate**

   Qingxian Wang, G.A. Saunders, E.F. Lambson, V.Bayot and J.-P. Michenaud.

   J. Non-Crystalline Solids **125**, 287-292, 1990.

6. **Ultrasonic Studies of Rare Earth Phosphate Glasses**

H.B. Senin, Q. Wang, G.A. Saunders, R.C.J. Draper, H.M.Farok, M. Cankurtaran, P.J.Ford.

Pros. Seminar Sains Keadaan Pepejal VIII (UPM), Malaysia. Sains & Teknologi Keadaan Pepejal (1991) pages 157-165.

7. **Nonlinear Acoustic Properties of High Purity Quartz as a Function of Temperature**

Q. Wang, G.A. Saunders, E.F. Lambson, P. Tschaufeser, S.C. Parker and B.J. James.

Developments in Acoustics and Ultrasonics, edited by M.J.W. Povey and D.J. McClements, IOP Publishing, Bristol (1992) pages 219-224.

8. **Ultrasonic Studies of Rare Earth Phosphate Glasses**

H.B. Senin, Q. Wang, G.A. Saunders, R.C.J. Draper, H.M. Farok, M. Cankurtaran, P.J. Ford, W. Poon, H. Vass and B. Bridge.

"Developments in Acoustics and Ultrasonics", edited by M.J.W. Povey and D.J. McClements, IOP Publishing, Bristol (1992) pages 197-201.

9. **Temperature Dependences of the Third Order Elastic Constants and Acoustic Mode Vibrational Anharmonicity of Vitreous Silica**

Q. Wang, G.A. Saunders H.B. Senin and E.F Lambson.

J. Non-Crystalline Solids **143**, 65-74 (1992).

10. **Temperature Dependences of the Acoustic Mode Vibrational Anharmonicity of Quartz from 243K to 393K**

Q. Wang, G.A. Saunders, E.F. Lambson, P. Tschaufeser, S.C. Parker and B.J. James.

Phys. Rev. B**45**, 10242-10254 (1992).

11. **High-pressure Ultrasonic Study of the Commensurate-Incommensurate Spin-Density-Wave Transition in an Antiferromagnetic Cr-0.3 at.% Ru Alloy Single Crystal**

M. Cankurtaran, G.A. Saunders, Q. Wang, P.J. Ford and H.L. Alberts.

Phys. Rev. B46, 14370-14380 (1992).

12. **Relationship of the Elastic and Non-Linear Acoustic Properties of Antiferromagnetic fcc $Fe_{60}Mn_{40}$ Single-Crystal Alloy to Invar Behaviour**

M. Cankurtaran, G.A. Saunders, P. Ray, Q. Wang, U.Kawald, J. Pelzl and H. Bach.

Phys. Rev. (in press).

13. **A Comparison Between the Elastic and Non-Linear Acoustic properties of Neodymium and Samarium Phosphate Glasses**

H.B. Senin, H.A.A. Sidek, P.J. Ford, G.A. Saunders, Q. Wang, R.C.J. Draper and W.A. Lambson.

Advances in Amorphous State Chemistry (to be published).

14. **Non-linear Acoustic Properties of Samarium Phosphate Glasses**

H.B. Senin, Q. Wang, G.A. Saunders and E.F.Lambson.

J. Non-Cryst. Solids (in press).

15. **Manufacture and Physical Properties of Rare Earth Phosphate Glasses**

H.B. Senin, Q. Wang, G.A.Saunders, R.C.J. Draper, E.F. Lambson, M. Cankurtaran, P.J. Ford, H.M. Farok, H.A.A. Sidek and W.A. Lambson.

J. of Glass Technology (to be published).

PAPERS PRESENTED IN CONFERENCES

1. **Elastic and Anelastic Properties of Rare Earth Phosphate Glasses**

   G. Carini, M. Cutroni, G. d'Angelo, M. Federico, G. Galli, G.A. Saunders, G. Tripodo and Wang Qingxian.

   17th IUPAP Int. Conf. on Thermodynamics and Statistical Mechanics, Rio de Janeiro, 31 July - 4 August 1989.

2. **Elastic and Anelastic Effects in the Orthorhombic and Tetragonal Forms of $GdBa_2Cu_3O_{7-x}$ as a Function in Pressure and Temperature**

   M. Cankurtaran, G.A. Saunders, D.P. Almond, A. Al-Kheffaji, J. Freestone, Wang Qingxian and E.F. Lambson.

   High Temperature Superconductors Physics and Materials Sciences, NATO Advanced Study Institute, Bad Windsheim, F.R.G., 13-26 August, 1989.

3. **Ultrasonics Studies of High T_C Superconductors**

   D.P. Almond, G.A. Saunders, A. Al-Kheffaji, J. Freeston, Qingxian Wang.

   High Temperature Superconductors, University of Birmingham, 19-21 September 1989.

4. **Elastic and Anelastic Effects in the Orthorhombic and Tetragonal Forms of $GdBa_2Cu_3O_{7-X}$**

   Qingxian Wang, D.P. Almond, J. Freeston, A. Al-Kheffaji, M. Cankurtaran, G.A. Saunders, P.J. Ford and E.F. Lambson.

   Solid State Physics Conference 1989, University of Warwick, 19-21 December, 1989.

5. **Ultrasonic Characteristics of High T_C Superconductors**

Chang Fanggao, M. Cankurtaran, A. Al-Kheffaji, D.P. Almond, G.A. Saunders, P.J. Ford, Qingxian Wang and J. Freestone.

High Temperature Superconductors Polar Solids Discussion Group, Royal Society of Chemistry, University of Bath, 17-19 September 1990.

6. **Nonlinear Acoustic Properties of High Purity Quartz as a Function of Temperature**

Wang Qingxian, G.A. Saunders and B.J. James.

11th General Conf. of the Condensed Matter Division (EPS), University of Exeter, 8-11 April 1991.

7. **Vibrational Anharmonicity of Vitreous Samarium Phosphate**

Wang Qingxian, H.B. Senin, G.A. Saunders, E.F. Lambson.

11th General Conf. of the Condensed Matter Division (EPS), University of Exeter, 8-11 April 1991.

8. **Ultrasonic Studies of Rare Earth Phosphate Glasses**

H.B. Senin, Q. Wang, G.A. Saunders, R.C.J. Draper, H.M. Farok, M. Cankurtaran, P.J. Ford, W. Poon, H. Vass and B. Bridge.

Developments in Acoustics and Ultrasonics, Univ. of Leeds, 24-25 Sept. 1991.

9. **Non-linear Acoustic Properties of Quartz**

Q. Wang, G.A. Saunders, E.F. Lambson, P. Tschaufeser, S.C. Parker and B.J. James.

Developments in Acoustics and Ultrasonics, Univ. of Leeds, 24-25 Sept. 1991.

10. **Ultrasonic Studies of Rare Earth Phosphate Glasses**

H.B. Senin, Q. Wang, G.A. Saunders, R.C.J. Draper, H.M. Farok, P.J. Ford, W. Poon, H. Vass and B. Bridge.

"Bengkel Peringkat Kebangsaan Mengenai Teknologi Sensor (24 October 1991)" and "Seminar Tahunan ke VIII Sains Keadaan Pepejal (25-26 October 1991)" at Universiti Pertanian Malaysia, Serdang, Selangor, Malaysia.

11. **Acoustic and Optical Properties of Rare Earth Phosphate Glasses**

H.B. Senin, H.M. Farok, G.A. Saunders, Q. Wang, M. Cankurtaran, R.C.J. Draper, P.J. Ford, W. Poon, H. Vass and B. Bridge.

Condensed Matter and Materials Physics Conference - 1991, University of Birmingham, 17-19 December 1991.

12. **The Third Order Elastic Stiffness Tensor Components and Non-linear Acoustic Properties of Very High Purity Quartz**

G.A. Saunders, Q. Wang, E.F. Lambson, P. Tschaufeser, S.C. Parker and B.J. James.

Condensed Matter and Materials Physics Conference - 1991, University of Birmingham, 17-19 December 1991.

13. **Linear and Nonlinear Acoustic Properties of Rare Earth Phosphate Glasses**

H.B. Senin, Q. Wang, R.C.J. Draper, G.A. Saunders, P.J. Ford, and M. Cankurtaran.

12th General Conference of the Condensed Matter Div. European Physical Society, Praha, Czechoslovakia, 6-9 April 1992.

14. **The Temperature Dependences of the Third Order Elastic Constants of the Very High Purity Quartz**

Q. Wang, G.A. Saunders, E.F. Lambson and B.J. James.

Annual Review of Progress in Physical Acoustics and Ultrasonics, Magdalen College, Oxford, UK, 22-23 September 1992.

15. **High Pressure Ultrasonic Study of an Antiferromagnetic Cr-0.3at.% Ru Alloy Single-Crystal**

M. Cankurtaran, G.A. Saunders, Q. Wang, P.J. Ford and H.L. Alberts.

Annual Review of Progress in Physical Acoustics and Ultrasonics, Magdalen College, Oxford, UK, 22-23 September 1992.

16. **Anomalous Elastic Behaviour under Pressure and with Temperature near 220K in $YB_2Cu_3O_{7-x}$ and Related High T_C Superconductors**

M. Cankurtaran, G.A. Saunders, P.J. Ford, D.P. Almond, Q. Wang, E.F. Lambson, W.A. Lambson, H.B. Senin and R.C.J. Draper.

Annual Review of Progress in Physical Acoustics and Ultrasonics, Magdalen College, Oxford, UK, 22-23 September 1992.

17. **Non-linear Acoustic Properties of Rare Earth Phosphate Glasses**

H.B. Senin, Q. Wang, G.A. Saunders, R.C.J. Draper, E.F. Lambson, M. Cankurtaran, P.J. Ford, H.A.A. Sidek and W.A. Lambson.

Annual Review of Progress in Physical Acoustics and Ultrasonics, Magdalen College, Oxford, UK, 22-23 September 1992.

18. **The Manufacture and Physical Properties of Rare Earth Phosphate Glasses**

H.B. Senin, Q. Wang, G.A. Saunders, R.C.J. Draper, E.F. Lambson, M. Cankurtaran, P.J. Ford, H.M. Farok, H.A.A. Sidek and W.A. Lambson.

Science and Art in Glass, The Royal Institution of Great Britain, London, 19-21 October (1992).

19. **Elastic and Non-linear Acoustic Properties of Neodymium and Samarium Phosphate Glasses**

H.B. Senin, H.A.A. Sidek, G.A. Saunders, P.J. Ford, Q. Wang, R.C.J. Draper and W.A. Lambson.

Advances in Amorphous State Chemistry, The Society of Glass Technology and the Applied Solid State Chemistry Group of the Royal Society, Scientific Societies Lecture Theatre, London, 1st December (1992).

20. **Comparison of Elastic Behaviour with Temperature and under Pressure in $YB_2Cu_3O_{7-x}$ and $YB_2Cu_4O_8$ High T_C Superconductors**

M. Cankurtaran, G.A. Saunders, P.J. Ford, D.P. Almond, Q. Wang, E.F. Lambson, W.A. Lambson, H.B. Senin and R.C.J. Draper.

Condensed Matter and Materials Conference - 1992, Institute of Physics, University of Sheffield, 15-17 December 1992.

21. **Nonlinear Acoustic Properties and Invar Behaviour of $Fe_{72}Pt_{28}$**

H.B. Senin, H.A.A. Sidek, G.A. Saunders, Q. Wang, L. l Mañosa, P.J. Ford and J. Pelzl.

Condensed Matter and Materials Conference - 1992, Institute of Physics, University of Sheffield, 15-17 December 1992.

22. **Third Order Elastic Constants of the Very High Purity Quartz**

Q. Wang, G.A. Saunders, E.F. Lambson and B.J. James.

Condensed Matter and Materials Conference - 1992, Institute of Physics, University of Sheffield, 15-17 December 1992.

23. **Nonlinear Acoustic Properties of Nd,Eu, and Sm Phosphate Glasses**

H.B. Senin, H.A.A. Sidek, G.A. Saunders, P.J. Ford, Q. Wang and R.C.J. Draper.

Condensed Matter and Materials Conference - 1992, Institute of Physics, University of Sheffield, 15-17 December 1992.

24. **High Pressure Ultrasonic Study of the I-C SDW Transition in Cr-0.3at.% Ru Single-Crystal**

M. Cankurtaran, G.A. Saunders, Q. Wang, P.J. Ford and H.L. Alberts.

Condensed Matter and Materials Conference - 1992, Institute of Physics,

University of Sheffield, 15-17 December 1992.